RADIO ENGINEERING and ELECTRONIC PHYSICS

English Edition of

РАДИОТЕХНИКА И ЭЛЕКТРОНИКА

Published by the American Institute of Electrical Engineers
with the aid of a grant from the National Science Foundation

No.1 January 1961

Translated and Produced by Royer and Roger, Inc.

AMERICAN INSTITUTE OF ELECTRICAL ENGINEERS

Established 1884

33 West Thirty-ninth Street
New York 18, New York

The English edition of RADIO ENGINEERING AND ELECTRONIC PHYSICS is published by the American Institute of Electrical Engineers with the aid of a grant from the National Science Foundation.

Also published under the same arrangement are the Russian electronic journals RADIO ENGINEERING and TELECOMMUNICATIONS.

RADIO ENGINEERING AND ELECTRONIC PHYSICS

(РАДИОТЕХНИКА И ЭЛЕКТРОНИКА)

Publication of the Institute of Radio Engineering and Electronic Physics,
Academy of Sciences of the USSR

Translated and Produced
by
Royer and Roger, Inc.

Translation Editor: Herbert Dern, Columbia University

Subscriptions to Radio Engineering and Electronic Physics should be sent to AIEE
Special Subscription Department
41 East 28th Street, New York 16, New York

1961 Subscription rates:

	$	£
Individuals	28.50	10
Libraries, institutes, govt. agencies	57.00	20

12 issues per annum comprising approximately 1900 pages

THERMAL FLUCTUATIONS IN NONLINEAR SYSTEMS

F. V. Bunkin

The article shows that the known fluctuation-dissipation theorem is strictly applicable for the description of the spectral intensity of thermodynamic equilibrium fluctuations in arbitrary (including nonlinear) passive systems. A qualitative evaluation of the subject is given from the standpoint of the kinetic theory of electrical conductivity.

1. There have recently appeared many theoretical works devoted to the study of thermodynamic equilibrium fluctuations in nonlinear systems [1-10], that is, systems whose macroscopic processes are described by nonlinear equations. The discussion of the problem in these works is based on the simplest example of an R-C mesh with a nonlinear volt-ampere characteristic. The authors proceed on the assumption that when the mean-square value of the thermal fluctuations in voltage at the capacitance $\sqrt{\overline{u^2}} = \sqrt{kT/C}$ * becomes so large (e.g., as the result of an increase in temperature T) as to depart from the region of linearity of the volt-ampere characteristic, the results of the conventional theory of Brownian movement of linear systems prove invalid. In addition, they attempt to construct a "more general" theory of Brownian movement which is valid however great the fluctuations (particularly at high temperatures). It is noteworthy that the final results of all these works differ in all but one respect: in Refs. [3, 5, 7, and 9] it is concluded that in the state of thermodynamic equilibrium the mean value of charge $\overline{q}$ at the capacitor in a nonlinear R-C mesh is other than zero and is $\overline{q} = -e/2$ (e is the electron charge). Notwithstanding the fact that this result, in the first place, contradicts the second principle of thermodynamics and, in the second place, contradicts the condition of continuity,** at no time do the authors consider this an indication of the incorrectness of their approach. On the contrary, in Refs. [7] and [9] in this connection, the authors question the applicability of the second principle of thermodynamics to nonlinear systems and also question the proof of relationship $q = -e/2$.

L. Brillouin [11] has already pointed to the difficulty encountered in a formal application of the Nyquist theorem in describing thermal fluctuations in nonlinear systems. He examined a system consisting of a linear impedance $Z = R + iX$ connected to a nonlinear element with a volt-ampere characteristic $V = ri + bi^2$ and showed that in describing thermal fluctuations in such a system by means of the Nyquist emf the second principle of thermodynamics is not violated if it is considered that the emf together with the fluctuation component e(t) has a constant component determined by the temperature T of the system and by its electrical parameters R, r, X and b. The role of component e_0 reduces to compensation for the rectifying effect of the nonlinear network (with $b = 0$, $e_0 = 0$). In

---

*In addition, it is assumed that the law of equipartition of energy according to degrees of freedom holds, i.e., in the given case, $C\overline{u^2}/2 = kT/2$.

**According to the formula $q = -e/2$ the mean value of charge is defined as a universal constant and does not depend on the properties of the resistance. In this case we do not have a continuous transition to a linear R-C mesh for which $\overline{q} = 0$.

addition, he showed that the spectral intensity of the fluctuations in e(t) must be defined by the linearized resistance of the network, that is,

$$\overline{e_\omega^2} = 4(R + r)kT. \tag{1}$$

2. The present report points out the fact that the fluctuation-dissipation theorem [12, 13]*, being a generalization of the classical Nyquist theorem for fluctuations of an arbitrary physical nature, is strictly valid for arbitrary (nonlinear) systems. This means that the spectral intensity of thermodynamic equilibrium fluctuations in an arbitrary system at temperature T is always precisely defined by the properties of the corresponding linearized system (e.g., its admittance) at the given temperature.

Thus, the nonlinear nature of the macroscopic equations of the system is not related to the problem of the spectrum of its equilibrium fluctuations.

If it is assumed that the above statement is proved (see below), we may proceed further. It is known that the complete theory of Brownian movement (that is, the theory dealing with n-variate probability distributions $w_n(x_1, x_2, \ldots, x_n)$ for equilibrium fluctuations $x(t)[x_i = x(t_i)]$** results from the spectral theory of Brownian movement, which is based on the fluctuation-dissipation theorem with the additional assumption of the specific nature of the fluctuations x(t). This assumption is usually made as follows [21]: either x(t) is a Gaussian process or it is a continuous Markoff Process.*** Each of these assumptions in conjunction with the fluctuation-dissipation theorem is sufficient (e.g., see Ref. 21 to establish the precise form of the function $w_n(x_1, x_2, \ldots, x_n)$, that is, to obtain exhaustive (in the probability sense) information concerning the fluctuations. It is important to note that in such a generalization of the theory the physical properties of the system, particularly the form of the macroscopic equations describing it, are no longer significant.**** Hence, it follows that if, for example, we postulate a Gaussian character for the equilibrium fluctuations in an arbitrary system, then the properties of the corresponding linearized system (e.g., its admittance $\alpha(\omega)$ or admittance matrix $\alpha_{nm}(\omega)$ in the case of several variables) will uniquely define not only the spectral properties of these fluctuations but also all of their statistics (i.e., the function $w_n(x_1, x_2, \ldots, x_n)$).

3. Let us turn now to our principal assertion, namely that the fluctuation-dissipation theorem is strictly applicable to an arbitrary passive system. For this purpose let us discuss the derivation of this theorem, presented in Ref. 13. For the sake of simplicity let us limit ourselves to the case of one fluctuating quantity x(t) (in the thermal equilibrium state the mean value $\overline{x} = 0$). The discussed derivation falls into two independent stages. First, with the single assumption of the stationary nature of the equilibrium fluctuations x(t) and the applicability of the Gibbs canonical distribution (to systems within a thermostat) quantum mechanics are employed to calculate the spectral intensity of $(x^2)_\omega$ of these fluctuations within an aribtrary system in terms of its temperature T, the matrix elements x_{nm} of the operator $\hat{x}$ relative to the stationary states of the system and the eigenvalues of energy E_i of these states (see Ref. 13, page 456):

$$(x^2)_\omega = \psi(\omega; T, x_{nm}, E_i). \tag{2}$$

Once the function ψ is derived, then, in principle, if we know the matrix elements x_{nm} and the energy E_i, the problem of the spectral properties of equilibrium fluctuations in an arbitrary system is already solved. The dynamic properties of the system (particularly the form of its macroscopic equations) do not enter into this stage.

---

* For a generalization of this theorem in the case of several fluctuating quantities and for field fluctuations see Refs 13-20.

** x(t) is regarded as a random process describing a physical quantity fluctuating in time.

*** In the case of several fluctuating quantities it is necessary to introduce the concept of multivariate or continuous Markoff process. A Markoff process is continuous if its transition probability satisfies the Einstein-Fokker equation.

****This is evident from the fact that the n-variate distribution is wholly determined by the mean values of $\overline{x}_k$ and the second-order movements $\overline{x}_i\overline{x}_k$, the values of which are given by the fluctuation-dissipation theorem.

The second stage consists in the quantum-mechanical calculation (in terms of the same quantities ω, T, x_{nm} and E_i) of the transfer function (admittance) $\alpha(\omega) = \alpha'(\omega) + i\alpha''(\omega)$ defining the mean linear response $\bar{x}_\omega$ to a sufficiently weak external harmonic input f_ω: $\bar{x}_\omega = \alpha(\omega) f_\omega$. In particular, this calculation yields the imaginary part of the admittance (see Ref. 13, page 456)

$$\alpha''(\omega) = \varphi(\omega; T, x_{nm}, E_i). \tag{3}$$

Thus, this stage provides a dynamic description of an arbitrary system in the presence of external inputs which are sufficiently weak that nonlinear effects in the response may be disregarded. In addition, fluctuations of the quantity x are completely disregarded.

The fluctuation-dissipation theorem arises from a comparison of the righthand members of Eqs. (2) and (3). It develops that, without any additional assumptions, the quantity $\psi(\omega; T, x_{nm}, E_i)$ (that is, $(x^2)_\omega$) can be expressed in general form in terms of the quantity $\varphi(\omega; T, x_{nm}, E_i)$ (that is, $\alpha''(\omega)$). In this case we obtain ([13], page 456)

$$(x^2)_\omega = \frac{\hbar}{2\pi} \alpha''(\omega) \operatorname{cth} \frac{\hbar\omega}{2kT}. \tag{4}$$

Thus, regardless of how the system behaves in the presence of strong influences (it may be as nonlinear as is desired), the spectral intensity of the equilibrium fluctuations within it is always determined by the properties of a linearized system (the function $\alpha''(\omega)$ in the case of one variable and the matrix $(\alpha^*_{mn} - \alpha_{nm})$ in the case of many variables) and its temperature T.* Hence it follows in particular that fluctuations x(t) may always (and not only for the dynamics of linear systems) be regarded as the response of a linearized system to an external random force f(t) with spectral intensity

$$(f^2)_\omega = \frac{\hbar}{2\pi} \frac{\alpha''(\omega)}{|\alpha(\omega)|^2} \operatorname{cth} \frac{\hbar\omega}{2kT}. \tag{5}$$

This result confirms that of L. Brillouin, Eq. (1), and eliminates the necessity for introducing the direct component of emf e_0.

In applying the fluctuation-dissipation theorem to fluctuations of an electromagnetic field in a nonlinear medium the spectral intensities of external random fields at each point of the medium must obviously be defined by the same formulas (similar to Eq. (5)) as in the case of a linear medium [13, 17-20]. As in the last case, these formulas may also be used for determining the intensity of the external field in nonuniformly heated bodies. In the case of nonlinear media there may also arise effects due to the rectification of inherent fluctuations. These do not, however, violate the second principle of thermodynamics, for nonuniform heating is present.

4. Let us now discuss from the physical point of view the reason why nonlinear effects within the system do not affect the statistical properties of its thermal equilibrium fluctuations (in any case, why they do not affect the spectral intensity of these fluctuations). Let us examine this problem through the example of electrical fluctuations in a system containing active resistances with nonlinear volt-ampere characteristics. For this purpose let us turn to the kinetic theory of electrical conductivity in strong quasi-static fields [22-26]. The quasi-static condition of the field in the given case means that the characteristic time τ_0 for a change of field must be great in comparison with all the microscopic relaxation times τ_{rel} in the conductor being discussed:

$$\tau_0 \gg \tau_{rel} \tag{6}$$

From the macroscopic point of view condition Eq. (6) signifies that the conductor being

---

* After the present report was completed there appeared Ref. 16 in which the authors arrive at the same conclusions concerning applicability of the fluctuation-dissipation theorem to nonlinear systems. In that paper, however, there is no evaluation of the problem from the kinetic point of view (see below).

discussed does not possess dispersion and its electrical properties may be characterized by means of one parameter — electrical resistance R. It is this case in which we are interested at this time.

As shown in Refs. 22-26, due to the fact that in each collision with a heavy particle an electron gives to it only a small part $\delta = \Delta\varepsilon/\varepsilon$ of its energy ε (for gases $\delta \sim m/M \ll 1$, for semiconductors and metals $\delta \sim mv_s^2/kT \ll 1$, where m and M are the electron and heavy-particle masses, respectively; v_s is the speed of sound; T is the lattice temperature), the distribution function f(**p**) of electrons in momentum space **p** may be represented with an accuracy up to terms of higher order relative to δ in the form

$$f(\mathbf{p}) = f_0(p) + f_1(p)\, p_x/p. \tag{7}$$

The symmetrical part of $f_0(p)$ is always (up to breakdown) considerably greater than asymmetrical part $f_1(p)p_x/p$ defining the electrical conductivity σ ($f_0 \gg f_1$) of the medium; the x-axis is directed along electric field E. In the equilibrium state, when E = 0, the symmetrical part $f_0(p)$ is a Maxwell (for gases and semiconductors) or Fermi (for metals) distribution, while $f_1(p) = 0$. The influence of the field on the electron distribution f(**p**) and the conductivity σ is defined by the parameter

$$\eta = \left(\frac{elE}{kT}\right)^2 \Big/ \delta, \tag{8}$$

where e and l are the charge and mean free path of electrons, respectively. In the case of a weak field, when $\eta \ll 1$, Ohm's law is applicable (σ is independent of E) with an accuracy up to terms of order η, while the symmetrical part $f_0(p)$ remains an equilibrium distribution corresponding to a lattice temperature T. Here the entire effect of the field reduces to the drift of electrons whose distribution within the momentum space remains an equilibrium distribution.

The chief result of the proposed theory for the discussed problem is the fact that departure from Ohm's law (occurring at $\eta \gtrsim 1$) is always accompanied by a departure of the function $f_0(p)$ (and, consequently, of the complete distribution function f(**p**)) from equilibrium. Thus, in the region of nonlinearity of the volt-ampere characteristic of the conducting element the distribution of electrical carriers within it is always essentially a nonequilibrium distribution.* Hence it is evident that nonlinearity of the volt-ampere characteristic (and, consequently, of the associated equations describing the macroscopic processes in the system) is not related to the problem of equilibrium fluctuations in this system. Since at any value of equilibrium fluctuation (in particular, at any temperature) the function $f_0(p)$ remains (by definition) an equilibrium distribution function, the system always behaves as a linear system in the sense that the properties of these fluctuations are defined by the corresponding linearized (in terms of the zero order solution) macroscopic equations of the system.

The examined "self-linearization" of the system with an increase in its temperature is qualitatively explained by the dependence of the parameter η on temperature: with an increase in T the region of linearity of the volt-ampere characteristic (the region of values of E wherein Ohm's law is still applicable) is expanded. It is easily shown that in the state of thermal equilibrium of the system the condition $\eta \ll 1$ is automatically fulfilled. For the sake of simplicity let us examine an R-C mesh. The quasi-static condition Eq. (6) in the given case reduces to the requirement $RC \gg \tau_{rel}$, where τ_{rel} is any relaxation micro-time, particularly the energy relaxation time $l/\bar{v}\delta$ ($\bar{v}$ is the mean thermal velocity of the electron). Let it be noted that with $RC \lesssim l/\bar{v}\delta$ the conducting element can no longer be considered as an inertial-less resistance R and the system itself is no longer an R-C

---

* In some cases (e.g., in metals [25, 26]) even in strong fields ($\eta \gtrsim 1$) the function $f_0(p)$ has the form of an equilibrium distribution corresponding to an electron temperature $\theta > T$. With regard to a thermostat with temperature T, this distribution is obviously a nonequilibrium distribution.

mesh as such.*

For an R-C mesh in thermal equilibrium $E \sim (kT/CL^2)^{1/2}$, where L is the length of resistor. Considering further that $R \sim L^2/\sigma V = L^2/en_e\mu V$, while the mobility $\mu \sim el/\sqrt{mkT}$ (n_e is the electron density, V is the volume of the resistor), for the parameter η we obtain

$$\eta \sim \left[\frac{l}{\bar{v}\delta} \Big/ RC\right] N_e^{-1}, \tag{9}$$

where N_e is the total number of free electrons in the resistor. Since $N_e \gg 1$, the parameter η is actually negligibly small.

The author wishes to express his gratitude to S. M. Rytov and L. I. Gudzenko for their advice concerning the problems discussed in this report.

REFERENCES

1. D. K. C. MacDonald, Philos. Mag., 1954, 45, 63.
2. D. Polder, Philos. Mag., 1954, 45, 69.
3. D. K. C. MacDonald, Phys. Rev., 1957, 108, 541.
4. N. G. van Kampen, Phys. Rev., 1958, 110, 319.
5. C. T. J. Alkemade, Physica, 1958, 24, 1029.
6. R. O. Davies, Physica, 1958, 24, 1055.
7. A. Marek, Czech. J. Phys., 1959, 9, 260.
8. V. B. Magolinskiy, ZhETF, 1959, 36, 1423.
9. A. Marek, Physica, 1959, 25, 1358.
10. M. Lax, Rev. Mod. Phys., 1960, 32, 25.
11. L. Brillouin, Phys. Rev., 1950, 78, 627.
12. H. B. Callen, T. A. Welton, Phys. Rev., 1951, 83, 34.
13. L. D. Landau, Ye. M. Lifshits, Electrodynamics of solid media, GIFML, 1959.
14. H. B. Callen, M. L. Barasch, J. L. Jackson, Phys. Rev., 1952, 88, 1382.
15. R. Kubo, J. Phys. Soc. Japan, 1957, 12, 570.
16. W. Bernard, H. B. Callen, Rev. Mod. Phys., 1959, 31, 1017.
17. S. M. Rytov, Theory of electrical fluctuations and thermal radiation, Izd. AN SSSR, 1953.
18. F. V. Bunkin, ZhETF, 1957, 32, 811.
19. S. M. Rytov, Dokl. AN SSSR, 1956, 110, 371.
20. V. P. Silin, Izv. vuzov MVO (Radiofizika), 1959, 2, 198.
21. M. C. Wang, G. E. Uhlenbeck, Rev. Mod. Phys., 1945, 17, 323.
22. L. Landau, A. Kompaneyets, ZhETF, 1935, 5, 276.
23. B. I. Davydov, ZhETF, 1936, 6, 471; 1937, 7, 1069.
24. B. I. Davydov, I. M. Shmushkevich, Uspekhi fiz. nauk, 1940, 24, 21.
25. V. P. Shabanskiy, ZhETF, 1954, 27, 147.
26. V. L. Ginzburg, V. P. Shabanskiy, Dokl. AN SSSR, 1955, 100, 445.

---

* Disturbance of the condition $RC \gg l/\bar{v}\delta$ with an increase in temperature may be expected, for example, in the case where the conducting element is a gas. If the temperature T is so great that the gas is almost wholly ionized, then the mean free path $l \sim T^2$ (collision with ions) and consequently the time $l/\bar{v}\delta$ will increase with temperature as $T^{3/2}$. However, it is well known that at frequencies $\omega \gtrsim \bar{v}\delta/l$ plasma has strongly pronounced dispersive properties.

P. N. Lebedev Physics Institute

AN SSSR

Submitted to the editors 24 June 1960

CROSS CORRELATION OF FIELD FLUCTUATIONS OF RECEIVING LENSES WITH FINITE DIMENSIONS

M. F. Bakhareva

The report derives the cross correlation coefficient R for field fluctuations at the foci of lenses when an incident monochromatic, initially plane wave passes through a medium with extensive random discontinuities in its refractive index. It is shown that if the dimensions of the lens are commensurate with the radius of cross correlation of the field fluctuations, then with an increase in the distance between receiving points the coefficient R decreases more slowly in the presence of lenses than in the absence of lenses.

INTRODUCTION

On the assumption that there are no lenses at the receiving points the cross correlation function of field fluctuations has been determined by L. A. Chernov [1] for the case of the passage of a plane monochromatic wave through a layer of a medium with extensive random discontinuities in its refractive index. However, in practice reception is always achieved with lenses or antennas of finite dimensions. If the antenna dimensions are commensurate with the correlation radius of the field fluctuations, the antenna gain is not wholly utilized, which leads, as is known [2, 3], to a decrease in the relative intensity of fluctuations at the antenna foci.

The present report investigates the influence of finite lens dimensions on the cross correlation coefficient R of field fluctuations at the lens foci. It also derives the dependence of R on the propagation parameter a relative to the lens dimension h/a (a is the mean extent of the discontinuity in the medium) and relative to the distance between lens foci (h + d)/a. It is shown that with lenses in which h is commensurate with a, the cross correlation coefficient decreases more slowly with an increase in distance between receiving points than in the absence of lenses.

1. STATEMENT OF THE PROBLEM

Let lenses be placed at two points for the reception of a random wave field. Let P_i represent the field strength at the focus of the i-th lens (i = 1, 2). The spatial correlation function K for field fluctuations at the receiving points is

$$K = \overline{\Delta P_1 \Delta P_2^*} = \overline{P_1 P_2^*} - \overline{P_1}\,\overline{P_2^*}. \tag{1}$$

It is assumed that the lenses are located in a plane perpendicular to the direction of propagation of the primary wave incident on a layer of thickness L of a statistically nonuniform medium (Fig. 1). The field strength P_i at the focus of the i-th lens is associated with the field p incident upon the lens by the relationship

$$P_i = \frac{jkA_0}{2\pi F} e^{-jkF} \int_{\Sigma_i} p(\vec{\rho})\, ds, \quad i = 1, 2, \tag{2}$$

where Σ_i is the area of the i-th lens, ds is an element of this area, $\vec{\rho}$ is the radius vector of this element, F is the focal length, k is the wave number, A_0^2 is the intensity of the waves incident upon the layer. We shall assume that both lens are identical. On the basis of Eqs. (1) and (2) the correlation function K may be written in the form

$$K = \frac{k^2 A_0^2}{4\pi^2 F^2} \int_{\Sigma_1}\int_{\Sigma_2} \overline{\Delta p(\vec{\rho})\, \Delta p^*(\vec{\rho}')}\, ds\, ds', \tag{3}$$

where $\Delta p = p - \bar{p}$ is the field fluctuation in the lens plane. The integrand in Eq. (3) is the cross correlation function of field fluctuation calculated by L. A. Chernov [2], namely:

$$\overline{\Delta p(\vec{\rho})\,\Delta p^*(\vec{\rho}')} = e^{\alpha\left[e^{-\frac{l^2}{a^2}}-1\right]} - e^{-\alpha}, \tag{4}$$

where

$$\alpha = \sqrt{\pi}\,\bar{\mu}^2 k^2 a L \tag{5}$$

is the propagation parameter, l is the distance between points $\vec{\rho}$ and $\vec{\rho}'$, $\bar{\mu}^2$ is the average intensity of the fluctuations in the refractive index of the medium

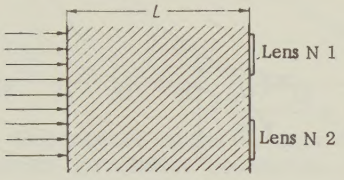

Fig. 1. Passage of a wave through a layer of thickness L. Arrows indicate the direction of propagation.

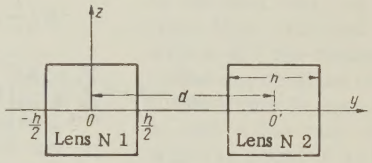

Fig. 2. Location of lenses in a plane perpendicular to direction of propagation. Points O and O' are the lens foci.

Let the lenses be bounded by square diaphragms with sides of length h. Then, in accordance with Eqs. (3) and (4), introducing integration limits corresponding to the dimensions of Fig. 2, the required correlation function is written in the form

$$K = \frac{A_0^2}{\lambda^2 F^2}\int_{-\frac{h}{2}}^{\frac{h}{2}}\int dz_1 dz_2 \int_{-\frac{h}{2}}^{\frac{h}{2}} dy_1 \int_{-\frac{h}{2}+d}^{\frac{h}{2}+d} e^{\alpha\left[e^{-\frac{l^2}{a^2}}-1\right]} - e^{-\alpha}\,dy^2, \tag{6}$$

wherein $l^2 = (y_1 - y_2)^2 + (z_1 - z_2)^2$.

2. CALCULATION OF THE CORRELATION FUNCTION

Let us expand the exponent of the integrand of Eq. (6) into a series:

$$\exp\left[\alpha e^{-\frac{l^2}{a^2}}\right] = 1 + \sum_{m=1}^{\infty}\frac{\alpha^m}{m!}e^{-m\frac{(y_1-y_2)^2+(z_1-z_2)^2}{a^2}} \tag{7}$$

Substituting Eq. (7) into Eq. (6), we find

$$K = \frac{A_0^2}{\lambda^2 F^2}e^{-\alpha}\sum_{m}^{\infty}\frac{\alpha^m}{m!}\int_{-\frac{h}{2}}^{\frac{h}{2}}\int e^{-\frac{m(z_1-z_2)^2}{a^2}}dz_1 dz_2 \int_{-\frac{h}{2}}^{\frac{h}{2}} dy_1 \int_{-\frac{h}{2}+d}^{\frac{h}{2}+d} e^{-\frac{m(y_1-y_2)^2}{a^2}}dy_2,$$

which after integration yields

$$K\left(\frac{h}{a},\ \frac{d}{a},\ \alpha\right) = \frac{A_0^2}{\lambda^2 F^2}e^{-\alpha}\pi a^4 \sum_{m=1}^{\infty}\frac{\alpha^m}{m!\,m^2}\left[\frac{h}{a}\sqrt{m}\,\Phi\left(\frac{h}{a}\sqrt{m}\right) + \frac{e^{-\frac{h^2}{a^2}m}-1}{\sqrt{\pi}}\right]\times$$

$$\times \left\{ \frac{d+h}{a} \sqrt{m}\,\Phi\left(\frac{d+h}{a}\right) - 2\frac{d}{a}\sqrt{m}\,\Phi\left(\frac{d}{a}\sqrt{m}\right) + \frac{d-h}{a}\sqrt{m}\,\Phi\left(\frac{d-h}{a}\sqrt{m}\right) + \right.$$

$$\left. + \frac{1}{\sqrt{\pi}}\left[e^{-\left(\frac{d+h}{a}\right)^2 m} - 2e^{-m\left(\frac{d}{a}\right)^2} + e^{-m\left(\frac{d-h}{a}\right)^2} \right] \right\}. \qquad (8)$$

As is seen from Eq. (8), the correlation function K depends on three parameters: the propagation parameter α (given by Eq. (5)), the relative lens size h/a and the relative distance between lens centers d/a.

Let us discuss a few limiting cases.

If there are no lenses at the receiving points (h/a = 0), then the quantity $K / \Sigma_1\Sigma_2 = K / h^4$ becomes Eq. (4) for the cross correlation function of field fluctuations.

If both lenses coincide (i.e., d/a = 0), then we obtain from Eq. (8) the expression for the intensity of field fluctuations $\overline{|\Delta P|^2}$ at the lens focus:

$$K\left(\frac{h}{a}, 0, \alpha\right) = \overline{|\Delta P|^2} =$$

$$= \frac{A_0^2}{\lambda^2 F^2}\pi a^4 e^{-\alpha} \sum_{m=1}^{\infty} \frac{\alpha^m}{m!\,m^2} \left[\sqrt{m}\,\frac{h}{a}\,\Phi\left(\sqrt{m}\,\frac{h}{a}\right) + \frac{e^{-m\left(\frac{h}{a}\right)^2} - 1}{\sqrt{\pi}} \right]^2 \qquad (9)$$

This expression differs somewhat from that obtained in M. N. Krom's paper Ref 3, namely:

$$\overline{|\Delta P|^2} = \frac{A_0^2}{\lambda^2 F^2}\pi a^4 e^{-\alpha} \sum_{m=1}^{\infty} \frac{\alpha^m}{m!\,m}.$$

The difference is associated with the fact that we have not extended the integration limits with respect to the normalized coordinate to infinity, as was done in Ref. 3.

On the basis of Eqs. (8) and (9) the correlation coefficient $R = \overline{\Delta P_1 \Delta P_2^*} / \overline{|\Delta P|^2}$ of field fluctuations at the foci of identical lenses may be written in the form

$$R = R\left(\frac{h}{a}, \frac{d}{a}, \alpha\right) = K\left(\frac{h}{a}, \frac{d}{a}, \alpha\right) \Big/ K\left(\frac{h}{a}, 0, \alpha\right). \qquad (10)$$

In the absence of lenses at the receiving points the correlation coefficient takes the form

$$R_0 = R\left(0, \frac{d}{a}, \alpha\right) = K\left(0, \frac{d}{a}, \alpha\right) \Big/ K(0, 0, \alpha) =$$

$$= \frac{e^{\alpha\left[e^{-\frac{d^2}{a^2}} - 1\right]} - e^{-\alpha}}{1 - e^{-\alpha}}. \qquad (11)$$

From Eq. (11) we find that in the case of small fluctuations ($\alpha \ll 1$)

$$R_0 = e^{-\frac{d^2}{a^2}}, \qquad (12)$$

and in the case of large fluctuations ($\alpha \gg 1$)

$$R_0 = e^{-\alpha\frac{d^2}{a^2}}. \qquad (13)$$

3. EVALUATION OF RESULTS

Figures 3 and 4 show the results of calculations from Eqs. (8)-(13) of the dependence of R (solid curves) and R_0 (dotted) on d/a for α = 4, 16, and $\alpha \ll 1$, and for h/a = 0.6, 1, 2.

The following conclusions may be drawn from the shape of the curves. First, for fixed values of h/a and α the value of R for any d/a is greater than R_0. In other words,

the correlation between field fluctuations at the lens foci decreases with increasing d/a more slowly than do the field correlations at the same points in the absence of lenses. This occurs because, with $h \neq 0$, the correlation of the fluctuations of the field in regions near the lens areas exceeds R_0, since the distance between these portions is less than the distance between lens centers. Second, in the case of small fluctuations ($\alpha \ll 1$) the difference between R and R_0 becomes significant when the lens dimensions are commensurate with the extent of the discontinuity of the medium a, and in the case where $\alpha \gg 1$, when the lens dimensions are considerably less than a. This is explained by the fact that, as follows from Eqs. (12) and (13), with $\alpha \ll 1$ the radius of cross correlation of field fluctuations is equal to a, and in the case where $\alpha \gg 1$ is equal to $a/\sqrt{\alpha}$, that is, is $\sqrt{\alpha}$ times less [1, 2].

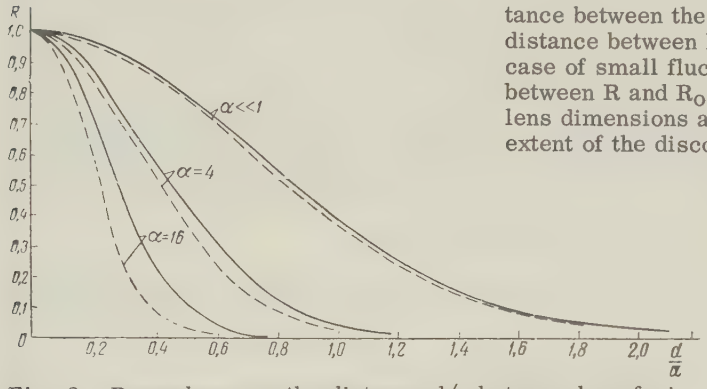

Fig. 3. Dependence on the distance d/a between lens foci of the cross correlation coefficient R (solid line) in the presence of a lens with h/a = 0.4 and cross correlation coefficient R_0 (broken line) in the absence of a lens. Propagation parameter $\alpha = 4$, 16, and $\alpha \ll 1$

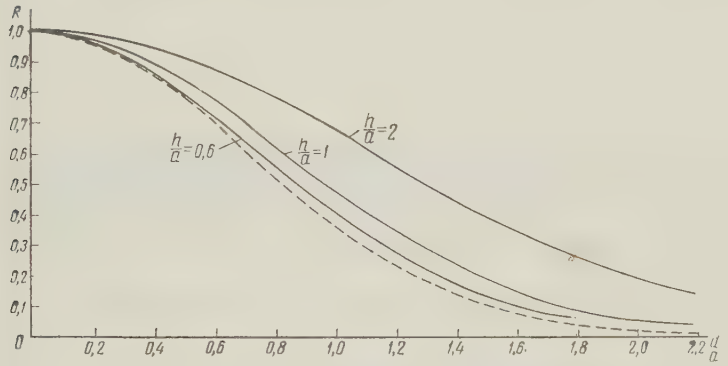

Fig. 4. Dependence on the distance d/a between lens foci of the cross correlation coefficient R (solid line) in the presence of a lens with h/a = 0.6, 1 and 2 and cross correlation coefficient R_0 (broken line) in the absence of a lens. Propagation parameter $\alpha \ll 1$.

The author takes this opportunity to express his thanks to S. M. Rytov for his counsel in this work.

REFERENCES

1. L. A. Chernov, Akust. zh., 1957, 3, 2, 192.
2. L. A. Chernov, Akust. zh., 1957, 3, 4, 360.
3. M. N. Krom, Akust. zh., 1959, 5, 1, 45.

Submitted to the editors

1 June 1960

CALCULATION OF CROSS NOISE POWER IN LONG-DISTANCE SCATTER COMMUNICATIONS SYSTEMS

A. V. Prosin

The paper determines the cross noise power arising in long-distance communications systems with frequency modulation and frequency multiplex, due to the multipath propagation of radio waves. It is shown that in the presence of the constant component of the field the value of cross noise in telephone communications channels using long-distance tropospheric microwave propagation may be extremely small.

INTRODUCTION

In long-distance tropospheric propagation of microwaves the total signal at the receiver input is caused by various propagation mechanisms which may act separately and simultaneously. As a result the field at the receiver is usually a combination of a field of constant intensity (caused by diffraction, reflection from various inversions, superrefraction and similar mechanisms of wave propagation) and a scatter field.

As an expansion of the work in Ref. 1 the present paper is devoted to determining the cross-noise distortion arising in long-distance communications systems with frequency modulation, due to the presence of the constant and scatter fields at the receiving site with relatively small delays of the constant wave. An analysis is performed in general form by use of the correlation function of turbulent discontinuities of air as introduced in Ref. 2.

1. CALCULATION PROCEDURE

In accordance with the procedure of correlation analysis presented in Ref. 3 the cross noise power is

$$P_{ct} = 10^9 K_g^2 W_\varepsilon(\Omega_K)\,\Delta F_K R_K^{-1} \quad \mu\mu\omega, \tag{1}$$

where the spectrum and correlation function of cross noise are determined from the expressions

$$W_\varepsilon(\Omega) = 4\Omega^2 \int_0^\infty \Psi_{\varepsilon_1}(\tau)\cos\Omega\tau d\tau, \tag{2}$$

$$\Psi_{\varepsilon_1}(\tau) = \overline{\varepsilon_1(t)\,\varepsilon_1(t+\tau)} = \frac{1}{\Delta\omega_m^2}\,\overline{\Psi(t)\,\Psi(t+\tau)}^{-} \tag{3}$$

In Eqs. (1)-(3) and thereafter the definitions of quantities not specifically indicated are as given in Ref. 1. In calculating the noise spectrum it is necessary in Eq. (3) to eliminate coherent terms which do not contribute to the cross noise in telephone channels.

2. CROSS NOISE CORRELATION FUNCTION

On the basis of Eqs. (4) and (5) of Ref. 1 and Eq. (3) above the correlation function will be

$$\Psi_{\varepsilon_1}(\tau) = \frac{1}{\Delta\omega_m^2}\int_{-\infty}^{\infty}\int_{-\infty}^{\infty}\int_{-\infty}^{\infty}\int_{-\infty}^{\infty} \operatorname{arc\,tg}\frac{B(t)}{1+A(t)}\operatorname{arc\,tg}\frac{B(t+\tau)}{1+A(t+\tau)}\,W[B(t),$$
$$A(t),\ B(t+\tau),\ A(t+\tau)]\,dB(t)\,dA(t)\,dB(t+\tau)\,dA(t+\tau), \tag{4}$$

where W [ ] is a quadrivariate distribution function.

It was shown in Ref. 1 that if the deviation of the dielectric constant from its mean value follows a normal probability distribution with mean zero, then A(t) and B(t) are uncorrelated random functions which follow the normal probability distribution.

A calculation of Eq. (4) with the statistical properties of A(t) and B(t) cited above is given in Ref. 4. For our case the correlation function of noise is defined by

$$\Psi_{\varepsilon_1}(\tau) = \frac{1}{\Delta\omega_m^2}\sum_{r=-\infty}^{\infty}\sum_{n=-\infty}^{\infty}\sum_{m=-\infty}^{\infty} A_{rmn}\frac{(-1)^{m+n}4\pi^2}{(n+r)(m-r)}, \quad n\neq -r,\ m\neq r, \tag{5}$$

$$A_{rmn} = \frac{1}{4\pi^2[1-R^2(\tau)]}e^{-\frac{2\gamma^2}{1+R(\tau)}}\int_0^\infty\int_0^\infty Z_1 Z_2 I_r\left(\frac{R(\tau)Z_1Z_2}{1-R^2(\tau)}\right)\times$$

$$\times I_m\left(\sqrt{2}\,\gamma\frac{Z_1}{1+R(\tau)}\right)I_n\left(\sqrt{2}\,\gamma\frac{Z_2}{1+R(\tau)}\right)e^{-\frac{Z_1^2+Z_2^2}{2(1-R^2(\tau))}}dZ_1dZ_2,$$

where $\gamma^2 = (V_g/V_p)^2$; V_p is the voltage attenuation factor of the scatter field components; I_r, I_m and I_n are Bessel functions, respectively, of the r-th, m-th and n-th orders, with imaginary arguments; $R(\tau)$ is a correlation coefficient, which with the given statistical properties of A(t) and B(t) is

$$R(\tau) = \frac{\Psi_{AA}(\tau)}{\Psi_{AA}(0)}. \tag{6}$$

Integration of Eq. (5) leads to an unwieldy expression for $\Psi_{\varepsilon_1}(\tau)$ which is extremely difficult to use in calculating the cross noise spectrum. With

$$\gamma^2 \frac{1 - R(\tau)}{1 + R(\tau)} < 1, \tag{7}$$

as shown in Ref. 5, the expression for the correlation function is somewhat simplified and has the form

$$\Psi_{\varepsilon_1}(\tau) \simeq \frac{1}{2\Delta\omega_m^2} e^{-\frac{2\gamma^2}{1+R(\tau)}} \sum_{r=1}^{\infty} \sum_{n=0}^{\infty} \frac{\Gamma^2\left(n + \frac{r}{2}\right)}{n!\,(n+r)!} R^{r+2n}(\tau), \tag{8}$$

where Γ is the gamma function.

The dependence of Eq. (8) on $R(\tau)$ is satisfactorily approximated by

$$\Psi_{\varepsilon_1}(\tau) \simeq \frac{\pi^2}{3\Delta\omega_m^2} e^{-\gamma^2} R^{n_\gamma}(\tau), \tag{9}$$

$$n_\gamma = \frac{4}{3} e^{0.35\gamma^2}.$$

In the case of a purely scattered microwave field $n_\gamma = 4/3$; when the intensities of the constant and scatter field components are equal, $n_\gamma = 1.9$.

In determining $R(\tau)$ it is necessary, in accordance with Eq. (6), to find the correlation function of A(t). With the assumptions made in Ref. 1 this function is equal to

$$\Psi_{AA}(\tau) \sim B_H(\tau) \int_V \Psi_z(\tau, T_z) \frac{f_{tr}(\alpha, \beta) f_{rec}(\alpha, \beta)}{R_{11}^2 R_{22}^2} \sigma dV. \tag{10}$$

$$\Psi_z(\tau, T_z) = \overline{\cos\{\Delta\omega_m [S(t) - S(t - T_z) - S(t + \tau) + S(t + \tau - T_z)]\}}, \tag{11}$$

where σ is the effective scatter cross-section (scatter coefficient); $f_{tr}(\alpha, \beta)$ and $f_{rec}(\alpha, \beta)$ are the power-gain characteristics of the receiving and transmitting antennas, respectively; $B_H(\tau)$ is the envelope of the scatter-signal time correlation coefficient. R_{11} and R_{22} are defined by Fig. 1.

The correlation function of Eq. (11) is from Ref. 6 equal to

$$\Psi_z(\tau, T_z) = e^{-m_{me}^2 y_1(\tau)}, \tag{12}$$

$$y_1(\tau) = \frac{4\Omega_2^2}{\Delta\Omega} \int_{\Omega_1}^{\Omega_2} \left(\frac{\sin\left(\frac{\Omega T_z}{2}\right)}{\Omega} \right)^2 (1 - \cos\Omega\tau)\, d\Omega, \tag{13}$$

where $m_{me} = \frac{\Delta\omega_{me}}{\Omega_2}$ is the effective modulation index; $\Delta\omega_{me} = 2\pi\Delta f_{me} = \Delta\omega_m \sqrt{\Psi_u(0)}$ (Δf_{me} is the effective frequency deviation); $\Psi_u(0)$ is the average power of the multichannel signals; $\Omega_2 = 2\pi F_2$; $\Omega_1 = 2\pi F_1$ (F_2 and F_1 are the upper and lower limit frequencies of the linear spectrum of u(t)); $\Delta\Omega = \Omega_2 - \Omega_1$.

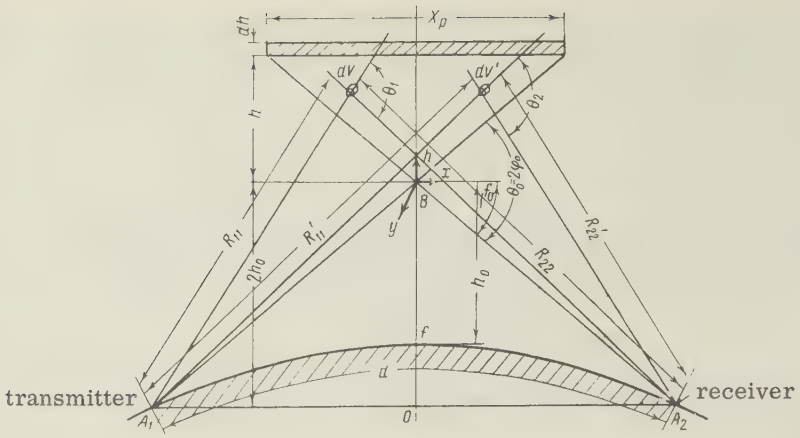

Figure 1

In communications systems with long-distance tropospheric propagation of microwaves the following condition is quite often fulfilled

$$\frac{\Omega_2 T_3}{2} \ll 1, \tag{14}$$

which corresponds to the case of relatively small delays of the constant component of the field, commensurate with the scatter field delays. Subject to the limitation of condition (14) (the procedure for the calculation of cross noise with delays of the constant wave is given in Ref. 1) we obtain for Eq. (12)

$$\Psi_z(\tau, T_z) = \exp\left\{-\Delta\omega_{me}^2 T_z^2 \left(1 - \frac{\sin \Omega_2 \tau}{\Omega_2 \tau}\right)\right\}. \tag{15}$$

The product of the directivity characteristics of the transmitting and receiving antennas in the vertical plane is approximated by

$$f_{\text{tr}}(\alpha) f_{\text{rec}}(\alpha) = \exp\left\{-1{,}38\left(\frac{h - n_x h_1}{h_1}\right)^2\right\}, \tag{16}$$

$$h_1 = \frac{\alpha_0 d}{\lambda}, \tag{17}$$

where α_0 is the angular width of the antenna radiation patterns in the vertical plane; n_X is a factor characterizing orientation of the antenna axis relative to the horizon. With the antenna axis oriented toward the horizon $n_X = 0$; with the antenna axis at an angle of $0.5\ \alpha_0$ above the horizon $n_X = 1$.

The scatter coefficient and decrease in fluctuation intensities with height are defined by Eqs. (31) and (32) in Ref. 1. The general nature of these equations permits the relation between cross noise and the statistical parameters of a turbulent troposphere to be written in a general form.

Substituting Eqs. (7), (8), (31) and (32) of Ref. 1 and Eqs. (15) and (16) above into Eq. (10) and reducing the volume integration to an integration over height alone [7], we obtain

$$\Psi_{AA}(\tau) \sim B_{\text{H}}(\tau) \int_0^\infty e^{-\left\{\left(\frac{\Delta\omega_{me} d}{CR_e}\right)^2 (1+y(\tau))(h-h_c)^2 + \frac{1{,}38}{h_1^2}(h-n_x h_1)^2 + \frac{a_x}{h_0^2}(h-b_x h_0)^2\right\}} dh =$$

$$= \Psi'_{AA}(\tau), \tag{18}$$

$$y(\tau) = \frac{\sin \Omega_2 \tau}{\Omega_2 \tau}; \quad h_c = \frac{\tau_{zg} CR_e}{d}; \tag{19}$$

$$a_x = \ln 2\,(1{,}4 e^{-0{,}33(p+0{,}5n_1-1)} - b_x)^{-2}; \tag{20}$$

$$b_x = (1 + p + 0{,}5 n_1)^{-1}. \tag{21}$$

Equations (20) and (21) are valid within the limits

$$1 \leqslant (p + 0{,}5\, n_1) \leqslant 3{,}5. \tag{22}$$

From Eq. (18) it follows that

$$\Psi_{AA}(0) \sim \int_0^\infty e^{-\left\{\frac{1{,}38}{h_1^2}(h-n_x h_1)^2 + \frac{a_x}{h_0^2}(h-b_x h_0)^2\right\}} dh = \Psi'_{AA}(0). \tag{23}$$

Substituting Eqs. (18), (23) and (6) into Eq. (9), we obtain

$$\Psi_{\varepsilon_1}(\tau) = \frac{\pi^2}{3\omega_m^2} e^{-\gamma^2 \Psi'^{-n_\gamma}_{AA}(0)} \Psi'^{n_\gamma}_{AA}(\tau). \tag{24}$$

In the integrand of Eq. (18) let us expand the exponential factor containing $y(\tau)$ into a power series:

$$e^{\left(\frac{\Delta\omega_{me} d}{CR_e}\right)^2 (h-h_c)^2 y(\tau)} = e^{A_1 y(\tau)} = 1 + \frac{A_1 y(\tau)}{1!} + \frac{A_1^2 y^2(\tau)}{2!} + \frac{A_1^3 y^3(\tau)}{3!}. \tag{25}$$

Hereafter we shall be limited by the condition

$$A_1 = \left(\frac{\Delta\omega_{me} d}{CR_e}\right)^2 (h-h_c)^2 = (\Delta\omega_{me} T_z)^2 \leqslant 1, \tag{26}$$

which is similar to the previously introduced condition (14). Hence in Eq. (25) we leave only three terms of expansion. Then, in accordance with Eqs. (18), (24) and (25), we obtain

$$\Psi'^{n_\gamma}_{AA}(\tau) = B_н^{n_\gamma}(\tau)\,[a_к + b_к y(\tau) + C_к y^2(\tau)]^{n_\gamma}, \tag{27}$$

$$a_к = \int_0^\infty e^{-f(h,\, h_c)}\, dh, \tag{28}$$

$$b_к = \frac{1}{1!}\left(\frac{\Delta\omega_{me} d}{CR_e}\right)^2 \int_0^\infty e^{-f(h,\, h_c)}\,(h-h_c)^2\, dh, \tag{29}$$

$$C_к = \frac{1}{2!}\left(\frac{\Delta\omega_{me} d}{CR_e}\right)^4 \int_0^\infty e^{-f(h,\, h_c)}\,(h-h_c)^4\, dh, \tag{30}$$

$$f(h,\, h_c) = \left[\left(\frac{\Delta\omega_{me} d}{CR_e}\right)^2 (h-h_c)^2 + \frac{1{,}38}{h_1^2}(h-n_x h_1)^2 + \frac{a_x}{h_0^2}(h-b_x h_0)^2\right]. \tag{31}$$

Experimental investigation of long-distance tropospheric propagation of microwaves has shown that the envelope of the scatter-signal time correlation coefficient decreases quite slowly with time ($B_н(\tau)$ decreases e times, where e is the natural log base, with τ equal to fractions and units of seconds). Consequently, the energy spectrum of the cross noise will be concentrated in the zero frequency region. Hence in subsequent use of Eq. (27) we shall discard the factor $B_н^{n_\gamma}(\tau)$.

Expanding Eq. (27) into a Maclaurin series in powers of $y(\tau)$ and, in accordance with Eq. (20), limiting ourselves to three terms of the expansion, we obtain

$$\Psi^{n_\gamma}_{AA}(\tau) = a_к^{n_\gamma} + \frac{1}{1!} n_\gamma a_к^{n_\gamma - 1} b_к y(\tau) + \frac{1}{2!} n_\gamma a_к^{n_\gamma - 2}\,[(n_\gamma - 1)\, b_к^2 + 2c_к a_к]\, y^2(\tau) + \cdots. \tag{32}$$

The first term of the expansion in Eq. (32) does not depend on τ and hence does not contribute to the shape of the spectrum. The second term of the expansion in Eq. (32) is the linear portion of the correlation function, which portion causes nonlinear distortion coherent with the signal itself. Consequently, the first and second terms in Eq. (32) will not create cross noise in the channels and it is necessary to eliminate them from Eq. (24) in determining the cross noise power.

3. CROSS NOISE POWER

Substituting Eqs. (2), (24) and (32) into Eq. (1) and integrating, we obtain the formula for the cross noise power measured at the point with zero reference level:

$$P_{ct} = \frac{\pi}{3} 10^9 K_g^2 e^{-\gamma^2} \frac{\Delta F_к F_2}{\Delta f_к^2} \frac{m^2}{(1+m)^{2+0,5\, n_\gamma}} b_1^2 (2 - b_1) f_1, \tag{33}$$

$$f_1 = \frac{e^{-mm_3^{2n_\gamma}} A_1^{n_\gamma - 2}}{[2 - P(2m_1, 1)]^{n_\gamma}} n_\gamma [(n_\gamma - 1) A_2^2 + 0,885 A_1 A_3], \tag{34}$$

$$A_1 = [2 - P(2m_2^2, 1)], \tag{35}$$

$$A_2 = 0,442 [2 - P(2m_2^2, 3)] + P(2m_2^2, 2) m_3 + 0,884 [2 - P(2m_2^2, 1)] m_3^2, \tag{36}$$

$$A_3 = 0,665 \{[2 - P(2m_2^2, 5)] + 3P(2m_2^2, 4) m_3 + 4 [2 - P(2m_2^2, 3)] m_3^2 + 3P(2m_2^2, 2) m_3^3 + 1,33 [2 - P(2m_2^2, 1)] m_3^2\}. \tag{37}$$

In Eqs. (33)-(37) $\Delta f_к = \Delta f_{me} e^{-b_{av}}$ is the effective value of frequency deviation per channel, b_{av} is the difference between the average power level of all channels and the measured level of a single channel (in nepers), $b_1 = \Omega_к / \Omega_2$, and Δf_2 is the troposphere bandwidth in the case where directional antennas are used:

$$\Delta f_2 = \Delta f_1 Q_1; \tag{38}$$

Δf_1 is the troposphere bandwidth in the case where nondirectional antennas are used

$$\Delta f_1 = \frac{C R_e^2}{d^3}, \tag{39}$$

Q is a factor which takes into account the influence of antenna directivity on the troposphere bandwidth:

$$Q = \sqrt{a_x + \frac{1,38}{a^2}}; \tag{40}$$

$a = \alpha_0 / \varphi_0$; $P(\chi^2, n)$ is the x^2 probability function, φ_0 is half of the zeroth scatter angle;

$$m = 0,62 \left(\frac{\Delta f_{me}}{\Delta f_2} \right)^2; \tag{41}$$

$$m_1 = 1,38 \frac{\left(n_x + \frac{a_x b_x}{1,38} a \right)^2}{1 + \frac{a_x}{1,38} a^2}; \tag{42}$$

$$m_2 = \sqrt{\frac{m_1}{1+m}} \left(1 + m \frac{h_c}{m_4} \right); \tag{43}$$

$$m_3 = \sqrt{\frac{m_1}{(1+m)}} \left(1 - \frac{h_c}{m_4} \right); \tag{44}$$

$$m_4 = \frac{1,38\, h_1}{a} \frac{1}{Q_1}; \tag{45}$$

$$Q_1 = \frac{1,38 + a_x a^2}{a n_x + \frac{b_x b_x}{1,38} a^2}. \tag{46}$$

Equation (33) is applicable upon satisfying conditions (14) and (7). The minimum value of the constant field component is determined from the condition $V_g^2 > V_{pH}^2$, , where V_{pH}^2 is the intensity of the field scattered by the most active turbulent discontinuity in the scatter space (i.e., the discontinuity causing the maximum value of the scatter field at the receiving point in comparison with other discontinuities). With $V_g = 0$ and $h_c = 0$ Eq. (33) defines the value of cross noise arising in the propagation of waves by scatter.

For a qualitative analysis of the cross distortion arising upon interaction of the constant and scatter fields let us derive a simpler formula for cross noise power. Integrating Eq. (18) and considering Eqs. (16) and (9), we have

$$\Psi_{\varepsilon_1}(\tau) = \frac{\pi^2}{3\Delta\omega_m^2} e^{-\gamma^2 B_H(\tau)} \exp\{-m_5 m_6 m_7\}, \tag{47}$$

$$m_5 = \frac{\pi^2}{16}\left(\frac{\Delta f_{me}}{\Delta f_2}\right)^2 (1 - y(\tau)), \tag{48}$$

$$m_6 = 0{,}99\, m_1 n_\gamma, \tag{49}$$

$$m_7 = 1 - \frac{h_c}{m_4} = 1 - \frac{h_c a Q_1}{1{,}38\, h_1}. \tag{50}$$

Equation (47) is obtained on the condition that m_5 and $m_5 \frac{h_c}{m_4}$ are substantially less than unity. The second condition is more rigid and extremely difficult to satisfy, particularly with a horizontal orientation of the antenna.

Isolating in Eq. (47) the coherent terms of cross distortion (the procedure for isolating coherent terms is approximately the same as that examined above) and discarding, as before, the function $B_H(\tau)$, we obtain in accordance with Eqs. (1), (2) and (47) the following expression for cross noise power measured at the point with zero reference level:

$$P_{ct} = 2\cdot 10^9 K_g^2 e^{-0{,}3\gamma^2} \frac{\Delta F_K F_2}{\Delta f_K^2}\left(\frac{\Delta f_{me}}{\Delta f_2'}\right)^4 \times$$

$$\times e^{-\left[1{,}67\left(\frac{\Delta f_{m9}}{\Delta f_2'}\right)^2 e^{0{,}35\gamma^2} m_7^2\right]} m_7^4 b_1^2 (2 - b_1)\, nbm, \tag{51}$$

where $\Delta f_2'$ is the troposphere bandwidth in the case where directional antennas are used:

$$\Delta f_2' = \Delta f_1 Q_1; \tag{52}$$

Q_1 is a factor which takes into account the increase in troposphere bandwidth with an increase in antenna directivity [see Eq. (46)].

It follows from Eq. (51) that the minimum value of cross noise will occur under the condition $m_7 = 0$. A quantitative determination of the minimum value of cross noise must be made with Eq. (33), for Eq. (51) does not consider second order terms.

In microwave scatter propagation (i.e., with $\gamma^2 = 0$, $h_c = 0$) Eq. (51) may be used for quantitative calculations, but in comparison with Eq. (33) it yields slightly lower values (by 2 db) of cross noise power.

4. DEPENDENCE OF CROSS NOISE POWER ON VARIOUS PARAMETERS

Investigation of the dependence of cross distortion on the position of the channel in the linear spectrum of multichannel communications has shown that the maximum cross noise power will occur in the channel with frequency $\Omega_K \simeq \frac{4}{3}\Omega_2$. Consequently, calculations of cross noise must be performed for the uppermost channel, that is, for $b_1 = 1$.

From Eqs. (33) and (51) it follows that the cross noise power is inversely proportional to the fourth power of the troposphere bandwidth, which in Ref. 8 is determined on the basis of the transfer characteristics of the troposphere. Consequently, the equations derived establish the relation between the value of cross noise and the troposphere bandwidth as defined on the basis of the transfer characteristics of the medium.

Figure 2 shows the dependence of Q^2 on a for a number of values of p and n_1. With increased antenna directivity, the coefficient Q and consequently the troposphere bandwidth increase rapidly. In the region $0.4 \leqslant a \leqslant 1.5$ the value of Q is considerably affected by the

statistical characteristics of the turbulent troposphere, in particular with an increase in p and n_1 the value of Q also rises. Since existing systems of microwave scatter propagation operate in the given range of a, in calculating cross noise it is necessary to consider the statistical parameters of the troposphere.

The table and Fig. 3 show the dependence of f_1 and P_{ct} on h_c/h_1 for a = 1 and a = 0.25, $n_\gamma = 4/3$ (the case of low intensity of the constant wave) and $n_\gamma = 1.9$ (the case where $V_g^2 = V_p^2$), $n_x = 0$ (horizontal orientation of the antennas) and $n_x = 1$ (antenna at an angle of 0.5 α_0 above the horizon). In the calculations it was assumed that d = 300 km, R_e = 8500 km, c = 300,000 km/sec, number of telephone channels N = 120, p = 1, and $n_1 = 2$ (the chosen values of p and n_1 permit a relatively simple explanation of the experimentally observed values of the field beyond the horizon). The dependence of P_{ct} and f_1 on h_c/h_1 is

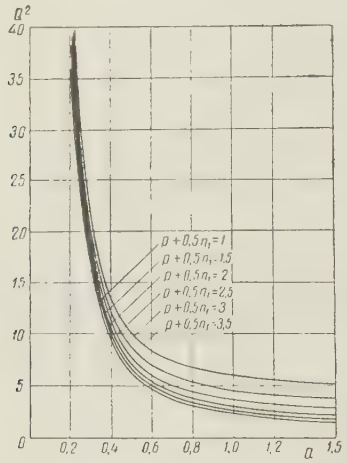

Fig. 2

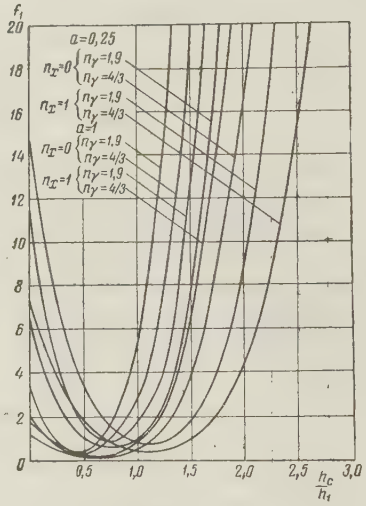

Fig. 3

resonant in nature, wherein there exists an optimum ratio of h_c/h_1 at which the value of cross noise will be minimum. For example, with a = 1 and $n_x = 1$ the value of P_{ct} is minimum at $h_c/h_1 = 0.81$, this ratio being practically independent of n_γ (i.e., the relation between the constant and scatter field components). Existence of the optimum $P_{ct} = f(h_c/h_1)$ may be explained by the symmetrical disposition of the scatter field components relative to the constant field components, which with constant amplitudes of scatter rays leads to a linear phase characteristic for the propagation medium.

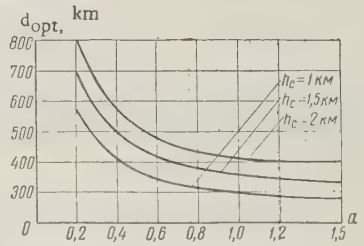

Fig. 4

The presence of a wave of constant intensity with corresponding delay considerably reduces the value of cross noise. Thus, with a = 1 and $n_x = 1$, in purely scatter propagation of microwaves $P_{ct} = 290 \cdot 10^3\ \mu\mu\omega$, and with n = 1.9 the value of cross noise at the minimum is only $P_{ct} = 130 \cdot 10^2\ \mu\mu\omega$ (i.e., 22 times less).

With a decrease in the elevation angles of the antennas, first, the value of optimum ratio h_c/h_1 decreases and, second, the value of P_{ct} is substantially reduced. For example, with a = 0.25, $n_x = 1$ and $n_\gamma = 1.9$ the optimum ratio $h_c/h_1 = 0.65$ and $P_{ct} = 280\ \mu\mu\omega$, and with $n_x = 0$ $h_c/h_1 = 1$ and $P_{ct} = 79\ \mu\mu\omega$.

From Eqs. (33), (34), (50) and (51) it follows that for a constant value of time delay of the wave of constant intensity we may in this manner select such parameters for the communications system as will provide minimum cross noise. These parameters are length of the transmission path, directivity of the transmitting and receiving antennas and antenna elevation angles. From Eqs. (50) and (51) it follows that the optimum path length will be

a=0,25													a=1											
n_x=0						n_x=1						n_x=0						n_x=1					
n_γ=4/3			n_γ=1,9			n_γ=4/3			n_γ=1,9			n_γ=4/3			n_γ=1,9			n_γ=4/3			n_γ=1,9		
$\frac{h_c}{h_1}$	f_1	P_{ct}	$\frac{h_c}{h_1}$	f_1	P_{ct}	$\frac{h_c}{h_1}$	f_1	P_{ct}	$\frac{h_c}{h_1}$	f_1	P_{ct}	$\frac{h_c}{h_1}$	f_1	P_{ct}	$\frac{h_c}{h_1}$	f_1	P_{ct}	$\frac{h_c}{h_1}$	f_1	P_{ct}	$\frac{h_c}{h_1}$	f_1	P_{ct}
0	1,2	$12\cdot10^2$	0	2,0	740	0	7,1	$72\cdot10^2$	0	14	$51\cdot10^2$	0	2,1	$95\cdot10^3$	0	3,3	$48\cdot10^3$	0	6,4	$29\cdot10^4$	0	11	$16\cdot10^4$
0,043	1,0	10^3	0,043	1,7	630	0,26	3,6	$37\cdot10^2$	0,26	7,0	$25\cdot10^2$	0,044	1,7	$78\cdot10^3$	0,044	2,7	$39\cdot10^3$	0,16	3,7	$17\cdot10^4$	0,16	6,3	$92\cdot10^3$
0,086	0,87	880	0,086	1,5	530	0,51	1,7	$18\cdot10^2$	0,51	3,2	$12\cdot10^2$	0,088	1,4	$63\cdot10^3$	0,088	2,1	$31\cdot10^3$	0,32	1,9	$88\cdot10^3$	0,32	3,3	$47\cdot10^3$
0,13	0,74	750	0,13	1,2	440	0,77	0,79	$8\cdot10^2$	0,77	1,4	520	0,13	1,1	$5\cdot10^4$	0,13	1,7	$25\cdot10^3$	0,49	1,0	$45\cdot10^3$	0,49	1,7	$24\cdot10^3$
0,17	0,62	630	0,17	1,0	370	1,0	0,43	430	1,0	0,77	280	0,22	0,71	$32\cdot10^3$	0,22	1,1	$16\cdot10^3$	0,65	0,57	$26\cdot10^3$	0,65	0,96	$14\cdot10^3$
0,26	0,44	450	0,26	0,71	260	1,3	0,48	480	1,3	0,89	320	0,31	0,45	$2\cdot10^4$	0,31	0,68	$98\cdot10^2$	0,81	0,54	$24\cdot10^3$	0,81	0,92	$13\cdot10^3$
0,30	0,37	380	0,30	0,60	220	1,5	1,0	10^3	1,5	1,9	$7\cdot10^2$	0,35	0,37	$17\cdot10^3$	0,35	0,56	$8\cdot10^3$	0,97	0,97	$44\cdot10^3$	0,97	1,7	$24\cdot10^3$
0,40	0,25	250	0,40	0,39	140	1,8	2,3	$24\cdot10^2$	1,8	4,6	$16\cdot10^2$	0,39	0,30	$14\cdot10^3$	0,39	0,47	$68\cdot10^2$	1,1	1,4	$66\cdot10^3$	1,1	2,8	$4\cdot10^4$
0,60	0,13	140	0,60	0,22	79	2,0	5,0	$5\cdot10^3$	2,0	9,9	$36\cdot10^2$	0,44	0,27	$12\cdot10^3$	0,44	0,42	$61\cdot10^2$	1,3	2,9	$13\cdot10^4$	1,3	5,6	$81\cdot10^3$
0,65	0,13	130	0,65	0,22	79	2,3	9,7	$98\cdot10^2$	2,3	20	$72\cdot10^2$	0,48	0,26	$12\cdot10^3$	0,48	0,41	$59\cdot10^2$	1,6	9,9	$45\cdot10^4$	1,6	1,8	$28\cdot10^4$
0,69	0,13	130	0,69	0,23	82	2,6	17	$17\cdot10^3$	2,6	36	$13\cdot10^3$	0,52	0,27	$12\cdot10^3$	0,52	0,44	$63\cdot10^2$	1,9	25	$12\cdot10^5$	1,9	46	$66\cdot10^4$
0,80	0,20	$2\cdot10^2$	0,80	0,38	140	2,8	29	$29\cdot10^3$	2,8	61	$22\cdot10^3$	0,61	0,39	$18\cdot10^3$	0,61	0,64	$92\cdot10^2$	2,3	49	$22\cdot10^5$	2,3	88	$13\cdot10^5$
0,90	0,28	290	0,90	0,52	190	3,1	51	$52\cdot10^3$	3,1	97	$35\cdot10^3$	0,7	0,8	$36\cdot10^3$	0,7	1,4	$2\cdot10^4$	2,4	64	$29\cdot10^5$	2,4	110	$16\cdot10^5$
1,0	0,47	480	1,0	0,87	310	3,3	70	$7\cdot10^4$	3,3	150	$54\cdot10^3$	1,0	2,8	$13\cdot10^4$	1,0	5,3	$77\cdot10^3$	2,6	81	$37\cdot10^5$	2,6	140	$20\cdot10^5$
2,0	17	$17\cdot10^3$	2,0	33	$12\cdot10^3$	3,6	10^2	10^5	3,6	220	$79\cdot10^3$	2,0	56	$25\cdot10^5$	2,0	110	$16\cdot10^5$	3,0	140	$64\cdot10^5$	3,0	220	$31\cdot10^5$
3,0	120	$12\cdot10^4$	3,0	240	$87\cdot10^3$	3,8	150	$15\cdot10^4$	3,8	310	$11\cdot10^4$	3,0	170	$79\cdot10^5$	3,0	250	$37\cdot10^5$	3,5	$2\cdot10^2$	$99\cdot10^5$	3,5	270	$4\cdot10^6$
4,0	470	$47\cdot10^4$	4,0	950	$34\cdot10^4$	4,0	$2\cdot10^2$	$2\cdot10^5$	4,0	430	$15\cdot10^4$	4,0	210	$98\cdot10^5$	4,0	220	$32\cdot10^5$	4,0	230	$11\cdot10^6$	4,0	260	$38\cdot10^5$

Note: Comma represents decimal point.

$$d_{opt} = \sqrt{5{,}8\, h_c R_e Q_1}. \quad (53)$$

This equation provides satisfactory quantitative results in the case of antenna elevation angles of $0.5\ \alpha_0$. For horizontally oriented antennas the optimum parameters must be determined from Eq. (33). Figure 4 shows the dependence of $d_{opt} = f(a)$ with $p = 1$, $n_1 = 2$, $R_e = 8500$ km and $n_x = 1$ for three values of h_c. With an increase in delay of the constant field component and with an increase in antenna directivity the optimum length of path increases.

CONCLUSIONS

1. In multichannel microwave-scatter communications systems with frequency modulation and frequency multiplex the maximum value of cross noise occurs in scatter propagation of waves on turbulent discontinuities of the troposphere. In this method of propagation the cross noise increases rapidly with distance.

2. The presence at the receiving point (in addition to the scatter component) of a component of constant intensity with relatively short delay decreases cross distortion. With this composite mechanism of wave propagation there exists the possibility (with known statistical parameters of the troposphere) of choosing communications system parameters which provide minimum cross noise. The dependence of cross noise on distance is resonant in nature, hence there exists an optimum distance between transmitter and receiver at which cross noise is minimum.

3. The statistical characteristics of the troposphere have considerable effect on the value of cross distortion. Hence for a more accurate calculation of cross noise power it is necessary to have exhaustive experimental data concerning the statistical characteristics of the troposphere (i.e., data concerning the correlation function of turbulent discontinuities in the dielectric constant of air, the extent of turbulent discontinuities, the decrease in intensity of discontinuities with height, etc.).

REFERENCES

1. A. V. Prosin, A theory of cross distortion in long-distance troposphere propagation of microwaves, Radiotekhnika i elektronika, 1960, 5, 7, 1052.
2. A. V. Prosin, Influence of the statistical characteristics of a turbulent troposphere on microwave scatter propagation, NDVSh (Radiotekhnika i elektronika), 1959, 1, 43.
3. A. V. Prosin, Toward calculation of cross distortion in multipath propagation of radio waves, HDVSh (Radiotekhnika i elektronika), 1959, 1, 53.
4. B. R. Levin, Theory of random processes and its application in radio engineering, Sovetskoye radio, 1957.
5. I. A. Gusyatinskiy, Signal distortion in microwave propagation beyond the line of sight, Proc. NII MS SSSR, 1959, 1(15), 15.
6. A. V. Prosin, Cross noise arising in relay links with frequence modulation due to multipath propagation or mismatch and discontinuities in antenna feeders. Sb. trudov Nauchno-tekhnicheskogo obshchestva radiotekhniki i elektrosvyazi im. A.S. Popova, 1958, No. II, 168.
7. A. V. Prosin, Toward calculation of scatter power in microwave scatter propagation, Elektrosvyaz', 1958, 8, 13.
8. A. V. Prosin, Distortions in microwave scatter propagation, Elektrosvyaz', 1959, 5, 32.

Submitted to the editors 16 July 1960

POWER SPECTRUM OF A SIGNAL OBTAINED BY SCANNING

N. K. Ignat'yev

The paper establishes the dependence of the power spectrum of a signal on the multi-dimensional statistical properties of the information from which this signal is obtained by scanning. The solutions derived are directly applicable in television, facsimile and radar engineering.

INTRODUCTION

In radio engineering there are encountered cases of the transformation of information in which the signal is formed by scanning (e.g., in television, facsimile, radar). The presence of scanning considerably complicates the spectra of the corresponding signals and at the same time leads to definite regularities in their structure which must be considered in all attempts to compress the band of frequencies occupied by the signal. From this point of view the determination of the power spectrum of the signal is of maximum interest.

Since in all three of the abovementioned areas of application the spectral properties of the signal are determined by the presence of scanning, the methods of investigating them are similar and hence it is expedient to examine them together.

1. THE PROBING ELEMENT

In the discussed systems information which is a function of two or three variables is transformed by scanning into a function of time known as the signal [1]. Scanning is achieved by a moving probing element periodically traversing the area of the information. In radar the probing element is a "packet" of waves propagated in space; in facsimile it is the cross-section of a light beam tracing the image elements; in television this role is filled by the cross-section of the electron beam traversing the target and by the persistence of the target.

The probing element is usually finite in all dimensions of the information space. Hence the resulting signal is proportional (within a certain approximation) to the effective changes in reflectivity or brilliance of the scanned object. In the given case the effect of the probing element is equivalent to the effect of a low-frequency filter generalized into the corresponding number of dimensions [1].

Thus, it may be considered that the process of scanning represents a process of low-frequency filtering. If the effect of the probing element in the dimensions x, y and t may be characterized by the weighting function $G_1(x, y, t)$*, then as the result of this filtering, the function $F_1(x, y, t)$, characterizing the initial information, is transformed into the function

$$F(x, y, t) = \iiint_{-\infty}^{\infty} F_1(\chi, \nu, \vartheta)\, G_1(x - \chi, y - \nu, t - \vartheta)\, d\chi\, d\nu\, d\vartheta.$$

* In television such a function may be formed by the product of the density distribution function of the current in the electron beam exploring the target by the transfer function characterizing the target persistence.

By so treating the filtering effect of the probing element we may consider that the ultimate transformation of the function F(x, y, t) reduces to "pure" scanning by an infinitely small probing element. The weighting function of this "ideal" probing element may be expressed by means of the delta-function as

$$G(x, y, t) = \delta(x)\,\delta(y)\,\delta(t).$$

Since in each specific case the real weighting function of the probing element is known and its effect on the initial information and its statistical properties may be determined relatively easily, it will hereafter be considered that we are speaking only of the scanning of the transformed function F(x, y, t) by an ideal probing element.

2. SCANNING ACTION

In television the scanning of an image F(x, y, t) which is a function of two spatial coordinates x and y and of the time t occurs. The dimensions of the scanned surface are always finite and hence it may be considered that

$$|x| \leqslant \frac{X}{2}; \quad |y| \leqslant \frac{Y}{2}.$$

It is easily seen that in this case the function

$$D_R(x, y, t, \tau) = \sum_{k_1} \delta\left[x - X\left(\frac{\tau}{T_1} + k_1\right)\right] \sum_{k_2} \delta\left[y - Y\left(\frac{\tau}{T_2} + k_2\right)\right] \delta(t - \tau) \tag{1}$$

describes the displacement of an ideal probing element in the space of the variables x, y, t as functions of present time τ [2]. Here T_1 is the scanning period along the x-axis (i.e., the line scan period) and T_2 is the scanning period along the y-axis (i.e., the field scan period). Henceforth we shall refer to this function as the discretizing function.

Multiplying the initial function F(x, y, t) by the discretizing function (1) and integrating, we obtain a sequence of separate values of this function forming a function of time (the signal)

$$f(\tau) = \iiint_{-\infty}^{\infty} F(x, y, t)\, D_R(x, y, t, \tau)\, dx\, dy\, dt. \tag{2}$$

In facsimile it may be considered that transmission of an image in the form of an infinite strip, with width lying within the limits of $|x| \leqslant |X|/2$, displaced along the y-axis at a velocity of v = y/t occurs. The result is that the transmitted image may be regarded as a function F(x, t) and the displacement of the ideal probing element in the scanning process may be represented by means of the discretizing function

$$D_R(x, t, \tau) = \sum_{k} \delta\left[x - X\left(\frac{\tau}{T} + k\right)\right] \delta(t - \tau), \tag{3}$$

where T is the line scan period.

As in the preceding case, the resulting facsimile signal may be expressed as

$$f(\tau) = \iint_{-\infty}^{\infty} F(x, t)\, D_R(x, t, \tau)\, dx\, dt. \tag{4}$$

Let a radar probe space along the coordinate x, wherein, due to displacement of the target or of the radar, the character of the reflected signals depends on time t. This means that scanning of function F(x, t) occurs. It is evident that if during pulse-repetition period T of the radar, the probing packet of waves travels a distance X, then the corresponding movement of the probing element is expressed by the same equation as in the preceding case, Eq. (3). If we neglect the fact that intensity of the reflected signals

decreases with distance to the target, or if we assume that high-speed automatic gain control is used, then the resulting signal may also be expressed by Eq. (4).

Thus, the bases of the transformation of a two-dimensional function into one-dimensional function are identical in facsimile and radar, whereas they are special cases of a more general form of the transformation of the three-dimensional function occurring in television.

3. CORRELATION FUNCTION

Let us assume that the scanned function $F(x, y, t)$ represents a random stationary process* for which the bivariate distribution function $\Phi(u_1, u_2; x_1, x_2; y_1, y_2; t_1, t_2)$, where u_1 and u_2 are the values of function $F(x, y, t)$ at points (x_1, y_1, t_1) and (x_2, y_2, t_2), is known. Assuming that $\chi = x_2 - x_1$, $\nu = y_2 - y_1$, and $\vartheta = t_2 - t_1$ by virtue of the stationary nature of the process we may write

$$\Phi(u_1, u_2; x_1, x_2; y_1, y_2; t_1, t_2) = \Phi(u_1, u_2; \chi, \nu, \vartheta).$$

Knowing this expression for the distribution function, we may give the three-dimensional correlation function

$$B(\chi, \nu, \vartheta) = \iint_{-\infty}^{\infty} u_1 u_2 \Phi(u_1, u_2; \chi, \nu, \vartheta) du_1, du_2, \tag{5}$$

which is the natural generalization of the one dimensional correlation function.

If a function $F(x, y, t)$ having the statistical characteristics mentioned is transformed by scanning into a function of time, then the latter will have a distribution function $\varphi(u_1, u_2, \tau)$, (depending only on the displacement of the examined points in time τ) and the corresponding correlation function

$$b(\tau) = \iint_{-\infty}^{\infty} u_1, u_2 \varphi(u_1, u_2, \tau) du_1 du_2. \tag{6}$$

It is easily concluded that if scanning is achieved in accordance with the discretizing function $D_R(x, y, t, \tau)$, then the relation between the displacements χ, ν, ϑ in three-dimensional space on one hand and the displacement of τ in one-dimensional space on the other will be defined by the discretizing function $D_R(\chi, \nu, \vartheta, \tau)$, and hence, as in Eq. (2), we will have

$$\varphi(u_1, u_2, \tau) = \iiint_{-\infty}^{\infty} \Phi(u_1, u_2; \chi, \nu, \vartheta) D_R(\chi, \nu, \vartheta, \tau) d\chi\, d\nu\, d\vartheta. \tag{7}$$

Substituting Eq. (7) in Eq. (6) and taking into account Eq. (5), we obtain

$$b(\tau) = \iiint_{-\infty}^{\infty} B(\chi, \nu, \vartheta) D_R(\chi, \nu, \vartheta, \tau) d\chi\, d\nu\, d\vartheta. \tag{8}$$

It is evident that for facsimile and radar we shall similarly have the correlation function

---

* The assumption of the stationary nature of the process examined (signifying that its distribution function does not depend on the coordinates in which this process is given) may be justified by the fact that in each case it is difficult even to indicate the cause whereby there may arise a given relationship disturbing the condition of stationarity. If in a certain case such a cause does occur, then the process acquires a nonstationary component and the results of the analysis presented here, remaining applicable only for its stationary component, are approximate in the broadest sense.

$$b(\tau)\iint_{-\infty}^{\infty} B(\chi, \vartheta) D_R(\chi, \vartheta, \tau)\, d\chi\, d\vartheta. \tag{9}$$

Thus, the correlation function of a signal obtained as a result of scanning may be determined as the result of scanning the correlation function of the initial information.

4. POWER SPECTRUM

As is known, the power spectrum of the signal is associated with the correlation function by the relationship

$$w(\omega) = \int_{-\infty}^{\infty} b(\tau)\, e^{-i\omega\tau} d\tau. \tag{10}$$

In a similar manner we may determine the power spectra of three-dimensional and two-dimensional information:

$$W(\omega_1, \omega_2, \omega_3) = \iiint_{-\infty}^{\infty} B(\chi, \nu, \vartheta)\, e^{-i(\omega_1\chi+\omega_2\nu+\omega_3\vartheta)} d\chi\, d\nu\, d\vartheta, \tag{11}$$

$$W(\omega_1, \omega_2) = \iint_{-\infty}^{\infty} B(\chi, \vartheta)\, e^{-i(\omega_1\chi+\omega_2\vartheta)} d\chi\, d\vartheta. \tag{12}$$

Let us introduce the concept of discretizing functions in the spectral region: three-dimensional $D_S(\omega_1, \omega_2, \omega_3, \omega)$ and two-dimensional $D_S(\omega_1, \omega_2, \omega)$, which satisfy the conditions

$$w(\omega) = \iiint_{-\infty}^{\infty} W(\omega_1, \omega_2, \omega_3)\, D_S(\omega_1, \omega_2, \omega_3, \omega)\, d\omega_1\, d\omega_2\, d\omega_3, \tag{13}$$

$$w(\omega) = \iint_{-\infty}^{\infty} W(\omega_1, \omega_2)\, D_S(\omega_1, \omega_2, \omega)\, d\omega_1\, d\omega_2. \tag{14}$$

Substituting Eq. (8) in Eq. (10) and comparing the result with Eq. (13), we have

$$\iiint_{-\infty}^{\infty} B(\chi, \nu, \tau) \int_{-\infty}^{\infty} D_R(\chi, \nu, \vartheta, \tau)\, e^{-i\omega\tau} d\tau\, d\chi\, d\nu\, d\vartheta =$$

$$= \iiint_{-\infty}^{\infty} W(\omega_1, \omega_2, \omega_3)\, D_S(\omega_1, \omega_2, \omega_3, \omega)\, d\omega_1\, d\omega_2\, d\omega_3.$$

Using here the value $B(\chi, \nu, \vartheta)$ obtained from Eq. (11), we have

$$\iiint_{-\infty}^{\infty} \left(\frac{1}{2\pi}\right)^3 \iiint_{-\infty}^{\infty} W(\omega_1, \omega_2, \omega_3)\, e^{i(\omega_1\chi+\omega_2\nu+\omega_3\vartheta)} d\omega_1\, d\omega_2\, d\omega_3 \times$$

$$\times \int_{-\infty}^{\infty} D_R(\chi, \nu, \vartheta, \tau)\, e^{-i\omega\tau}\, d\tau\, d\chi\, d\nu\, d\vartheta =$$

$$= \iiint_{-\infty}^{\infty} W(\omega_1, \omega_2, \omega_3)\, D_S(\omega_1, \omega_2, \omega_3, \omega)\, d\omega_1\, d\omega_2\, d\omega_3.$$

Differentiating both sides of this expression with respect to ω_1, ω_2, and ω_3 and simplifying, we obtain

$$D_S(\omega_1, \omega_2, \omega_3, \omega) = \left(\frac{1}{2\pi}\right)^3 \int_{-\infty}^{\infty} \int \int \int \int D_R(\chi, \nu, \vartheta, \tau)\, e^{i(\omega_1\chi + \omega_2\nu + \omega_3\vartheta - \omega\tau)}\, d\chi\, d\nu\, d\vartheta\, d\tau. \tag{15}$$

Substituting Eq. (9) in Eq. (10) and comparing the result with Eq. (14), in the same manner as in the previous case we obtain

$$D_S(\omega_1, \omega_2, \omega) = \left(\frac{1}{2\pi}\right)^2 \int_{-\infty}^{\infty} \int \int D_R(\chi, \vartheta, \tau)\, e^{i(\omega_1\chi + \omega_2\vartheta - \omega\tau)}\, d\chi\, d\vartheta\, d\tau. \tag{16}$$

Substituting Eq. (1) in Eq. (15) and Eq. (3) in Eq. (16), we obtain after integration the final expressions for the corresponding discretizing functions in the spectral region:

$$D_S(\omega_1, \omega_2, \omega_3, \omega) = \frac{1}{XY} \sum_{m_1} \delta\left(\omega_1 - m_1 \frac{2\pi}{X}\right) \sum_{m_2} \delta\left(\omega_2 - m_2 \frac{2\pi}{Y}\right) \times$$

$$\times\, \delta\left(\omega_3 - \omega + m_1 \frac{2\pi}{T_1} + m_2 \frac{2\pi}{T_2}\right), \tag{17}$$

$$D_S(\omega_1, \omega_2, \omega) = \frac{1}{X} \sum_{m} \delta\left(\omega_1 - m \frac{2\pi}{X}\right) \delta\left(\omega_2 - \omega + m \frac{2\pi}{T}\right). \tag{18}$$

Substituting Eq. (17) in Eq. (13), we obtain after integration the general expression for the power spectrum of a television signal

$$w(\omega) = \frac{1}{XY} \sum_{m_1} \sum_{m_2} W\left(m_1 \frac{2\pi}{X},\ m_2 \frac{2\pi}{Y},\ \omega - m_1 \frac{2\pi}{T_1} - m_2 \frac{2\pi}{T_2}\right). \tag{19}$$

Similarly, substituting Eq. (18) in Eq. (14), we obtain after integration the general expression for the power spectrum of facsimile or radar signals

$$w(\omega) = \frac{1}{X} \sum_{m} W\left(m \frac{2\pi}{X},\ \omega - m \frac{2\pi}{T}\right). \tag{20}$$

CONCLUSION

As is seen from the derived equations (19) and (20), just as a one-dimensional signal is formed by scanning from three-dimensional (or two-dimensional) information, so also in the spectral domain a one-dimensional power spectrum is formed by sequential exploration of points with different power density from a three-dimensional (or two-dimensional) power spectrum.

The more highly correlated the information, the greater its concentration of energy at low frequencies. The result is that the power spectrum, being the result of multiple, almost periodic probing of this space, acquires a characteristic structure which is almost periodic. Thus, in accordance with Eq. (19), the power spectrum of the television signal acquires maxima at frequencies which are multiples of $2\pi/T_1$ and $2\pi/T_2$ and, in accordance with Eq. (20), the power spectra of facsimile and radar signals acquire maxima at frequencies which are multiples of $2\pi/T$.

REFERENCES

1. N. K. Ignat'yev, Discretization of multivariate information, NDVSh (Radiotekhnika i elektronika), 1958, 1, 63.
2. N. K. Ignat'yev, Frequency spectrum in scanning n-dimensional information, Elektrosvyaz', 1959, 6, 74.

Submitted to editors 26 December 1959

PLANE AND CYLINDRICAL WAVE SCATTERING ON AN ELLIPTICAL CYLINDER AND THE THEORY OF DIFFRACTION RAYS

L. A. Vaynshteyn and A. A. Fedorov

We investigated the diffraction of cylindrical and plane waves on an ideally diffracting elliptical cylinder, the transverse dimensions and radii of curvature of which are large compared with the wavelength. A rigorous solution of this diffraction problem was obtained in the form of a series and a contour integral, which lead to special functions (attenuation coefficients) introduced by V. A. Fok when asymptotic expressions for the radial and angular functions of an elliptic cylinder are substituted. The asymptotic solution obtained in this way corresponds to J. B. Keller's concept of diffraction waves and is easily generalized to cover a convex cylinder of arbitrary shape. This concept thus gains additional justification (when applied to this type of problem) and at the same time it permits a certain generalization; in particular, the formulae derived make it possible to study the transformation of diffraction waves into ordinary waves and vice versa.

INTRODUCTION

The present-day state of development of the theory of diffraction of electromagnetic waves on convex conducting bodies is a result of the basic work done by V. A. Fok, [1-7]. In particular, he introduces (by means of contour integrals) special functions — attenuation coefficients which give the diffraction field for different positions of the source and points of observation. These functions originally related to the semi-shade region. In the illuminated region they become expressions of geometrical optics, and at the same time they can be used in the deep shadow region, as is clear from a consideration of diffraction on a sphere [9, 10] and circular cylinder [11]; however, a generalization of the corresponding formulae for a surface with a variable curvature, is not obvious.

J. B. Keller in Ref. 12 has made this generalization for two-dimensional problems by formulating the concept of diffraction rays which have curvilinear areas lying on the surface of the body and constitute waves which have undergone diffraction in the true sense of the word. According to this concept the total field is equal to the sum of the contributions made by ordinary rays, governed by geometrical optics, and by diffraction rays.

The concept of diffraction rays in its present form cannot be considered either fully substantiated or exhausted. It is rather an outline enabling us to give a physical interpretation and to make a brief formulation of the asymptotic diffraction laws for a definite class of problems. In this article we derive an asymptotic solution for the particular diffraction problem of a convex cylinder with variable surface curvature, and we use it to substantiate and make more precise the concept of diffraction rays. For the convex cylinder we took an elliptical cylinder, limiting ourselves to two-dimensional fields and very simple boundary conditions.

1. GREEN'S FUNCTION G

Let us introduce the elliptical coordinates ξ and η on the plane x, y by the formulae

$$x = f \operatorname{ch}\xi \cos\eta, \quad y = f \operatorname{sh}\xi \sin\eta,$$
$$dx^2 + dy^2 = f^2(\operatorname{ch}^2\xi - \cos^2\eta)(d\xi^2 + d\eta^2) \tag{1}$$

and let us consider the region $\xi > \bar{\xi}$ outside the elliptical cylinder with the semi-axes

$$a = f \operatorname{ch}\bar{\xi}, \quad b = f \operatorname{sh}\bar{\xi} \tag{2}$$

and with the interfocal distance 2f. The wave equation

$$\Delta U + k^2 U = 0 \tag{3}$$

in elliptical coordinates (1) becomes

$$\frac{\partial^2 U}{\partial \xi^2} + \frac{\partial^2 U}{\partial \eta^2} + c^2 (\mathrm{ch}^2 \xi - \cos^2 \eta) U = 0, \quad c = kf, \tag{4}$$

and we are only considering two-dimensional fields which are not a function of the third coordinate z.

Green's Function $G = G(\xi, \eta; \xi', \eta') = G(\xi', \eta'; \xi, \eta)$ is defined to be a function with the following properties.

1. It satisfies Eqs. (3) and (4) everywhere, except at the point ξ', η' at which the source is located ("the luminous line").

2. At the point ξ', η' it has the particular characteristic that the 0 on the right-hand side of (3) is replaced by a two-dimensional delta-function $-4\pi\delta(x-x', y-y')$. Elsewhere,

$$G = \pi i H_0^{(1)} (k\rho) + G^1, \tag{5}$$

where ρ is the distance between the source and the point of observation; $H_0^{(1)}$ is the Hankel function ($\pi i H_0^{(1)} (k\rho) \simeq -2 \ln k\rho$ for $k\rho \ll 1$); G^1 is a finite function.

3. For $\xi \xi \to \infty$ it satisfies the condition of Sommerfeld radiation.

4. On the surface of the elliptical cylinder $\xi = \bar{\xi}$ the function satisfies the boundary condition

$$G = 0 \quad \text{for} \quad \xi = \bar{\xi} \tag{6}$$

or, what amounts to the same thing, the boundary condition

$$\frac{\partial G}{\partial \xi} = 0 \quad \text{for} \quad \xi = \bar{\xi}. \tag{7}$$

5. It is a periodic function η with a period 2π.

We should point out that instead of condition (5) we can use either the continuity of G on the ellipse $\xi = \xi'$ together with the condition

$$\frac{\partial G}{\partial \xi}\Big|_{\xi=\xi'+0} - \frac{\partial G}{\partial \xi}\Big|_{\xi=\xi'-0} = -4\pi\delta(\eta - \eta'), \tag{8}$$

or the continuity of G on the hyperbola $\eta = \eta'$ together with the condition

$$\frac{\partial G}{\partial \eta}\Big|_{\eta=\eta'+0} - \frac{\partial G}{\partial \eta}\Big|_{\eta=\eta'-0} = -4\pi\delta(\xi - \xi'). \tag{9}$$

Particular solutions to Eq. (4) are found by the method of separation of variables. Setting

$$U = R(\xi, \varkappa) S(\eta, \varkappa), \tag{10}$$

we obtain the following equation for the "radial" function R

$$\frac{d^2 R}{d\xi^2} + c^2 (\mathrm{ch}^2 \xi - \varkappa) R = 0, \tag{11}$$

and for the "angular" function S we obtain the equation

$$\frac{d^2 S}{d\eta^2} + c^2 (\varkappa - \cos^2 \eta) S = 0, \tag{12}$$

in which $\varkappa$ is the separation constant. For certain values of $\varkappa$, Eq. (12) has a periodic solution (Mathieu function); using these functions and the solutions of Eq. (11) it is easy to plot an expression for G. However, this expression is only suitable for computation when the transverse dimensions of the cylinder are comparable with $\lambda = 2\pi/k$, or smaller.

When the dimensions of the cylinder are large compared with the wavelength, we have to approach the problem in a different way.

2. PLOTTING THE FUNCTION Γ

Let us use $\Gamma = \Gamma(\xi, \eta, \xi', \eta')$ to designate a function which has the same properties as G, with the exception of property (5), which is replaced by the condition

$$\Gamma(\xi, \eta; \xi', \eta') \to 0 \text{ when } |\eta - \eta'| \to \infty. \tag{13}$$

The function Γ can be called Green's function in an infinite plane, in which the values η, $\eta + 2\pi$, $\eta + 4\pi$ etc. correspond to the various points.

The functions G and Γ are clearly linked by the relationship

$$G(\xi, \eta; \xi', \eta') = \sum_{j=-\infty}^{\infty} \Gamma(\xi, \eta + 2\pi j; \xi', \eta'). \tag{14}$$

As we shall see later, this series converges rapidly, provided the cylinder dimensions exceed the wave length.

Let us plot the function Γ. Let us use R_1 and R_2 to designate the asymptotic solutions of the differential equation (12) as $\xi \to \infty$:

$$R_1 = R_1(\xi, \varkappa) \sim \frac{e^{ic \operatorname{ch} \xi}}{\sqrt{c \operatorname{ch} \xi}},$$
$$R_2 = R_2(\xi, \varkappa) \sim \frac{e^{-ic \operatorname{ch} \xi}}{\sqrt{c \operatorname{ch} \xi}}, \tag{15}$$

where R_1 represents waves propagating toward infinity, while R_2 represents waves propagating from infinity. Let us use S_1 and S_2 to designate the solutions to equation (12) which satisfy the relationships

$$S_1(\eta + 2\pi j, \varkappa) = \tau^{2j} S_1(\eta, \varkappa),$$
$$S_2(\eta - 2\pi j, \varkappa) = \tau^{2j} S_2(\eta, \varkappa), \tag{16}$$

i.e., Floke's theorem which we shall use for complex $\varkappa$ assuming that the parameter $\tau = \tau(\varkappa)$ satisfies the condition $|\tau| < 1$. S_1 will then represent waves which are attenuated as $\eta \to \infty$, and S_2 represents waves which are attenuated as $\eta \to -\infty$.

The function Γ can be expressed in the form s = 1, 2...)

$$\left.\begin{aligned} \Gamma(\xi, \eta; \xi', \eta') &= \Sigma A_s R_1(\xi, \varkappa_s) S_1(\eta, \varkappa_s) S_2(\eta', \varkappa_s) \quad \text{at} \quad \eta > \eta', \\ \Gamma(\xi, \eta; \xi', \eta') &= \Sigma A_s R_1(\xi, \varkappa_s) S_2(\eta, \varkappa_s) S_1(\eta', \varkappa_s) \quad \text{at} \quad \eta < \eta', \end{aligned}\right\} \tag{17}$$

where the A_s are unknown coefficients. The series (17) satisfy the conditions (1) and (3) and also condition (13). The boundary condition (6) is satisfied if

$$R_1(\bar{\xi}, \varkappa_s) = 0 \quad (s = 1, 2, \ldots), \tag{18}$$

and the boundary condition (7) will be satisfied if

$$\frac{\partial R_1}{\partial \xi}(\bar{\xi}, \varkappa_s) = 0 \quad (s = 1, 2, \ldots). \tag{19}$$

In Section 3 we shall see that both Eqs. (18) and (19) lead to complex $\varkappa_s$.

The coefficients A_s are determined from Eq. (9). Let us use $D = D(\varkappa)$ to designate the Wronskian

$$D = \frac{dS_1}{d\eta} S_2 - S_1 \frac{dS_2}{d\eta}, \tag{20}$$

Eq. (9) then takes the form

$$\Sigma A_s D(\varkappa_s) R_1(\xi, \varkappa_s) = -4\pi\delta(\xi - \xi') \text{ when } \bar{\xi} < \xi < \infty. \tag{21}$$

Using the relationship of orthogonality

$$\int_{\bar{\xi}}^{\infty e^{i\varepsilon}} R_1(\xi, \varkappa_s) R_1(\xi, \varkappa_r)\, d\xi = 0 \text{ when } s \neq r, \tag{22}$$

we obtain

$$A_s = -\frac{4\pi}{D(\varkappa_s) N_1(\varkappa_s)} R_1(\xi', \varkappa_s),$$

$$N_1(\varkappa_s) = \int_{\bar{\xi}}^{\infty e^{i\varepsilon}} R_1^2(\xi, \varkappa_s)\, d\xi. \tag{23}$$

Relationship (22) can easily be deduced from the identity

$$\frac{d}{d\xi}\left[\frac{dR_1}{d\xi}(\xi, \varkappa) R_1(\xi, \varkappa') - R_1(\xi, \varkappa)\frac{dR_1}{d\xi}(\xi, \varkappa')\right] + \\ + c^2(\varkappa' - \varkappa) R_1(\xi, \varkappa) R_1(\xi, \varkappa') = 0, \tag{24}$$

if we set $\varkappa = \varkappa_S$, $\varkappa' = \varkappa_r$, and integrate with respect to ξ, using relationship (18) or (19) and choose an $\epsilon > 0$ such that $R_1 \to 0$ as $\xi \to \infty$ $e^{i\epsilon}$. But if we set $\varkappa = \varkappa_S$, integrate and then let $\varkappa' \to \varkappa_S$, we obtain the following expression for the "norm" N_1

$$N_1(\varkappa_s) = \frac{1}{c^2}\frac{\partial R_1}{\partial \xi}(\bar{\xi}, \varkappa_s)\frac{\partial R_1}{\partial \varkappa}(\bar{\xi}, \varkappa_s), \tag{25}$$

if $\varkappa_S$ satisfies Eq. (18), and the expression

$$N_1(\varkappa_s) = -\frac{1}{c^2} R_1(\bar{\xi}, \varkappa_s)\frac{\partial^2 R_1}{\partial \bar{\xi}\, \partial \varkappa}(\bar{\xi}, \varkappa_s), \tag{26}$$

if $\varkappa_S$ is the root of Eq. (19).

The series

$$\Gamma(\xi, \eta; \xi', \eta') = \\ = -4\pi \sum_{s=1}^{\infty} \frac{1}{D(\varkappa_s) N_1(\varkappa_s)} R_1(\xi, \varkappa_s) R_1(\xi', \varkappa_s) \begin{Bmatrix} S_1(\eta, \varkappa_s) S_2(\eta', \varkappa_s) \\ S_2(\eta, \varkappa_s) S_1(\eta', \varkappa_s) \end{Bmatrix}, \tag{27}$$

in which the top line within the braces applies for $\eta > \eta'$, and the bottom line for $\eta < \eta'$, satisfies (at least formally) all of the conditions imposed on the function Γ, and gives the desired solution.

3. ASYMPTOTIC EXPRESSION FOR THE FUNCTION Γ NEAR THE CYLINDER

Formula (27) is accurate and in principle suitable for any value of c and $\bar{\xi}$. Next we shall assume that the least radius of curvature of the ellipse $\xi = \bar{\xi}$ (equal to b^2/a) is large compared with the wavelength:

$$k\frac{b^2}{a} = c\frac{\operatorname{sh}^2 \bar{\xi}}{\operatorname{ch} \bar{\xi}} \gg 1, \tag{28}$$

and, consequently, that all other dimensions and radii of curvature are still larger. Under

this condition we can asymptotically integrate the differential equation (11) using the "standard" equation (compare Ref. 16, Section 3)

$$w''(\varphi) - \varphi w(\varphi) = 0, \tag{29}$$

which is satisfied by the Airy functions $w_1(\varphi)$ and $w_2(\varphi)$. The above-determined radial functions R_1 and R_2 are approximately equal to

$$R_1(\xi, \varkappa) = \sqrt[4]{\frac{-\varphi}{c^2(\mathrm{ch}^2\xi - \varkappa)}}\, w_1(\varphi), \quad R_2(\xi, \varkappa) = \sqrt[4]{\frac{-\varphi}{c^2(\mathrm{ch}^2\xi - \varkappa)}}\, w_2(\varphi). \tag{30}$$

The correspondence between the variables φ and ξ for a real positive value $\varkappa = \mathrm{ch}^2\xi_0 (\xi_0 > 0)$ is established by the formulae

$$\left.\begin{aligned} \frac{2}{3}(-\varphi)^{3/2} &= c\int_{\xi_0}^{\xi} \sqrt{\mathrm{ch}^2\xi - \varkappa}\, d\xi \quad \text{when } \xi > \xi_0 \text{ и } \varphi < 0, \\ \frac{2}{3}\varphi^{3/2} &= c\int_{\xi}^{\xi_0} \sqrt{\varkappa - \mathrm{ch}^2\xi}\, d\xi \quad \text{when } \xi < \xi_0 \text{ и } \varphi > 0. \end{aligned}\right\} \tag{31}$$

If $\varkappa$ is complex, we have to use the method of analytical continuation. Using φ to designate t_s for $\xi = \bar{\xi}$, and $\varkappa = \varkappa_s$, Eq. (18) can be transformed into

$$w_1(t_s) = 0 \quad (s = 1, 2, \ldots), \tag{32}$$

and Eq. (19) into

$$w_1'(t_s) = 0 \quad (s = 1, 2, \ldots). \tag{33}$$

The complex roots $t_s = |t_s|\, e^{i\frac{\pi}{3}}$ have been thoroughly investigated (see Ref. 2, Section 7).

If it is assumed (as confirmed by the expressions in (35)) that $\xi_{0s} \simeq \bar{\xi}$, then the second formula (31) gives

$$\frac{2}{3} t_s^{3/2} = \frac{2}{3} c \sqrt{\mathrm{sh}\, 2\bar{\xi}}\, (\xi_{0s} - \bar{\xi})^{3/2} \qquad (\varkappa_s = \mathrm{ch}^2\xi_{0s}) \tag{34}$$

from which

$$\xi_{0s} = \bar{\xi} + \frac{t_s}{(c^2\, \mathrm{sh}\, 2\bar{\xi})^{1/3}}, \qquad \varkappa_s = \mathrm{ch}^2\bar{\xi} + \left(\frac{\mathrm{sh}\, 2\bar{\xi}}{c}\right)^{2/3} t_s. \tag{35}$$

Knowing $\varkappa_s$, we can find $R_1(\xi, \varkappa_s)$ and $R_2(\xi, \varkappa_s)$ from Eq. (30).

The asymptotic solution of Eq. (12) can be written in simpler form:

$$\left.\begin{aligned} S_1(\eta, \varkappa) &= \frac{1}{\sqrt[4]{c^2(\varkappa - \cos^2\eta)}}\, e^{iQ}, \quad S_2(\eta, \varkappa) = \frac{1}{\sqrt[4]{c^2(\varkappa - \cos^2\eta)}}\, e^{-iQ}, \\ Q &= c\int_{\eta_0}^{\eta} \sqrt{\varkappa - \cos^2\eta}\, d\eta, \end{aligned}\right\} \tag{36}$$

where the lower bound η_0 is arbitrary. For the functions (36) the Wronskian D = 2i.

For $\varkappa = \varkappa_s$ we obtain an approximate expression

$$c\int_{\eta_0}^{\eta} \sqrt{\varkappa_s - \cos^2\eta}\, d\eta = \sigma + t_s x, \tag{37}$$

where σ and χ are equal to:

$$\sigma = c\int_{\eta_0}^{\eta} \sqrt{\operatorname{ch}^2\bar{\xi} - \cos^2\eta}\, d\eta,$$

$$x = \frac{c}{2}\left(\frac{\operatorname{sh} 2\bar{\xi}}{c}\right)^{1/3}\int_{\eta_0}^{\eta} \frac{d\eta}{\sqrt{\operatorname{ch}^2\bar{\xi} - \cos^2\eta}}. \tag{38}$$

Furthermore, replacing $\varkappa$ by $\operatorname{ch}^2\bar{\xi}$ in the coefficients of the exponential forms, we obtain the final expressions for S_1 and S_2:

$$S_1(\eta, \varkappa_s) = \frac{1}{\sqrt[4]{c^2(\operatorname{ch}^2\bar{\xi} - \cos^2\eta)}} e^{i(\sigma + t_s x)},$$

$$S_2(\eta, \varkappa_s) = \frac{1}{\sqrt[4]{c^2(\operatorname{ch}^2\bar{\xi} - \cos^2\eta)}} e^{-i(\sigma + t_s x)}. \tag{39}$$

Let the source and the observation point be near the surface of the cylinder, so that $\xi \simeq \bar{\xi}$ and $\xi' \simeq \bar{\xi}$. Setting

$$y = (c^2 \operatorname{sh} 2\bar{\xi})^{1/3}(\xi - \bar{\xi}),$$
$$y' = (c^2 \operatorname{sh} 2\bar{\xi})^{1/3}(\xi' - \bar{\xi}) \tag{40}$$

and using the approximate expression

$$\varkappa_s - \operatorname{ch}^2\bar{\xi} = \left(\frac{\operatorname{sh} 2\bar{\xi}}{c}\right)^{2/3}(t_s - y) \quad (\varphi = t_s - y \text{ when } \varkappa = \varkappa_s), \tag{41}$$

we obtain the expressions

$$R_1(\xi, \varkappa_s) = (c^2 \operatorname{sh} 2\bar{\xi})^{-1/6} w_1(t_s - y),$$
$$\frac{\partial R_1}{\partial \bar{\xi}}(\xi, \varkappa_s) = -(c^2 \operatorname{sh} 2\bar{\xi})^{1/6} w_1'(t_s - y), \tag{42}$$

so that Eq. (25) is equal to

$$N_1(\varkappa_s) = -(c^2 \operatorname{sh} 2\bar{\xi})^{-2/3}[w_1'(t_s)]^2, \tag{43}$$

and Eq. (26) is equal to

$$N_1(\varkappa_s) = (c^2 \operatorname{sh} 2\bar{\xi})^{-2/3} t_s\, [w(t_s)]^2. \tag{44}$$

Introducing the quantity

$$M(\eta) = \left[\frac{k\rho(\eta)}{2}\right]^{1/3} = \left(\frac{c}{\operatorname{sh} 2\bar{\xi}}\right)^{1/3} \sqrt{\operatorname{ch}^2\bar{\xi} - \cos^2\eta}, \tag{45}$$

in which $\rho(\eta)$ is the radius of curvature of the ellipse $\xi = \bar{\xi}$, we can write the function Γ for the boundary conditions (6) in the form

$$\Gamma(\xi, \eta; \xi', \eta') =$$
$$= \frac{2\pi i}{\sqrt{M(\eta) M(\eta')}} e^{i|\sigma - \sigma'|} \Psi(|x - x'|, y, y', \infty), \tag{46}$$

and for the boundary condition (7) in the form

$$\Gamma(\xi, \eta; \xi', \eta') = \frac{2\pi i}{\sqrt{M(\eta) M(\eta')}} e^{i|\sigma - \sigma'|} \Psi(|x - x'|, y, y', 0). \tag{47}$$

where

$$\left.\begin{aligned}\Psi(x,\ y,\ y',\ \infty) &= -\sum e^{it_s x}\frac{w_1(t_s-y)}{w_1'(t_s)}\frac{w_1(t_s-y')}{w_1'(t_s)},\\ \Psi(x,\ y,\ y',\ 0) &= \sum e^{it_s x}\frac{1}{t_s}\frac{w_1(t_s-y)}{w_1(t_s)}\frac{w_1(t_s-y')}{w_1(t_s)}.\end{aligned}\right\} \tag{48}$$

The contour integral (assuming $y' \geqslant y$)

$$\Psi(x,y,y',\ q) =$$
$$= \frac{1}{4\pi}\int_C e^{itx}w_1(t-y')\left[w_2(t-y) - \frac{w_2'(t)-qw_2(t)}{w_1'(t)-qw_1(t)}w_1(t-y)\right]dt \tag{49}$$

leads to the series (48) for $q = \infty$ and $q = 0$. The contour C encloses all the poles t_s of the integrand in a positive direction, and, calculating the residues, we have to take into account the relationship

$$w_1'(t)\,w_2(t) - w_1(t)\,w_2'(t) = -2i. \tag{50}$$

The properties of the integral in Eq. (49) have been studied in detail. In particular, by using the transform for the function Ψ (cf. Ref. 16, Section 2) we obtain, for $\eta \simeq \eta'$

$$\Gamma(\xi,\ \eta;\ \xi',\ \eta') =$$
$$= \sqrt{\frac{2\pi}{|\sigma-\sigma'|}}\,e^{i\left(|\sigma-\sigma'|+\frac{\pi}{4}\right)}\left[e^{i\frac{(\eta-\eta')^2}{4|x-x'|}} \mp e^{i\frac{(\eta+\eta')^2}{4|x-x'|}}\right], \tag{51}$$

where the negative sign applies for the boundary condition of Eq. (6) and the positive sign for that of Eq. (7). The first term in square brackets determines the primary cylindrical wave, which according to formula (5) is equal to

$$\pi i H_0^{(1)}(k\rho) = \sqrt{\frac{2\pi}{k\rho}}\,e^{i\left(k\rho+\frac{\pi}{4}\right)} \quad \text{when } k\rho \gg 1, \tag{52}$$

while the second term gives the specular reflection of the wave from the cylinder.

4. FUNCTION Γ FAR AWAY FROM THE CYLINDER

Let us go on to study cases in which the coordinate ξ or ξ' is large (a characteristic of radiation when the source is near the cylinder or the diffraction field of a plane wave) or when both coordinates ξ and ξ' are large (scattering characteristic for a plane wave on a cylinder).

The series of Eq. (27) can be transformed into a contour integral for the boundary condition of Eq. (6)

$$\Gamma(\xi,\ \eta;\ \xi',\ \eta') =$$
$$= \frac{ic^2}{2}\int_C R_1(\xi',\varkappa)\left[R_2(\xi,\varkappa) - \frac{R_2(\bar{\xi},\varkappa)}{R_1(\bar{\xi},\varkappa)}R_1(\xi,\varkappa)\right]S_1(\eta,\varkappa)\,S_2(\eta',\varkappa)\,d\varkappa, \tag{53}$$

and into an integral for the boundary condition of Eq. (7)

$$\Gamma(\xi,\ \eta;\ \xi',\ \eta') =$$
$$= \frac{ic^2}{2}\int_C R_1(\xi',\varkappa)\left[R_2(\xi,\varkappa) - \frac{\frac{\partial R_2}{\partial\xi}(\bar{\xi},\varkappa)}{\frac{\partial R_1}{\partial\xi}(\bar{\xi},\varkappa)}R_1(\xi,\varkappa)\right]S_1(\eta,\varkappa)\,S_2(\eta',\varkappa)\,d\varkappa, \tag{54}$$

where the contour C encloses all the poles of $\varkappa_s$ in a positive direction. In these exact

integrals we assume $\xi' \geqslant \xi$ and $\eta \geqslant \eta'$, and that

$$D = \frac{dS_1}{d\eta} S_2 - S_1 \frac{dS_2}{d\eta} = 2i, \quad \frac{dR_1}{d\xi} R_2 - R_1 \frac{dR_2}{d\xi} = 2i. \tag{55}$$

As $\xi' \to \infty$ the function $R_1(\xi', \varkappa)$, by virtue of Eq. (30), takes the form

$$R_1(\xi', \varkappa) = \frac{1}{\sqrt[4]{c^2(\operatorname{ch}^2 \xi' - \varkappa)}} e^{i\left(c\int_{\xi_0}^{\xi'} \sqrt{\operatorname{ch}^2 \xi - \varkappa}\, d\xi + \frac{\pi}{4}\right)} \tag{56}$$

Using the identity

$$\int_{\xi_0}^{\xi'} \sqrt{\operatorname{ch}^2 \xi - \varkappa}\, d\xi = \operatorname{th} \xi' \sqrt{\operatorname{ch}^2 \xi' - \varkappa} - \int_0^{\arccos \frac{\sqrt{\varkappa}}{\operatorname{ch} \xi'}} \sqrt{\varkappa - \cos^2 \eta}\, d\eta, \tag{57}$$

we can rewrite Eq. (56) in a simpler form:

$$R_1(\xi', \varkappa) = \frac{1}{\sqrt{c \operatorname{ch} \xi'}} e^{i\left(c \operatorname{ch} \xi' + \frac{\pi}{4} - Q_0\right)},$$

$$Q_0 = c \int_0^{\frac{\pi}{2}} \sqrt{\varkappa - \cos^2 \eta}\, d\eta \tag{58}$$

and introduce a new function $\Gamma(\xi, \eta; \eta')$ — Green's function for a plane wave — by the formula

$$\Gamma(\xi, \eta; \xi', \eta') = \sqrt{\frac{2\pi}{c \operatorname{ch} \xi'}} e^{i\left(c \operatorname{ch} \xi' + \frac{\pi}{4}\right)} \Gamma(\xi, \eta; \eta') \quad (\xi' \to \infty). \tag{59}$$

Using the approximate formulae

$$\varkappa = \operatorname{ch}^2 \bar{\xi} + \left(\frac{\operatorname{sh} 2\bar{\xi}}{c}\right)^{2/3} t, \quad Q_0 = \sigma_0 + t x_0, \tag{60}$$

where

$$\sigma_0 = c \int_0^{\frac{\pi}{2}} \sqrt{\operatorname{ch}^2 \bar{\xi} - \cos^2 \eta}\, d\eta, \quad x_0 = \frac{c}{2} \left(\frac{\operatorname{sh} 2\bar{\xi}}{c}\right)^{2/3} \int_0^{\frac{\pi}{2}} \frac{d\eta}{\sqrt{\operatorname{ch}^2 \bar{\xi} - \cos^2 \eta}}, \tag{61}$$

and assuming $\xi \simeq \bar{\xi}$, we obtain the expression

$$\Gamma(\xi, \eta; \eta') = \frac{\sqrt{\operatorname{ch} \bar{\xi} \operatorname{sh} \bar{\xi}}}{\sqrt[4]{(\operatorname{ch}^2 \bar{\xi} - \cos^2 \eta)(\operatorname{ch}^2 \bar{\xi} - \cos^2 \eta')}} e^{i(|\sigma - \sigma'| - \sigma_0)} V_1(|x - x'| - x_0, y, q), \tag{62}$$

in which

$$V_1(x, y, q) = \frac{i}{2\sqrt{\pi}} \int_C e^{itx} \left[w_2(t - y) - \frac{w_2'(t) - q w_2(t)}{w_1'(t) - q w_1(t)} w_1(t - y)\right] dt \tag{63}$$

is an "attenuation coefficient" for the plane wave, assuming that q = ∞ for the boundary condition of Eq. (6) and that q = 0 for the boundary condition of Eq. (7).

In order to calculate the scattering characteristic, we have to separate the primary

(incident) wave from the secondary (scattered) wave in the integrals of Eqs. (53) and (54). Let us introduce the function

$$R_0(\xi, \varkappa) = \frac{R_1(\xi, \varkappa) - R_2(\xi, \varkappa)}{2i} \tag{64}$$

and rewrite the integral of Eq. (53) in the form

$$\Gamma(\xi, \eta; \xi', \eta') = c^2 \int_C R_1(\xi', \varkappa) \left[R_0(\xi, \varkappa) - \frac{R_0(\bar{\xi}, \varkappa)}{R_1(\bar{\xi}, \varkappa)} R_1(\xi, \varkappa) \right] S_1(\eta, \varkappa) S_2(\eta', \varkappa) \, d\varkappa. \tag{65}$$

It can be shown that the first term in square brackets is the primary wave, while the secondary wave is equal to

$$\gamma(\xi, \eta; \xi', \eta') = -c^2 \int_C R_1(\xi', \varkappa) R_1(\xi, \varkappa) S_1(\eta, \varkappa) S_2(\eta', \varkappa) \frac{R_0(\bar{\xi}, \varkappa)}{R_1(\bar{\xi}, \varkappa)} d\varkappa. \tag{66}$$

The scattering characteristic $\gamma(\eta, \eta')$ is obtained by the formula

$$\Gamma(\xi, \eta; \xi', \eta') = \frac{1}{c} \sqrt{\frac{2\pi}{c \sqrt{\xi \operatorname{ch} \xi'}}} e^{ic(\operatorname{ch}\xi + \operatorname{ch}\xi') + i\frac{\pi}{4}} \gamma(\eta, \eta') \quad \begin{pmatrix} \xi \to \infty \\ \xi' \to \infty \end{pmatrix} \tag{67}$$

and for the boundary condition of Eq. (6) it is equal to

$$\gamma(\eta, \eta') = -\frac{(c^2 \operatorname{sh}^2 2\bar{\xi})^{3/8}}{c \sqrt{2} \sqrt[4]{(\operatorname{ch}^2 \bar{\xi} - \cos^2 \eta)(\operatorname{ch}^2 \bar{\xi} - \cos^2 \eta')}} e^{i(|\sigma - \sigma'| - 2\sigma_0)} \hat{f}(|x - x'| - 2x_0), \tag{68}$$

where

$$\hat{f}(x) = \frac{e^{i\frac{\pi}{4}}}{\sqrt{\pi}} \int_C e^{itx} \frac{v(t)}{w_1(t)} dt. \tag{69}$$

For the boundary condition of Eq. (7), instead of Eq. (66) we have

$$\gamma(\xi, \eta; \xi', \eta') = -c^2 \int_C R_1(\xi', \varkappa) R_1(\xi, \varkappa) S_1(\eta, \varkappa) S_2(\eta', \varkappa) \frac{\frac{\partial R_0}{\partial \xi}(\bar{\xi}, \varkappa)}{\frac{\partial R_1}{\partial \xi}(\bar{\xi}, \varkappa)} d\varkappa, \tag{70}$$

so that

$$\gamma(\eta, \eta') = -\frac{(c^2 \operatorname{sh} 2\bar{\xi})^{3/8}}{c \sqrt{2} \sqrt[4]{(\operatorname{ch}^2 \bar{\xi} - \cos^2 \eta)(\operatorname{ch}^2 \bar{\xi} - \cos^2 \eta')}} e^{i(|\sigma - \sigma'| - 2\sigma_0)} \hat{g}(|x - x'| - 2x_0), \tag{71}$$

where

$$\hat{g}(x) = \frac{e^{i\frac{\pi}{4}}}{\sqrt{\pi}} \int_C e^{itx} \frac{v'(t)}{w_1'(t)} dt. \tag{72}$$

As will be shown later, the results of this section have to be made more precise if the functions $\Gamma(\xi, \eta, \eta')$ or $\gamma(\eta, \eta')$ correspond to waves approaching the point of observation according to the normal laws of geometrical optics (without diffraction). The original series of Eq. (27) after substitution of Eqs. (58) then diverges, but the contour integrals converge and make it possible to study the transition of the diffraction laws to those of geometrical optics.

5. MORE DETAILED STUDY OF GREEN'S FUNCTION FOR A PLANE WAVE

Let us first ascertain the physical meaning of Eq. (62). Let us determine the angles η'_1 and η'_2 by the relationships

$$\sin\eta'_\nu = \epsilon_\nu \frac{\operatorname{sh}\bar{\xi}\cos\eta'}{\sqrt{\operatorname{ch}^2\bar{\xi}-\cos^2\eta'}},$$

$$\cos\eta'_\nu = -\epsilon_\nu \frac{\operatorname{ch}\bar{\xi}\sin\eta'}{\sqrt{\operatorname{ch}^2\bar{\xi}-\cos^2\eta'}},$$

$$\sqrt{\operatorname{ch}^2\bar{\xi}-\cos^2\eta'} = \frac{\operatorname{ch}\bar{\xi}\operatorname{sh}\bar{\xi}}{\sqrt{\operatorname{ch}^2\bar{\xi}-\cos^2\eta'}}, \tag{73}$$

in which $\epsilon_1 = 1$ and $\epsilon_2 = -1$. As can easily be shown η'_1 and η'_2 are the coordinates of the points of contact between the ellipse and straight lines drawn to a point at infinity (see Fig. 1). Using the theorem of addition for elliptic integrals ([13], p. 315), we can prove the following identities:

$$\left.\begin{aligned} x'+x_0 &= x'_1, \quad \sigma'+\sigma_0 = \sigma'_1 - c\frac{\cos\eta'_1\cos\eta'}{\operatorname{ch}\bar{\xi}},\\ x'-x_0 &= x'_2, \quad \sigma'-\sigma_0 = \sigma'_2 - c\frac{\cos\eta'_2\cos\eta'}{\operatorname{ch}\bar{\xi}}, \end{aligned}\right\} \tag{74}$$

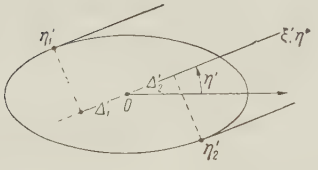

Fig. 1. Points of contact η'_1 and η'_2 on cylinder (in given case $\Delta'_1 < 0$ and $\Delta'_2 > 0$).

in which x'_ν and σ'_ν are the values of x and σ at $\eta = \eta'_\nu$. These identities can be directly checked at $\bar{\xi} \to \infty$, when the ellipse changes to a circle, and also at $\eta' = 0, \pm\pi/2, \pm\pi, \ldots$. They are only valid for certain values of η'_1 and η'_2 and when η'_ν is replaced by $\eta'_\nu + 2\pi j$, they become more complex. We obtain

$$\left.\begin{aligned} |x-x'|-x_0 &= x-x'_1, \quad |\sigma-\sigma'|-\sigma_0 = \sigma-\sigma'_1-k\Delta'_1 \quad \text{when } \eta>\eta',\\ |x-x'|-x_0 &= x'_2-x, \quad |\sigma-\sigma'|-\sigma_0 = \sigma'_2-\sigma-k\Delta'_2 \quad \text{when } \eta<\eta', \end{aligned}\right\} \tag{75}$$

in which the term (see Fig. 1)

$$-k\Delta'_\nu = -c(\operatorname{ch}\bar{\xi}\cos\eta'_\nu\cos\eta' + \operatorname{sh}\bar{\xi}\sin\eta'_\nu\sin\eta') = -c\frac{\cos\eta'_\nu\cos\eta'}{\operatorname{ch}\bar{\xi}} \tag{76}$$

determines the phase of the plane wave at the points of contact, while the term $\epsilon_\nu(\sigma-\sigma'_\nu)$, is proportional to the length of the arc of the ellipse from the point of contact η'_ν to the observation point, and determines the phase shift of the wave on the curvilinear section of the diffraction ray. The attenuation coefficient V_1 in Eq. (69) depends on the agrument of $\epsilon_\nu(x-x'_\nu)$ and determines the attenuation and phase shift of the diffraction ray on its curvilinear part. Equation (62) can finally be written in the form

$$\Gamma(\xi,\eta;\eta') = \sqrt{\frac{M(\eta'_\nu)}{M(\eta)}}\, e^{i[\epsilon_\nu(\sigma-\sigma'_\nu)-k\Delta'_\nu]}\, V_1(\epsilon_\nu(x-x'_\nu), y, q). \tag{77}$$

If the boundary condition is Eq. (6) it is advisable to introduce the function

$$\Gamma_\alpha(\eta, \eta') = \frac{\partial \Gamma}{\partial \bar{\xi}}(\bar{\xi}, \eta; \eta') = \\ = (c^2 \operatorname{sh} 2\bar{\xi})^{1/3} \sqrt{\frac{M(\eta'_\nu)}{M(\eta)}}\, e^{i[\epsilon_\nu(\sigma-\sigma'_\nu)-k\Delta'_\nu]} f(\epsilon_\nu(x-x'_\nu)), \tag{78}$$

in which

$$f(x) = \frac{1}{\sqrt{\pi}} \int_C \frac{e^{itx}\, dt}{w_1(t)}, \tag{79}$$

and if it is the boundary condition of Eq. (7) we introduce the function

$$\Gamma_\beta(\eta, \eta') = \Gamma(\bar{\xi}, \eta; \eta') = \sqrt{\frac{M(\eta'_\nu)}{M(\eta)}}\, e^{i[\epsilon_\nu(\sigma-\sigma'_\nu)-k\Delta'_\nu]} g(\epsilon_\nu(x-x'_\nu)), \tag{80}$$

where

$$g(x) = \frac{1}{\sqrt{\pi}} \int_C \frac{e^{itx}\, dt}{w'_1(t)}. \tag{81}$$

Using these formulae, it is assumed that $\nu = 1$ for $\eta > \eta'$ and $\nu = 2$ for $\eta < \eta'$. For $\eta - \eta'_1 > 2\pi m$ ($m = 1, 2, \ldots$) the formulae give a diffraction ray which has gone around the cylinder in a positive direction not less than m times, and for $\eta'_2 - \eta > 2\pi m$ they give a ray which has done the same in a negative direction. The contribution made by these rays, as a rule, is negligible, since the argument of $\epsilon_\nu(x - x'_\nu)$ for them exceeds $4mx_0$, and according to Eqs. (61) and (28) we have

$$x_0 > \frac{\pi}{2}\left(\frac{c}{2}\frac{\operatorname{sh}^2\bar{\xi}}{\operatorname{ch}\bar{\xi}}\right)^{1/3}, \tag{82}$$

i.e., the magnitude of x_0 is at least equal to three or four.

The highest value is shown by rays for which the argument $\epsilon_\nu(x - x'_\nu)$ is small or else negative. If the argument is large and negative, Eqs. (77), (78) and (80) do not represent a diffraction ray, but a pair of rays (direct ray and reflected ray from the cylinder) conforming to geometrical optics; in this case they need clarification, which, for the sake of simplicity we will only do in the case of Γ_α and Γ_β; by virtue of Eqs. (53), (54) and (58) these can be written in the following form for $\eta > \eta'$

$$\left.\begin{aligned} \Gamma_\alpha(\eta, \eta') &= \frac{c^2}{\sqrt{2\pi}} \int e^{-iQ_0} \frac{S_1(\eta, \varkappa)\, S_2(\eta', \varkappa)}{R_1(\bar{\xi}, \varkappa)}\, d\varkappa = \\ &= \frac{ce^{-i\frac{\pi}{4}}}{\sqrt{2\pi}} \int \frac{\sqrt[4]{c^2(\operatorname{ch}^2\bar{\xi} - \varkappa)}\, e^{i\omega(\varkappa)}\, d\varkappa}{\sqrt[4]{(\varkappa - \cos^2\eta)(\varkappa - \cos^2\eta')}}, \\ \Gamma_\beta(\eta, \eta') &= -\frac{c^2}{\sqrt{2\pi}} \int e^{-iQ_0} \frac{S_1(\eta, \varkappa)\, S_2(\eta', \varkappa)}{\frac{\partial R_1}{\partial \bar{\xi}}(\bar{\xi}, \varkappa)}\, d\varkappa = \\ &= \frac{ce^{i\frac{\pi}{4}}}{\sqrt{2\pi}} \int \frac{e^{i\omega(\varkappa)}\, d\varkappa}{\sqrt[4]{c^2(\operatorname{ch}^2\bar{\xi} - \varkappa)(\varkappa - \cos^2\eta)(\varkappa - \cos^2\eta')}}, \end{aligned}\right\} \tag{83}$$

in which the phase $\omega(\varkappa)$ is equal to

$$\omega(\varkappa) = c\int_{\eta'}^{\eta} \sqrt{\varkappa - \cos^2\eta}\, d\eta - c\int_{\bar{\xi}_0}^{\bar{\xi}} \sqrt{\operatorname{ch}^2\xi - \varkappa}\, d\xi - c\int_0^{\frac{\pi}{2}} \sqrt{\varkappa - \cos^2\eta}\, d\eta. \tag{84}$$

Since $\eta < \eta'$, η and η' have to change places in Eq. (84), and we can rewrite the equation $\omega'(\varkappa) = 0$ in the form

$$\epsilon_\nu\left[F\left(k, \frac{\pi}{2} - \eta'\right) - F\left(k, \frac{\pi}{2} - \eta\right)\right] + \\ + F\left(k, \frac{\pi}{2} + i\bar{\xi}_0\right) - F\left(k, \frac{\pi}{2} + i\bar{\xi}\right) - F\left(k, \frac{\pi}{2}\right) = 0, \tag{85}$$

in which $F(k, \varphi)$ is an elliptic integral of the first kind and, $k = 1/\sqrt{\varkappa}$. Applying the theorem for the addition of elliptic integrals three times, we obtain the following equation for a stationary phase point

$$\epsilon_\nu \frac{\sin\eta\cos\eta'\sqrt{\varkappa - \cos^2\eta} - \cos\eta\sin\eta'\sqrt{\varkappa - \cos^2\eta'}}{\varkappa - \cos^2\eta\cos^2\eta'} = \frac{1}{\operatorname{ch}\bar{\xi}}. \tag{86}$$

We need the $\varkappa_0$ root of this equation and it is equal to

$$\left.\begin{aligned} \varkappa_0 &= \operatorname{ch}^2\bar{\xi} - (\operatorname{sh}\bar{\xi}\cos\eta\cos\eta' + \operatorname{ch}\bar{\xi}\sin\eta\sin\eta')^2, \\ \sqrt{\operatorname{ch}^2\bar{\xi} - \varkappa_0} &= \operatorname{sh}\bar{\xi}\cos\eta\cos\eta' + \operatorname{ch}\bar{\xi}\sin\eta\sin\eta'. \end{aligned}\right\} \tag{87}$$

The following operations are valid provided the right-hand side of the last relationship is positive and not too small; it becomes zero at $\eta = \eta'_1$ and $\eta = \eta'_2$. After some rather cumbersome transformations we obtain

$$\left.\begin{aligned} \omega_0 &= \omega(\varkappa_0) = -c(\operatorname{ch}\bar{\xi}\cos\eta\cos\eta' + \operatorname{sh}\bar{\xi}\sin\eta\sin\eta'), \\ \omega''(\varkappa_0) &= -\frac{c}{4}\frac{i1}{\sqrt{(\operatorname{ch}^2\bar{\xi} - \varkappa_0)(\varkappa_0 - \cos^2\eta)(\varkappa_0 - \cos^2\eta')}}, \end{aligned}\right\} \tag{88}$$

and the stationary phase method yields expressions

$$\Gamma_\alpha(\eta, \eta') = 2i\frac{\partial\omega_0}{\partial\bar{\xi}}e^{i\omega_0}, \quad \Gamma_\beta(\eta, \eta') = 2e^{i\omega_0}, \tag{89}$$

corresponding to geometrical optics and approaching Eqs. (78) and (80) for $\eta \simeq \eta'_\nu$ and large negative values of $\epsilon_\nu(x - x'_\nu)$, when the asymptotic relationships

$$f(\zeta) = 2i\zeta e^{-\frac{i}{3}\zeta^3}, \quad g(\zeta) = 2e^{-\frac{i}{3}\zeta^3} \quad (\zeta \to -\infty). \tag{90}$$

6. SCATTERING CHARACTERISTIC

At the end of Section 4 we found expressions for the scattering characteristic $\gamma(\eta, \eta')$. The conclusion given should be supplemented, that is to say, it should be proved that the first term in the integral of Eq. (65) gives the first wave $\pi i H_0^{(1)}(k\rho)$, and, moreover, we should derive an expression for $\gamma(\eta, \eta')$ for the case in which it represents an ordinary ray. Here we will use a slightly different method based on the following formula

$$G = \pi i H_0^{(1)}(k\rho) + \frac{i}{4}\oint\left[G\frac{\partial H_0^{(1)}(kr)}{\partial n} - H_0^{(1)}(kr)\frac{\partial G}{\partial n}\right]dl, \tag{91}$$

which expresses Green's function G at any point in terms of the primary wave and in terms of the function G and its derivative with respect to the outer normal $\partial G/\partial n$ at the boundary ellipse $\xi = \bar{\xi}$; r is the distance between the point $\bar{\xi}$, $\bar{\eta}$ on the ellipse and the point of observation ξ, η. Under the boundary condition (6) we have

$$\gamma(\eta, \eta') = -\frac{e^{i\frac{\pi}{4}}}{2\sqrt{2\pi}}\int\Gamma_\alpha(\bar{\eta}, \eta')e^{i\psi}d\bar{\eta}, \tag{92}$$

and under the boundary condition (7) we have

$$\gamma(\eta, \eta') = -\frac{e^{-i\frac{\pi}{4}}}{2\sqrt{2\pi}} \int \Gamma_\beta(\bar{\eta}, \eta') \frac{\partial \psi}{\partial \bar{\xi}} e^{i\psi} d\bar{\eta}, \tag{93}$$

where

$$\psi = -c(\operatorname{ch}\bar{\xi}\cos\bar{\eta}\cos\eta + \operatorname{sh}\bar{\xi}\sin\bar{\eta}\sin\eta). \tag{94}$$

If Eqs. (78) and (80) are used for the functions Γ_α and Γ_β near the stationary phase point ($\bar{\eta} \simeq \eta_\nu$), the integrals of Eqs. (92) and (93) can be calculated by the more precise stationary phase method (see Ref. 11); in this case the "rapidly varying" phase of the integrand is equal to

$$\omega(\bar{\eta}) = \epsilon_\nu(\bar{\sigma} - \sigma'_\nu) + \psi. \tag{95}$$

The roots of η_1 and η_2 of the equation $\omega'(\bar{\eta}) = 0$ are determined by the relationships

$$\sin\eta_\nu = -\epsilon_\nu \frac{\operatorname{sh}\bar{\xi}\cos\eta}{\sqrt{\operatorname{ch}^2\bar{\xi} - \cos^2\eta}}, \quad \cos\eta_\nu = \epsilon_\nu \frac{\operatorname{ch}\bar{\xi}\sin\eta}{\sqrt{\operatorname{ch}^2\bar{\xi} - \cos^2\eta}},$$
$$\sqrt{\operatorname{ch}^2\bar{\xi} - \cos^2\eta_\nu} = \frac{\operatorname{ch}\bar{\xi}\operatorname{sh}\bar{\xi}}{\sqrt{\operatorname{ch}^2\bar{\xi} - \cos^2\eta}}. \tag{96}$$

The expansion of the function of Eq. (95) for $\bar{\eta} \simeq \eta_\nu$ takes the form

$$\left.\begin{aligned} \omega(\bar{\eta}) &= \omega(\eta_\nu) + \frac{\epsilon_\nu}{3} s^3, \quad s = \bar{x} - x_\nu, \\ \omega(\eta_\nu) &= \epsilon_\nu(\sigma_\nu - \sigma'_\nu) - c\frac{\cos\eta_\nu\cos\eta}{\operatorname{ch}\bar{\xi}} = \epsilon_\nu(\sigma_\nu - \sigma'_\nu) - k\Delta_\nu, \end{aligned}\right\} \tag{97}$$

the meaning of Δ_ν being the same as that of Δ'_ν (see Figs. 1 and 2).

Taking the coefficients $\sqrt{\frac{M(\eta'_\nu)}{M(\eta)}}$ and $\partial\psi/\partial\bar{\xi}$ outside the integral sign (for $\bar{\eta} = \eta_\nu$) and using the integral expressions (79) and (81) together with the relationship

$$v(t) = \frac{1}{2\sqrt{\pi}} \int_{-\infty}^{\infty} e^{i\epsilon_\nu\left(ts + \frac{1}{3}s^3\right)} ds, \tag{98}$$

we obtain the following equations

$$\gamma(\eta, \eta') = -\sqrt{2M(\eta_\nu)M(\eta'_\nu)}\, e^{i\epsilon_\nu(\sigma_\nu - \sigma'_\nu) - ik(\Delta_\nu + \Delta'_\nu)} \hat{f}(\epsilon_\nu(x_\nu - x'_\nu)) \tag{99}$$

and

$$\gamma(\eta, \eta') = -\sqrt{2M(\eta_\nu)M(\eta'_\nu)}\, e^{i\epsilon_\nu(\sigma_\nu - \sigma'_\nu) - ik(\Delta_\nu + \Delta'_\nu)} \hat{g}(\epsilon_\nu(x_\nu - x'_\nu)), \tag{100}$$

equivalent to Eqs. (68) and (71), respectively.

Equations (99) and (100) show that the scattered field is formed in the following way: rays coming from the source η' at infinity are tangent to the cylinder at points η'_1 and η'_2 and give rise to diffraction rays 1 and 2, where ray 1 circles the cylinder in the positive direction ($\epsilon_1 = 1$) and ray 2 does the same in a negative direction ($\epsilon_2 = -1$). Ray 1 may reach the observation point η at infinity, by merely leaving the cylinder at point η_1 and ray 2 may do the same by leaving the cylinder at point η_2 (Fig. 2), and in the process they may circle the cylinder any number of times before being separated.

If the argument $\epsilon_\nu(x_\nu - x'_\nu)$ is negative, the function $\gamma(\eta, \eta')$ does not give the diffraction,

but an ordinary ray which is governed by geometrical optics; if the ray grazes the surface (at a small and finite $|x_\nu - x'_\nu|$), the geometrical optics approach requires a more accurate representation by means of Eqs. (99) and (100). In other cases expressions (89) have to be substituted into Eqs. (92) and (93), and the rapidly varying phase will be equal to

$$\omega(\bar{\eta}) = -c\,[\mathrm{ch}\,\bar{\xi}\cos\bar{\eta}\,(\cos\eta + \cos\eta') + \mathrm{sh}\,\bar{\xi}\sin\bar{\eta}\,(\sin\eta + \sin\eta')]. \tag{101}$$

The stationary point η_0 is determined by the relationships

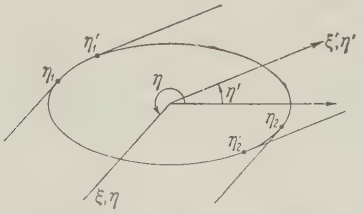

Fig. 2. Points of contact η'_1, η'_2, η_1 and η_2.

$$\cos\frac{\eta+\eta'}{2} = \frac{\mathrm{sh}\,\bar{\xi}\cos\eta_0}{\sqrt{\mathrm{ch}^2\bar{\xi} - \cos^2\eta_0}},$$

$$\sin\frac{\eta+\eta'}{2} = \frac{\mathrm{ch}\,\bar{\xi}\sin\eta_0}{\sqrt{\mathrm{ch}^2\bar{\xi} - \cos^2\eta_0}},$$

$$\sqrt{\mathrm{ch}^2\bar{\xi} - \cos^2\eta_0} = \frac{\mathrm{ch}\bar{\xi}\,\mathrm{sh}\,\bar{\xi}}{\sqrt{\mathrm{ch}^2\bar{\xi} - \sin^2\dfrac{\eta+\eta'}{2}}}, \tag{102}$$

while $\omega''(\eta_0) = -\omega(\eta_0) \neq 0$. The usual stationary phase method reduces to the equation

$$\gamma(\eta, \eta') = \mp\sqrt{\frac{k\upsilon(\eta_0)}{2}\cos\frac{\eta-\eta'}{2}}\,e^{i\omega(\eta_0)} = \mp\,[M(\eta_0)]^{1/2}\sqrt{\cos\frac{\eta-\eta'}{2}}\,e^{i\omega(\eta_0)}, \tag{103}$$

which corresponds to geometrical optics (compare Eq. (51)) and is close to Eqs. (99) and (100), since for large negative arguments, ζ, the functions $\hat{f}(\zeta)$ and $\hat{g}(\zeta)$ are approximately equal:

$$\hat{f}(\zeta) = \frac{\sqrt{-\zeta}}{2}e^{-\frac{i}{12}\zeta^3}, \quad \hat{g}(\zeta) = -\frac{\sqrt{-\zeta}}{2}e^{-\frac{i}{12}\zeta^3} \tag{104}$$

CONCLUSION

The principal results of this research can easily be generalized to cover a convex cylinder of arbitrary shape (oval, parabolic, hyperbolic, and so on). If the observation point and the source lie close to the surface of the cylinder, Eqs. (46) and (47) are applicable in them $M(\eta)$ is related to the radius of curvature of the cylinder $\rho(\eta)$ by

$$M(\eta) = \left[\frac{k\rho(\eta)}{2}\right]^{1/3}, \tag{105}$$

and σ, x, y and y' are obviously equal to

$$\sigma = k\int dl, \quad x = \frac{k}{2}\int\frac{dl}{M^2(\eta)}, \quad y = \frac{kh}{M(\eta)}, \quad y' = \frac{kh'}{M(\eta')}, \tag{106}$$

where dl is the element of the arc of the boundary contour, and h' and h are the shortest distance from the observation point and source to the surface of the cylinder (we are again designating the coordinates of the observation point by ξ, η and the coordinates of the source by ξ',η'). If one of the points tends to infinity ($\xi' \to \infty$), the corresponding coordinate η' loses its conventional meaning and becomes a polar angle, while Green's function takes the form

$$\Gamma(\xi, \eta; \xi', \eta') = \sqrt{\frac{2\pi}{kr'}}\,e^{i\left(kr' + \frac{\pi}{4}\right)}\Gamma(\xi, \eta; \eta'), \tag{107}$$

in which r' is the radius vector. The formula applicable to the function $\Gamma(\xi, \eta; \eta')$ is Eq. (77), which for large negative $\epsilon_\nu(x - x'_\nu)$ must be supplemented by the laws of geometrical optics (see Ref. 8). For functions (78) and (80) these laws assume the form of

Eq. (89), in which ω_0 is the phase of the plane wave on the surface of a cylinder.

If both points are removed to infinity ($\xi \to \infty$, $\xi' \to \infty$), then it is of interest to note the scattering characteristic $\gamma(\eta, \eta')$ as determined by the relationship,

$$\gamma(\xi, \eta; \eta') = \frac{e^{ikr}}{\sqrt{kr}}\gamma(\eta, \eta'), \tag{108}$$

in which $\gamma(\xi, \eta; \eta')$ is the "secondary" part of the function $\Gamma(\xi, \eta; \eta')$, i.e., the waves scattered by the cylinder, and r, η are the polar coordinates of the observation point. The scattering characteristic $\gamma(\eta, \eta')$ for an arbitrary convex cylinder is calculated from Eqs. (99), (100) and (103).

We should recall that each function Γ or γ corresponds to either a diffraction on an ordinary ray (or else a pair of ordinary rays) and Green's function, according to Eq. (14), is equal to the sum of the contributions of all the rays, with diffraction rays circling the cylinder more than once usually making a negligible contribution.

The limits of applicability of these asymptotic formulas can be estimated using the numerical results obtained earlier for a sphere [9, 10] and a circular cylinder [11]. Specifically, the scattering characteristics as given by these formulas are certainly valid for $k\rho_{min} > 5$, while the functions Γ_α and Γ_β are certainly valid for $k\rho_{min} > 10$, where ρ_{min} is the minimum radius of curvature of the cylinder.

We should point out that direct plotting of a series analogous to the series of Eq. (27) has been done before for other problems (see, for example, Ref. 14). But transformation of a series into a contour integral makes the method more flexible and effective. In particular the contour integrals (49), (63), (69), (72), (79) and (81) introduced by V. A. Fok and tabulated in [15] give the transformation of the diffraction rays into ordinary ones, and vice versa. Thus we have obtained a more complete solution than J. B. Keller [12] who limited himself to the residue series (diverging for $x < 0$).

This method can be applied to the asymptotic solutions of all diffraction problems (both electrodynamic as well as acoustic) which can be treated by the method of separation of variables.

REFERENCES

1. V. A. Fok, ZhETF, 1945, 15, 12, 693.
2. V. A. Fok, Diffraction of radio waves around earth's surface, Izd. AN SSSR, 1946.
3. V. A. Fok, Izv. AN SSSR, phys. ser., 1946, 10, 2, 171.
4. M. Leontovich, V.A. Fok, ZhETF, 1946, 16, 7, 557.
5. V. A. Fok, ZhETF, 1949, 19, 10, 916.
6. V. A. Fok, Advances in physical sciences, 1948, 36, 3, 308.
7. V. A. Fok, Advances in physical sciences, 1950, 43, 4, 587.
8. V. A. Fok, ZhETF, 1950, 20, 11, 961.
9. M. G. Belkina, L. A. Vaynshteyn. Coll. artic. "Diffraction of electromagnetic waves on certain bodies of rotation," Soviet Radio Press, 1957, pp. 57-125.
10. A. A. Fedorov, Radio Engineering and Electronics, 1958, 3, 12, 1451.
11. A. S. Goryainov, Radio Engineering and Electronics, 1958, 3, 5, 603 (see also Reports of Acad. Sci. USSR, 1956, 109, 3, 417).
12. J. B. Keller, IRE Trans., 1956, AP-4, 3, 312.
13. A. Erdelyi, W. Magnus, F. Oberhettinger, F. G. Tricomi, Higher transcendental functions, Bateman manuscript project, McGraw-Hill, 2, 1953.
14. A. Sommerfeld, Partial differential equations in Physics, For. Lit. Press, 1950, pp. 298-312.
15. P. A. Azrilyant, M. G. Belkina, Numerical results of theory of diffraction of radio waves around earth's surface, Soviet Radio Press, 1957.
16. V. A. Fok, Radio Engineering and electronics, 1956, 1, 5, 560.

Received by editors on May 3, 1960.

DIFFRACTION OF A PLANE ELECTROMAGNETIC WAVE PROPAGATING ALONG THE AXIS OF A CONE

A. S. Goryainov

This article gives the rigorous solution of the problem of the diffraction of a plane electromagnetic wave on an infinite conducting cone in the case in which the wave spreads along the axis of the cone. In the region where the scattered field takes the form of a spherical wave, formulas are derived for numerical calculation of the scattering characteristics, and the results of the calculation are given. Formulas are obtained for the functions of the correction field due to the narrowing of the surface at the apex of the cone. The graphs given for these functions make it possible to evaluate the part played by the point of the conde in diffraction of electromagnetic waves.

INTRODUCTION

During the diffraction of electromagnetic waves on a finite conical surface, the diffraction field can be considered to be composite and to consist of a field defined by the laws of physical optics and a correction field determined by additional currents near the edge and the apex of the cone. The physical optics field is defined as the field created by a current whose density is expressed in terms of the magnetic intensity vector $\vec{H}$ of the incident wave by the known relationship

$$\vec{j} = \frac{c}{2\pi} [\vec{n}\vec{H}] \qquad (1)$$

($\vec{n}$ is the external normal to the surface). Near the apex of the cone, the current defined by Eq. (1) is supplemented by the current whose origin is linked with the sharp convergence of the surface at the apex. This additional current is concentrated mainly near the apex, and the correction field created by it in a finite and infinite cone is therefore identical, provided $l \sin\gamma \gg \lambda$, where l is the length of the generator of the finite cone; λ is the wave length, and the angle γ is shown in Fig. 1. In this case the correction field caused by the apex can be defined as the difference between the field obtained when the problem of an infinite cone is rigorously solved, and the field obtained for it by the laws of physical optics. In view of the concentration of the additional current, the correction field will appear as a spherical wave at great distances from the apex of the cone.

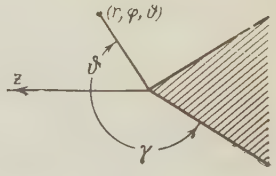

Fig. 1

This article considers the exact solution of the diffraction of a plane electromagnetic wave on an infinite cone with a flare $2(\pi-\gamma) < \pi$ in the case in which the plane wave is propagated along the axis of the cone. In the region $0 \leqslant \vartheta < 2\gamma-\pi$, where the scattered field takes the form of a spherical wave, formulas are derived for numerical calculation of the scattering characteristics, and the results of calculations are given. Functions are also obtained for the calculation of terms in the scattering characteristics corresponding to the correction field, and graphs are given for these functions in the same region $0 \leqslant \vartheta < 2\gamma-\pi$.

Thus, the article basically studies the effect of the apex of the cone on the diffraction field. Diffraction at the edges of a finite cone can be calculated on the basis of the results given in Ref. 1.

1. EXACT SOLUTION

In studying the diffraction of electromagnetic waves on an ideally conducting infinite cone in free space, we will use the Debye potentials, (u, v), through which the components of the electromagnetic field in a spherical system of coordinates (r, φ, ϑ) are determined from the equations

$$
\begin{aligned}
E_r &= \left(\frac{\partial^2}{\partial r^2} + k^2\right)(ru),\\
E_\vartheta &= \frac{1}{r}\frac{\partial^2}{\partial r\,\partial\vartheta}(ru) + \frac{ik}{\sin\vartheta}\frac{\partial v}{\partial\varphi},\\
E_\varphi &= \frac{1}{r\sin\vartheta}\frac{\partial^2}{\partial r\,\partial\varphi}(ru) - ik\frac{\partial v}{\partial\vartheta},\\
H_r &= \left(\frac{\partial^2}{\partial r^2} + k^2\right)(rv),\\
H_\vartheta &= -\frac{ik}{\sin\vartheta}\frac{\partial u}{\partial\varphi} + \frac{1}{r}\frac{\partial^2}{\partial r\,\partial\vartheta}(rv),\\
H_\varphi &= ik\frac{\partial u}{\partial\vartheta} + \frac{1}{r\sin\vartheta}\frac{\partial^2}{\partial r\,\partial\varphi}(rv),
\end{aligned}
\tag{2}
$$

where k is the wave number in free space. The Debye potentials are the solution of the wave equation

$$
\Delta u + k^2 u = 0, \quad \Delta v + k^2 v = 0; \tag{3}
$$

the presence of the cone $\vartheta = \gamma$, $\pi/2 < \gamma < \pi$ (Fig. 1) is taken into account by the boundary condition

$$
E_r = E_\varphi = 0 \text{ when } \vartheta = \gamma.
$$

When the plane electromagnetic wave is incident along the negative axis z

$$
E_x^0 = -H_y^0 = e^{-ikz}
$$

(the time factor $e^{-i\omega t}$ is omitted here and from now on) the total diffraction field has the potentials

$$
\left.
\begin{aligned}
u &= -\frac{\pi\cos\varphi}{ik^2 r}\sum_{n=1}^{\infty}\frac{(2\nu_n+1)\,e^{-i\frac{\pi\nu_n}{2}}}{\nu_n(\nu_n+1)\sin\pi\nu_n}\,\frac{P^1_{\nu_n}(-\cos\gamma)}{\frac{\partial}{\partial\nu_n}P^1_{\nu_n}(\cos\gamma)}\,P^1_{\nu_n}(\cos\vartheta)\,\psi_{\nu_n}(kr),\\
v &= \frac{\pi\sin\varphi}{ik^2 r}\sum_{n=1}^{\infty}\frac{(2\mu_n+1)\,e^{-i\frac{\pi\mu_n}{2}}}{\mu_n(\mu_n+1)\sin\pi\mu_n}\,\frac{\frac{d}{d\gamma}P^1_{\mu_n}(-\cos\gamma)}{\frac{\partial^2}{\partial\mu_n\partial\gamma}P^1_{\mu_n}(\cos\gamma)}\,P^1_{\mu_n}(\cos\vartheta)\,\psi_{\mu_n}(kr),
\end{aligned}
\right\}
\tag{4}
$$

where $P^1_\nu(\cos x)$ is the associated Legendre function; $\psi_\nu(x)$ is the spherical Bessel function related to the normal Bessel function by the following

$$
\psi_\nu(x) = \sqrt{\frac{\pi x}{2}}\,J_{\nu+\frac{1}{2}}(x);
$$

the numbers ν_n and μ_n are the eignevalues of the boundary problem and are determined from the equations

$$
P^1_{\nu_n}(\cos\gamma) = 0, \quad \frac{d}{d\gamma}P^1_{\mu_n}(\cos\gamma) = 0.
$$

The solution of Eq. (4) is exact, and it satisfies all known requirements; the method of obtaining it is given in Ref. 2. The series in Eq. (4) contain the usual inherent defects of exact solutions of diffraction problems: slow convergence at large values of the parameter kr, difficulty in finding the eigenvalues, the impossibility of physical interpretation of the solution, and the presence of untabulated functions. Hence, we will transform the series in Eq. (4) into contour integrals for further analysis, using the method of residues:

$$u = \frac{\cos\varphi}{2k^2r}\int\limits_{D_1} \frac{(2\nu+1)}{\nu(\nu+1)} \frac{e^{-i\frac{\pi\nu}{2}}}{\sin\pi\nu} \frac{P^1_\nu(-\cos\gamma)}{P^1_\nu(\cos\gamma)} P^1_\nu(\cos\vartheta)\,\psi_\nu(kr)\,d\nu,$$

$$v = -\frac{\sin\varphi}{2k^2r}\int\limits_{D_2} \frac{(2\nu+1)}{\nu(\nu+1)} \frac{e^{-i\frac{\pi\nu}{2}}}{\sin\pi\nu} \frac{\frac{d}{d\gamma}P^1_\nu(-\cos\gamma)}{\frac{d}{d\gamma}P^1_\nu(\cos\gamma)} P^1_\nu(\cos\vartheta)\,\psi_\nu(kr)\,d\nu.$$

The contour D_1 (or D_2) encloses the zero functions $P^1_\nu(\cos\gamma)$ (or $\frac{d}{d\gamma}P^1_\nu(\cos\gamma)$), excluding the points $\nu = 0$. Let us draw the contours C, C_1 and L as shown in Fig. 2. Let us replace the integration along D_1 (or D_2) by integration above the contours C_1 and C (contour L encloses the zeros in $\sin\pi\nu$, beginning at $\nu = 1$), after which in the integral above C_1 we replace ν by $\nu - \frac{1}{2}$, and represent the integrals along L by a series of residues, then

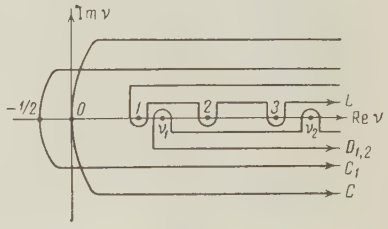

Fig. 2

$$u = u_1 + u_0, \quad v = v_1 + v_0,$$

in which

$$u_1 = -\frac{e^{i\frac{\pi}{4}}\cos\varphi}{k^2r}\int\limits_C \nu e^{-i\frac{\pi\nu}{2}} P_1(\nu)\,\psi_{\nu-\frac{1}{2}}(kr)\,d\nu - \\ - i\cos\varphi\,\mathrm{ctg}^2\frac{\gamma}{2}\,\mathrm{tg}\frac{\vartheta}{2}\frac{\sin kr}{k^2r};$$

$$v_1 = \frac{e^{i\frac{\pi}{4}}\sin\varphi}{k^2r}\int\limits_C \nu e^{-i\frac{\pi\nu}{2}} P_2(\nu)\,\psi_{\nu-\frac{1}{2}}(kr)\,d\nu - \\ - i\sin\varphi\,\mathrm{ctg}^2\frac{\gamma}{2}\,\mathrm{tg}\frac{\vartheta}{2}\frac{\sin kr}{k^2r};$$

$$u_0 = -\frac{i\cos\varphi}{k^2r}\sum_{n=1}^{\infty}\frac{2n+1}{n(n+1)}\,i^n\,\frac{P^1_n(-\cos\gamma)}{P^1_n(\cos\gamma)}\,P^1_n(\cos\vartheta)\,\psi_n(kr);$$

$$v_0 = \frac{i\sin\varphi}{k^2r}\sum_{n=1}^{\infty}\frac{2n+1}{n(n+1)}\,i^n\,\frac{\frac{d}{d\gamma}P^1_n(-\cos\gamma)}{\frac{d}{d\gamma}P^1_n(\cos\gamma)}\,P^1_n(\cos\vartheta)\,\psi_n(kr);$$

$$P_1(\nu) = \frac{P^1_{\nu-\frac{1}{2}}(-\cos\gamma)\,P^1_{\nu-\frac{1}{2}}(\cos\vartheta)}{P^1_{\nu-\frac{1}{2}}(\cos\gamma)\left(\nu^2-\frac{1}{4}\right)\cos\pi\nu};$$

$$P_2(\nu) = \frac{\frac{d}{d\gamma}P^1_{\nu-\frac{1}{2}}(-\cos\gamma)\,P^1_{\nu-\frac{1}{2}}(\cos\vartheta)}{\frac{d}{d\gamma}P^1_{\nu-\frac{1}{2}}(\cos\gamma)\left(\nu^2-\frac{1}{4}\right)\cos\pi\nu}.$$

(5)

The second terms in Eq. (5) give the residues at the point $\nu = 0$ when going from the contours $D_{1,2}$ to the contour C_1. Using the formula

$$\sum_{n=1}^{\infty}\frac{2n+1}{n(n+1)}(-i)^n\,P^1{}_n(\cos\vartheta)\,\psi_n(kr) = \\ = \frac{i}{\sin\vartheta}(\cos kr - i\cos\vartheta\sin kr - e^{-ikr\cos\vartheta}) \qquad (6)$$

and the relationship for integral n

$$P^1_n(-x) = (-1)^{n-1}P^1_n(x),$$

we obtain

$$u_0 = -\frac{\cos\varphi}{\sin\vartheta\, k^2 r}(\cos kr - i\cos\vartheta\sin kr - e^{-ikr\cos\vartheta}),$$
$$v_0 = \frac{\sin\varphi}{\sin\vartheta\, k^2 r}(\cos kr - i\cos\vartheta\sin kr - e^{-ikr\cos\vartheta}).$$

By substituting u_0 and v_0 into Eq. (2) we can see that the potentials (u_0, v_0) gives the incident wave field.

In this way, the transformation of the series of Eq. (4) into integrals has immediately made it possible to divide the potentials of the total diffraction field (u, v) into incident wave potentials (u_0, v_0) and secondary (scattered) field potentials (u_1, v_1). The integral representation of the potentials of Eq. (5) also makes it possible to obtain a diffraction field in the wave zone for the region $\vartheta < 2\gamma - \pi$ in the form of a spherical wave. Indeed, on account of the asymptotic behavior of the associated Legendre function and the spherical Bessel function

$$\left.\begin{aligned} P^1_{\nu-\frac{1}{2}}(\cos\vartheta) &= \sqrt{\frac{2\nu}{\pi\sin\vartheta}}\cos\left(\nu\vartheta + \frac{\pi}{4}\right) + O(\nu^{-1/2}),\\ \psi_{\nu-\frac{1}{2}}(x) &= \frac{\sqrt{x}}{2}e^{\nu+\nu\ln\frac{x}{2}-\left(\nu+\frac{1}{2}\right)\ln\nu},\\ |\nu| &\gg 1,\ |\arg\nu| \leqslant \pi-\varepsilon,\ \varepsilon>0 \end{aligned}\right\} \qquad (7)$$

and in Eq. (5) the integration along the contour C can be replaced by integration along the imaginary axis. Next, using the property of even numbers in the Legendre functions with respect to the variable ν, as well as by the relationship

$$e^{-i\frac{\pi\nu}{2}}\psi_{\nu-\frac{1}{2}}(x) = \frac{1}{2}\left[e^{-i\frac{\pi\nu}{2}}\psi_{\nu-\frac{1}{2}}(x) + e^{i\frac{\pi\nu}{2}}\psi_{-\nu-\frac{1}{2}}(x)\right] -$$
$$-\frac{i}{2}e^{i\frac{\pi\nu}{2}}\sin\pi\nu\,\zeta_{\nu-\frac{1}{2}}(x),$$

in which $\zeta_\nu(x)$ is a spherical Hankel function determined by means of the normal Hankel function by the equality

$$\zeta_\nu(x) = \sqrt{\frac{\pi x}{2}}H^{(1)}_{\nu+\frac{1}{2}}(x),$$

we obtain

$$\left.\begin{aligned} u_1 &= -\frac{e^{i\frac{\pi}{4}}\cos\varphi}{k^2 r}\int_0^\infty \nu e^{-\frac{\pi\nu}{2}}\operatorname{sh}\pi\nu P_1(i\nu)\,\zeta_{i\nu-\frac{1}{2}}(kr)\,d\nu -\\ &\quad - i\cos\varphi\operatorname{ctg}^2\frac{\gamma}{2}\operatorname{tg}\frac{\vartheta}{2}\frac{\sin kr}{k^2 r},\\ v_1 &= \frac{e^{i\frac{\pi}{4}}\sin\varphi}{k^2 r}\int_0^\infty \nu e^{-\frac{\pi\nu}{2}}\operatorname{sh}\pi\nu P_2(i\nu)\,\zeta_{i\nu-\frac{1}{2}}(kr)\,d\nu -\\ &\quad - i\sin\varphi\operatorname{ctg}^2\frac{\gamma}{2}\operatorname{tg}\frac{\vartheta}{2}\frac{\sin kr}{k^2 r}. \end{aligned}\right\} \qquad (8)$$

For $kr \gg \nu_0$, where ν_0 is the smallest value of the variable, for which we can omit the integration in Eq. (8), the spherical Hankel function can be replaced by its asymptotic representation

$$\zeta_{i\nu-\frac{1}{2}}(kr) = e^{i\left(kr - \frac{i\pi\nu}{2} - \frac{\pi}{4}\right)}.$$

Using Eq. (2) the components of the electromagnetic diffraction field in the wave zone for the region $\vartheta < 2\gamma - \pi$ can now be written in the form

$$E_r^1 = H_\vartheta^1 = 0,\ E_\nu^1 = H_\varphi^1 = \cos\varphi L_1^1(\vartheta, \gamma)\frac{e^{ikr}}{ikr},$$

$$E_\varphi^1 = -H_\vartheta^1 = -\sin\varphi L_2^1(\vartheta, \gamma)\frac{e^{ikr}}{ikr},$$

in which

$$\left.\begin{aligned} L_1^1(\vartheta, \gamma) &= \frac{d}{d\vartheta}\int_0^\infty \nu \operatorname{sh}\pi\nu P_1(i\nu)\,d\nu - \frac{1}{\sin\vartheta}\int_0^\infty \nu \operatorname{sh}\pi\nu P_2(i\nu)\,d\nu + \frac{\operatorname{ctg}^2\frac{\gamma}{2}}{2\cos^2\frac{\vartheta}{2}}, \\ L_2^1(\vartheta, \gamma) &= \frac{1}{\sin\vartheta}\int_0^\infty \nu \operatorname{sh}\pi\nu P_1(i\nu)\,d\nu - \frac{d}{d\vartheta}\int_0^\infty \nu \operatorname{sh}\pi\nu P_2(i\nu)\,d\nu - \frac{\operatorname{ctg}^2\frac{\gamma}{2}}{2\cos^2\frac{\vartheta}{2}}. \end{aligned}\right\} \quad (9)$$

In the wave zone at $\vartheta = 2\gamma - \pi$ (the direction of the specular reflection) the spherical wave develops into a conical wave spreading in the region $\vartheta > 2\gamma - \pi$. This is expressed by the fact that at $\vartheta \geqslant 2\gamma - \pi$ the integrals in Eq. (9) diverge.

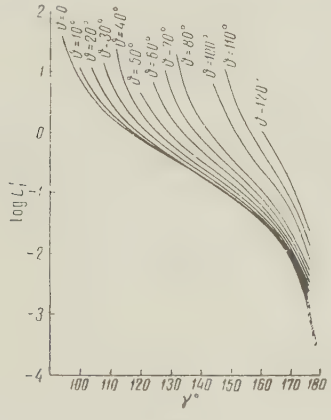

Fig. 3

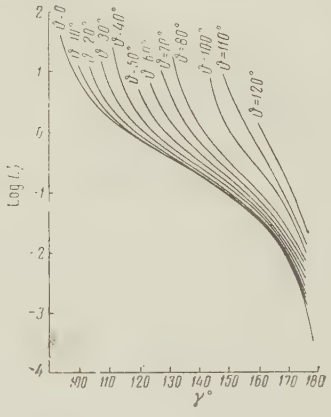

Fig. 4

The functions $L_{1,2}^1(\vartheta, \gamma)$ can be determined the scattering characteristics of the plane wave on the cone. They are positive, real and increase monotonically as $\vartheta \to 2\gamma - \pi$, They were calculated with a Strela (Arrow) electronic computer for $0 \leqslant \vartheta \leqslant 2\gamma - \pi - 2°$, $96° \leqslant \gamma \leqslant 178°$; $\Delta\vartheta = 2°$, $\Delta\gamma = 2°$. About forty hours of computing time were required for these calculations. The results for some parameters are given in Figs. 3 and 4.

Equations (9) for narrow-angle ($\gamma \leqslant \pi$) and wide angle ($\gamma \geqslant \pi/2$) cones at $\vartheta = 0$ can be simplified by using approximate formulas in the first case

$$P^1_{i\nu-\frac{1}{2}}(\cos\gamma) = -\frac{1}{\pi}\operatorname{tg}\frac{\gamma}{2}\operatorname{ch}\pi\nu,\ P^1_{i\nu-\frac{1}{2}}(-\cos\gamma) = -\frac{1}{2}\left(\nu^2 + \frac{1}{4}\right)\sin\gamma,$$

and by using the first formula in (7) for the second case. For narrow-angle cones the scattering characteristics are approximately equal to

$$L^1_{1,2}(\vartheta, \gamma) = \left(\frac{\pi - \gamma}{2}\right)^2,$$

and for wide angle cones they are

$$L^1_{1,2}(\vartheta, \gamma) = \frac{1}{(2\gamma - \pi)^2}.$$

These results agree with those given in Ref. 3, and also with the results of physical optics.

2. THE FIELD ACCORDING TO THE LAWS OF PHYSICAL OPTICS

The physical optics potentials u_p, v_p (the subscript p is used to designate values pertaining to the physical optics solution) satisfying Eqs. (3) will be sought in the form

$$\left.\begin{aligned} u_p &= \frac{\cos\varphi}{r}\int_{C_2} F(\nu)\,\psi_{\nu-\frac{1}{2}}(kr)\begin{Bmatrix} P^1_{\nu-\frac{1}{2}}(\cos\vartheta)\,P^1_{\nu-\frac{1}{2}}(-\cos\gamma) \\ P^1_{\nu-\frac{1}{2}}(-\cos\vartheta)\,P^1_{\nu-\frac{1}{2}}(\cos\gamma) \end{Bmatrix} d\nu, \\ v_p &= \frac{\sin\varphi}{r}\int_{C_2} G(\nu)\,\psi_{\nu-\frac{1}{2}}(kr)\begin{Bmatrix} P^1_{\nu-\frac{1}{2}}(\cos\vartheta)\,\frac{d}{d\gamma}P^1_{\nu-\frac{1}{2}}(-\cos\gamma) \\ P^1_{\nu-\frac{1}{2}}(-\cos\vartheta)\,\frac{d}{d\gamma}P^1_{\nu-\frac{1}{2}}(\cos\gamma) \end{Bmatrix} d\nu, \end{aligned}\right\} \qquad (10)$$

in which the top line in the braces should be taken for $\vartheta < \gamma$, and the bottom line for $\vartheta > \gamma$. The contour C_2 is shown in Fig. 5. The boundary conditions follow from Eq. (1) and can be written as

$$\left.\begin{aligned} H^p_r\big|_{\vartheta=\gamma-0} - H^p_r\big|_{\vartheta=\gamma+0} &= 2H^0_r, \\ H^p_\varphi\big|_{\vartheta=-\gamma-0} - H^p_\varphi\big|_{\vartheta=\gamma+0} &= 2H^0_\varphi, \end{aligned}\right\}$$

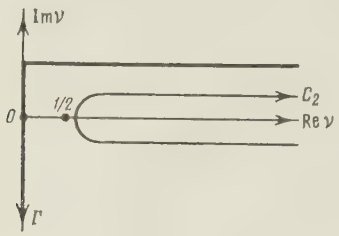

Fig. 5.

in which the components of the magnetic intensity vector of the incident wave are

$$\left.\begin{aligned} H^0_r &= -\sin\varphi\sin\gamma e^{-ikr\cos\gamma} \\ H^0_\varphi &= -\cos\varphi e^{-ikr\cos\gamma}. \end{aligned}\right\}$$

Using Eqs. (2) these boundary conditions and the expressions for the Wronskian

$$P^1_{\nu-\frac{1}{2}}(\cos\gamma)\frac{d}{d\gamma}P^1_{\nu-\frac{1}{2}}(-\cos\gamma) - \frac{d}{d\gamma}P^1_{\nu-\frac{1}{2}}(\cos\gamma)\,P^1_{\nu-\frac{1}{2}}(-\cos\gamma) = \frac{2}{\pi\sin\gamma}\left(\nu^2-\frac{1}{4}\right)\cos\pi\nu \qquad (11)$$

can be reduced to the form

$$\left.\begin{aligned} &\frac{1}{\pi r^2\sin^2\gamma}\int_C G(\nu)\left(\nu^2-\frac{1}{4}\right)^2\psi_{\nu-\frac{1}{2}}(kr)\cos\pi\nu d\nu = -e^{-ikr\cos\gamma}, \\ &\frac{ik}{\pi r\sin\gamma}\int_{C_2} F(\nu)\left(\nu^2-\frac{1}{4}\right)\psi_{\nu-\frac{1}{2}}(kr)\cos\pi\nu d\nu - \frac{k}{\pi r\sin^2\gamma}\int_{C_2} G(\nu)\left(\nu^2-\frac{1}{4}\right)\times \\ &\qquad\times\frac{d}{d(kr)}\psi_{\nu-\frac{1}{2}}(kr)\cos\pi\nu\,d\nu = e^{-ikr\cos\gamma}. \end{aligned}\right\} \qquad (12)$$

To determine the functions $G(\nu)$ let us multiply the first equation in (12) by $\xi_{\mu-\frac{1}{2}}(kr)$ in which $\mathrm{Re}\,\nu > \mathrm{Re}\,\mu$) and integrate with respect to r from 0 to ∞, and then we obtain

$$ik\int_{C_2} G(\nu)\left(\nu^2-\frac{1}{4}\right)^2\cos\pi\nu\,\frac{e^{i(\nu-\mu)\frac{\pi}{2}}}{\nu^2-\mu^2}\,d\nu = \pi\sin^2\gamma\int_0^\infty e^{-ikr\cos\gamma}\,\zeta_{\mu-\frac{1}{2}}(kr)\,dr. \qquad (13)$$

Here we have changed the order of integration and used the relation

$$\int_0^\infty \zeta_{\mu-\frac{1}{2}}(kr)\,\psi_{\nu-\frac{1}{2}}(kr)\,\frac{dr}{r^2} = -\frac{ik}{\nu^2-\mu^2}\,e^{i(\nu-\mu)\frac{\pi}{2}},\quad \operatorname{Re}\nu > \operatorname{Re}\mu.$$

From now on in the calculation of the function $G(\nu)$ from Eq. (13) we will follow the method set forth in detail in Ref. 4; as a result we obtain

$$G(\nu) = -\frac{\sin^2\gamma}{k}\,\frac{\nu}{\left(\nu^2-\frac{1}{4}\right)^2\cos\pi\nu}\int_0^\infty e^{-ikr\cos\gamma}\,\zeta_{\nu-\frac{1}{2}}(kr)\,dr. \tag{14}$$

When finding the function $F(\nu)$ we use the fact that

$$\left(\frac{d^2}{dr^2}+k^2\right)\psi_\nu(kr) = \frac{\nu(\nu+1)}{r^2}\,\psi_\nu(kr).$$

Applying the operator $\left(\frac{d^2}{dr^2}+k^2\right)$ to the left-hand and right-hand sides of the second equation in (12) and using Eq. (14), we obtain

$$\frac{1}{r^2}\int_{C_z} F(\nu)\left(\nu^2-\frac{1}{4}\right)^2\psi_{\nu-\frac{1}{2}}(kr)\cos\pi\nu\,d\nu = -\pi\sin\gamma\,(\cos\gamma + ikr\sin^2\gamma)\,e^{-ikr\cos\gamma}.$$

Using the same method as in solving Eq. (13), we obtain

$$F(\nu) = -\frac{\nu}{\left(\nu^2-\frac{1}{4}\right)^2\cos\pi\nu}\left[i\sin^3\gamma\int_0^\infty e^{-ikr\cos\gamma}\,\zeta_{\nu-\frac{1}{2}}(kr)\,r\,dr + \frac{\cos\gamma\sin\gamma}{k}\int_0^\infty e^{-iks\gamma}\,\zeta_{\nu-\frac{1}{2}}(kr)\,dr\right]. \tag{15}$$

The integrals on the right-hand side of Eqs. (14) and (15) can be calculated using the relation

$$\left.\begin{aligned}\int_0^\infty e^{-ikr\cos\gamma}\,r^q\,\zeta_{\nu-\frac{1}{2}}(kr)\,dr &= \frac{\pi e^{-i\frac{\pi}{4}}}{(ik\sin\gamma)^{q+1}}\,\frac{e^{-i\frac{\pi\nu}{2}}}{\cos\pi\nu}\,P^{(q+1)}_{\nu-\frac{1}{2}}(-\cos\gamma),\\ \operatorname{Re}\left(q+\frac{3}{2}\pm\nu\right) &> 0,\ \operatorname{Im}k>0.\end{aligned}\right\} \tag{16}$$

This relation may be obtained by expressing the integral in terms of a hypergeometric function, which is one of the representations of the associated Legendre function (see Ref. 5).

Let us replace the right-hand sides in Eqs. (14) and (15) on the basis of Eq. (16) and substitute $G(\nu)$ and $F(\nu)$, into Eq. (10), and we will then obtain integral representations for the physical optics potentials; in the region $\vartheta < \gamma$ we will have

$$\frac{u_p}{\cos\varphi} = \frac{v_p}{\sin\varphi} = \frac{\pi e^{i\frac{\pi}{4}}\sin\gamma}{k^2 r}\int_{C_z}\frac{\nu e^{-i\frac{\pi\nu}{2}}}{\left(\nu^2-\frac{1}{4}\right)^2\cos^2\pi\nu}\,P_{\nu-\frac{1}{2}}(-\cos\gamma)\times \times\frac{d}{d\gamma}P^1_{\nu-\frac{1}{2}}(-\cos\gamma)\,P^1_{\nu-\frac{1}{2}}(\cos\vartheta)\,\psi_{\nu-\frac{1}{2}}(kr)\,d\nu. \tag{17}$$

To check whether or not the solution is correct, let us substitute the functions $G(\nu)$ and $F(\nu)$ given by Eqs. (14) and (15), having first substituted Eq. (16), into Eq. (12). The integrals obtained thereby will then be represented by a series of residues. Next, using Eq. (6) we can see that the substitution makes Eqs. (12) into identities.

We have thus obtained an integral representation of the potentials in accordance with physical optics; it is similar to the integral representation of potentials in the exact solution; both solutions are plotted by means of associated Legendre functions and spherical Bessel functions, and the integration contours enclose the positive part of the real axis. This fact makes it possible to represent the correction field potentials in the wave zone fairly simply in the form of a spherical wave spreading from the apex of the cone.

As was pointed out earlier, we calculated the characteristics of $L_{1,2}(\vartheta, \gamma)$ for the wave zone in the region $\vartheta < 2\gamma - \pi$, hence there is no need in this region to make any particular calculations of the correction field. All we need do is derive simple results for physical optics for $kr \gg 1$ and $\vartheta < 2\gamma - \pi$. These results may be derived by setting up an expression for the vector potential using the current determined by Eq. (1). The transformations arising in the process are elementary; the final expressions take the form of

$$E_r^p = H_r^p = 0,\ E_\vartheta^p = H_\varphi^p = \cos\varphi L(\vartheta, \gamma)\frac{e^{ikr}}{ikr},\ E_\varphi^p = -H_\vartheta^p = \\ = -\sin\varphi L(\vartheta, \gamma)\frac{e^{ikr}}{ikr},$$

$$kr \gg 1,\ 0 \leqslant \vartheta < 2\gamma - \pi,$$

in which

$$L(\vartheta, \gamma) = \left| \frac{\sin^2\gamma\cos\gamma}{4\cos\frac{\vartheta}{2}\left[\cos\left(\gamma - \frac{\vartheta}{2}\right)\cos\left(\gamma + \frac{\vartheta}{2}\right)\right]^{1/2}} \right|; \qquad (18)$$

In particular at $\vartheta = 0$, we obtain the well-known equations

$$E_\vartheta^p = H_\varphi^p = \frac{1}{4}\sin\varphi\,\mathrm{tg}^2\gamma\frac{e^{ikr}}{ikr},$$

$$E_\varphi^p = -H_\vartheta^p = -\frac{1}{4}\cos\varphi\,\mathrm{tg}^2\gamma\frac{e^{ikr}}{ikr}.$$

The numerical values of the scattering characteristics of $L_{1,2}(\vartheta, \gamma)$ from Eqs. (9) together with the simple equation (18) solve the problem of the accuracy of physical optics in the region in which the scattered field takes the form of a spherical wave ($kr \gg 1$, $\vartheta < 2\gamma - \pi$), and also makes it possible to determine the correction wave in this region numerically.

3. THE CORRECTION FIELD

By definition, the potentials of the correction field (u_q, v_q) are determined in the form

$$u_q = u_1 - u_p,\ v_q = v_1 - v_p.$$

Let us substitute into this equation the earlier derived exact solution potentials (5) and the physical optics potentials (17), and let us reduce the contour C_2 in the latter to the contour C temporarily; then using the Wronskian from Eq. (11) we obtain

$$u_q = -\frac{e^{i\frac{\pi}{4}}}{k^2 r}\cos\varphi\, I_1(\vartheta, r, \gamma),\ v_q = -\frac{e^{i\frac{\pi}{4}}}{k^2 r}\sin\varphi\, I_2(\vartheta, r, \gamma),$$

in which

$$I_{1,2}(\vartheta, r, \gamma) = \int_C \nu e^{-i\frac{\pi\nu}{2}} P_{1,2}(\nu) f(\nu) \psi_{\nu-\frac{1}{2}}(kr)\, d\nu;$$

$$f(\nu) = -\frac{\pi}{2} \frac{\sin\gamma}{\left(\nu^2 - \frac{1}{4}\right)\cos\pi\nu} \frac{d}{d\gamma}\left[P^1_{\nu-\frac{1}{2}}(\cos\gamma) P^1_{\nu-\frac{1}{2}}(-\cos\gamma)\right].$$

Let us show that for all values of ϑ in the wave zone u_q and v_q are spherical wave potentials. To do this we will represent the integrals $I_{1,2}(\vartheta, r, \gamma)$ in the form

$$\left.\begin{aligned} I_{1,2}(\vartheta, r, \gamma) = \int_C \nu e^{-i\frac{\pi\nu}{2}} P_{1,2}(\nu)\,[f(\nu) - F(\nu)]\,\psi_{\nu-\frac{1}{2}}(kr)\, d\nu + \\ + \int_C \nu e^{-i\frac{\pi\nu}{2}} P_{1,2}(\nu)\, F(\nu)\, \psi_{\nu-\frac{1}{2}}(kr)\, d\nu, \\ F(\nu) = \frac{\sin[(2\gamma - \pi)\nu]}{\cos\pi\nu}. \end{aligned}\right\} \tag{19}$$

With the aid of the first of Eqs. (7) it is easy to see that at $|\nu| \gg 1$, $|\arg\nu| \leqslant \pi - \epsilon$, $\epsilon > 0$ we have

$$f(\nu) = F(\nu) + O(\nu^{-1}),$$

and the module of the functions $\nu e^{-i\frac{\pi\nu}{2}} P_{1,2}(\nu)[f(\nu) - F(\nu)]$ decrease as $\nu^{-3/2}$. This fact makes it possible to replace the spherical Bessel function for the wave zone in the first integral of the right-hand side of Eq. (19) by its asymptotic expression

$$\psi_{\nu-\frac{1}{2}}(kr) = \cos\left(kr - \frac{\pi\nu}{2} - \frac{\pi}{4}\right). \tag{20}$$

In the second integral in Eq. (19) we will replace the integration along C by integration along the imaginary axis, which is possible on account of the asymptotic formula (7). Then repeating the same arguments as for transformation of Eq. (8), we replace the spherical Bessel function in this integral by Eq. (20) and obtain

$$\begin{aligned} I_{1,2}(\vartheta, r, \gamma) = \frac{e^{-i\frac{\pi}{4}}}{2} e^{ikr} \int_C \nu e^{-i\pi\nu} P_{1,2}(\nu)\,[f(\nu) - F(\nu)]\, d\nu + \\ + \frac{e^{i\frac{\pi}{4}}}{2} e^{-ikr} \int_C \nu P_{1,2}(\nu)\,[f(\nu) - F(\nu)]\, d\nu + \\ + \frac{e^{i\frac{\pi}{4}}}{2} e^{-ikr} \int_{i\infty}^{-i\infty} \nu P_{1,2}(\nu) F(\nu)\, d\nu + \frac{e^{-i\frac{\pi}{4}}}{2} e^{ikr} \int_{i\infty}^{-i\infty} \nu e^{-i\pi\nu} P_{1,2}(\nu) F(\nu)\, d\nu. \end{aligned}$$

If we now replace C in the second integral on the right-hand side by the imaginary axis, the terms with the coefficient e^{-ikr} disappear because the functions $P_{1,2}(\nu)$ and $F(\nu)$ are even. We finally obtain

$$\begin{aligned} u_q = -\frac{\cos\varphi}{2k^2 r} e^{ikr} \left\{ \int_C \nu e^{-i\pi\nu} P_1(\nu)\,[f(\nu) - F(\nu)]\, d\nu - \right. \\ \left. - 2\int_0^{i\infty} \nu\cos\pi\nu\, P_1(\nu)\, F(\nu)\, d\nu \right\}, \end{aligned}$$

$$v_q = -\frac{\sin\varphi}{2k^2r}e^{ikr}\left\{\int_C \nu e^{-i\pi\nu}P_2(\nu)[f(\nu)-F(\nu)]\,d\nu - \right.$$
$$\left. -2\int_0^{i\infty}\nu\cos\pi\nu P_2(\nu)\,F(\nu)\,d\nu\right\}. \qquad (21)$$

In these expressions the contour C may be replaced by the contour Γ, shown in Fig. 5. The integrals in Eq. (21) converge for the entire range of the parameter ϑ. The numerical calculation of the non-uniform component of the field using Eq. (21) has not been made,

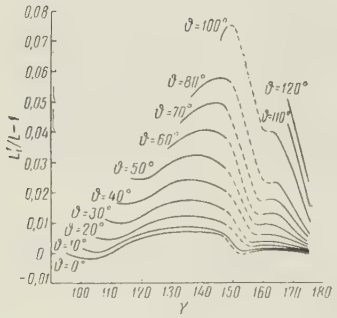

Fig. 6

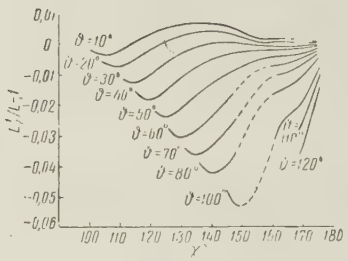

Fig. 7

but we have calculated the functions $L^q_{1,2}(\vartheta, \gamma)$ corresponding to the correction field for the region $\vartheta < 2\gamma - \pi$. They are determined from the equation

$$L^q_{1,2}(\vartheta,\gamma) = L^1_{1,2}(\vartheta,\gamma) - L(\vartheta,\gamma).$$

Graphs showing the functions $\frac{L^q_{1,2}}{L} = \frac{L^1_{1,2}}{L}$ — for certain values of ϑ and γ are given in Figs. 6 and 7.

Comparison of the results shown in Figs. 3, 4 and 6 and 7 suggest that the physical optics field is close to the true field at $\vartheta \simeq 0$; when ϑ increases over the range $0 \leqslant \vartheta < 2\gamma - \pi$, the functions $L^q_{1,2}(\vartheta, \gamma)$ increase monotonically and provide a correction of the order of 10%, which shows the part played by the correction field in diffraction on a finite body with an apex. In Figs. 6 and 7 the graphical interpolation areas are shown with dotted lines. At $\vartheta \simeq 0$ the non-uniform component can obviously be ignored.

In conclusion I would like to express my appreciation to L. A. Vaynshteyn who was in charge of the project.

REFERENCES

1. P. Ya. Ufimtsev. Approximate calculation of diffraction of plane electromagnetic waves on certain metallic bodies. ZhTF, 1957, 27, 8, 1840.
2. L. A. Vaynshtayn. Electromagnetic waves. Sov. Radio Press, 1957.
3. L. B. Felsen, Backscattering from wide-angle and narrow-angle cones, J. Appl. Phys., 1955, 26, 2, 138.
4. M. I. Kontorovich and N. N. Lebedev. One method of solving certain problems of diffraction and allied topics. ZhETF, 1938, 8, 10-11, 1192.
5. A. Erdelyi, W. Magnus, F. Oberhettinger, F. G. Tricomi, Higher Transcendental Functions, 2, McGraw-Hill, 1953, p. 50, 124.

Received by the editors 14 May 1960

INCIDENCE OF A PLANE ELECTROMAGNETIC WAVE ON A PLANE GRID (CASE IN WHICH THE H VECTOR IS PARALLEL TO THE WIRES)

A. N. Sivov

A solution is found for the electrodynamic problem of finding the coefficients of reflection and transmission when a plane wave strikes a plane grid at an angle in a case in which the H vector is parallel to the wires of the grid. The grid spacing is taken as small compared with the wavelength. The shape of the wire and the dielectric filler, which is different, generally speaking, on different sides of the grid, have been taken into account. The equations derived allow, in particular, a limiting process when the wires are brought together to an unlimited extent. The fields near the wires are also found. Equivalent boundary conditions are also derived for a grid and for a system consisting of a grid and a solid metal screen.

1. FORMULATION OF THE PROBLEM. INTRODUCTION

An electromagnetic wave, in which the magnetic field vector is oriented parallel to the wires, strikes a plane infinite grid formed by parallel wires obliquely. The space is filled with a homogeneous dielectric but, generally speaking, the dielectric is different on each side of the grid. On the assumption that the grid spacing is small compared with the wavelength, we have to find the transmitted and reflected fields. The solution of this problem is undertaken to investigate the attenuation and phase characteristics of waves in periodic waveguides, taking into account the period, geometry of the wire and dielectric.

Let us introduce the rectangular system of coordinates x, ξ, y) related to the grid in the following way: the axis ox is perpendicular to the wires and lies in the plane of the grid, oξ is directed along the wires and passes through the center of the section of one of them, oy coincides with the normal to the grid plane.

The space above (y > 0) and below (y < 0) the grid is filled with homogeneous dielectrics with dielectric constants ϵ_1 and ϵ_2. Throughout all space $\mu = 1$. The grid is formed by parallel, ideally conducting metal wires of an arbitrary cross-section, which have two axes of symmetry ox and oy. The grid spacing p is small compared with the wavelength in free space λ, in such a way that the dimensionless parameter kp ($k = 2\pi/\lambda$) is small. The dependence of the fields on time is taken in the form of exp ($i\omega t$). Since the directions of the propagation of waves are perpendicular to the wires, and the grid is uniform in the direction ξ, the problem is plane (the field does not depend on the coordinates ξ, i.e., $\partial \ldots / \partial \xi \equiv 0$). Fig. 1 shows a typical field area bounded by the contours Γ_1 (5' - 4' - 3' - 2 - 3 - 4 - 5) and Γ_2 (4 - 3 - $\overline{2}$' - 3' - 4' - $\overline{5}$'). A plane wave with components $H\xi$, E_x, and E_y strikes the grid from y' < 0 at an angle φ_1. The reflected wave goes off in a negative direction of the axis y'', and the original wave, now passed, spreads at a refraction angle φ_2 $\left(\sin\varphi_2 = \sin\varphi_1 \sqrt{\frac{\varepsilon_1}{\varepsilon_2}}\right)$ in the positive direction of the axis $\overline{y}$'. The areas 5' - 5 and $\overline{5}$' - $\overline{5}$ are at sufficient distances from the grid to ensure the formation of plane waves.

2. AN EXPRESSION FOR THE FIELDS IN THE FAR ZONE IN TERMS OF THE FIELDS AT THE WIRE CONTOUR AND THE PLANE y = 0

To discover the link between the fields in the far zones (areas 5' - 5 and $\overline{5}$' - $\overline{5}$) and the fields close to the wires we will apply the Lorentz lemma (see, for example, Ref. 1) on the contours Γ_1 and Γ_2. As auxiliary fields E^i and H^i (i = 1;2) figuring in the lemma, it is more convenient to take the fields of the plane waves in space without a grid and with a plane interface between dielectrics at y = 0. The directions of propagation of the

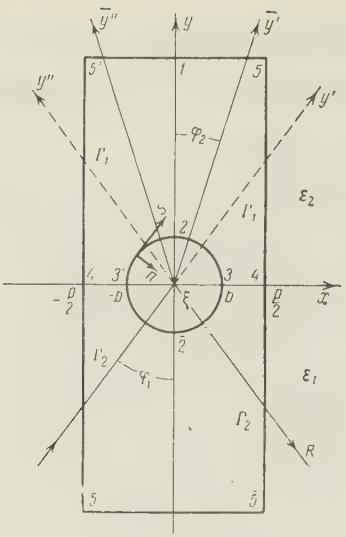

Fig. 1

auxiliary waves will be selected in such a way that they are "head-on" with respect to the true fields, i.e., the field E^1, H^1 (head-on field with respect to the reflected wave) comes after the wave striking the interface in the positive direction of the axis y'', and the field E^2, H^2 (head-on with respect to the transmitted wave) is the field of the wave striking the interface on the opposite side in the negative direction of the axis $\bar{y}'$ (see Fig. 1).

Let us designate $\alpha_i = \sin\varphi_i$, and $\beta_i = \cos\varphi_i$. Let us write the expressions for the true fields in the far zone and for the auxiliary fields:

$$\left.\begin{aligned}
&H_\xi = Te^{-ik\sqrt{\varepsilon_2}\bar{y}'};\quad E_x = \frac{\beta_2 T}{\sqrt{\varepsilon_2}}e^{-ik\sqrt{\varepsilon_2}\bar{y}'};\quad E = \frac{-\alpha_2 T}{\sqrt{\varepsilon_2}}e^{-ik\sqrt{\varepsilon_2}\bar{y}'};\\
&H^1_\xi = T_1 e^{-ik\sqrt{\varepsilon_2}\bar{y}''};\quad E^1_x = \frac{\beta_2 T_1}{\sqrt{\varepsilon_2}}e^{-ik\sqrt{\varepsilon_2}\bar{y}''};\quad E^1_y = \frac{\alpha_2 T_1}{\sqrt{\varepsilon_2}}e^{-ik\sqrt{\varepsilon_2}\bar{y}''};\\
&H^2_\xi = e^{ik\sqrt{\varepsilon_2}\bar{y}'} + R_2 e^{-ik\sqrt{\varepsilon_2}\bar{y}''};\quad E^2_x = \frac{-\beta_2}{\sqrt{\varepsilon_2}}(e^{ik\sqrt{\varepsilon_2}\bar{y}'} - R_2 e^{-ik\sqrt{\varepsilon_2}\bar{y}''});\\
&E^2_y = \frac{\alpha_2}{\sqrt{\varepsilon_2}}(e^{ik\bar{y}'\sqrt{\varepsilon_2}} + R_2 e^{-ik\sqrt{\varepsilon_2}\bar{y}''});
\end{aligned}\right\}\quad y>0 \qquad (1)$$

$$\left.\begin{aligned}
&H_\xi = e^{-ik\sqrt{\varepsilon_1}\bar{y}'} + Re^{ik\sqrt{\varepsilon_1}\bar{y}''};\quad E_x = \frac{\beta_1}{\sqrt{\varepsilon_1}}(e^{-ik\sqrt{\varepsilon_1}\bar{y}'} - Re^{ik\sqrt{\varepsilon_1}\bar{y}''});\\
&E_y = \frac{-\alpha_1}{\sqrt{\varepsilon_1}}(e^{-ik\sqrt{\varepsilon_1}\bar{y}'} + Re^{ik\sqrt{\varepsilon_1}\bar{y}''});\\
&H^1_\xi = e^{-ik\sqrt{\varepsilon_1}\bar{y}''} + R_1 e^{ik\sqrt{\varepsilon_1}\bar{y}'};\quad E^1_x = \frac{\beta_1}{\sqrt{\varepsilon_1}}(e^{-ik\sqrt{\varepsilon_1}\bar{y}''} - R_1 e^{ik\sqrt{\varepsilon_1}\bar{y}'});\\
&E^1_y = \frac{\alpha_1}{\sqrt{\varepsilon_1}}(e^{-ik\sqrt{\varepsilon_1}\bar{y}''} + R_1 e^{ik\sqrt{\varepsilon_1}\bar{y}'});\\
&H^2_\xi = T_2 e^{ik\sqrt{\varepsilon_1}\bar{y}'};\quad E^2_x = -\frac{\beta_1 T_2}{\sqrt{\varepsilon_1}}e^{ik\sqrt{\varepsilon_1}\bar{y}'};\quad E^2_y = \frac{\alpha_1 T_2}{\sqrt{\varepsilon_1}}e^{ik\sqrt{\varepsilon_1}\bar{y}'}
\end{aligned}\right\}\quad y<0$$

Here R and T are the known coefficients of reflection and transmission; R_i and T_i are the coefficients of reflection and transmission for the auxiliary waves which are found from the simple problem of the incidence of plane waves on a plane interface between two homogeneous dielectrics:

$$R_1 = \frac{\beta_1\sqrt{\varepsilon_2} - \beta_2\sqrt{\varepsilon_1}}{\beta_1\sqrt{\varepsilon_2} + \beta_2\sqrt{\varepsilon_1}};\quad T_1 = \frac{2\beta_1\sqrt{\varepsilon_2}}{\beta_1\sqrt{\varepsilon_2} + \beta_2\sqrt{\varepsilon_1}};\quad R_2 = -R_1;\quad T_2 = T_1\frac{\beta_2\sqrt{\varepsilon_1}}{\beta_1\sqrt{\varepsilon_2}} \qquad (2)$$

On the straight lines $\bar{5}'$ - 5' and 5 - $\bar{5}$ the relations

$$H(p/2) = H(-p/2)e^{-\gamma};\quad E(p/2) = E(-p/2)e^{-\gamma};$$

$$H^i(p/2) = H^i(-p/2)\,e^{\gamma};\ E^i(p/2) = E^i(-p/2)\,e^{\gamma};\ \gamma = ik\sqrt{\varepsilon_1}\,\alpha_1 p. \tag{3}$$

are satisfied. This leads to the vanishing of the integrals along the segments $\bar{5}'$ - 5' and 5 - $\bar{5}$. Taking it into account that on the wire contour the tangential component of the electric field $E_S = 0$, we come onto the known relations linking the fields in the far zone with those at the wire contour and on the line y = 0 between the wires:

$$\begin{aligned}
\int\limits_{(5'-5)} (E_x^i H_\xi - E_x H_\xi^i)\,dx &= \int\limits_{(3'-\bar{2}-3)} E_s^i H_\xi ds + \int\limits_{(4'-3'),\,(3-4)} (E_x^i H_\xi - E_x H_\xi^i)\,dx;\\
\int\limits_{(\bar{5}'-\bar{5})} (E_x H_\xi^i - E_x^i H_\xi)\,dx &= \int\limits_{(3-\bar{2}-3')} E_s^i H_\xi ds - \int\limits_{(4'-3'),\,(3-4)} (E_x^i H_\xi - E_x H_\xi^i)\,dx.
\end{aligned} \tag{4}$$

Substituting expressions for the fields from Eq. (1) into the left-hand side, we obtain

$$\begin{aligned}
0 &= \int\limits_{(3'-\bar{2}-3)} E_s^1 H_\xi ds + \int\limits_{(4'-3'),\,(3-4)} (E_x^1 H_\xi - E_x H_\xi^1)\,dx;\\
\frac{2\beta_1 p}{\sqrt{\varepsilon_1}}(R_1 - R) &= \int\limits_{(3-\bar{2}-3')} E_s^1 H\,ds - \int\limits_{(4'-3'),\,(3-4)} (E_x^1 H_\xi - E_x H_\xi^1)\,dx;\\
-\frac{2\beta_2 p}{\sqrt{\varepsilon_2}}\,T &= \int\limits_{(3'-\bar{2}-3)} E_s^2 H_\xi ds + \int\limits_{(4'-3'),\,(3-4)} (E_x^2 H_\xi - E_x H_\xi^2)\,dx;\\
\frac{2\beta_1 p}{\sqrt{\varepsilon_1}}\,T_1 &= \int\limits_{(3-\bar{2}-3')} E_s^2 H_\xi ds - \int\limits_{(4'-3'),\,(3-4)} (E_x^2 H_\xi - E_x H_\xi^2)\,dx.
\end{aligned} \tag{5}$$

Thus, the coefficients R and T (i.e., the fields in the far zone) are expressed in terms of the field on the wire contour c:

$$\begin{aligned}
\frac{2\beta_1 p}{\sqrt{\varepsilon_1}}(R_1 - R) &= \oint\limits_c E_s^1 H_\xi ds;\\
\frac{2\beta_2 p}{\sqrt{\varepsilon_2}}(T_1 - T) &= \oint\limits_c E_s^2 H_\xi ds.
\end{aligned} \tag{6}$$

3. FIELDS NEAR THE WIRES

Let us find expressions for the fields near the wires. Replacement of the wave equation by the Laplace equation leads in our case to an error of the order of $(kp)^2$. Hence, if the solution of the equation $\nabla^2 H = 0$ is found to an accuracy within terms of the order $(kp)^2$, we can take it that this solution represents a true field with the same degree of accuracy. We should stress, as follows from Eqs. (5), that this solution will only be used at a wire contour and on a line between the wires. Thus, we will find the quasi-static solution satisfying the requirements:

1) The values H_ξ and $\frac{1}{\varepsilon_i}\frac{\partial H_\xi}{\partial y}$ are continuous on 4' - 3' and on 3 - 4;

2) $\partial H_\xi / \partial n = 0$ on the cross section contour of the wire (n is the external normal to the contour).

The first requirement follows from the continuity of the tangential components, and the second from the fact that the tangential component of the electric field on the metal E_S is equal to zero. To determine the type of solution we must make some conformal transformations of $z_1(z)$ and $z_2(z)$, transposing the regions D_1 and D_2 of the planes of the complex variables $z_1 = x_1 + iy_1$ and $z_2 = x_2 + iy_2$ to the region D of the complex variable $z = x + iy$. The correspondence of the points is shown in Fig. 2. Let us seek the solution to the problem throughout the region under consideration in the form

$$H_{\xi 2} = (A_2 + B_2 y_1)(1 + C_2 x_2)$$
$$y \geqslant 0,$$
$$H_{\xi 1} = (A_1 + B_1 y_1)(1 + C_1 x_2)$$
$$y \leqslant 0. \qquad (7)$$

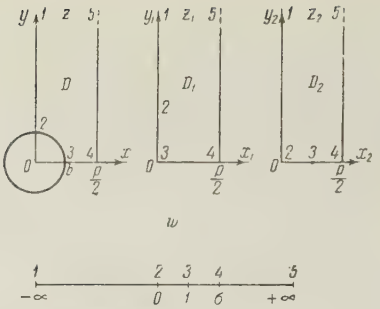

Fig. 2

Here $y_1(x, y)$ and $x_2(x, y)$ are the imaginary and real parts of the transformations $z_1(z)$ and $z_2(z)$; A_i, B_i and C_i are constants.

Let us determine the functions x_2 and y_1 beyond the bounds of the region D from the conditions

$$\begin{aligned} y_1(-x, y) &= y_1(x, y); \\ y_1(x, -y) &= -y_1(x, y); \\ x_2(-x, y) &= -x_2(x, y); \\ x_2(x, -y) &= x_2(x, y). \end{aligned} \qquad (8)$$

Let us join the constants.

1) At the segment 3-4 $H_{\xi 2} = H_{\xi 1}$, $y_1 = 0$. This gives us $A_1 - A_2 = (C_2 A_2 - A_1 C_1)x_2$ and since $x_2 \neq$ const, this equality is only possible at $A_1 = A_2$, $C_1 = C_2$ (we can set $C_1 = C$, $A_1 = A$).

2) The component of the electric field E_x is found by the formula $E_{xi} = \frac{-1}{ik\varepsilon_i} \frac{\partial H_{\xi i}}{\partial y}$, and since 3-4 $\partial x_2 / \partial y = 0$, the conditions $E_{x2} = E_{x1}$ leads to the relationship $B_1 = B_2 \frac{\epsilon_1}{\epsilon_2}$ (we can set $B_1 = B$).

3) From the condition $H_{\xi i}(p/2) = H_{\xi i}(-p/2)e^{-\gamma}$ and $x_2(-x, y) = -x_2(x, y)$ we can easily find $C = -ik\sqrt{\epsilon_1 \alpha_1}$. Thus, the field near the wires can be represented by two constants A and B in the form

$$H_{\xi 2} = \left(A + \frac{\varepsilon_2}{\varepsilon_1} B y_1\right)(1 - ik\sqrt{\varepsilon_2}\alpha_2 x_2) \text{ for } y \geqslant 0,$$
$$H_{\xi 1} = (A + B y_1)(1 - ik\sqrt{\varepsilon_1}\alpha_1 x_2) \text{ for } y \leqslant 0. \qquad (9)$$

A and B are determined from the basic equations in (5). It is further shown that B is of the order of kp, hence $\nabla^2 H_\xi$ is of the order of $(kp)^2$, i.e., the solution found is the true field with the assumed accuracy.

4. CALCULATION OF KNOWN VALUES

Let the contour of the cross-section of the wire be given by the equation $y = y(x)$. When calculating the integrals along the wire contour of Eqs. (6) we will replace the exponents by the first two terms in an expansion with respect to ky (the vertical dimensions of the wire will be assumed to be small compared with the wavelength). Omitting long intermediate calculations, we will write expressions for R and T in terms of the constants A and B:

$$\frac{2\beta_2}{T_2}(R_1 - R) = -ikp\sqrt{\varepsilon_2}\left[2l + \alpha_2^2\left(1+\frac{\varepsilon_2}{\varepsilon_1}\right)L\right]A + \left[\beta_2\left(1+\frac{\varepsilon_2}{\varepsilon_1}\right)\Delta_1 + \right.$$
$$\left. + ikp\sqrt{\varepsilon_2}\left(1-\frac{\varepsilon_2}{\varepsilon_1}\right)\Delta_2\right]Bp;$$

$$\frac{2\beta_1}{T_1}(T_1 - T) = -ikp\sqrt{\varepsilon_1}\left[2l + \alpha_1^2\left(1+\frac{\varepsilon_1}{\varepsilon_2}\right)L\right]A + \tag{10}$$
$$+\left[\beta_1\left(1+\frac{\varepsilon_2}{\varepsilon_1}\right)\Delta_1 - ikp\sqrt{\varepsilon_2}\left(1-\frac{\varepsilon_2}{\varepsilon_1}\right)\Delta_2\right]Bp;$$
$$l = \frac{S}{2p^2};\ L = \frac{2!}{p^2}\int_0^b x_2 y'dx;\ \Delta_1 = \frac{2}{p^2}\int_0^b y_1 dx;\ \Delta_2 = \frac{2}{p^3}\int_0^b yy_1 dx.$$

The functions under the integral sign are taken at the points of the contour; y' is the derivative of the function y (x); S is the area of the wire section; 2b is the maximum dimension of the wire in the direction of the axis ox. A and B are found from the first and fourth equations in (5). When calculating the integrals along the segments 4' - 3' and 3 - 4 it is essential to know the value $\int_b^{p/2} \frac{\partial y_1}{\partial y} dx$. This integral can easily be found by noting the condition under which the integral along the closed contour Γ_1 from the function $\partial y_1 / \partial n$ is equal to zero; it proves equal to p. As a result we find the constants A and B:

$$A = \frac{2\beta_1}{G_{22}} \frac{1}{\frac{G_{11}}{G_{22}} + \sqrt{\frac{\varepsilon_1}{\varepsilon_2}}\frac{D_{11}}{D_{22}}};\qquad B = -\frac{2\beta_1}{D_{11}} \frac{ik\sqrt{\varepsilon_1}}{\sqrt{\frac{\varepsilon_2}{\varepsilon_1}}\frac{G_{11}}{G_{22}} + \frac{D_{11}}{D_{22}}}. \tag{11}$$

Substituting A and B into Eq. (10), we find the final values for R and T:

$$R = \frac{\frac{G_{12}}{G_{22}} - \frac{D_{12}}{D_{22}}}{\frac{G_{11}}{G_{22}} + \sqrt{\frac{\varepsilon_1}{\varepsilon_2}}\frac{D_{11}}{D_{22}}} T_1\sqrt{\frac{\varepsilon_1}{\varepsilon_2}} + R_1;\qquad T = \frac{\frac{G_{21}}{G_{22}} + \sqrt{\frac{\varepsilon_1}{\varepsilon_2}}\frac{D_{21}}{D_{22}}}{\frac{G_{11}}{G_{22}} + \sqrt{\frac{\varepsilon_1}{\varepsilon_2}}\frac{D_{11}}{D_{22}}} T_1 \tag{12}$$

Here

$$G_{jn} = \beta_n - (-1)^{j+n} ikp\sqrt{\varepsilon_n}\,(l + \alpha_j^2 L);$$

$$D_{jn} = 1 + (-1)^{j+n} ikp\frac{\varepsilon_j}{\sqrt{\varepsilon_n}}\beta_n\Delta_1 + (kp)^2\,\varepsilon_j\,(\beta_j^2\Delta_2 - \alpha_j^2\Delta_3);$$

$$\Delta_3 = \frac{2}{p^3}\int_0^b (x - x_2)\, y_1 y' dx.$$

5. THE VERIFICATIONS OF THE LIMITING CASES

For q = 2b/p → 0 (b → 0) the coefficients R and T become R_1 and T_1. But this limiting process only occurs as kp → 0. In other words a reduction in the spacing leads to an increase in the leakage of the field through the grid.

Let us ascertain the behavior of R and T as q → 1 (transition to solid filling, i.e., to corrugation). To do this it is simpler to use another transformation, to wit, we make a conformal transformation of the upper half plane of the auxilliary complex plane w (Fig. 2) into the region D_1 of the plane z_1 in such a way that the points $-\infty$, 0, 1, σ, $+\infty$ of the actual axis of w become the points 1, 2, 3, 4 and 5 of the plane z_1, respectively. The transformation is written in the form

$$z_1 = \frac{p}{\pi} \arcsin\sqrt{\frac{w-1}{\sigma-1}}. \tag{13}$$

The parameter σ depends on the shape and relative size of the wire. To calculate Δ_i we have to know the values of y_1 along the segment 2 - 3. For this segment $0 \leqslant \omega \leqslant 1$, hence

$$y_1 = \operatorname{Im} z_1 = \frac{p}{\pi} \ln \frac{\sqrt{1-w} + \sqrt{\sigma - w}}{\sqrt{\sigma - 1}}. \tag{14}$$

As $q \to 1$ (the wires approach one another without limit, $b \to p/2$ $\sigma \to 1$, $y_1 \to \infty$ (we should recall that the requirement $ky_1 \ll 1$ has not been made, we have only had $ky \ll 1$). Here we note carefully in the integrals determining Δ_i, the main terms tending to infinity (it can be shown that the singularity of the expression $(\sqrt{1-w} + \sqrt{\sigma - w})$ at the point w = 1 is integrable for $\sigma \to 1$):

$$\Delta_1 \to \frac{y_1}{p}; \quad \Delta_2 \to \frac{y_1}{p} l; \quad \Delta_3 \to -\frac{y_1}{p}(l + L); \quad \beta_i^2 \Delta_2 - \alpha_i^2 \Delta_3 \to \frac{y_1}{p}(l + \alpha_i^2 L). \tag{15}$$

Substituting these expressions into (12), we find for q = 1

$$T = 0; \qquad R = \frac{\beta_1 + ikp\sqrt{\varepsilon_1}(l + \alpha_1^2 L)}{\beta_1 - ikp\sqrt{\varepsilon_1}(l + \alpha_1^2 L)}; \quad |R| = 1, \tag{16}$$

which was indeed expected. At the normal incidence $\varphi_1 = 0$ ($\beta_1 = 1$; $\alpha_1 = 0$) we can write Eq. (16) for R in our approximation as

$$R = e^{ik\sqrt{\varepsilon_1}\frac{S}{p}}. \tag{17}$$

For a rectangular wire, this equation, as should be the case, gives the phase lead for a simple shift in the negative direction in an ideally conducting plane. Thus, given normal incidence of a plane wave onto a plane corrugated surface with an arbitrarily shaped corrugation, the phase lead in the coefficient of reflection is proportional to the cross-section of the figure formed by the corrugation.

6. WIRES WITH ROUND AND RETANGULAR CROSS-SECTIONS

For a grid made of round wires we can use the exact Bloch transformation [2] for our calculations

$$z_1 = z - \frac{mb}{2\pi} \ln \frac{\sin\frac{\pi}{p}(z + \lambda b)}{\sin\frac{\pi}{p}(z - \lambda b)}. \tag{18}$$

Here b is the radius of the wire; m and λ are parameters depending on q. If the wire is thin ($q \ll 1$), the incidence is normal ($\varphi_1 = 0$) and $\epsilon_1 = \epsilon_2 = 1$, use of this transformation leads to the equations

$$R = 3ikl, \quad T = 1 - ikl, \tag{19}$$

coinciding with those obtained in Ref. 3. The results obtained by Lamb [4] and Gans [5] for this case in a problem under the same assumptions are erroneous. Their results do not take into account the ring current around the perimeter of the wire section, which led to an error in the reflection coefficient of 1-1/2 times. A numerical calculation of R and T was made from Eqs. (12) using the transformations (18) for the parameters $\epsilon_1 = 1$, $\epsilon_2 = 3$, $\varphi_1 = 84°$*, and kp = 0.1, 0.2. The results of the calculation of the function of q are given in

---

* This angle is equal to the Brillouin angle in the expansion of the waveguide E_{01} wave in a circular waveguide into plane waves, ka = 23.13 (a is the radius of the waveguide).

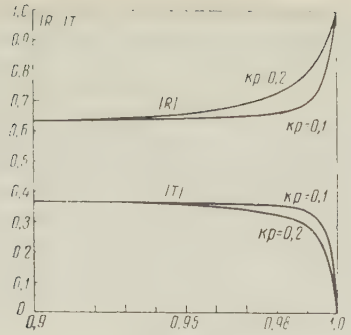

Fig. 3

Fig. 3

For rectangular wires the conformal transformations z(w) and $z_1(w)$ take the form

$$z = \frac{p}{2\pi}\int_0^w \frac{1}{\sqrt{u(1-u)}}\sqrt{\frac{u-t}{u-\sigma}}\,du + \\ + ic;\ z_1 = \frac{p}{\pi}\arcsin\sqrt{\frac{w-1}{\sigma-1}} = \\ = \frac{p}{2\pi}\int_{w-1}^{w} \frac{du}{\sqrt{u(\sigma-1-u)}}. \qquad (20)$$

Here 2c is the dimension of the wire in the direction of the y axis. The parameters σ and t, which depend on the relative dimentions of the wire, are found from Eqs. (5) and (6) in Ref. 6. For some values of the relative dimensions of the wire in this work calculations of σ and t have been made. The dimensionless parameter l, L and Δ_i are determined from

$$l = \frac{2bc}{p^2};\ L = -\frac{2}{p^2}\int_0^c x_2(b,\ y)\,dy;\ \Delta_1 = \frac{2}{p^2}\int_0^b y_1(x,\ c)\,dx;\ \Delta_2 = \Delta_1\frac{c}{p}; \qquad (21)$$

$$\Delta_3 = \frac{2}{p^2}\int_0^c [x_2(b,\ y) - b]\,y_1(b,\ y)\,dy.$$

7. EQUIVALENT BOUNDARY CONDITIONS

The derived coefficients of reflection and transmission make it possible to set up the local boundary conditions equivalent to the actions of a grid. Indeed, after the calculation of R and T from Eqs. (1) we know the true fields for regions lying above the straight line 5' - 5 and below $\bar{5}'$ — $\bar{5}$ (It should be recalled that these segments are found in the plane y = 0, as plane wave fields (bearing in mind that this extension is not a true field), we thereby introduce at y = 0 a certain semi-transparent infinitely thin film on which there are definite discontinuities in the field components:

$$H_{\xi 2} - H_{\xi 1} = (T - R - 1)\,e^{-\gamma};$$
$$E_{x2} - E_{x1} = \left[\frac{\beta_2}{\sqrt{\varepsilon_2}}T + \frac{\beta_1}{\sqrt{\varepsilon_1}}(R-1)\right]e^{-\gamma}; \qquad (22a)$$
$$E_{y2} - E_{y1} = \left[\frac{\alpha_1}{\sqrt{\varepsilon_1}}(1+R) - \frac{\alpha_2}{\sqrt{\varepsilon_2}}T\right]e^{-\gamma}.$$

correspondingly,

$$H_{\xi 2} + H_{\xi 1} = (T + R + 1)\,e^{-\gamma};$$
$$E_{x2} + E_{x1} = \left[\frac{\alpha_2}{\sqrt{\varepsilon_2}}T + \frac{\beta_1}{\sqrt{\varepsilon_1}}(1-R)\right]e^{-\gamma}; \qquad (22b)$$
$$E_{y2} + E_{y1} = -\left[\frac{\alpha_2}{\sqrt{\varepsilon_2}}T + \frac{\alpha_1}{\sqrt{\varepsilon_1}}(1+R)\right]e^{-\gamma}.$$

Clearly, the effect of this hypothetical film is equivalent to the action of a true grid, since the fields in the far zone are maintained. The discontinuity in the components of the field of Eq. (2) can be considered as equivalent boundary conditions, which have to be posed at y = 0. These boundary conditions can be used to calculate the attenuation and phase characteristics of E_{0n} waves in a spiral waveguide. For the particular case when the grid is made of strips (c = 0) and $\epsilon_1 = \epsilon_2 = 1$, these boundary conditions coincide with the corresponding conditions obtained in Ref. 7.

8. CALCULATION OF THE EFFECTIVE REFLECTION COEFFICIENT FOR A GRID-SCREEN SYSTEM. BOUNDARY CONDITIONS.

Let us consider a system (Fig. 4) formed by a grid and an ideally conducting metal plane placed at a distance r from the grid (r is sufficient for the formation of plane waves). The space between the grid and the solid screen is filled with a dielectric with a dielectric constant ϵ_2; underneath the grid ($y < 0$) the dielectric filler has a dielectric constant ϵ_1. Let us calculate the coefficient of reflection for this system R_{ef}.

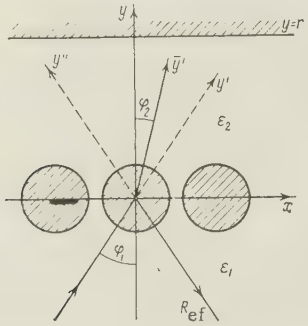

Fig. 4

Let us replace the grid by an equivalent film: the field in the region $y \leqslant 0$ will then be represented in the form

$$H_{\xi 1} = e^{-ik\sqrt{\epsilon_2}\,y'} + Re^{ik\sqrt{\epsilon_1}\,y''} + \sum_{n=1}^{\infty} H_{\xi 1}^{(n)}, \quad (23)$$

in which the sum in the right-hand side is the field which arises as a result of multiple reflections occurring in the region between the film and the screen. By calculating this sum, for example, at the point x = 0, y = 0, we find an expression for the effective coefficient of reflection

$$R_{ef} = R + \frac{TT^*}{e^{ik\sqrt{\epsilon_2}\beta_2 2r} - R^*}. \quad (24)$$

Here R* and T* are the coefficients of reflection and transmission when a wave from the medium (2) strikes the medium (1). They are obtained from Eqs. (12) for R and T by replacing the subscripts (1 by 2 and 2 by 1). The derived coefficient of reflection makes it possible to set up the boundary condition equivalent to the action of a grid-solid screen system, for y = 0:

$$E_{x1} = \eta H_{\xi 1}, \quad \eta = \frac{1 - R_{ef}}{1 + R_{ef}} \frac{\beta_1}{\sqrt{\epsilon_1}}. \quad (25)$$

The boundary condition can be used for calculating the phase velocities of E_{on} waves in a helical waveguide with an all-metal sheath. By substituting the expression for the field components into Eq. (25) we obtain the dispersion equation

$$\frac{xJ_0(x)}{J_1(x)} = -i\eta ka. \quad (26)$$

In conclusion the author wishes to thank B. Z. Katsenelenbaum for the great interest shown by him in the above work, and also for very valuable advice.

REFERENCES

1. Zakson, M B., Modification of a method of calculating the excitation of waveguides Reports of AS USSR, 1949, 66, 4, 637.
2. Bloch, E. Investigation of a plane grid made of theoretical profiles of finite

---

* This angle is equal to the Brillouin angle in the transformation of the Eq wave in a circular wave guide into plane waves, ka = 23.13 (a is the radius of the (waveguide).

thickness, Proc. TsAGI, 1947, No. 611.
3. B.E. Katsenelenbaum. Calculation of the coefficient of reflection of an electromagnetic wave from a thin metal rod perpendicular to the electric field in a rectangular waveguide, Izv. Vuzov MVO SSSR, (Radio Engineering), 1960, 5.
4. G. Lamb, Hydromechanics, GITTL, 1947, p. 673.
5. R. Gans, Das Verhalten Hertzseher Gitter, Ann. Physik, 1920, 61, 5, 447.
6. Malin, V.V., Sivov, A.N., Theory of propagation of H_{01} waves in a helical waveguide, Radio Engineering and Electronics, 1959, 4, 3, 433.
7. Smirnov, N.N., Propagation of electromagnetic waves in round waveguides with periodic slots, ZhTF, 1958, 28, 7, 1494.

Received by the editors 10 May 1960

π AND T RIDGED WAVEGUIDES UNIFORMLY BENT IN THE E PLANE

Ya. A. Yashkin

Systems of equations are derived relating the cutoff wavelength to the dimensions of the cross section of π and T ridged waveguides uniformly bent in the E-plane*. The application of the equations is illustrated by the calculation of the cutoff wavelength of the bent π ridged waveguide.

INTRODUCTION

The transverse TE waves usually used in straight π and T ridged waveguides, as is known, have two electric field components in the plane of the cross section, one of which (the main component) determines the wave's polarization (the polarization shown in Fig. 1 by the vector E is usually used).

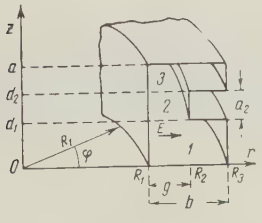

Fig. 1

In studying bent waveguides we shall consider a type of wave which also has both electric field components in the plane of the cross-section. This condition in bent wave-guides is satisfied by E waves [2]. The other possible wave (H type) does not have an E_z-component, and does not degenerate into a transverse wave as the bent wave guide goes over into a straight section, as might be expected, but into a longitudinal wave [3], which is not normally used in straight π and T ridged waveguides. Since the propagation of waves in bent waveguides is in the coordinate direction φ, if we use the cylindrical system of coordinates z, r and φ, there is no propagation in this direction at cutoff frequencies and, consequently, the terms containing derivatives with respect to φ drop out of the initial equations. From now on it will be assumed that the waveguide has perfectly conducting walls and is filled with air ($\epsilon = \mu = 1$). Omitting the term containing the harmonic time dependence of the field, we can write the field components in terms of the electric potential function $\Pi_E = \Pi$:

$$\Pi = \Pi_z \Pi_r = [A' \cos sz + B' \sin sz]\,\Pi_r = A \cos s\,(z - \alpha)\,\Pi_r; \qquad (1)$$

* Waveguides bent in the H-plane are considered in Ref. 1.

$$E_r = \frac{\partial^2 \Pi}{\partial z \partial r}; \quad H_\varphi = -jk \frac{\partial \Pi}{\partial r}; \quad E_z = \left[\frac{\partial^2}{\partial z^2} + k^2\right] \Pi; \; E_\varphi = H_r = H_z = 0, \tag{2}$$

which in its turn, satisfies the wave equation

$$\frac{\partial^2 \Pi}{\partial z^2} + \frac{1}{r}\left[\frac{\partial}{\partial r}\left(r \frac{\partial \Pi}{\partial r}\right)\right] + k^2 \Pi = 0, \tag{3}$$

in which $k = 2\pi/\lambda$ is the propagation constant of the wave in free space (λ is the wavelength).

The function π_r is the solution of the Bessel equation

$$\frac{1}{r} \frac{\partial}{\partial r}\left(r \frac{\partial \Pi_r}{\partial r}\right) + \varkappa^2 \Pi_r = 0, \tag{4}$$

where

$$\varkappa^2 = k^2 - s^2, \tag{5}$$

and s^2 is the separation constant.

The solution of Eq. (4) when $\varkappa$ is not zero is expressed in the general case by the linear combination of Bessel and Neumann functions of zero order:

$$\Pi_r = A_1 Z_0(\varkappa r) = A_2 J_0(\varkappa r) + A_3 N_0(\varkappa r). \tag{6}$$

As is known [4], an E wave in a bent waveguide of simple rectangular shape or a TM wave in a coaxial waveguide (the cutoff case in a bent waveguide corresponds to steady-state oscillations in a short-circuited segment of the coaxial line) may degenerate into a TEM wave, whose components are related to the potential function π, which is the solution of the Laplace equation obtained from Eq. (4) when $\varkappa = 0$. The solution of this Laplace equation takes the form [4]

$$\Pi = B_1 \ln r + B_2. \tag{7}$$

In what follows we shall use the solutions of Eq. (4) for various $\varkappa$, including $\varkappa = 0$.

1. π RIDGED WAVEGUIDE

Let us split the section of the bent π ridged waveguide (Fig. 1) into three simple rectangular regions 1, 2 and 3, and for each of them let us write the general solution of the wave equation (3) in the form of an infinite sum of partial solutions corresponding to different values of $\varkappa$, but corresponding to one value of k (since according to Eq. (5) for $\varkappa = 0$ s = k):

$$\Pi_i = \sum_{m=0}^{\infty} \Pi_{im} = A_{i0} \cos k(z - \alpha_i) \; (\ln r + B_2) + \sum_{m=1}^{\infty} A_{im} \cos s_{im}(z - \alpha_i) Z_0(\varkappa_{im} r), \tag{8}$$

in which i = 1, 2 and 3 is the number of the region.

From the boundary conditions at the walls of the waveguide

$$(\Pi_{im})_{r=R_i} = 0; \quad \left(\frac{\partial \Pi_{im}}{\partial z}\right)_{z=0,\, a} = 0 \tag{9}$$

it is not difficult to show that: $\alpha_1 = 0$; $\alpha_3 = a$ (α_2 is the unknown parameter determined from the continuity conditions); $\varkappa_{1m} = \varkappa_{3m} = m$-e are the roots of the equation

$$J_0(\varkappa R_1) N_0(\varkappa R_3) - N_0(\varkappa R_1) J_0(\varkappa R_3) = 0; \tag{10}$$

$\varkappa_{2m}$ are the roots of the equation

$$J_0(\varkappa R_1) N_0(\varkappa R_2) - N_0(\varkappa R_1) J_0(\varkappa R_2) = 0. \tag{10'}$$

Since the $\varkappa_{im}$ are determined from the boundary conditions, the constant s_{im} can be calculated, given the propagation wavenumber k:

$$s_{im} = \sqrt{k^2 - \varkappa_{im}^2}. \tag{11}$$

The problem is to determine the wavenumber k of Eq. (3) for the boundary conditions of π along the complex contour of the waveguide cross section. To do this we shall "join" the solutions at the boundaries of the simple regions.

The continuity requirements on the field components Eq. (2), along the line $z = d_1$

$$\frac{\partial^2 \Pi_1}{\partial z \partial r} = \frac{\partial^2 \Pi_2}{\partial z \partial r} \sim E_r; \qquad \frac{\partial \Pi_1}{\partial r} = \frac{\partial \Pi_2}{\partial r} \tag{12}$$

lead to two equations

$$A_{10} \frac{k \sin k d_1}{r} - \sum_{m=1}^{\infty} A_{1m} \varkappa_{1m} s_{1m} \sin(s_{1m} d_1) Z_1(\varkappa_{1m} r) =$$

$$= A_{20} \frac{k \sin k(d_1 - \alpha_2)}{r} - \sum_{m=1}^{\infty} A_{2m} \varkappa_{2m} s_{2m} \sin s_{2m}(d_1 - \alpha_2) Z_1(\varkappa_{2m} r) = \frac{\Psi(r)}{r}, \tag{13}$$

$$A_{10} \frac{\cos k d_1}{r} - \sum_{m=1}^{\infty} A_{1m} \varkappa_{1m} \cos(s_{1m} d_1) Z_1(\varkappa_{1m} r) =$$

$$= A_{20} \frac{\cos k(d_1 - \alpha_2)}{r} - \sum_{m=1}^{\infty} A_{2m} \varkappa_{2m} \cos s_{2m}(d_1 - \alpha_2) Z_1(\varkappa_{2m} r). \tag{14}$$

Considering Eq. (13) to be the expansion of the function $\Psi(r)/r$ into a Fourier-Bessel series with respect to $Z_1(\varkappa_{1m} r)$ in the interval $(R_1 R_3)$, and with respect to $Z_1(\varkappa_{2m} r)$ in the interval $(R_1 R_2)$ $(m = 0, 1, 2 \ldots)$, and taking into account the fact that the function $\Psi(r)$ under the integral sign is zero along the conducting segment $(R_3 - R_2)$, we can express the coefficients A_{1m}, and A_{2m} in terms of the unknown function $\Psi(r)$:

$$A_{10} = \frac{\int_{R_1}^{R_3} \frac{\Psi(\xi)}{\xi} d\xi}{k \sin k d_1 \ln \frac{R_3}{R_1}}; \quad A_{1m} = -\frac{2 \int_{R_1}^{R_3} \Psi(\xi) Z_1(\varkappa_{1m} \xi) d\xi}{s_{1m} \varkappa_{1m} \sin(s_{1m} d_1) [R_3^2 Z_1^2(\varkappa_{1m} R_3) - R_1^2 Z_1^2(\varkappa_{1m} R_1)]}; \tag{15}$$

$$A_{20} = \frac{\int_{R_1}^{R_2} \frac{\Psi(\xi)}{\xi} d\xi}{k \sin k(d_1 - \alpha_2) \ln \frac{R_2}{R_1}};$$

$$A_{2m} = -\frac{2 \int_{R_1}^{R_2} \Psi(\xi) Z_1(\varkappa_{2m} \xi) d\xi}{s_{2m} \varkappa_{2m} \sin s_{2m}(d_1 - \alpha_2) [R_2^2 Z_1(\varkappa_{2m} R_2) - R_1^2 Z_1^2(\varkappa_{2m} R_1)]}. \tag{16}$$

Substituting the above coefficients into Eq. (14) and transposing all terms to the left-hand side of the equality, we obtain the integral equation containing $\Psi(\xi)$:

$$\int_{R_1}^{R_3} \Psi(\xi) P(r, \xi) d\xi = 0, \tag{17}$$

in which the symmetrical kernel is represented by the expression

$$P(r, \xi) = \frac{\operatorname{ctg} kd_1}{\ln \frac{R_3}{R_1}} \frac{1}{r} \frac{1}{\xi} - \frac{\operatorname{ctg} k(d_1 - \alpha_2)}{k \ln \frac{R_2}{R_1}} \frac{1}{r} \frac{1}{\xi} +$$
$$+ \sum_{m=1}^{\infty} \frac{2 \operatorname{ctg} s_{1m} d_1}{s_{1m} [R_3^2 Z_1^2 (\varkappa_{1m} R_3) - R_1^2 Z_1^2 (\varkappa_{1m} R_1)]} Z_1 (\varkappa_{1m} r) Z_1 (\varkappa_{1m} \xi) - \tag{18}$$
$$- \sum_{m=1}^{\infty} \frac{2 \operatorname{ctg} s_{2m} (d_1 - \alpha_2)}{s_{2m} [R_2^2 Z_1^2 (\varkappa_{2m} R_2) - R_1^2 Z_1^2 (\varkappa_{2m} R_1)]} Z_1 (\varkappa_{2m} r) Z_1 (\varkappa_{2m} \xi).$$

The solution of the integral equation (17) will be found by the Bubnov-Galerkin method. As a first approximation, the unknown function $\Psi(\xi)$ is assumed to equal some constant, and we obtain the relationship

$$\int_{R_1}^{R_2} \int_{R_1}^{R_3} P(r, \xi) \, dr \, d\xi = 0, \tag{19}$$

which relates the wavenumber (and, therefore, the cutoff wavelength), as well as the unknown parameter α_2, to the dimensions of the two neighboring rectangular regions. The solution of Eq. (19) takes the following form:

$$\operatorname{ctg} k(d_1 - \alpha_2) = \frac{\ln \frac{R_2}{R_1}}{\ln \frac{R_3}{R_1}} \left\{ \operatorname{ctg} kd_1 + \right.$$
$$\left. + \frac{\ln \frac{R_3}{R_1}}{\ln^2 \left(\frac{R_2}{R_1} \right)} 2k \sum_{m=1}^{\infty} \frac{\operatorname{ctg} s_{1m} d_1 Z_0^2 (\varkappa_{1m} R_2)}{s_{1m} \varkappa_{1m}^2 [R_3^2 Z_1^2 (\varkappa_{1m} R_3) - R_1^2 Z_1^2 (\varkappa_{1m} R_1)]} \right\}. \tag{20}$$

Let us write Eq. (20) in a slightly different form. Let us express Z_0 and Z_1 in terms of functions [5] of a small radial sine (sn) and cosine (cs) according to the following relationships:

$$Z_0 (\varkappa_{1m} R_j) = \frac{J_0 (\varkappa_{1m} R_j) N_0 (\varkappa_{1m} R_1) - N_0 (\varkappa_{1m} R_j) J_0 (\varkappa_{1m} R_1)}{N_0 (\varkappa_{1m} R_1)} =$$
$$= \frac{\operatorname{sn} (\varkappa_{1m} R_j, \varkappa_{1m} R_1)}{N_0 (\varkappa_{1m} R_1)}, \tag{21}$$
$$Z_1 (\varkappa_{1m} R_j) = \frac{J_1 (\varkappa_{1m} R_j) N_0 (\varkappa_{1m} R_1) - N_1 (\varkappa_{1m} R_j) J_0 (\varkappa_{1m} R_1)}{N_0 (\varkappa_{1m} R_1)} =$$
$$= \frac{\operatorname{cs} (\varkappa_{1m} R_j, \varkappa_{1m} R_1)}{N_0 (\varkappa_{1m} R_1)}. \tag{22}$$

Noting that the radial cosine for identical independent variables takes the simple form [6]

$$\operatorname{cs} (\varkappa_{1m} R_1, \varkappa_{1m} R_1) = - \frac{2}{\pi \varkappa_{1m} R_1},$$

Eq. (20) can be written in final form as follows:

$$\operatorname{ctg} k(d_1 - \alpha_2) = \frac{\ln \frac{R_2}{R_1}}{\ln \frac{R_3}{R_1}} \left\{ \operatorname{ctg} kd_1 + \right.$$

$$+\frac{\ln\frac{R_3}{R_1}}{\ln^2\left(\frac{R_2}{R_1}\right)}2k\sum_{m=1}^{\infty}\frac{\operatorname{ctg}s_{1m}d_1\,\mathrm{sn}^2(\varkappa_{1m}R_2,\varkappa_{1m}R_1)}{s_{1m}\varkappa_{1m}^2\left[R_3^2\,\mathrm{cs}^2(\varkappa_{1m}R_3,\varkappa_{1m}R_1)-\frac{4}{\pi^2\varkappa_{1m}^2}\right]}\Bigg\}. \tag{23}$$

It is not difficult to show that for large R_j and R_1, the radial sines and cosines may be replaced by the asymptotic expressions

$$\begin{aligned}\mathrm{sn}(\varkappa_{1m}R_j,\varkappa_{1m}R_1)&\simeq\frac{2}{\pi\varkappa_{1m}\sqrt{R_jR_1}}\sin[\varkappa_{1m}(R_j-R_1)],\\ \mathrm{cs}(\varkappa_{1m}R_j,\varkappa_{1m}R_1)&=\frac{2}{\pi\varkappa_{1m}\sqrt{R_jR_1}},\end{aligned} \tag{24}$$

while the number $\varkappa_{1m}$ can be replaced by the expression

$$\varkappa_{1m}=\frac{m\pi}{R_3-R_1}. \tag{25}$$

From Eqs. (25) and (24), setting $R_3 - R_1 = b$; $R_2 - R_1 = g$, and letting the following expressions approach their limits $\ln\frac{R_2}{R_1}\Big/\ln\frac{R_3}{R_1}\to\frac{g}{b}$; $R_2\ln\frac{R_2}{R_1}\to g$, $\left(\frac{R_j}{R_1}\to 1\right)$, it is easy to obtain the expression for Eq. (23) at the limit, which applies to a straight waveguide:

$$\begin{aligned}&\operatorname{ctg}k(d_1-\alpha_2)=\\ &=\frac{g}{b}\left\{\operatorname{ctg}kd_1+2k\sum_{m=1}^{\infty}\frac{\operatorname{ctg}s_{1m}d_1}{s_{1m}}\frac{\sin^2\left(\frac{m\pi}{b}g\right)}{\left(\frac{m\pi}{b}g\right)^2}\right\}.\end{aligned} \tag{26}$$

Equation (26) proves to be identical to the corresponding equation obtained in Ref. 7 by a direct solution for the straight non-symmetrical π ridged waveguide, which justifies our treatment of Eq. (23). Equation (23) contains two unknown quantities, k and α_2. In order to determine them we require a second equation, which can be obtained from the continuity conditions of the solutions along the line $z = d_2$:

$$\begin{aligned}\operatorname{ctg}k(d_2-\alpha_2)=\frac{\ln\frac{R_2}{R_1}}{\ln\frac{R_3}{R_1}}\Bigg\{&\operatorname{ctg}k(d_2-a)+\\ &+\frac{\ln\frac{R_3}{R_1}}{\ln^2\left(\frac{R_2}{R_1}\right)}2k\sum_{m=1}^{\infty}\frac{\operatorname{ctg}s_{1m}(d_2-a)\,\mathrm{sn}^2(\varkappa_{1m}R_2,\varkappa_{1m}R_1)}{s_{1m}\varkappa_{1m}^2\left[R_3^2\,\mathrm{cs}^2(\varkappa_{1m}R_3,\varkappa_{1m}R_1)-\frac{4}{\pi^2\varkappa_{1m}^2}\right]}\Bigg\}.\end{aligned} \tag{27}$$

Thus, Eqs. (23 and (27) form a characteristic system for a π ridged waveguide bent in the E-plane, when the bend occurs on the smooth side (Fig. 1). If the bend occurs on the ridged side (Fig. 2), the characteristic system has a different form:

$$\begin{aligned}\operatorname{ctg}k(d_1-\alpha_2)=\frac{\ln\frac{R_3}{R_2}}{\ln\frac{R_3}{R_1}}\Bigg\{&\operatorname{ctg}kd_1+\\ &+\frac{\ln\frac{R_3}{R_1}}{\ln^2\left(\frac{R_3}{R_2}\right)}2k\sum_{m=1}^{\infty}\frac{\operatorname{ctg}s_{1m}d_1\,\mathrm{sn}^2(\varkappa_{1m}R_2,\varkappa_{1m}R_3)}{s_{1m}\varkappa_{1m}^2\left[\frac{4}{\pi^2\varkappa_{1m}^2}-R_1^2\,\mathrm{cs}^2(\varkappa_{1m}R_1,\varkappa_{1m}R_3)\right]}\Bigg\},\end{aligned} \tag{28}$$

$$\operatorname{ctg} k(d_2 - \alpha_2) = \frac{\ln \frac{R_3}{R_2}}{\ln \frac{R_3}{R_1}} \left\{ \operatorname{ctg} k(d_2 - a) + \right.$$

$$\left. + \frac{\ln \frac{R_3}{R_1}}{\ln^2 \left(\frac{R_3}{R_2}\right)} 2k \sum_{m=1}^{\infty} \frac{\operatorname{ctg} s_{1m}(d_2 - a)\, \mathrm{sn}^2 (\varkappa_{1m} R_2, \varkappa_{1m} R_3)}{s_{1m} \varkappa_{1m}^2 \left[\frac{4}{\pi^2 \varkappa_{1m}^2} - R_1^2 \mathrm{cs}^2 (\varkappa_{1m} R_1, \varkappa_{1m} R_3) \right]} \right\}. \quad (29)$$

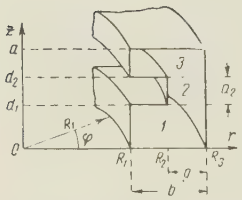

Fig. 2

The system of equations (28) and (29) is not identical with the system of equations (23) and (27), hence the result of bending a π ridged waveguide on one side or the other in the E-plane will not be the same. Obviously, this difference gradually disappears as the waveguide becomes straight.

2. T RIDGED WAVEGUIDE

The characteristic system of equations for a bent T ridged waveguide is obtained by joining the solutions for each of the three regions (Fig. 3) along the lines $z = d_1, d_2$. Omitting the derivations (which are exactly the same as for the above case), we shall write the final expressions obtained to a first approximation

$$\operatorname{ctg} k d_1 = \frac{\ln \frac{R_2}{R_1}}{\ln \frac{R_3}{R_1}} \left\{ \operatorname{ctg} k(d_1 - \alpha_2) + \right.$$

$$\left. + \frac{\ln \frac{R_3}{R_1}}{\ln^2 \left(\frac{R_2}{R_1}\right)} 2k \sum_{m=1}^{\infty} \frac{\operatorname{ctg} s_{2m}(d_1 - \alpha_2)\, \mathrm{sn}^2 (\varkappa_{2m} R_2, \varkappa_{2m} R_1)}{s_{2m} \varkappa_{2m}^2 \left[R_3^2 \mathrm{cs}^2 (\varkappa_{2m} R_3, \varkappa_{2m} R_1) - \frac{4}{\pi^2 \varkappa_{2m}^2} \right]} \right\}, \quad (30)$$

$$\operatorname{ctg} k(d_2 - a) = \frac{\ln \frac{R_2}{R_1}}{\ln \frac{R_3}{R_1}} \left\{ \operatorname{ctg} k(d_2 - \alpha_2) + \right.$$

$$\left. + \frac{\ln \frac{R_3}{R_1}}{\ln^2 \left(\frac{R_2}{R_1}\right)} 2k \sum_{m=1}^{\infty} \frac{\operatorname{ctg} s_{2m}(d_2 - \alpha_2)\, \mathrm{sn}^2 (\varkappa_{2m} R_2, \varkappa_{2m} R_1)}{s_{2m} \varkappa_{2m}^2 \left[R_3^2 \mathrm{cs}^2 (\varkappa_{2m} R_3, \varkappa_{2m} R_1) - \frac{4}{\pi^2 \varkappa_{2m}^2} \right]} \right\}. \quad (31)$$

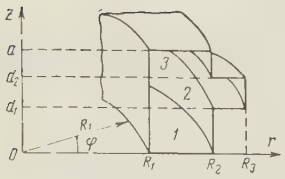

Fig. 3

Just as for the π ridged waveguide, the effects of the possible E plane bends in the T ridged waveguide will not be the same. The differences in the result of the bend again disappear when the waveguide becomes straight and the system of equations (30) and (31) at $R_1 R_1 \to 1$ goes over into the known system [7] for a straight non-symmetrical T ridged waveguide.

3. SOME DESIGN DATA

If we seek the smallest k for the waveguides under consideration, it ought to be found, according to Eq. (11), among the values less than any arbitrary $\varkappa_{im}$. This condition means that

$$s_{im} = j\sqrt{\varkappa_{im}^2 - k^2} = js'_{im} \tag{32}$$

are pure imaginary quantities for all m = 1, 2, ...

Thus, the characteristic systems for the waveguides being discussed here in the case of the smallest k will have negative hyperbolic cotangents in the summation, instead of circular cotangents.

Below, we give results from the calculation of the least wavenumber k for a nonsymmetrical π ridged waveguide bent on its smooth side (Fig. 1). The calculation was made on the basis of Eqs. (23) and (27). Only the first term of the sum was calculated (it is not difficult to show by using the asymptotic behavior of the Bessel functions that when m increases, the terms of the sum decrease at least as fast as $1/m^2$). The values of the roots of $\varkappa_{im}$ were taken from Tables in Ref. 5.

Figure 4 (curve 1) gives the results of the calculation of k as a function of d_1 which is the distance of the protrusion (Fig. 1) of fixed dimensions ($a_2 = 0.34$; $b/g = 2$) from the sidewall of the bent π ridged waveguide. The curvature is characterized by $R_3/R_1 = 4$. In the calculation it was assumed that: $a = \pi$, $a/b = 2$. Curve 2 in Fig. 4 shows the same relationship $k = f(d_1)$ for a straight π ridged waveguide. The dotted line in Fig. 4 shows k for a bent rectangular waveguide ($R_3/R_1 = 4$) without a ridge ($g = b$). This value can be obtained from Eqs. (23) and (27) in the limit as $R_2 \to R_3$.

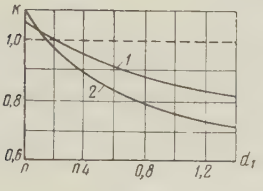

Fig. 4

From the given data it is clear that the bend in the π ridged waveguide in the E-plane leads (with the exception of small d_1) to an increase in the wavenumber and, therefore, to a decrease in the cutoff wavelength with respect to that of the π ridged waveguide. On the other hand, the addition of a ridge in an already bent rectangular waveguide leads to an increase in the cutoff wavelength for all d_1 which are not very small. For small d_1 the addition of a ridge in a bent rectangular waveguide may, in fact, lead to a reduction in the cutoff wavelength.

REFERENCES

1. Yashkin, A. Ya., π and T ridged waveguides uniformly bent in the H-plane, Radio Engineering and Electronics, 1959, 4, 11, 1831.
2. Voskresenskiy, D.I., Uniformly bent waveguide of rectangular section. Problems of radio engineering at superhigh frequencies, Oborongiz, 1957.
3. Vvedenskiy, B. A., Arenburg, A.G., Radio waveguides, GTI, 1946.
4. Gurevich, A.G., Hollow resonators and waveguides, Soviet Radio Herald, 1952.
5. Waveguide reference book, Soviet Radio Herald, 1952.
6. Watson, G.N., Theory of Bessel Functions, For. Lit. Press, 1949.
7. Yashkin, A. Ya., Calculation of cutoff lower wavelengths for nonsymmetrical π and T ridged waveguides and some others of different shapes. Radio Engineering and Electronics, 1957, 2, 8, 989,

Received by the editors 28 December 1959

INVESTIGATION OF CAVITY SYSTEMS WITH ANISOTROPIC REGIONS BY THE EIGENFUNCTION METHOD. PART III. WAVEGUIDES

V. V. Nikol'skiy

Part I investigated a cavity resonator with an anisotropic region; the present paper investigates an analogous waveguide. The problem is presented in a form which permits application of machine computing techniques.

1. STATEMENT OF THE PROBLEM

Let us discuss a waveguide (see figure) — an ideal conducting tube (cross-section S_0 with contour L_0) — containing an anisotropic cylinder of cross-section S. It is required to find the propagation constants, i.e., the longitudinal (complex) wave numbers of the possible modes of the system.

The medium (compare Ref. 1) is characterized by permeability tensors $\overleftrightarrow{\varepsilon}(\vec{r})$ and $\overleftrightarrow{\mu}(\vec{r})$,, which are given as

$$\left.\begin{aligned}\overleftrightarrow{\varepsilon}(\vec{r}) &= \varepsilon_0 \overleftrightarrow{I}\\ \overleftrightarrow{\mu}(\vec{r}) &= \mu_0 \overleftrightarrow{I}\end{aligned}\right\} \text{ within } S - S_0, \qquad \left.\begin{aligned}\overleftrightarrow{\varepsilon}(\vec{r}) &= \overleftrightarrow{\varepsilon}\\ \overleftrightarrow{\mu}(\vec{r}) &= \overleftrightarrow{\mu}\end{aligned}\right\} \text{ within S.} \tag{1}$$

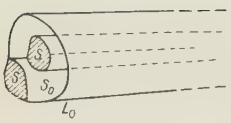

It is assumed that for a "hollow" waveguide the complete system of eigenfunctions is known (see Ref. 2, section 22) as a combination of longitudinal and transverse components of the possible H- and E-fields. These fields obey Maxwell's equations, which in the present case are conveniently expressed in the form

$$\operatorname{curl}_\perp \vec{H}_k + j\Gamma_k [\vec{H}_k, \vec{z}_0] = j\omega\varepsilon_0 \vec{E}_k. \tag{2}$$

Here Γ_k are the logitudinal wave numbers of the possible (E or H) modes of the waveguide, associated, as is known, by the equality

$$\Gamma_k^2 = k_0^2 - \chi_k^2 \qquad (k_0^2 = \omega^2\varepsilon_0\mu_0), \tag{3}$$

where χ_k represents the transverse wave numbers.

Let us introduce the quantities:

$$\left.\begin{aligned}\vec{E}_k &= \vec{E}_{zk} + \vec{E}_{\perp k}\\ \vec{H}_k &= \vec{H}_{\perp' k}\end{aligned}\right\} \text{ for E-fields} \qquad \left.\begin{aligned}\vec{E} &= \vec{E}_{\perp' k}\\ \vec{H}_k &= \vec{H}_{zk} + \vec{H}_{\perp k}\end{aligned}\right\} \text{ for H-fields} \tag{4}$$

where

$$\left.\begin{aligned}\vec{E}_{\perp k} &= -j\frac{\Gamma_k}{\chi_k^2}\nabla_\perp E_{zk}, \quad \vec{H}_{\perp' k} = j\frac{\omega\varepsilon_0}{\chi_k^2}[\nabla_\perp E_{zk}, \vec{z}_0],\\ \vec{H}_{\perp k} &= -j\frac{\Gamma_k}{\chi_k^2}\nabla_\perp H_{zk}, \quad \vec{H}_{\perp' k} = j\frac{\omega\mu_0}{\chi^2}[\vec{z}_0, \nabla_\perp H_{zk}].\end{aligned}\right\} \tag{5}$$

Orthonormalizing the $\vec{E}_k$, $\vec{H}_k$ fields in the form

$$\varepsilon_0 \int_{S_0} \vec{E}_k^* \vec{E}_n ds = \mu_0 \int_{S_0} \vec{H}_k^* \vec{H}_n ds = \delta_{kn}, \tag{6}$$

we also have relationships

$$\varepsilon_0 \int_{S_0} \vec{E}_\perp^* \vec{E} \, ds = \frac{\Gamma_k^2}{k_0^2} \delta_{kn}, \quad \mu_0 \int_{S_0} \vec{H}_{\perp k}^* \vec{H}_{\perp n} ds = \frac{\Gamma_k^2}{k_0^2} \delta_{kn}, \tag{7}$$

$$\varepsilon_0 \int_{S_0} \vec{E}_{zk}^* \vec{E}_{zn} ds = \frac{\chi_k^2}{k_0^2} \delta_{kn}, \quad \mu_0 \int_{S_0} \vec{H}_{zk}^* \vec{H}_{zn} ds = \frac{\chi_k^2}{k_0^2} \delta_{kn}, \tag{8}$$

$$\varepsilon_0 \int_{S_0} \vec{E}_{\perp' k}^* \vec{E}_{\perp n} ds = \mu_0 \int_{S_0} \vec{H}_{\perp' k}^* \vec{H}_{\perp n} = 0, \tag{9}$$

$$\int_{S_0} [\vec{E}_k^*, \vec{H}_n] ds = \frac{}{k_0^2} \delta_{kn}. \tag{10}$$

In addition, the following equalities will be used:

$$\vec{E}_{\perp' k} = \frac{\omega \mu_0}{\Gamma_k} [\vec{H}_{\perp k}, \vec{z}_0], \quad \vec{H}_{\perp k} = \frac{\Gamma_k}{\omega \mu_0} [\vec{z}_0, \vec{E}_{\perp' k}], \tag{11}$$

$$\vec{E}_{\perp k} = \frac{\Gamma_k}{\omega \varepsilon_0} [\vec{H}_{\perp' k}, \vec{z}_0], \quad \vec{H}_{\perp' k} = \frac{\omega \varepsilon_0}{\Gamma_k} [\vec{z}_0, \vec{E}_{\perp k}], \tag{12}$$

$$\operatorname{curl}_\perp \vec{E}_{zk} = -j \frac{\chi_k^2}{\omega \varepsilon_0} \vec{H}_{\perp' k}, \tag{13}$$

$$\operatorname{curl}_\perp \vec{E}_{\perp k} = 0, \tag{14}$$

$$\operatorname{curl}_\perp \vec{E}_{\perp' k} = -j \omega \mu_0 \vec{H}_{zk}, \tag{15}$$

$$\operatorname{curl}_\perp \vec{H}_{zk} = j \frac{\chi_k^2}{\omega \mu_0} \vec{E}_{\perp' k}, \tag{16}$$

$$\operatorname{curl}_\perp \vec{H}_{\perp k} = 0, \tag{17}$$

$$\operatorname{curl}_\perp \vec{H}_{\perp' k} = j \omega \varepsilon_0 \vec{E}_{zk}. \tag{18}$$

2. EIGENFUNCTION EXPANSIONS

Let us designate a certain possible mode of a waveguide with an anisotropic cylinder as $\vec{E}$, $\vec{H}$ and its corresponding longitudinal wave number as Γ. Since because of the conditions of the problem, within the waveguide the only possible discontinuities are those of the transverse components of the vectors $\vec{E}$ and $\vec{H}$ and we have solenoidal $(\vec{E}_{\perp' k}, \vec{H}_{\perp' k})$ as well as $(\vec{E}_{\perp k}, \vec{H}_{\perp k})$ transverse eigenfunctions, there is no direct necessity to convert from field intensities to the corresponding inductions (as was done in Ref. 1). In the given case the expansion may be based on the form

$$\left.\begin{aligned} \vec{E} &= \sum_m (A'_{zm} \vec{E}_{zm} + A'_{\perp m} E_{\perp m}) + \sum A'_{\perp' n} \vec{E}_{\perp' n}, \\ \vec{H} &= \sum B'_{\perp' m} \vec{H}_{\perp' m} + \sum_n (B'_{zn} H_{zn} + B'_{\perp n} \vec{H}_{\perp n}) \end{aligned}\right\} \tag{19}$$

and then from Maxwell's equations

$$\left.\begin{aligned} \operatorname{curl}_\perp \vec{E} - j\Gamma [\vec{z}_0, \vec{E}] &= -j \omega \overleftrightarrow{\mu}(r) \vec{H}, \\ \operatorname{curl}_\perp \vec{H} + j\Gamma [\vec{H}, \vec{z}_0] &= j \omega \overleftrightarrow{\varepsilon}(r) \vec{E} \end{aligned}\right\} \tag{20}$$

we may find the relation between the unknown coefficients in the form of six infinite systems of equations. However, it is even more convenient to use the expansions of the inductions $\vec{D} = \overleftrightarrow{\varepsilon}^{-1}(\vec{r})\vec{E}$ and $\vec{B} = \overleftrightarrow{\mu}^{-1}(\vec{r})\vec{H}$.

$$\left.\begin{aligned}\vec{D} &= \varepsilon_0 \sum_m (A_{zm}\vec{E}_{zm} + A_{\perp m}\vec{E}_{\perp m}) + \varepsilon_0 \sum_n A_{\perp' n}\vec{E}_{\perp' n},\\ \vec{B} &= \mu_0 \sum_m B_{\perp' m}\vec{H}_{\perp' m} + \mu_0 \sum_n (B_{zn}\vec{H}_{zn} + B_{\perp n}\vec{H}_{\perp n}),\end{aligned}\right\} \tag{21}$$

since in this case the number of infinite systems is reduced to four.

Thus, with a view to using expansion (21), let us proceed from Maxwell's equations, written for $\vec{D}$ and $\vec{B}$:

$$\left.\begin{aligned}\operatorname{curl}_\perp \overleftrightarrow{\varepsilon}^{-1}(\vec{r})\vec{D} - j\Gamma[\vec{z}_0, \overleftrightarrow{\varepsilon}^{-1}(\vec{r})\vec{D}] &= -j\omega\vec{B},\\ \operatorname{curl}_\perp \overleftrightarrow{\mu}^{-1}(\vec{r})\vec{B} + j\Gamma[\overleftrightarrow{\mu}^{-1}(\vec{r})\vec{B}, \vec{z}_0] &= j\omega\vec{D}.\end{aligned}\right\} \tag{22}$$

Taking the first of these equations, let us multiply all of its terms by H^*_{zk} and both sides of the complex-conjugate of Eq. (16) by $\overleftrightarrow{\varepsilon}^{-1}(\vec{r})\vec{D}$. Combining the results, and taking into account the identity

$$\vec{B}\operatorname{curl}_\perp \vec{A} - \vec{A}\operatorname{curl}_\perp \vec{B} = \operatorname{div}_\perp [\vec{A}, \vec{B}],$$

integrating over S_0 and using the two dimensional analog of the Ostrogradskiy-Gauss theorem, we find

$$\int_{L_0} [\overleftrightarrow{\varepsilon}^{-1}(\vec{r})\vec{D}, \vec{H}^*_{zk}]\vec{n}_0 dl = -j\omega \int_{S_0} \vec{B}\vec{H}^*_{zk}\, ds + j\frac{\chi_k^2}{\omega\mu_0}\int_{S_0} \vec{E}_{\perp' k}\overleftrightarrow{\varepsilon}^{-1}(\vec{r})\vec{D}\, ds \tag{23}$$

($\vec{n}_0$ is the unit normal to S_0).

Introducing here Eq. (21) and considering the properties of the medium of Eq. (1) as well as the orthonormalizations (6)-(9), we obtain

$$\begin{aligned}A_{\perp' k} = \sum_m A_{zm}\varepsilon_0 \int_S \vec{E}^*_{\perp' k}\Delta\overleftrightarrow{\varepsilon}_r^{-1}\vec{E}_{zm}\, ds + \sum_m A_{\perp m}\varepsilon_0 \int_S \vec{E}^*_{\perp' k}\Delta\overleftrightarrow{\varepsilon}_r^{-1}\vec{E}_{\perp m}\, ds +\\ + \sum_n A_{\perp' n}\varepsilon_0 \int_S \vec{E}^*_{\perp' k}\Delta\overleftrightarrow{\varepsilon}_r^{-1}\overleftrightarrow{E}_{\perp' n}\, ds = B_{zk}.\end{aligned} \tag{24}$$

Subsequent operations are similar. From the first line of Eq. (22) and of Eq. (17) we have the equality

$$\int_{L_0} [\overleftrightarrow{\varepsilon}(\vec{r})\vec{D}, \vec{H}^*_{\perp k}]\vec{n}_0 dl - j\frac{\Gamma\Gamma_k}{\omega\mu_0}\int_{S_0} \vec{E}^*_{\perp' k}\overleftrightarrow{\varepsilon}^{-1}(\vec{r})\vec{D}\, ds = -j\omega\int_{S_0} \vec{B}\vec{H}^*_{\perp k}\, ds, \tag{25}$$

which leads to

$$\begin{aligned}A_{\perp' k} + \sum_m A_{zm}\varepsilon_0 \int_S \vec{E}^*_{\perp' k}\Delta\varepsilon_r^{-1}\vec{E}_{zm}\, ds + \sum A_{\perp m}\varepsilon_0 \int_S \vec{E}^*_{\perp' k}\Delta\overleftrightarrow{\varepsilon}_r^{-1}\vec{E}_{\perp m}\, ds +\\ + \sum_n A_{\perp' n}\varepsilon_0 \int_S \vec{E}^*_{\perp' k}\Delta\overleftrightarrow{\varepsilon}_r^{-1}\vec{E}_{\perp' n}\, ds = \frac{\Gamma_k}{\Gamma}B_{\perp k}.\end{aligned} \tag{26}$$

From the first line of Eq. (22) and of Eq. (18) we have

$$\int_L [\overleftrightarrow{\varepsilon}^{-1}(\vec{r})\,\vec{D},\ \vec{H}^*_{\perp' k}]\,\vec{n}_0\,dl - j\omega\varepsilon_0\frac{\Gamma}{\Gamma_k}\int_{S_0}\vec{E}^*_{\perp k}\overleftrightarrow{\varepsilon}^{-1}(\vec{r})\,\vec{D}ds =$$

$$= -j\omega\int_{S_0}\vec{H}^*_{\perp' k}\vec{B}ds + j\omega\varepsilon_0\int_{S_0}\vec{E}^*_{zk}\overleftrightarrow{\varepsilon}^{-1}(\vec{r})\,\vec{D}ds, \tag{27}$$

whence

$$A_{zk} + \frac{k_0^2}{\chi_k^2}\Big\{\sum_m A_{zm}\varepsilon_0\int_S \vec{E}^*_{zk}\,\overleftrightarrow{\Delta\varepsilon}_r^{-1}\vec{E}_{zm}\,ds + \sum_m A_{\perp m}\varepsilon_0\int_S \vec{E}^*_{zk}\,\overleftrightarrow{\Delta\varepsilon}_r^{-1}\vec{E}_{\perp m}\,ds +$$

$$+\sum_n A_{\perp' n}\varepsilon_0\int_S \vec{E}^*_{zk}\,\overleftrightarrow{\Delta\varepsilon}_r^{-1}\vec{E}_{\perp' n}\,ds\Big\} + \frac{\Gamma\Gamma_k}{\chi_k^2}A_{\perp k} +$$

$$+\frac{\Gamma}{\Gamma_k}\frac{k_0^2}{\chi_k^2}\Big\{\sum_m A_{zm}\varepsilon_0\int_S \vec{E}^*_{\perp k}\,\overleftrightarrow{\Delta\varepsilon}_r^{-1}\vec{E}_{zm}\,ds + \sum_m A_{\perp m}\varepsilon_0\int_S \vec{E}^*_{\perp k}\,\overleftrightarrow{\Delta\varepsilon}_r^{-1}\vec{E}_{\perp m}\,ds +$$

$$+\sum_n A_{\perp' n}\varepsilon_0\int_S \vec{E}^*_{\perp k}\,\overleftrightarrow{\Delta\varepsilon}_r^{-1}\vec{E}_{\perp' n}\,ds\Big\} = \frac{k_0^2}{\chi_k^2}B_{\perp' k}. \tag{28}$$

In the same manner let us combine the second Maxwell equation (22) first with Eq. (13), then with Eq. (14) and, finally, with Eq. (15). We thus obtain the following three equations:

$$\frac{\chi_k^2}{\omega^2\varepsilon_0}\int_{S_0}\vec{H}^*_{\perp' k}\overleftrightarrow{\mu}^{-1}(\vec{r})\,\vec{B}ds = \int_{S_0}\vec{D}\vec{E}^*_z\,ds, \tag{29}$$

$$\frac{\Gamma\Gamma_k}{\omega^2\varepsilon_0}\int_{S_0}\vec{H}^*_{\perp' k}\overleftrightarrow{\mu}^{-1}(\vec{r})\,\vec{B}ds = \int_{S_0}\vec{D}\vec{E}^*_{\perp k}\,ds, \tag{30}$$

$$\frac{\Gamma}{\Gamma_k}\mu_0\int_{S_0}\vec{H}^*_{\perp k}\overleftrightarrow{\mu}^{-1}(\vec{r})\,\vec{B}ds = -\mu_0\int_{S_0}\vec{H}^*_z\overleftrightarrow{\mu}^{-1}(\vec{r})\,\vec{B}ds + \int_S \vec{D}\vec{E}^*_{\perp' k}\,ds. \tag{31}$$

From Eq. (29)-(31), as was done above, we obtain

$$B_{\perp' k} + \sum_n B_{zn}\mu_0\int_S \vec{H}^*_{\perp' k}\,\overleftrightarrow{\Delta\mu}_r^{-1}\vec{H}_{zn}\,ds + \sum_n B_{\perp n}\mu_0\int_S \vec{H}^*_{\perp' k}\,\overleftrightarrow{\Delta\mu}_r^{-1}\vec{H}_{\perp n}\,ds +$$

$$+\sum_m B_{\perp' m}\mu_0\int_S \vec{H}^*_{\perp' k}\overleftrightarrow{\Delta\mu}^{-1}\vec{H}_{\perp' m}\,ds = A_{zk}, \tag{32}$$

$$B_{\perp' k} + \sum_n B_{zn}\mu_0\int_S \vec{H}^*_{\perp' k}\,\overleftrightarrow{\Delta\mu}_r^{-1}\vec{H}_{zn}\,ds + \sum_n B_{\perp n}\mu_0\int_S \vec{H}^*_{\perp' k}\,\overleftrightarrow{\Delta\mu}_r^{-1}\vec{H}_{\perp n}\,ds +$$

$$+\sum_m B_{\perp' m}\mu_0\int_S \vec{H}^*_{\perp' k}\,\overleftrightarrow{\Delta\mu}_r^{-1}\vec{H}_{\perp' m}\,ds = \frac{\Gamma_k}{\Gamma}A_{\perp k}, \tag{33}$$

$$B_{zk} + \frac{k_0^2}{\chi_k^2}\Big\{\sum_n B_{zn}\mu_0\int_S \vec{H}^*_{zk}\,\overleftrightarrow{\Delta\mu}_r^{-1}\vec{H}_{zn}\,ds +$$

$$+\sum_n B_{\perp n}\mu_0\int_S \vec{H}^*_{zk}\,\overleftrightarrow{\Delta\mu}_r^{-1}\vec{H}_{\perp n}\,ds + \sum_m B_{\perp' m}\mu_0\int_S \vec{H}^*_{zk}\,\overleftrightarrow{\Delta\mu}_r^{-1}\vec{H}_{\perp' n}\,ds\Big\} + \tag{34}$$

$$+\frac{\Gamma\Gamma_k}{\chi_k^2}B_{\perp k} + \frac{\Gamma}{\Gamma_k}\frac{k_0^2}{\chi_k^2}\Big\{\sum_n B_{zn}\mu_0\int_S \vec{H}^*_{\perp k}\,\overleftrightarrow{\Delta\mu}_r^{-1}\vec{H}_{zn}\,ds +$$

$$+\sum_n B_{\perp n}\mu_0\int_S \vec{H}^*_{\perp k}\overleftrightarrow{\Delta\mu_r^{-1}}\vec{H}_{\perp n}\,ds+\sum_m B_{\perp' m}\mu_0\int_S \vec{H}^*_{\perp k}\overleftrightarrow{\Delta\mu_r^{-1}}\vec{H}_{\perp' m}\,ds\Big\}=\frac{k_0^2}{\chi_k^2}A_{\perp' k}.$$

Thus we have derived six relationships, Eqs. (24), (26), (28) and (32)-(34) relating the unknown coefficients A_{zm}, $A_{\perp m}$, $A_{\perp' n}$, B_{zn}, $B_{\perp n}$ and $B_{\perp' m}$. With a variation in the subscript k (k = 1, 2, 3, . . .) they give rise to six infinite systems of equations. Introducing for the sake of simplification the infinite-dimensional vectors

$$\begin{aligned}
A_1&=(A_{z1},\ A_{z2},\ A_{z3},\ \ldots),\\
A_2&=(A_{\perp 1},\ A_{\perp 2},\ A_{\perp 3},\ \ldots),\\
A_3&=(A_{\perp' 1},\ A_{\perp' 2},\ A_{\perp' 3},\ \ldots),\\
B_1&=(B_{z1},\ B_{z2},\ B_{z3},\ \ldots),\\
B_2&=(B_{\perp 1},\ B_{\perp 2},\ B_{\perp 3},\ \ldots),\\
B_3&=(B_{\perp' 1},\ B_{\perp' 2},\ B_{\perp' 3},\ \ldots),
\end{aligned}$$

we thus have

$$\left.\begin{aligned}
\|\mathfrak{E}^{11}_{ik}\|A_1+\|\mathfrak{E}^{12}_{ik}\|A_2+\|\mathfrak{E}^{13}_{ik}\|\ A_3&=B_1,\\
\|\mathfrak{E}^{21}_{ik}\|A_1+\|\mathfrak{E}^{22}_{ik}\|A_2+\|\mathfrak{E}^{23}_{ik}\|\ A_3&=B_2,\\
\|\mathfrak{E}^{31}_{ik}\|A_1+\|\mathfrak{E}^{32}_{ik}\|A_2+\|\mathfrak{E}^{33}_{ik}\|\ A_3&=B_3,\\
\|\mathfrak{M}^{11}_{ik}\|B_1+\|\mathfrak{M}^{12}_{ik}\|B_2+\|\mathfrak{M}^{13}_{ik}\|B_3&=A_1,\\
\|\mathfrak{M}^{21}_{ik}\|B_1+\|\mathfrak{M}^{22}_{ik}\|B_2+\|\mathfrak{M}^{23}_{ik}\|B_3&=A_2,\\
\|\mathfrak{M}^{31}_{ik}\|B_1+\|\mathfrak{M}^{32}_{ik}\|B_2+\|\mathfrak{M}^{33}_{ik}\|B_3&=A_3.
\end{aligned}\right\}\qquad(35)$$

The form of the matrices $\|\mathfrak{E}^{\alpha\beta}_{ik}\|$ and $\|\mathfrak{M}^{\alpha\beta}_{ik}\|$ is easily seen from Eqs. (24), (26), etc. Thus, for example,

$$\|\mathfrak{M}^{23}_{ik}\|=\Gamma\left\{[\Gamma_i^{-1}]+\left\|\Gamma_i^-\ \mu_0\int_S \vec{H}^*_{\perp' i}\overleftrightarrow{\Delta\mu_r^{-1}}\vec{H}_{\perp' k}\,ds\right\|\right\}$$

(not all of the matrices are written out).

3. DETERMINING THE PROPAGATION CONSTANT

As is seen from Eqs. (32) and (33) and, consequently, from Eqs. (24) and (26),

$$A_{zk}=\frac{\Gamma_k}{\Gamma}A_{\perp k}\qquad(36)$$

and

$$B_{zk}=\frac{\Gamma_k}{\Gamma}A_{\perp k},\qquad(37)$$

so that the number of independent vectors Γ reduces to four.

By means of Eqs. (36) and (37) let us eliminate vectors A_1 and B_1 from Eqs. (35). Thus there remain only four matrix equations

$$\left.\begin{aligned}
\|\widetilde{\mathfrak{E}}^{22}_{ik}\|A_2+\|\widetilde{\mathfrak{E}}^{23}_{ik}\|A_3&=B_2,\\
\|\widetilde{\mathfrak{E}}^{32}_{ik}\|A_2+\|\widetilde{\mathfrak{E}}^{33}_{ik}\|A_3&=B_3,\\
\|\widetilde{\mathfrak{M}}^{22}_{ik}\|B_2+\|\widetilde{\mathfrak{M}}^{23}_{ik}\|B_3&=A_2,\\
\|\widetilde{\mathfrak{M}}^{32}_{ik}\|B_2+\|\widetilde{\mathfrak{M}}^{33}_{ik}\|B_3&=A_3,
\end{aligned}\right\}\qquad(38)$$

wherein the elements of matrix $\|\widetilde{\mathfrak{E}}_{ik}^{\alpha\beta}\|$ have the form

$$\widetilde{\mathfrak{E}}_{ik}^{22} = \varepsilon_0 \int_S \vec{E}^*_{\perp' i} \overleftrightarrow{\Delta\varepsilon_r^{-1}} \vec{E}_{zk}\, ds + \frac{\Gamma}{\Gamma_i} \varepsilon_0 \int_S \vec{E}^*_{\perp' i} \overleftrightarrow{\Delta\varepsilon_r^{-1}} \vec{E}_{\perp k}\, ds,$$

$$\widetilde{\mathfrak{E}}_{ik}^{23} = \frac{\Gamma}{\Gamma_i}\left(\delta_{ik} + \varepsilon_0 \int_S \vec{E}^*_{\perp' i} \overleftrightarrow{\Delta\varepsilon_r^{-1}} \vec{E}_{\perp' k}\, ds\right),$$

$$\widetilde{\mathfrak{E}}_{ik}^{32} = \frac{\Gamma_i}{\Gamma} \frac{\chi_i^2 + \Gamma^2}{k_0^2} \delta_{ik} + \frac{\Gamma_i}{\Gamma} \varepsilon_0 \int_S \vec{E}^*_{zi} \overleftrightarrow{\Delta\varepsilon_r^{-1}} \vec{E}_{zk}\, ds + \varepsilon_0 \int_S \vec{E}^*_{zi} \overleftrightarrow{\Delta\varepsilon_r^{-1}} \vec{E}_{\perp k}\, ds +$$

$$+ \varepsilon_0 \int_S \vec{E}^*_{\perp i} \overleftrightarrow{\Delta\varepsilon_r^{-1}} \vec{E}_{zk}\, ds + \frac{\Gamma}{\Gamma_i} \varepsilon_0 \int_S \vec{E}^*_{\perp i} \overleftrightarrow{\Delta\varepsilon_r^{-1}} \vec{E}_{\perp k}\, ds,$$

$$\widetilde{\mathfrak{E}}_{ik}^{33} = \varepsilon_0 \int_S \vec{E}^*_{zi} \overleftrightarrow{\Delta\varepsilon_r^{-1}} \vec{E}_{\perp' k}\, ds + \frac{\Gamma}{\Gamma_i} \varepsilon_0 \int_S \vec{E}^*_{\perp i} \overleftrightarrow{\Delta\varepsilon_r^{-1}} \vec{E}_{\perp' k}\, ds,$$

and those of $\widetilde{\mathfrak{M}}_{ik}^{\alpha\beta}$ are obtained from $\widetilde{\mathfrak{E}}_{ik}^{\alpha\beta}$ by replacing $\vec{E}$ (with appropriate subscripts) with $\vec{H}$ (with the same subscripts), ϵ_0 with μ_0 and $\overleftrightarrow{\Delta\varepsilon_r^{-1}}$ with $\overleftrightarrow{\Delta\mu_r^{-1}}$.

It is not difficult to eliminate all but one of the vectors in Eq. (38). With B_2 remaining, let us write the following matrix equation:

$$\{\|\widetilde{\mathfrak{E}}_{ik}^{22}\|\,\|\widetilde{\mathfrak{M}}_{ik}^{22}\| + \|\widetilde{\mathfrak{E}}_{ik}^{23}\|\,\|\widetilde{\mathfrak{M}}_{ik}^{32}\| - 1\}\, B_2 - \{\|\widetilde{\mathfrak{E}}_{ik}^{22}\|\,\|\widetilde{\mathfrak{M}}_{ik}^{23}\| + \|\widetilde{\mathfrak{E}}_{ik}^{23}\|\,\|\widetilde{\mathfrak{M}}_{ik}^{33}\|\} \times$$
$$\times \{\|\widetilde{\mathfrak{E}}_{ik}^{32}\|\,\|\widetilde{\mathfrak{M}}_{ik}^{23}\| + \|\widetilde{\mathfrak{E}}_{ik}^{33}\|\,\|\widetilde{\mathfrak{M}}_{ik}^{33}\| - 1\}^{-1} \{\|\widetilde{\mathfrak{E}}_{ik}^{32}\|\,\|\widetilde{\mathfrak{M}}_{ik}^{22}\| + \|\widetilde{\mathfrak{E}}_{ik}^{33}\|\,\|\widetilde{\mathfrak{M}}_{ik}^{32}\|\} \qquad (39)$$

or, more briefly,

$$\|G_{ik}\|\, B_2 = 0. \qquad (39a)$$

The equation for the propagation constant Γ is obtained by setting the determinant of this matrix to zero:

$$\begin{vmatrix} G_{11} & G_{12} & G_{13} \ldots \\ G_{21} & G_{22} & G_{23} \ldots \\ \ldots & \ldots & \ldots \\ \ldots & \ldots & \ldots \end{vmatrix} = 0. \qquad (40)$$

CONCLUSION

Compared with the problem of the waveguide transformer [3], the problem of the waveguide with a regular anisotropic region discussed herein is more abstract. This, however, does not exclude the practical significance of the results obtained, for computations may in a number of cases prove considerably less laborious than for the problem in Ref. 3. It is particularly easy to determine the propagation constants of waveguides completely filled with an anisotropic (e.g., gyromagnetic) medium.

LITERATURE

1. V.V. Hikol'skiy. Investigation of cavity systems with anisotropic regions by the eigenfunction method. Part I, Cavity Resonator. Radio Engineering and Electronics, 1960, 5, 11, 1802.
2. G.V. Kisun'ko, Electrodynamics of cavity systems, Izd. VKAS, 1949.
3. V. V. Nikol'skiy, Investigation of cavity systems with anisotropic regions by the eigenfunction method. Part II, Waveguide transformer. Radio Engineering and Electronics, 1960, 5, 12, 1960.

Submitted to the editors 13 May 1960

ERRATA

1. Throughout the paper (parts I-III) the problem has been formulated in Maxwell's equations. It is more convenient (particularly in Part I) to take as a basis one of the second-order equations, e.g.,

$$L\vec{D} = \omega^2\vec{D}, \quad L \equiv \mathrm{curl}\overleftrightarrow{\mu}^{-1}(\vec{r})\,\mathrm{curl}\overleftrightarrow{\varepsilon}^{-1}(\vec{r}) \tag{1}$$

or

$$M\vec{B} = \omega^2\vec{B}, \quad M \equiv \mathrm{curl}\overleftrightarrow{\varepsilon}^{-1}(\vec{r})\,\mathrm{curl}\overleftrightarrow{\mu}^{-1}(\vec{r}). \tag{1a}$$

Then the elements of the matrices $\|\mathfrak{E}_{kn}\|$ and $\|\mathfrak{M}_{kn}\|$ in Part I Eq. (10') assume the simple form:

$$\mathfrak{E}_{kn} = \varepsilon_0 \int_{V_0} \vec{E}_k^* L\vec{E}_n\, dv \text{ and } \mathfrak{M}_{kn} = \mu_0 \int_{V_0} \vec{H}_k^* M\vec{H}_n\, dv. \tag{2}$$

2. In the expansion of the vector $\vec{B}$ in Part II, in accordance with Gubo's theorem (Part I, Ref. 13), it was necessary, in addition to the rotational functions, to take the potential functions ($B_n \neq 0$ at $S\Sigma$!). The need for this was called to the author's attention by V.G. Sukhov. In inserting the corrections it is necessary to consider that in Eq. (2) of Part II among the $\vec{H}_{k'}$ there are also those ($k = k'$) for which $\mathrm{curl}\,\vec{H}_{k'} = 0$, which is equivalent to the requirement $\omega_{k'} = 0$ in Eq. (2). Then, instead of Eq. (2) of Part II, we have

$$\left.\begin{aligned} \{[\omega_k] + \|\omega_k \vartheta_{kn}\|\}\, A &= \omega B - jF, \\ \{[\omega_k] + \|\omega_k M_{kn}\|\}\, B &= \omega A - j\frac{1}{\omega}\|\omega_k M_{kn'}\|\, F' \end{aligned}\right\}, \quad B' = \frac{j}{\omega}F' \tag{3}$$

(the prime indicates that the expression deals with a totational function rather than a potential function).

In using the results of Part II it is necessary to proceed from the corrected Eqs. (3) or in Eq. (6) of Part II to consider only Eq. (5) of the same part.

Nor is it difficult to obtain the shorter formulation of the auxiliary problem of excitation in Part II on the basis of one of the second-order equations. The differential operator of Eq. (1) or (1a) is transformed so that the surface integral may be isolated. In essence, both $\vec{B}$ and $\vec{D}$ are expanded into magnetic functions. The corresponding results are not written out here.

UNIDIRECTIONAL PROPAGATION OF WAVES IN A HELICAL WAVEGUIDE PLACED IN A FERRITE MEDIUM

B.M. Bulgakov, V.P. Shestopalov, L.A. Shishkin and I.P. Yakimenko

We investigated the propagation of electromagnetic waves in a helical waveguide placed in a ferrite medium when a constant magnetic field was applied along the axis of the system. We determined the attenuation factor and made numerical calculations of the attenuation for forward and backward waves.

INTRODUCTION

The survey [1] points out that if a helix is surrounded by a ferrite medium and a constant magnetic field H_0 is applied along the axis of the system, it is reasonable to expect a considerable gyromagnetic effect in this system. It is also pointed out that "no theoretical explanations have been offered for this effect so far." At the same time, the directivity coefficient (ratio of backward attenuation to forward attenuation) for this system has been found experimentally to be equal to 6:1. The authors of Ref. 2 believe that this directivity coefficient is considerably greater than would follow from elementary theory, which defines the degree of directivity as a function of the eccentricity of an ellipse described by the fector of the magnetic field in the plane perpendicular to the constant magnetic field. It is rightly assumed in Ref. 2 that the discrepancy between the experimental results and the elementary theory is due to the effect of magnetic permeability of the ferrite on the eccentricity of the ellipses described by the magnetic vectors.

The electrodynamic solution of this problem should, of course, yield the correct value of the directivity factor. The problem of the propagation of waves along a helical system in a ferrite medium with logitudinal magnetization is solved by the authors of Ref. 3 for an ideal case in which there are neither dielectric nor magnetic losses in the medium. They show that the phase velocities of forward and backward waves differ from each other; the smaller the cotangent of the pitch angle, the greater is this difference.

This article studies the propagation of waves in a helical waveguide when imposed in an actual ferrite medium possessing both dielectric and magnetic losses of a ferroresonant nature. The calculations clearly demonstrate the possibility of obtaining fairly large directivity factors in the system under consideration (up to 8:1), and this fact can be effectively applied in designing ferrite attenuators in travelling wave tube amplifiers.

1. THE DISPERSION EQUATION AND ITS SOLUTION WHEN LOSSES ARE SMALL

If the system under investigation consists of a helical waveguide (helix radius R, pitch angle Θ), inside a ferrite casing of infinite thickness, its dispersion equation, as shown in Ref. 3 (the case of a longitudinal exciting field), can be represented as:

$$f_1 = f_2 + f_3, \tag{1}$$

in which

$$\begin{aligned}
f_1 &= y^2\left\{1 + \frac{K_0(|y|/\sqrt{\mu})\,I_1(|y|)}{K_1(|y|/\sqrt{\mu})\,I_0(|y|)}\right\}\frac{I_0(|y|)\,K_0(|y|)}{I_1(|y|)\,K_1(|y|)};\\
f_2 &= x^2\operatorname{ctg}^2\Theta\left\{\varepsilon + \frac{I_1(|y|)\,K_0(|y|)}{I_0(|y|)\,K_1(|y|)}\right\};\\
f_3 &= -2\varepsilon\frac{x^2\varkappa}{\mu-1}\operatorname{ctg}\Theta\left\{1 - \frac{I_0(|y|/\sqrt{\mu})\,K_1(|y|)}{K_1(|y|/\sqrt{\mu})\,K_0(|y|)}\right\}\frac{K_0(|y|)}{K_1(|y|)}\operatorname{sign} y;\\
x &= \frac{\omega}{c}R = kR;\quad y = \frac{\omega}{v_\Phi}R = \beta R,\quad \operatorname{sign} y = \begin{cases}+1, & y>0,\\ -1, & y<0\end{cases}
\end{aligned} \tag{2}$$

(ω is the angular frequency of the signal, k is the wavenumber in free space; v_Φ is the phase velocity of the wave; c is the speed of light in vacuum; ϵ is the dielectric constant; μ and $\varkappa$ are the components of the magnetic permeability tensor).

Equation (1) is valid for the case of very slow waves and in the frequency region determined by the inequality

$$\frac{y^2}{x^2}\sigma^2 \gg 4\varepsilon \tag{3}$$

($\sigma = \omega_0/\omega$; ω_0 is the resonant frequency). The case of large slowdown implies the condition

$$y^2 \gg x^2\varepsilon\mu. \tag{4}$$

is satisfied. Since Eq. (1) is taken in this article as the initial dispersion equation, all further results will be valid provided conditions (3) and (4) are assumed to hold.

Equation (1) is derived on the assumption that there are no dielectric or magnetic losses. When there are losses in the system, the dispersion equation maintains its general form as in Eq. (1), but $\mu, \varkappa, \epsilon$ and y have complex values:

$$\mu = \mu' + i\mu''; \quad \varkappa = \varkappa' + i\varkappa''; \quad \varepsilon = \varepsilon' + i\varepsilon''; \quad y = y' + iy''. \tag{5}$$

The values μ and $\varkappa$ may be obtained from the equation for the motion of the magnetic moment [4]

$$\frac{d\vec{M}}{dt} = \gamma [\vec{M}, \vec{H}] - \frac{\alpha\gamma}{M} [\vec{M} [\vec{M}, \vec{H}]], \tag{6}$$

where γ is the gyromagnetic ratio; $\alpha = \Delta H/2H_{res}$ is the parameter calculated from the width of the resonant curve (ΔH is the width of the curve at the level $\mu'' = \mu''_{res}/2$). If the variable components in the magnetic field are small compared with the axially-directed constant field, and if the variable field has a harmonic time dependence of the form exp (—iωt), then

$$\mu' - 1 = \frac{\left(1 - \frac{x^2}{u^2}\right) + 2\frac{x^2}{u^2}\alpha^2}{\left(1 - \frac{x^2}{u^2}\right)^2 + 4\frac{x^2}{u^2}\alpha^2} \frac{v}{u}; \qquad \mu'' = \frac{\frac{vx}{u^2}\left(1 + \frac{x^2}{u^2}\right)\alpha}{\left(1 - \frac{x^2}{u^2}\right)^2 + 4\frac{x^2}{u^2}\alpha^2};$$

$$\varkappa' = \frac{\frac{vx}{u^2}\left(\frac{x^2}{u^2} - 1\right)}{\left(1 - \frac{x^2}{u^2}\right)^2 + 4\frac{x^2}{u^2}\alpha^2}; \qquad \varkappa'' = \frac{2\frac{vx^2}{u^3}\alpha}{\left(1 - \frac{x^2}{u^2}\right)^2 + 4\frac{x^2}{u^2}\alpha^2}, \tag{7}$$

where $u = \frac{\gamma H_0}{c} R$, $v = \frac{4\pi\gamma M}{c} R$, are dimensionless parameters (M is the intensity of magnetization at the saturation point; H_0 is the constant field in the ferrite).

Typical resonance curves for μ' and μ'' are shown in Fig. 1. It is clear from these curves that at frequencies near the resonant frequency, μ'' may become equal to μ', or even exceed it. This article deals with a case in which there are small losses, for which the following inequalities are valid:

$$\mu'' \ll \mu'; \quad \varkappa'' \ll \varkappa'; \quad \varepsilon'' \ll \varepsilon'; \quad y'' \ll y'. \tag{8}$$

Thus, conditions (8) are added to conditions (3) and (4). When the values of cotangent Θ are fairly high, all these limiting conditions can be reduced to the fact that the results cannot be used at frequencies too close to resonant frequencies for cotangent Θ = 10 at frequencies greater than 0.95 ω_0).

If the conditions in (8) are satisfied, all the functions contained in Eq. (1) can be expanded into a Taylor series:

$$f_1 = f_1' + if_1''; \quad f_2 = f_2' + if_2''; \quad f_3 = f_3' + if_3'', \tag{9}$$

in which

$$f_1' = f_1(y', \zeta'); \quad f_2' = f_2(y', \varepsilon'); \quad f_3' = f_3(y', \varkappa', \varepsilon', \zeta');$$

$$f_1'' = y'' \frac{\partial f_1'}{\partial y'} + \zeta'' \frac{\partial f_1'}{\partial \zeta'}; \quad f_2'' = y'' \frac{\partial f_2'}{\partial y'} + \varepsilon'' \frac{\partial f_2'}{\partial \varepsilon'}; \tag{10}$$

$$f_3'' = y'' \frac{\partial f_3'}{\partial y'} + \varkappa'' \frac{\partial f_3'}{\partial \varkappa'} + \varepsilon'' \frac{\partial f_3'}{\partial \varepsilon'} + \zeta'' \frac{\partial f_3'}{\partial \zeta'},$$

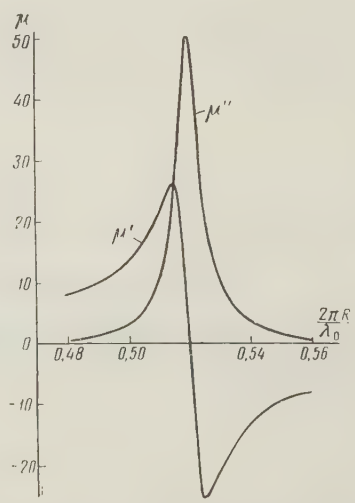

Fig. 1. μ as function of parameter $2\pi R/\lambda_0$ at v = 0.52, u = 0.52, and $\alpha = 10^{-2}$

and the dispersion equation (1) takes the form

$$f'_1 + if''_1 = f'_2 + if''_2 + f'_3 + if''_3. \tag{11}$$

Equating the real parts in Eq. (11), we obtain

$$f'_1 = f'_2 + f'_3, \tag{12}$$

which coincides with the dispersion equation (1) for the case of no losses. Equating the imaginary parts in Eq. (11) gives the attenuation factor for the system

$$y'' = \frac{\varepsilon''\left(\frac{\partial f'_2}{\partial \varepsilon'} + \frac{\partial f'_3}{\partial \varepsilon'}\right) + \zeta''\left(\frac{\partial f'_3}{\partial \zeta'} - \frac{\partial f'_1}{\partial \zeta'}\right) + \varkappa''\frac{\partial f'_3}{\partial \varkappa'}}{\frac{\partial f'_1}{\partial y'} - \frac{\partial f'_2}{\partial y'} - \frac{\partial f'_3}{\partial y'}}. \tag{13}$$

Let us first consider a case in which the Bessel functions can be replaced by their asymptotic values (large values of the arguments of the Bessel functions). This is the case when $R \to \infty$ (the cylindrical helical waveguide becomes an anisotropically conducting plane, i.e., a plane helix) or when the frequency of the signal is very high. The functions f'_1, f'_2, and f'_3, will then have the following form:

$$f'_1 = y'^2(1+\zeta'); \; f'_2 = (\varepsilon'+1)x^2 \operatorname{ctg}^2\Theta; \; f'_3 = -2\varepsilon' x^2 \operatorname{ctg}\Theta \frac{\varkappa'\zeta'^2}{1+\zeta'} \operatorname{sign} y. \tag{14}$$

Substituting Eq. (14) into Eq. (13), we find

$$y'' = \frac{1}{2y'(1+\zeta')}\left\{\varepsilon'' x^2 \operatorname{ctg}^2\Theta\left[1 - \frac{2\varkappa'\zeta'^2}{(1+\zeta')\operatorname{ctg}\Theta}\operatorname{sign} y\right] + \right.$$
$$\left. + \zeta''\left[y'^2 + \frac{2x^2\zeta'\varkappa'\varepsilon'(2+\zeta')}{(1+\zeta')^2}\operatorname{sign} y\right] - \frac{2\varkappa''\varepsilon'\zeta'^2 x^2 \operatorname{ctg}\Theta}{1+\zeta'}\operatorname{sign} y\right\}, \tag{15}$$

in which

$$\zeta' = 1/\sqrt{\mu}; \; \zeta'' = \mu''/2\mu'\sqrt{\mu'}.$$

In a general case we have to use the functions f'_1, f'_2, and f'_3 in the form of Eq. (10). By substituting Eq. (10) into Eq. (13) and making the corresponding transformations, we obtain an expression for the loss factor in the form

$$y'' = \frac{\varepsilon'' x^2 \operatorname{ctg}^2\Theta(1-\varkappa' A) - \varkappa'' x^2 \operatorname{ctg}^2\Theta\varepsilon' A + }{y'^2 B - x^2 \operatorname{ctg}^2\Theta C + 2\varepsilon' x^2 \operatorname{ctg}\Theta \frac{\varkappa'\zeta'^2}{1-\zeta'^2} D}$$
$$\frac{+\zeta''\left[\zeta' y'^3 \frac{K_0}{K_1}\Phi + \frac{2\varkappa'\varepsilon' x^2 \operatorname{ctg}\Theta}{1-\zeta'^2}\left(\frac{A\operatorname{ctg}\Theta}{\zeta'} - \zeta' y'\Phi \operatorname{sign} y\right)\right]}{y'^2 B - x^2 \operatorname{ctg}^2\Theta C + 2\varepsilon' x^2 \operatorname{ctg}\Theta \frac{\varkappa'\zeta'^2}{1-\zeta'^2} D}, \tag{16}$$

in which

$$A = \frac{2\zeta'^2 \operatorname{tg}\Theta}{1-\zeta'^2}\left(\frac{K_0}{K_1} - \frac{K'_0}{K'_1}\zeta'\right)\operatorname{sign} y; \; C = \frac{(I_1K_0 + I_0K_1)(I_0K_0 - I_1K_1)}{I_0^2K_1^2};$$

$$B = \frac{K_1K_0(I_1^2 - I_0I_2) + I_1I_0(K_0K_2 - K_1^2)}{I_1^2K_1^2} +$$
$$+ \zeta'\frac{K'_0K'_1(K_0K_2 - K_1^2) + \zeta' K_0K_1(K'_0K'_2 - K'^2_1)}{K_1^2K'^2_1}; \tag{17}$$

$$D = \left\{K_1^{-2}\left(\frac{1}{y'}K_0K_1 + K_0^2 - K_1^2\right) - \zeta'^2K_1'^{-2}\left(\frac{1}{\zeta' y'}K_0'K_1' + K_1'^2 - K_2'^2\right)\right\} \operatorname{sign} y;$$

$$\Phi = \frac{K_0'K_2' - K_1'^2}{K_1'^2}$$

(The primed Bessel functions have arguments equal to $|y'|/\sqrt{\mu'}$, while the remaining unprimed ones have arguments equal to $-|y'|$).

If we use the asymptotic values of the Bessel functions when the values of their arguments are large, we obtain the following for A, B, C, D, and Φ in Eq. (17):

$$A = \frac{2\zeta'^2 \operatorname{sign} y}{(1+\zeta')\operatorname{ctg}\Theta};\ B = \frac{2(1+\zeta')}{y'};\ C = O\left(\frac{1}{y'}\right) \to 0;$$
$$D = O\left(\frac{1}{y'}\right) \to 0;\ \Phi = \frac{1}{\zeta' y'}. \tag{18}$$

After substituting Eq. (18) into Eq. (16) we obtain, as expected, formula (15), which determines the attenuation factor for a flat helix.

As $H_0 \to 0$, when the ferrite is demagnetized, $\varkappa' \to 0$, $\varkappa'' \to 0$, $\mu'' \to 0$, $\xi \to 1$, and from Eq. (16) we have

$$y'' = \varepsilon''\left\{\frac{y'^2}{x^2\operatorname{ctg}^2\Theta}\left[\frac{K_0}{I_1^2K_1}(I_1^2 - I_0I_2) + \frac{K_0}{K_1^3}(K_0K_2 - K_1^2)\right] + \right.$$
$$\left. + \frac{y'(K_0K_2 - K_1^2)}{I_1K_1^3x^2\operatorname{ctg}^2\Theta} - \frac{(I_1K_0 + I_0K_1)(I_0K_0 - I_1K_1)}{I_0^2K_1^2}\right\}^{-1} \tag{19}$$

The dispersion equation of the system for the case under consideration is

$$\frac{y'^2}{x^2\operatorname{ctg}^2\Theta} = \frac{I_1K_1}{I_0K_0}(I_1K_0 + \varepsilon' I_0K_1). \tag{20}$$

Substituting Eq. (20) into Eq. (19), after a series of transformations we obtain

$$y'' = \varepsilon''\left\{\left(\frac{K_0}{I_0^2K_1} + \frac{y'^2}{x^2\operatorname{ctg}^2\Theta}\frac{K_0}{I_1^2K_0}\right)(I_1^2 - I_0I_2) + \right.$$
$$\left. + \left(\frac{\varepsilon'}{K_0K_1} + \frac{y'^2}{x^2\operatorname{ctg}^2\Theta}\frac{K_0}{K_1^3}\right)(K_0K_2 - K_1^2)\right\}^{-1},$$

which coincides exactly with the expression for the attenuation in the system consisting of the helix plus dielectric obtained in Ref. 5 (taking into account the fact that the dielectric is inside the helix).

2. DETERMINING THE ATTENUATION FACTOR BY THE ENERGY METHOD

The attenuation of electromagnetic waves propagating through the system due to the medium can also be determined by calculating the losses in the medium and the total power flux along the axis of the system, using the relationship

$$y'' = \frac{\overline{P}_{el} + \overline{P}_m}{2P_\Sigma}, \tag{21}$$

in which

$$P_\Sigma = \frac{c}{8\pi}\int_S [\vec{E}, \vec{H}^*]_z\, ds \tag{22}$$

(P_Σ is the total power flux along the axis; $\vec{E}$ and $\vec{H}$ are the vectors of the electric and magnetic fields; S is the surface enclosing volume V); and

$$\bar{P}_{el} = \int_V \bar{p}_{el} dv; \quad \bar{p}_{el} = \frac{\omega \varepsilon''}{8\pi} |\vec{E}|^2 \tag{23}$$

($\bar{p}_{el}$ is the density of electric losses at the given single frequency ω);

$$\bar{P}_m = \int_V \bar{p}_m \, dv, \tag{24}$$

$$\bar{p}_m = \frac{\omega \mu''}{8\pi} (|H_\varphi|^2 + |H_r|^2) + \frac{\omega \varkappa''}{4\pi} (H_{r2} H_{\varphi 1} - H_{r1} H_{\varphi 2}) \tag{25}$$

($\bar{p}_m$ is the density of the magnetic losses at the single frequency ω; $H_r = H_{r1} + iH_{r2}$; $H_\varphi = H_{\varphi 1} + iH_{\varphi 2}$ in a general case). The total power flux along the axis of the system [1] is expressed as follows:

$$P_\Sigma = \frac{cx}{8y'} R^2 E_0^2 \frac{I_0^2}{K_0^2} F(m, \operatorname{ctg}\Theta, \varepsilon', \varkappa', \mu'), \tag{26}$$

in which

$$F = (I_1^2 - I_0 I_2) \left(m^2 \frac{K_0^2}{I_1^2} \operatorname{tg}^2 \Theta + \frac{K_0^2}{I_0^2} \right) + \frac{m^2 \Pi^2}{\mu'} \left(\frac{K_0' K_2'}{K_1'^2} - 1 \right) +$$
$$+ \varepsilon' (K_0 K_2 - K_1^2) + \frac{2\varepsilon' \varkappa' \Pi}{y' (\mu' - 1) K_1'} \left(K_1' K_0 - \frac{K_0' K_1}{\sqrt{\mu'}} \right) \operatorname{sign} y; \tag{27}$$

$$\Pi^2 = \frac{\varepsilon' \varkappa' K_1}{m^2 (\mu' - 1)} \operatorname{sign} y - K_0 \operatorname{tg}\Theta; \; m = \frac{y'}{x}.$$

As in expressions (17), the primed Bessel functions have arguments $|y'|/\sqrt{\mu'}$, while those without a prime have arguments $-|y'|$.

The field components in Eq. (23), according to Ref. 1, can be expressed in the following way

$$E_r = i \left(\frac{\Pi}{\sigma K_1'} K_{1r}' + K_{1r} \right) \frac{I_0}{K_0} E_0 \operatorname{sign} y;$$
$$E_\varphi = \frac{\varepsilon'}{m^2 \sigma} \left(\frac{m^2 \sigma \Pi}{\varepsilon' K_1'} K_{1r}' - K_{1r} \right) \frac{I_0}{K_0} E_0 \operatorname{sign} y;$$
$$E_z = \left(\frac{\Pi}{\sigma \sqrt{\mu'} K_1'} K_{0r}' + K_{0r} \right) \frac{I_0}{K_0} E_0; \tag{28}$$
$$H_\varphi = i \frac{\varepsilon'}{m} \left(\frac{\Pi}{\sigma K_1'} K_{1r}' + K_{1r} \right) \frac{I_0}{K_0} E_0 \operatorname{sign} y;$$
$$H_r = -\frac{\varepsilon'}{m\sigma} \left(\frac{m^2 \sigma \Pi}{\varepsilon' \mu' K_1'} K_{1r}' - K_{1r} \right) \frac{I_0}{K_0} E_0 \operatorname{sign} y$$

(the Bessel functions with the subscript r have an argument which is a function of the current radius r).

Substituting Eqs. (23) through (27) into Eq. (21) we obtain

$$\nu'' = \frac{\int_0^R [\varepsilon'' |\vec{E}|^2 + \mu'' (|H_\varphi|^2 + |H_r|^2) + 2\varkappa'' (H_{r2} H_{\varphi 1} - H_{r1} H_{\varphi 2})] \, r \, dr}{\frac{R^2 E_0^2}{|y'|} \frac{I_0^2}{K_0^2} F}. \tag{29}$$

Finally, after substituting the field components from Eq. (28) into Eq. (29), we can determine the attenuation factor

$$y'' = \frac{K_0 K_1}{x^2 \operatorname{ctg}^2 \Theta F} \left\{ \varepsilon'' x^2 \operatorname{ctg}^2 \Theta (1 - \varkappa' A) - \varkappa'' x^2 \operatorname{ctg}^2 \Theta \varepsilon' A + \right.$$

$$+\zeta''\left[\zeta' y'^3 \frac{K_0}{K_1}\Phi + \frac{2\varkappa'\varepsilon' x^2 \operatorname{ctg}\Theta}{1-\zeta'^2}\left(\frac{A\operatorname{ctg}\Theta}{\zeta'} - \zeta'^3 y'\Phi \operatorname{sign} y\right)\right]\Bigg\} \tag{30}$$

(when deriving Eq. (23) the second order terms were discarded, in accordance with Eqs. (3) and (4).

After certain transformations the expression for y'', of Eq. (30), can be reduced exactly to the form of Eq. (16).

Thus, the formulas for the attenuation factor, Eqs. (16) and (30), obtained by the two methods, coincide exactly. Before going on to a quantitative analysis of the relationships we should make one important comment. It is easy to see that the possibility of obtaining $y'' < 0$ for a forward wave (sign y = 1) follows from Eq. (15).

Indeed, if

$$y'^2 = -2x^2 \operatorname{ctg}\Theta \frac{\zeta'\varepsilon'\varkappa'(2+\zeta')}{(1+\zeta')^2} \tag{31}$$

and

$$2\varkappa'' x^2 \operatorname{ctg}\Theta \frac{\varepsilon'\zeta'^2}{1+\zeta'} > \varepsilon'' x^2 \operatorname{ctg}^2\Theta\left[1 - \frac{2\varkappa'\zeta'^2}{(1+\zeta')\operatorname{ctg}\Theta}\right], \tag{32}$$

then $y'' < 0$.

It follows from the dispersion equation for the system under consideration that Eq. (31) can be satisfied, for example, for cotangent $\Theta = 10$ at frequencies $= 0.9\,\omega_0$. The inequality (32) is also satisfied at these frequencies (on account of the great increase in $\varkappa''$ according to Eq. (7), whereas $\epsilon'' = \text{const.}$). But if $y'' < 0$, this implies an amplification of the forward wave, which in the given case has no physical meaning. In order to explain the result obtained, let us turn to the limiting conditions (3) and (4). For a case in which μ, $\varkappa$, and ϵ are complex, conditions (3) and (4) are expressed by the following four inequalities:

$$y'^2 \gg x^2\varepsilon\mu';\ y'^2 \gg \frac{4x^2\varepsilon'}{\sigma^2};\ 2y'y'' \gg x^2(\varepsilon'\mu'' + \mu'\varepsilon'');\ 2y'y'' \gg \frac{4x^2\varepsilon''}{\sigma^2}. \tag{33}$$

The first two inequalities (33) are definitely satisfied at the frequencies and time delays which we are considering; the other two inequalities in (33) cannot hold for $y'' \leqslant 0$. Hence, when obtaining the dispersion equation for the field components and power flux of this system, $x^2\epsilon\mu$ compared with y'^2 is significant and cannot be discarded. It can be shown that if we only use the first two inequalities (33) when deriving the dispersion equation, and consider that the other two inequalities (33) are not satisfied in the general case, the real part of the dispersion equation takes the form of Eq. (12), while the imaginary part is slightly changed, leading to a different value

$$y'' = \frac{\varepsilon'' L + \varkappa'' Q + \mu'' T}{2y'\left(1 + \frac{1}{\sqrt{\mu'}}\right)}, \tag{34}$$

in which

$$L = x^2 \operatorname{ctg}^2\Theta\left[1 - 2\operatorname{tg}\Theta\left(1 - \frac{1}{\sqrt{\mu'}}\right)\frac{x}{u}\operatorname{sign} y\right];$$

$$Q = -\frac{2\varepsilon' x^2 \operatorname{ctg}\Theta}{\mu'\left(1 + \frac{1}{\sqrt{\mu'}}\right)}\operatorname{sign} y;\quad T = T_1 + \delta; \tag{35}$$

$$T_1 = \frac{1}{\mu'\sqrt{\mu'}}\left[y'^2 - 2x^2 \operatorname{ctg}\Theta\left(\frac{2\sqrt{\mu'}}{1 + \frac{1}{\sqrt{\mu'}}} - 1\right)\varepsilon'\frac{x}{u}\operatorname{sign} y\right];$$

$$\delta = 2x^2\varepsilon'\left(1 - \frac{1}{\sqrt{\mu'}}\right).$$

Comparing Eq. (34) with Eq. (15) we note that L, Q and T coincide with the corresponding terms in Eq. (15), and δ is an added term not previously taken into account. It can now be shown, using the dispersion equation (12), that there cannot be any zero or negative values of y''.

Equation (34) is more exact than Eq. (15) for calculating the attenuation factor; it is valid for all frequencies at which the first two inequalities in (33) are valid. As resonance is approached, Eq. (15) becomes invalid before Eq. (34) does. Hence, from here on in the quantitative analysis of the attenuation of forward and backward waves, Eq. (34) will be used for y".

We should also point out that up to now in our arguments we have not taken into account losses in the helix; this can be done in the same way as in Ref. 5. The losses in the helix calculated in Ref. 5 were of the order of 10^{-3}. hence their influence as resonance is approached is small.

3. ANALYSIS OF RESULTS

As an illustration let us consider a number of calculations which suggest certain conclusions regarding the nature of the propagation of forward and backward waves in the system. Let us determine the attenuation factor y" for a number of values of the constant magnetic field H_0 characterized by $u = \gamma H_0 R/c$; the intensity of the magnetization of the ferrite M proportional to $v = 4\pi\gamma MR/c$; the dielectric constant of the ferrite; the attenuation factor α and two values of cotangent Θ (10 and 20).

At the frequencies and values of cotangent Θ for which we are performing the calculation there is no need to use the rather complex formula (16), since Eq. (34) gives fairly accurate results (i.e., all the theoretical cases approach a high frequency case). Hence, all the calculations are made on the basis of Eq. (34) using the tensor components μ_{ik} determined in accordance with Eq. (7). Since for the losses determined by condition (8) the dispersion equation for calculating y' maintains the same form as in the case of an ideal ferrite, the values of y' in (34) will be taken from the relevant graphs in Ref. 3.

The theoretical curves are given in Figs. 2 - 5. They determine the attenuation of forward and backward waves for two magnetic fields (u = 0.56 and u = 0.19), two magnetization intensities (v = 0.52 and v = 0.19), two values of the imaginary part of the dielectric constance ($\epsilon'' = 10^{-2}$ and $\epsilon'' = 10^{-1}$; $\epsilon' = 10$), and two parameters α ($\alpha = 10^{-3}$ and $\alpha = 10^{-2}$).

We should point out that the curves in Figs. 2a - 5a may also be used to calculate the attenuation at $\alpha = 10^{-2}$ and $\epsilon' = 10^{-1}$. Here all that needs to be done, as follows from Eq. (34), is to multiply the ordinates in the corresponding graphs by 10.

Analysis of the curves in Figs. 2 - 5 suggests the following:

1. Waves propagated in the system in the direction +z (forward waves) and in the direction -z (backward waves) have a different attenuation factor. The difference between the attenuation in a forward and backward direction increases as we approach the resonant frequency and may attain extremely high values (for example, at cotangent $\Theta = 10$, u = 0.52, v = 0.19; at x = 0.5 the ratio of backward to forward attenuation is 7.7 (Fig. 2c). The directivity factor may attain a maximum, and then decrease (for the given example the factor drops from 7.7 to 4.5 for a variation in x from 0.5 to 0.51).

2. The dependence of the attenuation on the intensity of magnetization in the given magnetic field is small, particularly when cotangent Θ increases (in view of this, in Figs. 4a, 4c, 5a and 5c only the curves showing v = 0.52 are given for the forward waves, since they nearly coincide with the curves showing v = 0.19).

3. At frequencies equidistant from the resonant frequency (x/u = const.) there is a great deal of attenuation when the magnetic fields are small. For example, at cotangent Θ = 20 and x/u = 0.9, the attenuation at u = 0.52 is double that at u = 0.19 (Figs. 4a and 5a).

4. If the dielectric losses are high, it is possible that there are frequency regions in which the attenuation in the backward direction is less than in the forward direction. (For example, at cotangent $\Theta = 20$, $\alpha = 10^{-2}$, and $\epsilon'' = 10^{-1}$ the attenuation of the backward wave is less than that of the forward wave up to x/u = 0.79 (Fig. 5b). This is a direct corollary of Eq. (34), from which it follows that the dielectric losses are greater for forward waves than for backward ones.

Thus, in seeking to ensure the greatest directivity factor (for example, when designing the isolator for a traveling wave tube), it is essential to choose a ferrite with the least possible dielectric losses. This is also advisable, of course, from the point of view of reducing the absolute attenuation.

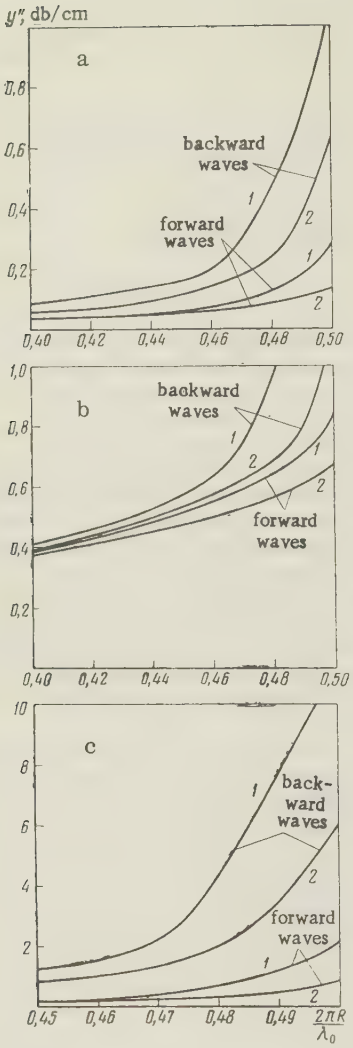

Fig. 2

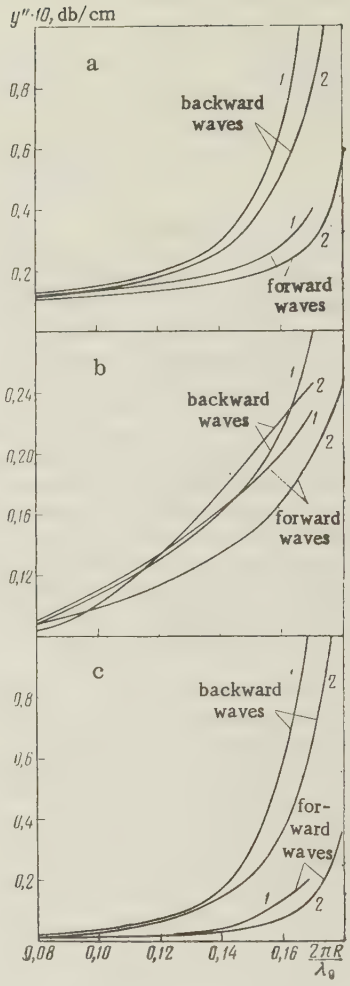

Fig. 3

Fig. 2. Attenuation of the helix-ferrite system as a function of the parameter $2\pi R/\lambda_0$ for cotangent $\theta = 10$, $u = 0.52$, $\alpha = 10^{-3}$, $\epsilon'' = 10^{-2}$ (a); $\alpha = 10^{-3}$, $\epsilon'' = 10^{-1}$ (b); $\alpha = 10^{-2}$, $\epsilon'' = 10^{-2}$ (c) and two values of the parameter v(1 — $v = 0.52$; 2 — $v = 0.19$)

Fig. 3. Attenuation of the helix-ferrite system as a function of the parameter $2\pi R/\lambda_0$ for cotangent $\theta = 10$, $v = 0.19$ (the remaining parameters are the same as in Fig. 2 a, b and c)

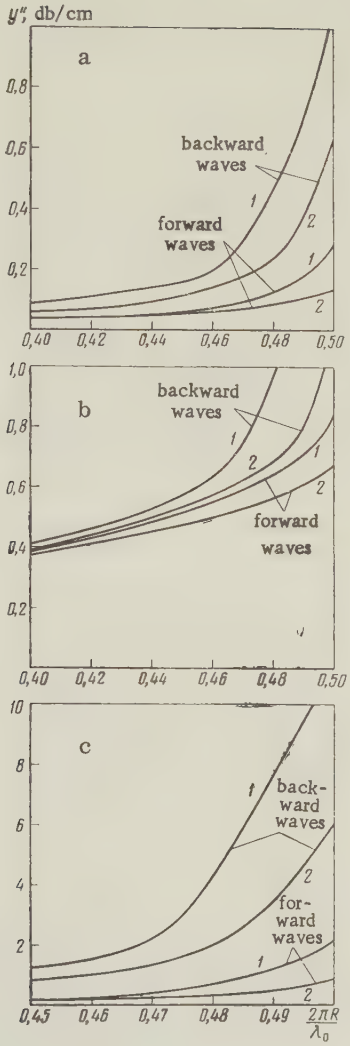

Fig. 4

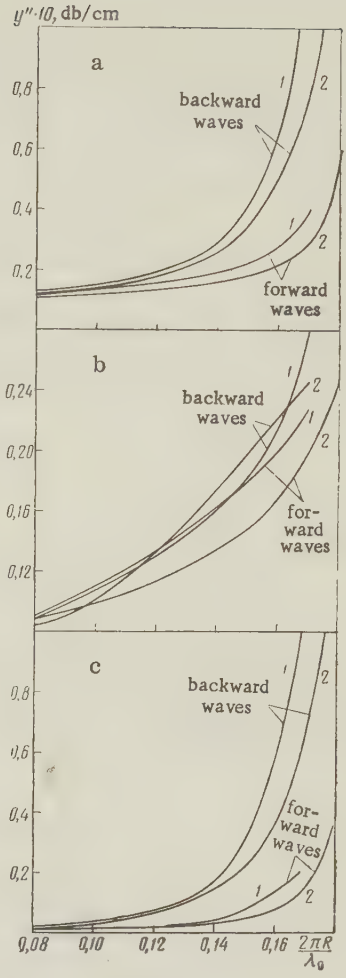

Fig. 5

Fig. 4. Attenuation of the helix-ferrite system as a function of the parameter $2\pi R/\lambda_0$ for cotangent $\theta = 20$ (the remaining parameters are the same as in Fig. 2 a, b and c)

Fig. 5. Attenuation of the helix-ferrite system as a function of the parameter $2\pi R/\lambda_0$ for cotangent $\theta = 20$ (the remaining parameters are the same as in Fig. 2 a, b and c)

REFERENCES

1. S. Sensiper, Proc. I.R.E., 1955, 43, 2, 149 (Russian translation see Quest. radar techniques, For. Lit. Press, 1955, 5(29)).
2. J.A. Rich, S.E. Weber, Proc. I.R.E., 1955, 43, 1, 100.
3. B.M. Bulgakov, V.P. Shestopalov, L.A. Shishkin and I.P. Yakimenko, Radio Engineering and Electronics, 1960, 5, 11, 1818.
4. L.D. Landau, Ye. M. Lifshits, Sow. Phys., 1935, 8, 153.
5. V.P. Shestopalov, K.P. Yatsuk, I.P. Yakimenko, ZhTF, 1959, 29, 11, 1330.

Kharkov (Gor'kiy) State University Received by the editors 15 February 1960

COAXIAL BIFILAR CONTRA-WOUND HELIX IMMERSED IN A MAGNETO-DIELECTRIC MEDIUM

V.P. Shestopalov and A.A. Bulgakov

We obtained and investigated a dispersion equation for a coaxial bifilar contra-wound helix immersed in a magneto-dielectric medium for the case in which the helices are arranged symmetrically. We calculated the effect of the magneto dielectric on the stored energy and impedance of the system. We also investigated the dispersion properties of the system experimentally.

INTRODUCTION

In Ref. 1 the variational method is used to investigate the properties of a bifilar contra-wound helix in free space. A slow wave system of this kind has a number of advantages over the ordinary helix, particularly in travelling-wave tube amplifiers. Indeed, at high voltages, in the ordinary helix the impedance to electron interaction is reduced, while certain space harmonics (-1) exhibit such a high impedance that backward wave interaction may exist. In a contra-wound bifilar helix, the symmetry of the system ensures that the concentration of most of the electric energy will be in the fundamental component, and most of the magnetic energy in the space harmonics. This leads to a higher impedance for the fundamental component and a reduction of the impedance for the higher space harmonics. As shown in Ref. 1, at a voltage of 10 kv, the impedance of the fundamental component of the bifilar helix is approximately double the corresponding impedance in simple helix, while the impedance of the -1 harmonic in the bifilar helix is smaller than in the single helix by a factor of 20.

Apart from the positive properties, the bifilar helix does have some shortcomings. The system is more dispersive than the single helix, and cannot therefore be used over a very wide frequency band when the voltage is fixed.

In actual practice the bifilar helix is used as a slow wave system only with the aid of various kinds of dielectric supports. This leads to the need to take into account the effect of the dielectric medium on the dispersion properties of the system. We are also faced with the problem of investigating the possibility of using the magneto-dielectric medium to improve both the dispersion and other properties of the bifilar helix.

In the present article we show that the introduction of a magneto-dielectric medium into a bifilar helix, when the entire system is placed in a metal waveguide, and when the values

ϵ and μ of the magneto-dielectric medium are suitably distributed and selected, provides the most suitable dispersion characteristic of the system for a high impedance of the fundamental space harmonic, and reduces the impedance of the first space harmonic. The metal sheath in the source-free system under investigation also makes it possible to consider the fast waves which may propagate through the system.

1. FIELDS AND CURRENTS IN THE SYSTEM

Let us assume that two helices of identical radius a (Fig. 1) are wound symmetrically (pitch angle Θ). We will designate the pitch of this system as p; the width of the helix band is δ. The bifilar helix is placed in a metal sheath of radius c. Inside the helix there is a magneto-dielectric medium with dielectric constant ϵ_1 and permeability μ_1; between the helix and the waveguide is a medium with properties ϵ_2, μ_2.

If the axes of the cylindrical system of coordinates r, φ and z are selected in such a way that z coincides with the axis of the bifilar helix, the system in question remains unchanged at any of the following transitions:

$$(r, \varphi, z) \leftrightarrow (r, \varphi, -z);$$
$$(r, \varphi, z) \leftrightarrow (r, -\varphi, z);$$
$$(r, \varphi, z) \leftrightarrow (r, \varphi, z \pm p);$$
$$(r, \varphi, z) \leftrightarrow \left(r, \varphi \pm \frac{\pi}{2}, z + \frac{p}{2}\right).$$

This latter property is typical of bifilar helices with identical spacing.

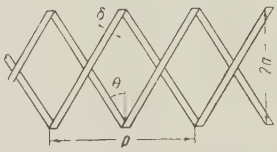

Fig. 1. Bifilar contra-wound (symmetrical arrangement of helices).

For a bifilar helix the solution of the wave equation for logitudinal components of the electric field E_z and the magnetic field H_z can be assumed to have the form

$$\sum_{l=-\infty}^{\infty} \sum_{m=-\infty}^{\infty} A_{lm} R_{lm}(r) \exp\left\{i\left[\beta_{00} + \frac{2\pi}{p}(l + 2m)\right]z\right\} \exp(-il\varphi) \exp(-i\omega t). \tag{1}$$

The functions are determined by the solution of a Bessel equation in the applicable region of the system.

Assuming that along one helix (a right-hand winding designated by a - superscript) there exists the current

$$\vec{\mathcal{J}}(a^-) = \vec{e}_\varphi \mathcal{J}_\varphi(a^-) + \vec{e}_z \mathcal{J}_z(a^-), \tag{2}$$

and along the other (a left-hand winding designated by a + superscript) the current is

$$\vec{\mathcal{J}}(a^+) = \vec{e}_\varphi \mathcal{J}_\varphi(a^+) + \vec{e}_z \mathcal{J}_z(a^+), \tag{3}$$

and using the boundary conditions on the helix (at r = a)

$$E_{1z} = E_{2z};\ E_{1\varphi} = E_{2\varphi};\ H_{1z} - H_{2z} = \mathcal{J}_\varphi(a^-) + \mathcal{J}_\varphi(a^+) = \mathcal{J}_\varphi;$$
$$H_{2\varphi} - H_{1\varphi} = \mathcal{J}_z(a^-) + \mathcal{J}_z(a^+) = \mathcal{J}_z, \tag{4}$$

as well as the boundary conditions on the ideally conducting sheath, we obtain the following expressions for the Fourier components of the longitudinal field intensities inside and outside the helices:

$$(E_{1z})_{lm} = -i \frac{\gamma_{lm} a}{k_1 a} \sqrt{\frac{\mu_1}{\varepsilon_1}} \left[\mathcal{J}_{zlm} - \frac{\beta_{lm} a l}{(\gamma_{lm} a)^2} \mathcal{J}_{\varphi lm}\right] \frac{I_l(\gamma_{lm} r)}{I_l'(\gamma_{lm} a)} \frac{1}{1 - \frac{\varepsilon_2}{\varepsilon_1}\frac{\Delta_2}{\Delta_1}}; \tag{5}$$

$$(H_{1z})_{lm} = \mathcal{J}_{\varphi lm} \frac{I_l(\gamma_{lm} r)}{I_l(\gamma_{lm} a)} \frac{1}{1 - \frac{\mu_1}{\mu_2}\frac{\Delta_3}{\Delta_4}}; \tag{6}$$

$$(E_{2z})_{lm} = -i \frac{\gamma_{lm} a}{k_1 a} \sqrt{\frac{\mu_1}{\varepsilon_1}} \left[\mathcal{J}_{zlm} - \frac{\beta_{lm} a l}{(\gamma_{lm} a)^2} \mathcal{J}_{\varphi lm} \right] \frac{I_l(\gamma_{lm} r)}{I_l'(\gamma_{lm} a)} \frac{\Delta_5}{\Delta_1} \frac{1}{1 - \frac{\varepsilon_2}{\varepsilon_1}\frac{\Delta_2}{\Delta_1}}; \tag{7}$$

$$(H_{2z})_{lm} = \mathcal{J}_{\varphi lm} \frac{I_l(\gamma_{lm} r)}{I_l(\gamma_{lm} a)} \Delta_6 \left(\frac{1}{\Delta_4} \frac{1}{1 - \frac{\mu_1}{\mu_2}\frac{\Delta_3}{\Delta_4}} - \frac{1}{\Delta_3} \right), \tag{8}$$

where

$$\begin{gathered}
\gamma_{lm}^2 = \beta_{lm}^2 - k_0^2;\ \beta_{lm} = \beta_{00} + \frac{2\pi}{a}(l + 2m);\ k_0 = \frac{\omega}{c};\ B_{00} = \frac{\omega}{v_{\Phi\,00}};\ k_1 = \frac{k_0}{\sqrt{\varepsilon_1 \mu_1}}; \\
\mathcal{J}_{zlm} = \mathcal{J}_{zlm}(a^+) + \mathcal{J}_{zlm}(a^-);\ \mathcal{J}_{\varphi lm} = \mathcal{J}_{\varphi lm}(a^+) + \mathcal{J}_{\varphi lm}(a^-); \\
\Delta_1 = \frac{K_l}{I_l}(\gamma_{lm} c) - \frac{K_l}{I_l}(\gamma_{lm} a);\ \Delta_2 = \frac{K_l}{I_l}(\gamma_{lm} c) - \frac{K_l'}{I_l'}(\gamma_{lm} a); \\
\Delta_3 = \frac{K_l'}{I_l'}(\gamma_{lm} c) - \frac{K_l}{I_l}(\gamma_{lm} a);\ \Delta_4 = \frac{K_l'}{I_l'}(\gamma_{lm} c) - \frac{K_l'}{I_l'}(\gamma_{lm} a); \\
\Delta_5 = \frac{K_l}{I_l}(\gamma_{lm} c) - \frac{K_l}{I_l}(\gamma_{lm} r);\ \Delta_6 = \frac{K_l'}{I_l'}(\gamma_{lm} c) - \frac{K_l}{I_l}(\gamma_{lm} r).
\end{gathered} \tag{9}$$

In Eqs. (5) - (8) the fact has already been taken into account that the transverse constants of propagation in the first and second regions have approximately the same values. The expression $\frac{K_l}{I_l}(\gamma_{lm} c)$ should be read as $K_l(\gamma_{lm} c)/I_l(\gamma_{lm} c)$.

2. DISPERSION EQUATION

To obtain a dispersion equation let us use the variational method developed in Refs. 1-3. If we use the expression for the Lagragian of the given problem in the form

$$\begin{gathered}
\dot{I} = \text{const} \sum_{l,\,m} \{(E_\varphi^*(a))_{lm} [\mathcal{J}_{\varphi lm}(a^-) + \mathcal{J}_{\varphi lm}(a^+)] + \\
+ (E_z^*(a))_{lm} [\mathcal{J}_{zlm}(a^-) + \mathcal{J}_{zlm}(a^+)]\},
\end{gathered} \tag{10}$$

the solution in the case of a one term approximation takes the form

$$\dot{I}\{\mathcal{J}_{\parallel lm}(a^-)\} = 0, \tag{11}$$

in which $\mathcal{J}_{\parallel lm}(a^-)$ is the parallel component of the surface current density on the right-hand helix. Let us select $\mathcal{J}_{\parallel lm}(a^-)$ in the form

$$\mathcal{J}_{\parallel lm}(a^-) = A \frac{\delta}{2\pi a \operatorname{tg}\Theta} \frac{\sin \frac{l\delta}{2a \operatorname{tg}\Theta}}{\frac{l\delta}{2a \operatorname{tg}\Theta}} \delta(m);\quad \delta(m) = \begin{cases} 1, & m = 0, \\ 0, & m \neq 0. \end{cases} \tag{12}$$

Using Eqs. (5) - (9) and Eqs. (11) and (12), we obtain a dispersion equation for the system

$$2Q_{00} + \sum_{l=1}^{\infty} \frac{\sin^2 \frac{l\delta}{2a \operatorname{tg}\Theta}}{\left(\frac{l\delta}{2a \operatorname{tg}\Theta}\right)^2} (Y_{l0} + Y_{-l0}) = 0, \tag{13}$$

in which $Y_{lm} = \gamma_{lm} a \sin^2\Theta \frac{I_l}{I_l'}(\gamma_{lm} a) \frac{1}{1 - \frac{\varepsilon_2}{\varepsilon_1}\frac{\Delta_2}{\Delta_1}} - \sin 2\Theta \frac{l\beta_{lm} a}{\gamma_{lm} a} \frac{I_l}{I_l'}(\gamma_{lm} a) \frac{1}{1 - \frac{\varepsilon_2}{\varepsilon_1}\frac{\Delta_2}{\Delta_1}} +$

$$+\cos^2\Theta\left\{\frac{(l\beta_{lm}a)^2}{(\gamma_{lm}a)^3}\frac{I_l}{I_l'}(\gamma_{lm}a)\frac{1}{1-\frac{\varepsilon_2}{\varepsilon_1}\frac{\Delta_2}{\Delta_1}}-\frac{(k_1a)^2}{(\gamma_{lm}a)^2}\frac{I_l}{I_l'}(\gamma_{lm}a)\frac{1}{1-\frac{\mu_1}{\mu_2}\frac{\Delta_3}{\Delta_4}}\right\};$$

$$Q_{00}=\gamma_{00}a\sin^2\Theta\frac{I_0}{I_0'}(\gamma_{00}a)\frac{1}{1-\frac{\varepsilon_2}{\varepsilon_1}\frac{\Delta_{02}}{\Delta_{01}}}; \tag{14}$$

$$\Delta_{01}=\frac{K_0}{I_0}(\gamma_{00}c)-\frac{K_0}{I_0}(\gamma_{00}a);\ \Delta_{02}=\frac{K_0}{I_0}(\gamma_{00}c)-\frac{K_0'}{I_0'}(\gamma_{00}a),$$

and the remaining quantities are as defined in Eq. (9).

3. GRAPHICAL ANALYSIS OF EQ. 13.

The analysis of the dispersion equation (13) will be made graphically. In order to plot the dispersion curves let us rewrite Eq. (13) in the form

$$Q_{00}(\gamma_{00})=-[Q_{-10}(\gamma_{-10})+Q_{+10}(\gamma_{+10})+\ldots+Q_{-n0}(\gamma_{-n0})+Q_{+n0}(\gamma_{+n0})], \tag{15}$$

where

$$Q_{l0}=\frac{\sin^2\frac{l\delta}{2a\operatorname{tg}\Theta}}{\left(\frac{l\delta}{2a\operatorname{tg}\Theta}\right)^2}Y_{l0};$$

$$Q_{-l0}=\frac{\sin^2\frac{l\delta}{2a\operatorname{tg}\Theta}}{\left(\frac{l\delta}{2a\operatorname{tg}\Theta}\right)^2}Y_{-l0}. \tag{16}$$

Next the curves for the left-hand and right-hand sides in Eq. (15) are plotted. Here $\beta_{00}a$ is fixed, but we vary $k_1a=k_0a/\sqrt{\varepsilon_1\mu_1}$. The points of intersection of these curves make it possible (at the given λ_0 and all other parameters of the system) to determine k_1a as a function of $\beta_{00}a$. In this way we can plot graphs for the variation of k_0a/cotangent Θ as a function of $\beta_{00}a$/cotangent Θ.

As shown by the calculation, to plot the dispersion curves in Eq. (15) it is sufficient to single-out three terms by representing Eq. (15) in the form

$$Q_{00}=-(Q_{-10}+Q_{+10}). \tag{17}$$

The intersection points of the curves for the left-hand and right-hand sides of Eq. (17) were found in the following way. At first we plotted the curves Q_{00}, Q_{-10} and Q_{+10}, separately in each case. They are shown in Fig. 2. For a number of values of k_1a the graphs Q_{00} represent straight lines, almost parallel to the axis K_1a. The curves for $-Q_{+10}$ begin close to zero with negative values and increase continuously $+\infty$, passing through $-Q_{+10}=0$. The behavior of the curves $-Q_{-10}$ is somewhat different from

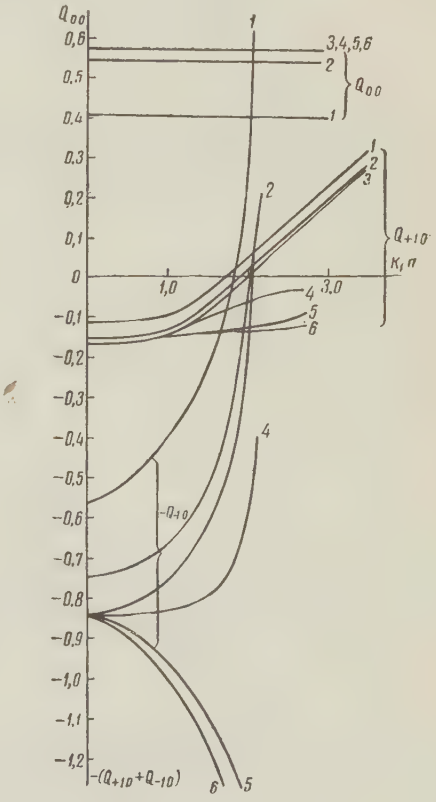

Fig. 2. Graphical solution of Eq. (17): 1, 2 and 3) curves Q_{00}, $-Q_{+10}$ and $-Q_{-10}$ for $\mu_1=1$, $\epsilon_1=2$, 6.5 and 10; 4, 5, and 6) curves for $\epsilon_1=10$, $\mu_1=2$, 10 and 20 (cotangent $\theta=5$, $\delta/p=0.1$, $c/a=3$ at $\beta_{00}a=1.5$).

Q_{00} and $-Q_{+10}$; the curves for $-Q_{-10}$ begin at negative values, and then, depending upon ϵ and μ, continue in a positive or negative direction.

As can be seen from Figs. 3 and 4, the dispersion properties of the system depend substantially on ϵ_1 and ϵ_2 (at the given value of cotangent $\theta = 5$; $\delta/p = 0.1$).

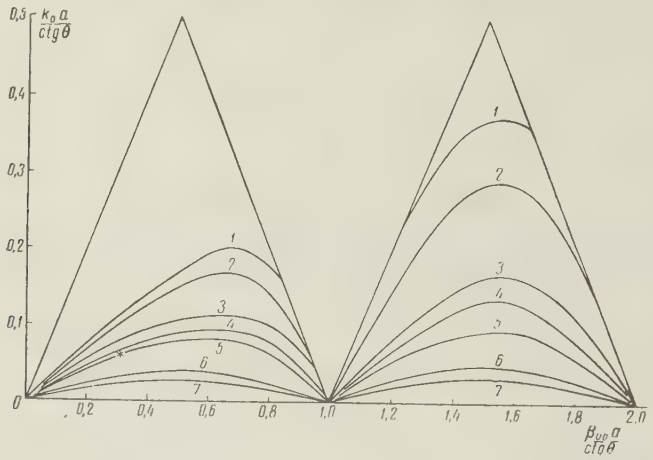

Fig. 3. Dispersion curves for slow waves in a bifilar helix in a magneto-dielectric medium at different values of ϵ_1, μ_1 ($\epsilon_2 = 1$, $\mu_2 = 1$): 1, 2, 3 and 4) for $\mu_1 = \mu_2 = 1$, $\epsilon_2 = 1$, $\epsilon_1 = 1$; 2; 6, 5; 10; 5, 6 and 7) curves for $\mu_2 = 1$, $\epsilon_2 = 1$, $\epsilon_1 = 10$, $\mu_1 = 2$; 10; 20

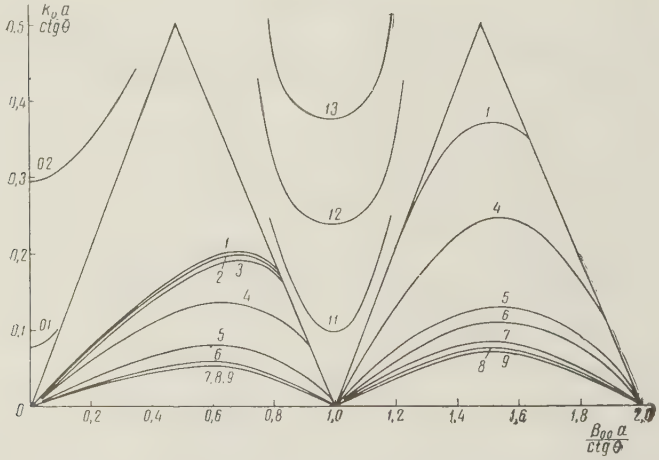

Fig. 4. Dispersion curves for slow and fast waves in a bifilar helix in a magneto-dielectric medium at different values ϵ_2, μ_2, c/a ($\epsilon_1 = 1$, $\mu_1 = 1$): 1, 4, 5 and 6) curves for $\epsilon_1 = 1$, $u_1 = \mu_2 = 1$, $\epsilon_2 = 1$; 2; 6, 5; 10; 7, 8 and 9) curves for $\epsilon_1 = 1$, $\mu_1 = 1$, $\epsilon_2 = 10$, $\mu_2 = 2$; 10; 20; 1, 2 and 3) curves for different values c/a = 3, 2, 1.1; curves 01, 02, 11, 12 and 13 are for case $\epsilon_2/\epsilon_1 = 1$, $\mu_2/u_1 = 1$, $\delta/p = 0$, 1, cotangent $\theta = 5i$ c/a = 3

We also investigated the dispersion of the system as a function of the ratio between the sheath diameter and the helix diameter. Figure 4 shows that the dispersion properties of the system vary slightly as a function of the selected c/a. Thus, using the magneto-dielectric and metallic sheath the dispersion properties of a bifilar helix can be controlled.

4. FAST WAVES IN A BIFILAR CONTRA-WOUND HELIX IN A METALLIC SHEATH

The presence of a metal waveguide, in which the bifilar helix is placed, makes it possible to consider the propagation of fast waves in this system, i.e., the oscillations with $v_\phi > c$. The transverse constant of propagation for these waves γ_{1m} takes the form

$$\gamma_{lm} = iq_{lm}, \tag{18}$$

while the dispersion equation (13) can be written as follows:

$$2P_{00} + \sum_{l=1}^{\infty} \frac{\sin^2 \frac{l\delta}{2a \operatorname{tg} \Theta}}{\left(\frac{l\delta}{2a \operatorname{tg} \Theta}\right)^2} (P_{l0} + P_{-l0}) = 0, \tag{19}$$

where

$$P_{lm} = q_{lm}a \sin^2 \Theta \frac{J_l}{J_l'}(q_{lm}a) \frac{1}{1 - \frac{\varepsilon_2}{\varepsilon_1}\frac{\delta_2}{\delta_1}} + \sin 2\Theta \frac{lh_{lm}a}{q_{lm}a} \frac{1}{1 - \frac{\varepsilon_2}{\varepsilon_1}\frac{\delta_2}{\delta_1}} +$$

$$+ \cos^2\Theta \left\{ \frac{(lh_{lm}a)^2}{(q_{lm}a)^2} \frac{J_l}{J_l'}(q_{lm}a) \frac{1}{1 - \frac{\varepsilon_2}{\varepsilon_1}\frac{\delta_2}{\delta_1}} + \frac{(k_1a)^2}{(q_{lm}a)^2} \frac{J_l'}{J_l}(q_{lm}a) \frac{1}{1 - \frac{\mu_1}{\mu_2}\frac{\delta_3}{\delta_4}} \right\};$$

$$P_{00} = (q_{00}a) \sin^2 \Theta \frac{J_0}{J_0'}(q_{00}a) \frac{1}{1 - \frac{\varepsilon_2}{\varepsilon_1}\frac{\delta_{02}}{\delta_{01}}}; \quad (q_{lm}a)^2 = (k_1a)^2 - (h_{lm}a)^2; \tag{20}$$

$$\delta_1 = \frac{N_l}{J_l}(q_{lm}c) - \frac{N_l}{J_l}(q_{lm}a); \qquad \delta_2 = \frac{N_l}{J_l}(q_{lm}a) - \frac{N_l'}{J_l'}(q_{lm}a);$$

$$\delta_3 = \frac{N_l'}{J_l'}(q_{lm}c) - \frac{N_l}{J_l}(q_{lm}a);$$

$$\delta_4 = \frac{N_l'}{J_l'}(q_{lm}c) - \frac{N_l'}{J_l'}(q_{lm}a); \qquad \delta_{01} = \frac{N_0}{J_0}(q_{00}c) - \frac{N_0}{J_0'}(q_{00}a);$$

$$\delta_{02} = \frac{N_0}{J_0}(q_{00}c) - \frac{N_0'}{J_0'}(q_{00}a).$$

Calculation of the dispersion curves was made in the same way as for slow waves. These curves passed through forbidden regions for slow waves. In view of the fact that the functions $J_l(x)$ and $N_l(x)$ may become zero when the argument varies, there may be a number of dispersion curves for fixed values of the system parameters, as distinct from the case of slow waves.

5. THE STORED ENERGY AND IMPEDANCE OF THE SYSTEM.

If we use W_{00H_φ} to designate the energy stored by the basic component of the magnetic field, and $W_{00E_z} + W_{00E_r}$ to denote the energy stored by the basic component of the electric field, then at $\gamma_{00}a \gg 3$

$$\left(\frac{W_{00H_\varphi}}{W_{00E_z} + W_{00E_r}}\right)_{\gamma_{00}a \gg 3} \simeq \left(\frac{k_0a}{\gamma_{00}a}\right)^2 \mu_1\varepsilon_2 \frac{3\left(\frac{\varepsilon_1}{\varepsilon_2}\right)^2 + \pi^2 \frac{\mu_2}{\mu_1}}{2\pi^2 + 4\frac{\varepsilon_1}{\varepsilon_2}};$$

$$\lim_{\gamma_{00}a \to \infty} \left(\frac{W_{00H_\varphi}}{W_{00E_z} + W_{00E_r}}\right) = 0. \tag{21}$$

Thus, there is considerably less magnetic field energy in the system than electric field energy. This fact agrees with the conclusion drawn in Ref. 1. Nevertheless, the presence of a magnetodielectric in the system, as is clear from the first formula in (21) somewhat impairs this relationship. Figure 5 gives the energy of the z and r - components of the electric field, normalized for the total energy of the system and normalized for the total energy of the φ component of the magnetic field for a bifilar helix in a sheath with and without a magnetodielectric. The calculations were made for a point on the dispersion curve 5 (Fig. 3) with the values $\beta_{00}a = 1.5$; $k_0a = 0.3$; cotangent $\Theta = 5$; $\epsilon_2 = 1$; $\mu_2 = 1$; $\epsilon_1 = 10$; $\mu_1 = 2$ (this point is shown in Fig. 3 by an asterisk). For a free space bifilar helix the parameters of the system had the following values; cotangent $\Theta = 10$; $\beta_{00}a = 1.5$; $k_0a = 0.3$ (Fig. 2 of Ref. 1). We also compared the stored energies of this system and those of an ordinary bifilar helix for the -1 and +1 harmonics. It is clear from Fig. 6 that the magnetodielectric increases the stored energy and redistributes it from the +1 to the -1 harmonic.

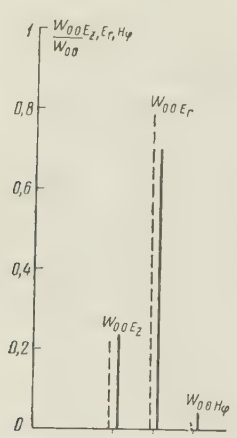

Fig. 5

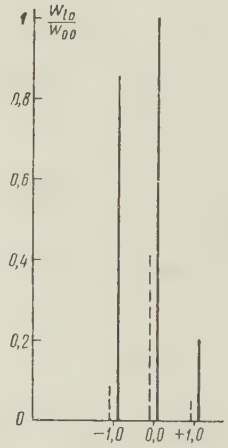

Fig. 6

Fig. 5. Comparison of the stored energy of the fundamental component for a bifilar helix with a sheath (solid line) and without it (dotted line).

Fig. 6. Comparison of the stored energy of fundamental, +1 and -1 harmonics for a bifilar helix with a sheath (solid line) and without (dotted line).

The impedance of the bifilar helix can be determined in the following way:

$$Z_{00} = \frac{|E_{z00}|^2_{r=a}}{\beta^2_{00} v_{rp} W_{00}}, \tag{22}$$

in which $v_{rp} = d(k_0a)/d(\beta_{00}a)$ is the group velocity which is calculated by graphical differentiation of the curves of Fig. 3. For $l \neq 0$ E_{z0} depends on φ and therefore

$$Z_{l0} = \frac{1}{\beta^2_{l0} v_{rp} W_{l0}} \frac{1}{2\pi} \int_0^{2\pi} |E_{zl0}|^2_{r=a} \, d\varphi. \tag{23}$$

The results of the calculation of the impedance are given in Fig. 7. The parameters of the system under investigation and the ordinary bifilar helix are the same as those used in calculating the stored energy. As is clear from Fig. 7. the magneto-dielectric in the system leads to a considerable variation in the impedance of the fundamental component and to a sharp drop in the impedance of the -1 and +1 harmonics. This decrease in impedance is due to an increase in the stored energy of these harmonics. This property of coaxial bifilar

helical guides may be used in travelling wave tubes to eliminate the generation of the -1 space harmonic in the amplifier.

6. EXPERIMENTAL INVESTIGATION OF DISPERSION

The main theoretical results of the investigation were checked experimentally. The dispersion properties of the bifilar helix in free space, and of a helix wound on ebonite ($\varepsilon \simeq 2$) and porcelain ($\varepsilon \simeq 6{,}5$) rods, (rod diameter 2a = 10 mm were studied. Two helices of copper tape, 0.1 mm thick and $\delta \simeq 0.6$ mm wide, were wound in opposite directions with cotangent $\Theta = 5$ (p = 6 mm). The bifilar helix without the dielectric consisted of two helices of copper wire, 0.6 mm in diameter (2a = 10 mm; p = 6 mm; cotangent $\Theta = 5$). The measurements were made by means of the instrumentation described in Refs. 4 and 5. The results of the measurements and a comparison with theoretical curves are given in Fig. 8. The points from which the continuous curve in Fig. 8 was plotted are taken from Fig. 3 (curves 1, 2 and 3). Here the relationship between λ_0, λ_g and k_0, β_{00} is determined by the formulae

$$\lambda_0 = \frac{2\pi a}{k_0 a}; \quad \lambda_g = \frac{2\pi a}{\beta_{00} a}. \qquad (24)$$

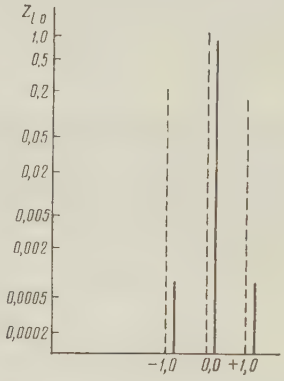

Fig. 7. Comparison of the impedance of the fundamental, +1 and -1 harmonics for a bifilar helix with a sheath (solid line) and without (dotted line)

A number of measurements were made in a copper sheath, c = 30 mm in diameter. Since the diameters of the helices were 2a = 10 mm, then c/a = 3, and the effect of the sheath on the dispersion of the system, as shown above, (Fig. 4, curves 1, 2 and 3) should be insignificant, which was in fact confirmed by the measurements made. The Table gives the results of these measurements. Let us note that both in the theoretical and experimental investigation of a coaxial helix immersed in a magnetodielectric we did not take into account the variation in the surface currents through the cross-section of the helices. This approximation, as shown by the analysis, was quite justified in the case of thin bands.

	λ_0, см	15	12	10	8,6
$\varepsilon_1 = 2$	λ_g, см (in sheath)	6,05	4,30	2,83	2,00
	λ_g, см (without sheath)	6,25	4,37	2,88	2,09
$\varepsilon_1 = 6{,}5$	λ_g, см (in sheath)	5,09	3,50	2,38	1,81
	λ_g, см (without sheath)	5,11	3,54	2,41	1,82

The authors wish to thank S. V. Troitskiy for his assistance in calculating the dispersion equations.

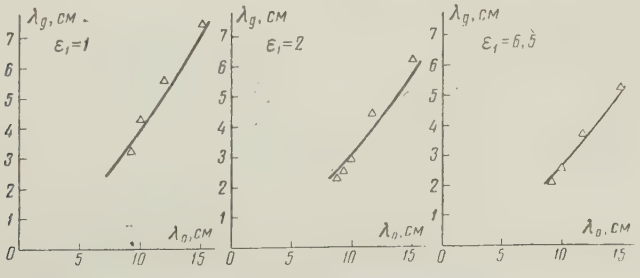

Fig. 8. Results of experimental measurements (triangles) of dispersion for a bifilar helix in free space ($\epsilon_1 = 1$) or wound on ebonite ($\epsilon_1 = 2$) and porcelain ($\epsilon_1 = 6.5$) rods.

REFERENCES

1. M. Chodorow, E.I. Chu, J. Appl. Phys., 1955, 26, 1, 33.
2. S. Sensiper, Proc. I.R.E.,1955, 43, 2, 149.
3. L. Stark, J. Appl. Phys., 1954, 25, 9, 1155.
4. Shestopalov, V.P., Yatsuk, K.P., Radio Engineering and Electronics, 1959, 4, 3, 547.
5. Shestopalov, V.P., Yatsuk, K.P., ZhTF, 1959, 29, 7, 819.

Kharkov (Gor'kiy) State University Received by editors 2 April 1960

SOME METHODS FOR THE SOLUTION OF A PROBLEM CONCERNING THE OSCILLATIONS OF A SMALL GYROTROPIC SPHERE. PART II, SERIES METHOD

Syuy Yan'-shen

This paper presents an approximate method for the solution of a problem concerning the oscillations of a gyrotropic sphere — the series method. Rules for the inter-relation of the various modes are established. It is shown that it is possible to achieve indirect excitation of Walker oscillations by means of an electric Debye potential. Indirect excitation occurs in particular upon placement of a ferrite sphere at the node of the magnetic field in a rectangular waveguide.

1. SOLUTION OF THE ELECTROMAGNETIC PROBLEM FOR A SMALL GYROTROPIC SPHERE BY THE SERIES METHOD

In the previous work [1] it was shown that by the method of successive approximations it is possible to solve the electromagnetic problem with the required degree of accuracy. However, this method does not provide a general representation of the rules for the transformation of oscillation modes. Hence it is advisable that we examine a method which is physically more descriptive.

In spherical coordinates Maxwell's equations for magnetized ferrites have the form

$$\begin{aligned}
\frac{\partial}{\partial\theta}(\sin\theta H_\varphi) - \frac{\partial}{\partial\varphi} H_\theta &= ik_0 \varepsilon r \sin\theta E_r,\\
\frac{\partial}{\partial\varphi} H_r - \frac{\partial}{\partial r}(r\sin\theta H_\varphi) &= ik_0 \varepsilon r \sin\theta E_\theta,\\
\frac{\partial}{\partial r}(rH_\theta) - \frac{\partial}{\partial\theta} H_r &= ik_0 \varepsilon r E_\varphi,\\
\frac{\partial}{\partial\theta}(\sin\theta E_\varphi) - \frac{\partial}{\partial\varphi} E_\theta &= -ik_0 r \sin\theta [(\mu\sin^2\theta + \cos^2\theta) H_r +\\
&+ (\mu - 1)\sin\theta\cos\theta H_\theta - ikH_\varphi \sin\theta],\\
\frac{\partial}{\partial\varphi} E_r - \frac{\partial}{\partial r}(r\sin\theta E_\varphi) &= -ik_0 r \sin\theta [(\mu - 1)\sin\theta\cos\theta H_r +\\
&+ (\mu\cos^2\theta + \sin^2\theta) H_\theta - ikH_\varphi \cos\theta],\\
\frac{\partial}{\partial r}(rE_\theta) - \frac{\partial}{\partial\theta} E_r &= -ik_0 r [\mu H_\varphi + ik(H_r \sin\theta + H_\theta \cos\theta)].
\end{aligned} \tag{1}$$

In comparing the system of equations (1) with Maxwell's equations for an isotropic medium and with their solutions (expressed as Debye potentials with indexes n and m) it is readily seen that dependence of the solutions of Eqs. (1) on φ may be expressed in terms of

$e^{\pm im\varphi}$, wherein coupling between modes with different indexes m is not present. This is due to the fact that in Eqs. (1) differentiation is expressed only in terms of φ, which does not yield a new dependence on φ. Gyrotropicity of the medium is characterized solely by the dependence of the righthand members of the last three of Eqs. (1) in θ. Consequently, the solution contains the sums of associated Legendre polynomials of cos θ with different indexes. As for the dependence on r, it is seen from the method of successive approximations [1] that it may be expressed in terms of power series with even or odd powers of $(k_0 r)$. In addition, associated Legendre polynomials with large indexes appear only after a large number of successive approximations and, consequently, their coefficients have higher powers of $(k_0 r)$.

It follows from the above that the components of the fields of the quasi-H $(n, \pm m)$ mode may be expressed as follows:

$$E_r = \sum_{p=0}^{\infty}\sum_{q=0}^{\infty} A_{p,q}(k_0 r)^{n+2p+2q} P^m_{n+2p+1}(\cos\theta)\, e^{\pm im\varphi} + \\ + \sum_{p'=1}^{N}\sum_{q=0}^{\infty} A_{p',q}(k_0 r)^{n+2q} P^m_{n-2p'+1}(\cos\theta)\, e^{\pm im\varphi},$$

$$E_\theta = \sum_{p=0}^{\infty}\sum_{q=0}^{\infty} B_{p,q}(k_0 r)^{n+2p+2q} \frac{\partial}{\partial\theta} P^m_{n+2p+1}(\cos\theta)\, e^{\pm im\varphi} + \\ + \sum_{p'=1}^{N}\sum_{q=0}^{\infty} B_{p',q}(k_0 r)^{n+2q} \frac{\partial}{\partial\theta} P^m_{n-2p'+1}(\cos\theta)\, e^{\pm im\varphi} + \\ + \sum_{p=0}^{\infty}\sum_{q=0}^{\infty} F_{p,q}(k_0 r)^{n+2p+2q} \frac{P^m_{n+2p}(\cos\theta)}{\sin\theta} \frac{\partial}{\partial\varphi} e^{\pm im\varphi} + \\ + \sum_{p'=1}^{N'}\sum_{q=0}^{\infty} F_{p',q}(k_0 r)^{n+2q} \frac{P^m_{n-2p'}(\cos\theta)}{\sin\theta} \frac{\partial}{\partial\varphi} e^{\pm im\varphi},$$

$$E_\varphi = \sum_{p=0}^{\infty}\sum_{q=0}^{\infty} B_{p,q}(k_0 r)^{n+2p+2q} \frac{P^m_{n+2p+1}(\cos\theta)}{\sin\theta} \frac{\partial}{\partial\varphi} e^{\pm im\varphi} + \\ + \sum_{p'=1}^{N}\sum_{q=0}^{\infty} B_{p',q}(k_0 r)^{n+2q} \frac{P^m_{n-2p'+1}(\cos\theta)}{\sin\theta} \frac{\partial}{\partial\varphi} e^{\pm im\varphi} - \\ - \sum_{p=0}^{\infty}\sum_{q=0}^{\infty} F_{p,q}(k_0 r)^{n+2p+2q} \frac{\partial}{\partial\theta} P^m_{n+2p}(\cos\theta)\, e^{\pm im\varphi} - \\ - \sum_{p'=1}^{N'}\sum_{q=0}^{\infty} F_{p',q}(k_0 r)^{n+2q} \frac{\partial}{\partial\theta} P^m_{n-2p'}(\cos\theta)\, e^{\pm im\varphi},$$

$$H_r = \sum_{p=0}^{\infty}\sum_{q=0}^{\infty} C_{p,q}(k_0 r)^{n+2p+2q-1} P^m_{n+2p}(\cos\theta)\, e^{\pm im\varphi} + \\ + \sum_{p'=1}^{N'}\sum_{q=0}^{\infty} C_{p',q}(k_0 r)^{n+2q-1} P^m_{n-2p'}(\cos\theta)\, e^{\pm im\varphi},$$

$$H_\theta = \sum_{p=0}^{\infty}\sum_{q=0}^{\infty} D_{p,q}(k_0 r)^{n+2p+2q-1} \frac{\partial}{\partial\theta} P^m_{n+2p}(\cos\theta)\, e^{\pm im\varphi} + \\ + \sum_{p'=1}^{N'}\sum_{q=0}^{\infty} D_{p',q}(k_0 r)^{n+2q-1} \frac{\partial P^m_{n-2p'}(\cos\theta)}{\partial\theta} e^{\pm im\varphi} + \\ + \sum_{p=0}^{\infty}\sum_{q=0}^{\infty} G_{p,q}(k_0 r)^{n+2p+2q+1} \frac{P^m_{n+2p+1}(\cos\theta)}{\sin\theta} \frac{\partial}{\partial\varphi} e^{\pm im\varphi} + \\ + \sum_{p'=1}^{N}\sum_{q=0}^{\infty} G_{p',q}(k_0 r)^{n+2q+1} \frac{P^m_{n-2p'+1}(\cos\theta)}{\sin\theta} \frac{\partial}{\partial\varphi} e^{\pm im\varphi},$$

$$H_\varphi = \sum_{p=0}^{\infty}\sum_{q=0}^{\infty} D_{p,q}(k_0 r)^{n+2p+2q-1}\frac{P_{n+2p}^m(\cos\theta)}{\sin\theta}\frac{\partial}{\partial\varphi}e^{\pm im\varphi} +$$
$$+ \sum_{p'=1}^{N'}\sum_{q=0}^{\infty} D_{p',q}(k_0 r)^{n+2q-1}\frac{P_{n-2p'}^m(\cos\theta)}{\sin\theta}\frac{\partial}{\partial\varphi}e^{\pm im\varphi} -$$
$$- \sum_{p=0}^{\infty}\sum_{q=0}^{\infty} G_{p,q}(k_0 r)^{n+2p+2q+1}\frac{\partial}{\partial\theta}P_{n+2p-1}^m(\cos\theta)e^{\pm im\varphi} -$$
$$- \sum_{p'=1}^{N}\sum_{q=0}^{\infty} G_{p',q}(k_0 r)^{n+2q+1}\frac{\partial}{\partial\theta}P_{n-2p'+1}^m(\cos\theta)e^{\pm im\varphi}.$$

Here $A_{p,q}$, $B_{p,q}$, C_{pq}, $D_{p,q}$, $F_{p,q}$, $G_{p,q}$ are coefficients, one of which characterizes the amplitude of the oscillations and the others are determined after substituting the series in Eqs. (1);

$$\text{with } (n-m) \text{ even, } N = N' = \frac{n-m}{2},$$

$$\text{with } (n-m) \text{ odd, } N = \frac{n-m+1}{2},\ N' = \frac{n-m-1}{2}.$$

The field components may be expressed in another, simpler manner. However, for convenience in imposing the boundary conditions, let us give them a form more similar to the expressions for the field components in an isotropic medium, described by means of Debye potentials.

Substituting the series (2) into Eqs. (1) and equating the coefficients of corresponding terms of both sides, we obtain an infinite system of equations with an infinite number of unknowns (i.e., the coefficients in Eqs. (2)). In addition, it is necessary to use the following known formulas for associated Legendre polynomials:

$$\cos\theta P_n^m(\cos\theta) = \frac{1}{2n+1}[(n-m+1)P_{n+1}^m(\cos\theta) + (n+m)P_{n-1}^m(\cos\theta)],$$
$$\sin\theta\frac{\partial}{\partial\theta}P_n^m(\cos\theta) = \frac{1}{2n+1}[n(n-m+1)P_{n+1}^m(\cos\theta) -$$
$$-(n+1)(n+m)P_{n-1}^m(\cos\theta)],$$

as well as the formulas for $\cos\theta\sin\theta\frac{\partial}{\partial\theta}P_n^m(\cos\theta)$, $\cos^2\theta P_n^m(\cos\theta)$, $\sin\theta\frac{\partial}{\partial\theta}\left[\sin\theta\frac{\partial}{\partial\theta}P_n^m(\cos\theta)\right]$, $\cos^3\theta P_n^m(\cos\theta)$ and $\cos^2\theta\sin\theta\frac{\partial}{\partial\theta}P_n^m(\cos\theta)$. These quantities may be expressed as the sum of polynomials $P_{n\pm3}^m(\cos\theta)$, $P_{n\pm2}^m(\cos\theta)P_{n\pm1}^m(\cos\theta)$, $P_n^m(\cos\theta)$ with appropriate coefficients. The infinite system of equations may be divided into a series of systems with a finite, gradually increasing number of unknowns and these systems may be solved successively: first it is necessary to solve simultaneously the equations containing unknowns with indexes q = 0, p = 0 and all p', then it is necessary to solve the system of equations containing unknowns with indexes p = 1, q = 0 and q = 1, p = 0, p' being arbitrary. Generally speaking, it is necessary to solve simultaneously equations containing as unknowns the coefficients with indexes p + q = s and q = s, p' arbitrary; here s is some constant.

By this method we may calculate all the coefficients required for any prescribed degree of accuracy. The existence of a method of calculation confirms the validity of Eqs. (2) and, consequently, the validity of the resulting rules for the relationship between modes as discussed below.

In a similar manner we may express the field components of the quasi-E mode by means of series and calculate the required coefficients. We will not discuss this subject in detail.

In the case of a small sphere, in Eqs. (2) it is necessary to take only the terms with the lowest power of $k_0 r$. Then the quasi-H mode waves and the quasi-E mode waves are converted into oscillations of the corresponding Walker types of analogous electrostatic types.

2. METHOD OF SOLUTION OF THE PROBLEM OF THE EXCITATION OF NATURAL OSCILLATIONS OF A SMALL GYROTROPIC SPHERE. RELATIONSHIP BETWEEN VARIOUS MODES.

In the preceding work [1] it was shown that in setting the boundary conditions of the electromagnetic problem, continuity of the tangential components of the fields at the surface of a sphere may be replaced by continuity of appropriately chosen potentials ψ_E and ψ_H and the normal components of induction B_r and D_r at the surface of the sphere. It was also shown that the higher order terms in Eqs. (2) (i.e., terms with higher powers of r than occur in the first terms) result in two phenomena: coupling between the various modes [2] and the effect of wave propagation in the ferrite on the resonance conditions. Coupling between different modes consists in the fact that, generally speaking, the following modes are always simultaneously excited (with all values of the index p):

$$\begin{cases} \text{quasi-E} & (|m| + 2p,\ m), \\ \text{quasi-H} & (|m| + 2p + 1,\ m), \end{cases}$$

or

$$\begin{cases} \text{quasi-E} & (|m| + 2p + 1,\ m), \\ \text{quasi-H} & (|m| + 2p,\ m), \end{cases}$$

where $p = 0, 1, 2, \ldots$

The cause of coupling between the quasi-E and quasi-H modes is explained in greater detail in Appendix 1.

The resonance conditions are determined from the requirement of an infinite or (in the presence of losses) of a maximum build up in the amplitudes of oscillations. They apply only to the magnetic field (and the associated electric field). In the case of a small sphere all the higher order terms in Eqs. (2) are small and the Walker resonance conditions are excellent approximations for the corresponding quasi-H modes. However, terms with higher powers of r whose dependence on θ, φ is identical with that of the principal mode still impart a small correction to the resonance condition. This subject is discussed in detail in Ref. 1.

The terms of the series with other dependences on θ, φ which enter into the solution establish the coupling between various modes and also, although weakly, affect the resonant frequency or field. This is due to the fact that, while the coupling between different modes is mutual (that is, if the first mode affects the second, then the second affects the first), the amplitude of oscillation rises significantly only at resonance and we may usually disregard the reverse effect of such a mode (on the original mode) for which resonance does not occur. However, if the resonance conditions of both coupled modes are approximately the same, their amplitudes increase simultaneously. Then it is necessary to consider both effects (forward and reverse); in this case at the resonance conditions there occurs the phenomenon of interference between these two modes, which was first observed by Fletcher and Solt in experimental investigations [2].

3. EXCITATION OF NATURAL OSCILLATIONS OF A SMALL GYROTROPIC SPHERE BY AN H_{10} WAVE IN A RECTANGULAR WAVEGUIDE

The problem of the excitation of a small gyrotropic sphere by an H_{10} wave in a rectangular waveguide has been discussed in Ref. 3. However, this dealt only with the solution of the zeroth-order approximation for the oscillations in the sphere and the results given therein may be rendered more accurate by approximations of higher order.

For practical purposes we are interested only in the amplitude of oscillations at resonance. As stated in Ref. 3, the amplitudes of the incident and reflected waves of different modes decrease rapidly with an increase in the index n. This leads to an important conclusion: it is necessary to consider only the influence of modes with smaller indexes n on modes with larger n and the influence of the resonant mode on other nearby modes. As shown above, coupling exists only between modes with identical indexes m. Consequently, in calculating the amplitudes of (m, -m) modes at resonance we may disregard the influence of other modes and the results given for these modes in Ref. 3 are acceptable. For other modes it is necessary to introduce corrections for the effect of modes with smaller indexes n.

For example, in calculating the amplitudes of reflected waves $v^s(n, m)$ it is necessary to consider the influence of modes u (n - 2p - 1, m) and v (n - 2p, m) with index values p = 0, 1, 2, ... In such cases it is first necessary to calculate the higher-order approximations defining the coupling between all modes $\psi_H(n - 2p, m)$ and $\psi_E(n - 2p - 1, m)$. Then it is necessary to simultaneously set the boundary conditions for all these modes considering the coupling between them. We then obtain a system of equations the solution of which will give the amplitudes of the reflected waves and oscillations of all the given modes in the ferrite.

It is important to note that due to coupling between modes quasi-H oscillations may also be excited by means of a transverse-magnetic wave (characterized by a Debye potential u) with appropriate indexes n and m. An example is the excitation of oscillations of type (2, 0) in a waveguide at the node of the magnetic field (see Figure), which has been observed by a number of authors [4, 5, 6].

On the other hand, an analysis of the H_{10} wave at the given point in a waveguide does not contain the Debye potential v(2, 0) [3]. In the given case, the specimen is placed at the antinode of the electric field parallel to the fixed magnetic field. Hence, within it there are excited oscillations of the $\psi_E(1, 0)$ mode which are coupled with oscillations of the $\psi_H(2, 0)$ mode. At a certain frequency the oscillations of both modes have a common resonance. If the fixed magnetic field is deflected at an angle φ to the waveguide wall, then there are also simultaneously excited oscillations of the $\psi_E(1, -1)$ mode and coupled oscillations of the $\psi_H(2, -1)$ mode. This problem is discussed in greater detail for $\psi_E(1, 0)$ and $\psi_H(2, 0)$ in Appendix 2.

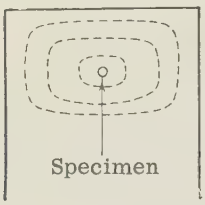

From the expressions given therein for the amplitude of the reflected wave (characterized by the Debye potential u^s) it is possible to determine for both modes the common resonance frequency, which proves to be close to the resonance frequency of the $\psi_H(2, 0)$ mode as calculated after Walker.

The reflected transverse-electric spherical wave (characterized by the Debye potential v^s) will in the given case create within the waveguide waves of the higher modes (beyond cutoff modes) only.

I wish to express my profound gratitude to A.A. Pistol'kors for supervision of this work and for much valuable advice.

APPENDIX 1

If it is assumed that coupling between the quasi-E and quasi-H modes is absent, then for the quasi-H mode the electric field components take the form

$$E_r = 0, \quad E_\theta = \frac{1}{\sin\theta}\frac{\partial}{\partial\varphi}\Phi, \quad E_\varphi = -\frac{\partial}{\partial\theta}\Phi. \tag{I}$$

Here Φ is some function of r, θ, φ.

Substituting Eq. (I) into the last two of Eqs. (1), we obtain

$$\frac{\partial}{\partial r}\left(r\sin\theta\frac{\partial}{\partial\theta}\Phi\right) = -ik_0 r\sin\theta\,[(\mu-1)\sin\theta\cos\theta\,H_r + (\mu\cos^2\theta + \sin^2\theta)\,H_\theta - ik\cos\theta H_\varphi], \tag{II}$$

$$\frac{\partial}{\partial r}\left(r\frac{\partial}{\partial\varphi}\Phi\right) = -ik_0 r\sin\theta\,[\mu H_\varphi + ik\,(H_r\sin\theta + H_\theta\cos\theta)]. \tag{III}$$

Consequently,

$$\frac{\partial}{\partial\varphi}[(\mu-1)\sin\theta\cos\theta\,H_r + (\mu\cos^2\theta + \sin^2\theta)\,H_\theta - ikH_\varphi\cos\theta] - \frac{\partial}{\partial\theta}\sin\theta\,[\mu H_\varphi + ik\,(H_r\sin\theta + H_\theta\cos\theta)] = 0. \tag{IV}$$

In the case of an isotropic medium ($u = \mu_z = 1$, $k = 0$) this equation is transformed into the first of Eqs. (1).

From $E_r = 0$ it follows that

$$H_\theta = \frac{\partial}{\partial\theta}\psi, \quad H_\varphi = \frac{1}{\sin\theta}\frac{\partial}{\partial\varphi}\psi. \tag{V}$$

Substituting Eqs. (I) and (V) into Eq. (IV) and the remaining equations of Eqs. (1), and eliminating H_r, we obtain two equations for the determination of ψ and Φ:

$$\frac{\partial}{\partial\varphi}\left[(\mu-1)\sin\theta\cos\theta\left\{\frac{\partial}{\partial r}(r\psi)+ik_0\varepsilon r\Phi\right\}+(\mu\cos^2\theta+\sin^2\theta)\frac{\partial}{\partial\theta}\psi-\right.$$
$$\left.-ik\frac{\cos\theta}{\sin\theta}\frac{\partial}{\partial\varphi}\psi\right]-\frac{\partial}{\partial\theta}\left[\mu\frac{\partial}{\partial\varphi}\psi+ik\sin^2\theta\left\{\frac{\partial}{\partial r}(r\psi)+ik_0\varepsilon r\Phi\right\}+\right.$$
$$\left.+ik\sin\theta\cos\theta\frac{\partial}{\partial\theta}\psi\right]=0, \tag{VI}$$

$$\frac{\partial}{\partial\theta}\left[\sin\theta\left(-\frac{\partial}{\partial\theta}\Phi\right)\right]-\frac{\partial^2}{\partial\varphi^2}\left(\frac{\Phi}{\sin\theta}\right)=-ik_0r\sin\theta\left[(\mu\sin^2\theta+\cos^2\theta)\times\right.$$
$$\left.\times\left\{\frac{\partial}{\partial r}(r\psi)+ik_0\varepsilon r\Phi\right\}+(\mu-1)\sin\theta\cos\theta\frac{\partial}{\partial\theta}\psi-ik\frac{\partial}{\partial\varphi}\psi\right]. \tag{VII}$$

In addition, ψ and Φ must still satisfy the condition stemming from Eq. (III):

$$\frac{\partial}{\partial r}\left(r\frac{\partial}{\partial\varphi}\Phi\right)=-ik_0r\sin\theta\left[\frac{\mu}{\sin\theta}\frac{\partial}{\partial\varphi}\psi+ik\sin\theta\left\{\frac{\partial}{\partial r}(r\psi)+ik_0\varepsilon r\Phi\right\}+ik\cos\theta\frac{\partial}{\partial\theta}\psi\right]. \tag{VIII}$$

With the three equations (VI) - (VII) for the two unknowns ψ and Φ the problem may be solved only by the introduction of fields corresponding to the potential Φ_E. Consequently, in fulfilling the boundary conditions at the surface of the sphere it is necessary to take as the fields within the sphere the sum of oscillations of the quasi-E and quasi-H modes.

APPENDIX 2

Let us assume that a wave with potential $u_i(1, 0) = B_1 j_1(k_0 r)\cos\theta$ is incident on a gyrotropic sphere. We are required to calculate the amplitudes of the $\psi_H(2, 0)$ and $\psi_E(1, 0)$ modes in the ferrite and the reflected waves $u^s(1, 0)$ and $v^s(2, 0)$ at resonance for mode $\psi_H(2, 0)$. Let us assume that

$$u^s(1, 0) = c_1 h_1^{(r)}(k_0 r)\,P_1(\cos\theta), \qquad v^s(2, 0) = c_2 h_2^{(r)}(k_0 r)\,P_2(\cos\theta)$$

and

$$\psi_E(1, 0) = A_1 r\cos\theta, \qquad \psi_H(2, 0) = \frac{A_2}{a}\left\{r^2\left(\frac{\sin^2\theta}{2}-\mu\cos^2\theta\right)-(1-\mu)\frac{a^2}{3}\right\}.$$

By the method of successive approximations it is not difficult to determine that the following components of the field and induction are associated with the $\psi_H(2, 0)$ and $\psi_E(1, 0)$ potentials

$$E_r(1, 0) = -\frac{k_0 A_2 k r^2}{5a}\cos\theta,$$
$$E_\theta(1, 0) = \frac{2k_0 A_2 k r^2}{5a}\sin\theta,$$
$$B_r(2, 0) = \frac{-e(k_0 r)\,A_1 k}{2\mu+1}P_2(\cos\theta).$$

Upon fulfillment of the boundary conditions for $D_r(1, 0)$, $E_\theta(1, 0)$, $B_r(2, 0)$, $\psi_E(2, 0)$ at the surface of the sphere we obtain the following systems of equations:

$$\varepsilon\left[-\frac{k_0A_2ka^2}{5a}\cos\theta+A_1\cos\theta\right]=\frac{2c_1h_1^{(2)}(k_0a)\cos\theta}{a}+\frac{2B_1j_1(k_0a)\cos\theta}{a},$$

$$\left[\frac{2k_0A_2k}{5a}\;a^2\sin\theta-A_1\sin\theta\right]=\frac{1}{a}\,c_1\left[\frac{\partial\,(rh_1^{(2)}(k_0r))}{\partial r}\right]_{r=a}(-\sin\theta)+$$

$$+\frac{B_1}{a}\left[\frac{\partial\,(rj_1(k_0r))}{\partial r}\right]_{r=a}(-\sin\theta),$$

$$\left(-\frac{2}{3}a\right)A_2\left(\mu+\frac{1}{2}\right)P_2(\cos\theta)=c_2\left[\frac{\partial}{\partial r}\{rh_2^{(2)}(k_0r)\}\right]_{r=a}P_2(\cos\theta),$$

$$-2\mu A_2-\frac{\varepsilon(k_0a)A_1k}{2\mu+1}=c_2\frac{6h_2^{(r)}(k_0a)}{a}.$$

Considering the approximate expressions $h_1^{(2)}(k_0a)$, $h_2^{(2)}(k_0a)$, $j_1(k_0a)$ and $j_2(k_0a)$ for small k_0a, it is not difficult to determine the solution of these equations:

$$A_1=\frac{2B_1k_0}{\frac{(k_0a)^2\varepsilon k^2}{5(4\mu+1)(2\mu+1)}(\varepsilon+4)+\varepsilon+2},\qquad A_2=\frac{-\varepsilon(k_0a)kA_1}{(4\mu+1)(2\mu+1)},$$

$$c_1=\frac{iB_1(k_0a)^3}{3}\left[1-\frac{3\varepsilon\left(1+\frac{k^2(k_0a)^2\varepsilon}{5(4\mu+1)(2\mu+1)}\right)}{(4+\varepsilon)\frac{(k_0a)^2\varepsilon k^2}{5(4\mu+1)(2\mu+1)}+(\varepsilon+2)}\right].$$

Resonance occurs with

$$\mathrm{Re}\,(4\mu+1)=-\left(\frac{\varepsilon+4}{\varepsilon+2}\right)\mathrm{Re}\left[\frac{k^2\varepsilon(k_0a)^2}{5(2\mu+1)}\right]\ll 1.$$

In the case of a small sphere $k_0^2a^2\epsilon\ll 1$ this condition differs but little from the Walker resonance condition for the $\psi_H(2,\ 0)$ mode:

$$\mathrm{Re}\,(4\mu+1)=0.$$

REFERENCES

1. Syuy Yan'-shen, Some methods for solution of a problem concerning oscillations of a small gyrotropic sphere. Part I, Successive approximation method. Radio Engineering and Electronics, 1960, 5, 12, 1951.
2. P. Fletcher, I.H. Solt, Coupling of the magnetostatic modes, J. Appl. Phys., 1959, Suppl. to 30, 4, 181 s.
3. Syuy Yan'-shen, Diffraction of electromagnetic waves at a gyrotropic sphere within a rectangular waveguide. Radio Engineering and Electronics, 1960, 5, 1, 15.
4. Ya. A. Monosov, A.V. Vashkovskiy, Ferromagnetic resonance of homogenous precession in a ferrite. Radio Engineering and Electronics, 1959, 4, 10, 1632.
5. J.F. Dillon, Magnetostatic modes in ferrimagnetic spheres, Phys. Rev., 1958, 112, 1, 59.
6. P. Fletcher, I.H. Solt, R. Bell, Identification of the magnetostatic modes of ferrimagnetic resonant spheres, Phys. Rev., 1959, 114, 3, 739.

Submitted to the editors 11 March 1960

LINEAR ACCELERATOR RESONATOR AS A MICROWAVE OSCILLATOR LOAD

A. P. Fedotov and B. K. Shembel'

We consider here an equivalent circuit for a linear accelerator resonator with a heavy beam load and derive the dependence of this load on the amplitude and phase of the field. The equivalent circuit enables us to calculate the input resistance of the accelerator resonator. We give the experimental results of the operation of an accelerator mode with a heavy beam load.

INTRODUCTION

In standing-wave linear accelerators, highly loaded with a beam of accelerated particles [1, 2], the latter affect the amplitude and phase of the accelerating field in the resonator and its input resistance as viewed by the high frequency oscillator. On the other hand, the amplitude and phase of the accelerating field excited by the oscillator determine the particle capture* in the resonator, and, therefore, the current in the accelerated particle beam. The interaction between the oscillator and the resonator becomes strong and hypotheses have been advanced that the oscillator accelerator system may become unstable when the beam loading is high.

To calculate the high frequency supply systems for high beam load accelerators we have to know the input resistance of the resonator and its dependence on the operating conditions of the accelerator and the oscillator. This means that we must know the equivalent electric circuit of the resonator of the beam loaded accelerator its parameters and their dependence on the given operating conditions.

This article considers an equivalent circuit of this kind. The experimental part of the work was carried out with a model of the electronic accelerator consisting of a single gap buncher of the klystron type and the principal resonator (see Fig. 1 and Appendix 1). The

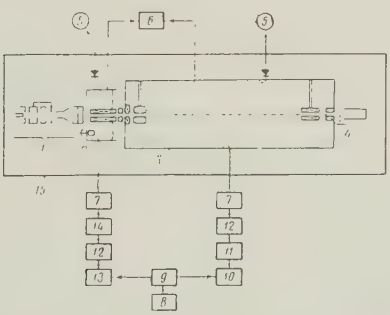

Fig. 1. Block diagram of model accelerator: 1) electron gun; 2) buncher; 3) principal resonator; 4) energy spectrum analyzer; 5) field amplitude indicator; 6) phase difference measuring device; 7) measuring line; 8) exciter, frequency multiplying channel; 9) power division bridge; 10) intermediate oscillator; 11) end oscillator; 12) phase inverter; 13) auxiliary oscillator; 14) attenuator; 15) vacuum container (steel tube).

model meets two basic requirements: 1) the power P_t transferred to the beam by the principal resonator field constitutes a substantial part of the power P_p put into it, i.e., the principal resonator of the accelerator has a high efficiency $\eta = P_t/P_p$; 2) the principal resonator is "long," i.e., under acceleration conditions the particles have a longer period of phase oscillation.

* The capture factor $\varkappa$ is equal to the ratio of the accelerated particle current at the resonator output to the current at the input.

1. EXPERIMENTAL RESULTS

a) Measuring the energy spectrum of particles at the output of a "long" accelerator operating without a buncher, Grishina [3] found two groups of particles in it: one group has energies close to that of the synchronous particle (accelerated particles), while the other had energies close to that of the injection particle (unaccelerated particles), while the other had energies close to that of the injection particle (unaccelerated particles).

Consequently, the power P_p transferred into the resonator is used, first, to create the accelerating field (power loss P_c in the resonator walls); and, second, is transferred to the group of accelerated particles (P_t). Thus, $P_p = P_t + P_c$ (the unaccelerated particles do not affect the power balance). This energy balance has been confirmed experimentally using a model without a buncher at high beam loads (see table). The measurements were made with different synchronous phases φ_c and the same input current $I_{im} = 1.2$ ma.

$\varphi_c°$	P_c, ω	P_t, ω	$\frac{3}{P_t + P_c}$,	P_p, ω	$\eta = \frac{P_t}{P_t + P_c}$
20	1,66	1,38	2,44	2,52	0,57
25	1,13	2,1	3,23	3,11	0,65
30	1,25	2,65	3,9	4,41	0,68
35	1,4	2,93	4,33	4,78	0,68
40	1,6	3,26	4,86	5,7	0,67

Table 1. Note: P_p and P_c are measured using an LI-4 line. The power P_t is calculated from measurements of the current I_0 of accelerated particles and their energy ΔU acquired in the accelerator ($P_t = I_0 \Delta U$). The energy of the synchronous particle at the accelerator output is 10.5 kev.

It is clear from the table that $P_p = P_t + P_c$ to within the accuracy of the measurements (the measurement error in P_p and P_c is 10 - 12%, the error in P_t is 3 - 5%).

b) Measurements on the model accelerator without a buncher showed that when we include a beam which greatly loads the resonator (in the experiments, for η up to 0.7), the pattern of distribution of the accelerating field along its axis (of electrical length 2.3λ) remains unchanged to within the measurement error, (0.5%). Consequently, under these conditions the beam does not contribute any undesirable effect due to a disturbance of the field structure, which would have to be taken into account in an equivalent circuit.

c) When the principal resonator with a buncher, with the second identical resonator operating at 76% efficiency, instability in the oscillator-accelerator system was not observed.

2. EQUIVALENT CIRCUIT*

The loading of a high Q accelerator resonator by a beam of accelerated particles can be represented in an equivalent circuit by a sinusoidal current generator I_c operating as an energy sink in parallel with the equivalent circuit of the resonator (Fig. 2a)**. It can be assumed in a long resonator-accelerator that the beam as a whole has an effect on the accelerating field in such a way that the particles in each bunch are drawn towards a synchronous particle. Since the latter leads the maximum voltage in the resonator U by the angle φ_c, in the equivalent circuit the current I_c should lead U by the same angle φ_c. The amplitude of I_c is determined from the condition of equality of the power obtained by the beam in the accelerator-resonator and the power in the equivalent circuit:

$$I_0 \Delta U = \frac{1}{2} I_c U \cos \varphi_c. \tag{1}$$

Here I_0 is the mean current of the accelerator particles: ΔU is the equivalent potential difference through which the accelerated particles fall in the accelerator; U is the amplitude of the voltage in the resonator and across the equivalent circuit of the resonator. But

$$\Delta U = \bar{\nu} U \cos \varphi_c, \tag{2}$$

---

* The circuit does not take into account the loading of the accelerator resonator by secondary particles.

** Mentioned by B.K. Shembel' in 1953.

in which $\bar{\nu}$ is the mean effectiveness of the accelerator gaps*. Equations (1) and (2) give

$$I_c = 2\bar{\nu} I_0. \tag{3}$$

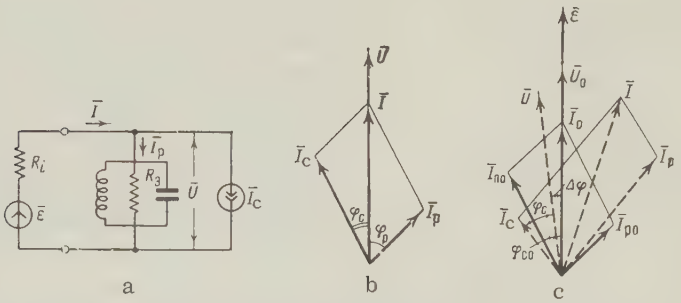

Fig. 2. Equivalent circuit for beam-loaded accelerator resonator and oscillator. Vector diagrams.

Since there is a phase difference φ_c between $\bar{U}$ and $\bar{I}_c$, a purely resistive input impedance of the resonator during the existence of the beam is attained by detuning the resonator with respect to the generator frequency. The phase angle of this detuning can be determined from Fig. 2b.

$$\operatorname{tg}\varphi_p = \frac{I_c \sin\varphi_c}{I_p \cos\varphi_p} = \frac{\eta}{1-\eta}\operatorname{tg}\varphi_c^{**}. \tag{4}$$

where

$$\eta = \frac{P_c}{P_c + P_c} = \frac{I_c \cos\varphi_c}{I_c \cos\varphi_c + I_p \cos\varphi_p}.$$

If the power source is represented by the parameters $\bar{\epsilon}$ and R_i in conjunction with the resonator circuit (Fig. 2a), it turns out that when the beam is switched off the voltage phase in the resonator is shifted by

$$\operatorname{ctg}\Delta\varphi = \operatorname{ctg}\varphi_p\left(1 + \frac{R_e}{R_i}\frac{1}{\cos^2\varphi_p}\right).$$

For $R_i \gg R_e$

$$\Delta\varphi \simeq \varphi_p. \tag{5}$$

The accelerator model without a buncher with an oscillator operating under conditions ($R_i \gg R_e$) was used to measure phase shifts $\Delta\varphi$ when the beam was being switched off at $\varphi_c = 35°$ and various values of η. The measurement of $\Delta\varphi$ was made with the use of a phase difference meter [5] by comparing the phase in the resonator with the reference phase. The frequency of the oscillator was tuned in such a way that the resonator input impedance was

---

* The effectiveness of the accelerating gap ν is the ratio of the potential difference through which the "maximum" particle in the gap falls to the amplitude of the potential difference at the gap the maximum particle is the one which passes the middle of the gap at the moment of the field maximum [3].

** The formula has been derived in another way by Prokunin [3]. For standing-wave accelerators the relationship between the variation in phase of the accelerating field and the particle beam was first determined by Kompaneyets [4].

purely resistive, and this was checked by a transmission line. The length of the transmission line between the oscillator anode circuit and the resonator of the accelerator is approximately a multiple of $\lambda/2$. The points on Fig. 3 are experimental. The theoretical curve in Fig. 3 is plotted from Eq. (4). The scattering of the experimental points may be explained by the difficulty of obtaining a purely resistive input in practice. Although the exciting oscillator is not an ideal current generator, the experimental points are fairly close to the theoretical curve. This makes it possible to claim that formula (4) is correct, and consequently, that the equivalent circuit is correct.

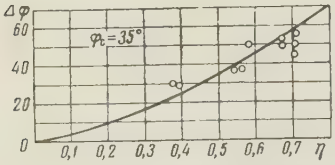

Fig. 3. Shift in voltage phases in resonator when beam is switched off.

The function $I_c(U)$ for two cases of accelerator operation is given in Appendix 2.

3. RESONATOR INPUT IMPEDANCE

Using the equivalent circuit we can calculate the input impedance of the accelerator resonator.

a) The input impedance of a long resonator loaded by a beam (Fig. 2a) is

$$\bar{Z}_{in} = \frac{\bar{\varepsilon} - \bar{I}_c(\bar{U})\, R_i}{\frac{\bar{\varepsilon}}{\bar{Z}} + \bar{I}_c(\bar{U})}.$$

Here the impedance of the unloaded resonator is $\bar{Z} = R_e + jx$. The value of the purely resistive component of the input impedance of the resonator, regardless of the parameters of the oscillator or the state of the particles at the resonator input, is equal to

$$R_0 = R_e(1 - \eta), \tag{6}$$

Here $x = R_e \tan \varphi_c \frac{\eta}{1-\eta}$. When the beam is switched off, the magnitude of the input impedance becomes

$$|\bar{Z}_{in}| = R_0 \frac{1}{\sqrt{1 - 2\eta + \frac{\eta^2}{\cos^2 \varphi_c}}}.$$

for $\varphi_c < 45°$ at any η $R_0 \Delta [\bar{Z}_{in}]$.

To calculate the input impedance of the resonator for a change in the beam current, amplitude, and phase of the field in the resonator we have to take into account the interdependence of these parameters. Let us assume the operation of a long resonator (case 2 in Appendix 2) and that in the initial state (in Fig. 2c the vectors $\bar{U}_0$ and $\bar{I}_{c0}$ are solid lines) $\bar{Z}_{in} = R_0$, $\eta = 0.5$ and $\varphi_{c0} = 40°$, the capture factor $\varkappa = 1$, and $R_e/R_i = 5$. Let us assume that the beam current at the resonator input varies in such a way that the voltage drops by 10% ($U/U_0 = 0.9$). In order to find the expression for this change in current and the new values of φ_c, $\varkappa$, and the phase of the voltage $\Delta\varphi$, we have to use the function $I_c(\bar{U})$ (case 2 in Appendix 2), which is given in Appendix 3. The derived values enable us to calculate the resonator input impedance directly for a change in the beam current.

APPENDIX 1

ACCELERATOR MODEL

The principal cylindrical resonator excited by TM_{01} type waves was made of copper, and was 1250 mm long and 360 mm in diameter. It contained 17 drift tubes with 12 mm diameter holes in them. The tubes were insulated against dc, which makes it possible to

measure the current of the particles impinging upon them and to record the electron-resonance breakdown between them. The wave length was $\lambda = 53.3$ cm. The mean electric field intensity for the acceleration period (the latter is equal to $\beta\lambda$, in which β is the particle velocity referred to the speed of light) was $\bar{E} = 80$ v/cm. The quality factor $Q_0 = 34,400$. The equivalent resonant resistance is $R_e = 53.4 \cdot 10^6$ ohms. The gap length is $0.3\beta\lambda$. The detuning equals 15% [6]. The efficiency of the gaps ν varies from 0.71 for the first to 0.82 for the last; $\Delta\beta/\beta$ at the first gap is 7.1% and 3.6% at the last gap. The uniformity of the accelerating field along the resonator axis is equal to $\pm$ 3% and is obtained by varying the natural frequencies of the end partitions.

The buncher is a toroidal resonator ($Q_0 = 1500$, $R_e = 170 \cdot 10^3$ ohm) with a beam hole diameter of 8 mm. The length of the bunching gap is 12.8 mm ($0.25\beta\lambda$); $\nu = 0.81$. To make it easier to focus the electron beam, which at low energy is rather difficult to do at the front end of the accelerator*, the distance between the middle of the gap in the buncher and the middle of the first gap in the principal resonator is fixed and designed to provide maximum capture, taking into account the space charge [7] for the following conditions: injection voltage 1,800 v, beam current 1.7 ma, beam diameter 8 mm. The distance is 240 mm (corresponding to a transit angle $\Theta = 33.7$ radians).

The modernized particle source with an accelerating electrode provides a maximum current of approximately 2 ma at an accelerating voltage of 1800 ± 1.5 v.

The beam is focused by a longitudinal magnetic field, the intensity of which is approximately 40 oersteds. The vacuum in the steel tube is kept constant to within $(3 - 9) \cdot 10^{-6}$ mm of mercury.

The exciter in the high frequency supply system is a thermostatically regulated continuous range exciter. The exciter frequency of 2.94 mc is multiplied 192 times. The intermediate oscillator in the principal resonator channel, the auxiliary oscillator, and the attenuator in the buncher channel are used for decoupling the channels, making it easier to conduct the experiment.

APPENDIX 2

DEPENDENCE OF THE AMPLITUDE OF CURRENT I_c ON THE AMPLITUDE AND PHASE OF THE VOLTAGE IN THE RESONATOR**

In Eq. (3) the current $I_0 = I_{in}\varkappa(\bar{U})$, where I_{in} is the current in the beam at the input of the resonator under consideration and $\varkappa$ is the capture factor. The function $\varkappa(\bar{U})$ will be different for different states of the particles at the resonator input. Let us consider it in the case of a long accelerator-resonator in two typical cases: 1) when the resonator receives particles from the output of a single gap buncher, and 2) when it receives particles from the output of a similar long resonator, on the supposition that the particle velocity in the gaps varies very slightly and that there is no space charge.

Case 1. The stability region in the phase plane of the accelerator or the region of phases φ and velocities $y = (\beta - \beta_0)/\beta_0$ (β_0 is the velocity of the synchronous particle), at which the particles are captured under the condition of synchronous acceleration, is bounded by the function***

$$\frac{2\pi\Theta_{fu}}{\sin\varphi_c - \varphi_c\cos\varphi_c} y_m^2 = 4 - 3\left(\frac{\varphi}{\varphi_c}\right)^2 - \left(\frac{\varphi}{\varphi_c}\right)^3. \qquad (7)$$

Here y_m is the velocity of the maximum particle; $\Theta_{fu} = 2\,U/\nu U_3$ is the transit angle up

---

* The effect of the spurious magnetic fields (including the earth's) on the trajectory of the beam was considerably reduced by taking steps suggested by Teplyakov; the steel tube containing the model was bound on the outside with high strength tape 0.2 mm thick; a permalloy screen 1 mm thick was fitted on the principal resonator.

** In a long accelerator $\bar{I}_c$ leads $\bar{U}$ by the angle φ_c (§ 2).

*** Equations (7) and (8) are taken from Teplyakov's work, for example Ref. 3.

to the focusing of the accelerator gap (U is the potential difference through which the particles have passed; U_3 is the high frequency voltage at the gap). In Fig. 4 curve C is the

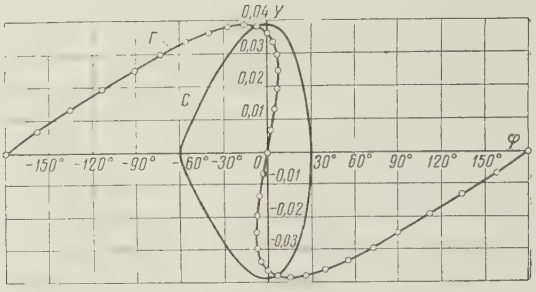

Fig. 4. Phase plane. C is the boundary limiting the region of stability of the principal resonator ($\varphi_c = 30°$, $\Theta_{fu} = 19$ radians), Γ is the curve showing the particle state at the buncher output ($\Theta = 33.7$ radians, $\Theta_{fg} = 25.9$ radians, $\varkappa = 0.45$).

boundary function for the principal resonator in the model at $\varphi_c = 30°$ and $\Theta_{fu} = 19$ radians. The particle state at the input to the principal resonator after a single gap buncher in the same phase plane is described in the following way

$$\varphi = \varphi_0 - \frac{\Theta}{\Theta_{fg}} \sin \varphi_0; \qquad y = -\frac{\sin \varphi_0}{\Theta_{fg}}. \tag{8}$$

and here Θ_{fg} is the transit angle up to the focusing of the buncher; φ_0 is the initial phase of the particles. In Fig. 4, the curve Γ is plotted from Eq. (8) for $\Theta = 33.7$ radians and $\Theta_{fg} = 25.9$ radians (in the principal resonator with $\varphi_c = 30°$ and $\Theta_{fu} = 19$ radians at a given $\Theta = 33.7$ radians the maximum capture factor $\varkappa = 0.45$ occurs at $\Theta_{fu} = 25.9$ radians). The small circles on the curve show the particles whose initial phases were different from each other by 10°; $\varkappa$ is calculated as the ratio of the number of intervals between the small circles enclosed by the boundary function to the total number of such intervals which is equal in the given case to 36.

Variation in the phase of oscillations in the resonator at a constant amplitude corresponds to a shift of the boundary C in Fig. 4 with respect to the curve Γ along the phase axis. The dependence of $\varkappa$ on the phase differences ($\Delta\varphi$) of the oscillations of the buncher and principal resonator system (Fig. 1), calculated in this way for the data in Fig. 4, is given in Fig. 5 ($\varkappa$ is the capture factor when operating with a buncher; $\varkappa_0$ is the capture factor without the buncher, when $\varphi_c = 30°$ is 0.25). Figure 5 shows an experimental

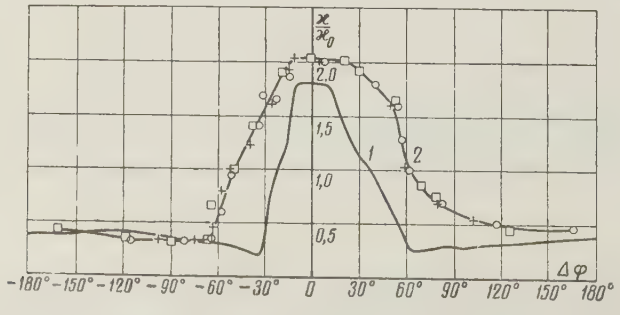

Fig. 5. Dependence of the capture factor for the principal resonator operating after the buncher on the phase difference in oscillations between the buncher and the principal resonator: 1) theoretical curve $\varphi_c = 30°$, $\Theta = 33.7$ radians, $\Theta_{fu} = 19$ radians, $\Theta_{fg} = 25.9$ radians; 2) experimental curve.

curve, 2, which is the result of three series of measurements. In these measurements the amplitude of the voltage in the buncher was selected in such a way as to ensure maximum $\varkappa$ in the principal resonator with an optimum phase difference $\Delta\varphi_{opt}$.

The experimental curve $\frac{\varkappa}{\varkappa_0}(\Delta\varphi)$ is somewhat broader than the theoretical one. This may be due to the fact that the actual region of capture in the principal resonator model is greater than that described by Eq. (7) because of an appreciable increment in the velocity in its gaps [8].

When calculating the dependence of $\varkappa$ in the principal resonator on the amplitude of the oscillations in it at a constant $\Delta\varphi$, the boundary function for the principal resonator is recalculated each time. Here the point on the boundary corresponding to the maximum particle remains at the same spot when the boundary itself varies.

Case 2. Let us assume that the particles at the output of the foregoing resonator are uniformly distributed in the phase space limited by the boundary function, which is the same for both resonators. The dependence of $\varkappa$ in the latter resonator on the amplitude and phase of the field in it may be found by varying the boundary for this resonator in accordance with the variation in amplitude, and shifting it with respect to the boundary of the former resonator which describes the state of the particles, as a function of the variation in phase and by calculating the area common to the bounded regions.

When the phase difference between resonators under consideration is constant, $\varkappa$ remains equal to unity when the amplitude U is increased from the initial value U_0, which corresponds to the synchronous phase φ_{co}. It can be shown* that when U is reduced in this resonator from U_0 to $U_0 \cos\varphi_{co}$, the function $\varkappa(U)$ can be idealized by the straight line

$$\varkappa = \frac{\frac{U}{U_0} - \cos\varphi_{c0}}{1 - \cos\varphi_{c0}}. \tag{9}$$

The dependence of $\varkappa$ on the phase difference $\Delta\varphi$ between the resonators for an increase ($U > U_0$) and reduction ($U < U_0$) in amplitude are given in Fig. 6 (the decremental segments $\varkappa(\Delta\varphi)$ are also approximated by straight lines).

APPENDIX 3

It follows from the circuit in Fig. 2a for two values $\bar{I}_{c0}$ and $\bar{I}_c$ (corresponding to $\bar{U}_0$ and $\bar{U}$) that

$$\frac{\bar{I}_c}{\bar{I}_{c0}} = \frac{\bar{U}}{\bar{U}_0} + \frac{1}{\bar{I}_{c0}}\frac{\bar{\varepsilon}}{R_i}\left(1 - \frac{\bar{U}}{\bar{U}_0}\right). \tag{10}$$

All phases are computed from $\bar{\epsilon}$. Since $\eta = I_{c0}\cos\varphi_{c0}/I_0$ and $I_0 = \epsilon/(R_i + R_0)$, then, from Eq. (6), we obtain

$$I_{co} = \frac{\eta}{\cos\varphi_{c0}}\frac{\varepsilon}{R_i + R_e(1-\eta)}. \tag{11}$$

After a change in the beam current at the resonator input (in Fig. 2c the vectors are shown by a dotted line)

$$\bar{U} = Ue^{j\Delta\varphi}. \tag{12}$$

The new current $\bar{I}_c$ leads $\bar{U}$ by the angle φ_c, determined by U,

$$\bar{I}_c = I_c e^{j(\Delta\varphi+\varphi_c)} \tag{13}$$

---

* By the graphical method discussed above or by the ratio of the areas of the bounded regions $s/s_0 = \sqrt{(\varphi_c/\varphi_{c0})^5}$ which follows, e.g. from Ref. 9.

Here

$$\varphi_c = \arccos \frac{\cos \varphi_{c0}}{U/U_0}. \tag{14}$$

But in the initial state

$$\bar{I}_{c0} = I_{c0} e^{j\varphi_{c0}}. \tag{15}$$

Substituting Eqs. (11), (12), (13), and (15) in Eq. (10), we obtain

$$\frac{I_c}{I_{c0}} = \frac{U}{U_0} e^{j(\varphi_{c0} - \varphi_c)} + \cos \varphi_{c0} \frac{1}{\eta} \left[1 + \frac{R_e}{R_i} (1 - \eta) \right] \left(1 - \frac{U}{U_0} e^{j\Delta\varphi} \right) e^{-j(\Delta\varphi + \varphi_c)} \tag{16}$$

Equating the imaginary part of the right-hand side of Eq. (16) to zero, we obtain

$$\sin(\Delta\varphi + \varphi_c) = \frac{U}{U_0} \left[\sin \varphi_c + \frac{\sin(\varphi_{c0} - \varphi_c)}{\cos \varphi_{c0}} \frac{\eta}{1 + \frac{R_e}{R_i}(1 - \eta)} \right] \tag{17}$$

Equating the real parts of Eq. (16) gives

$$\frac{I_c}{I_{c0}} = \frac{U}{U_0} \cos(\varphi_{c0} - \varphi_c) + \cos \varphi_{c0} \frac{1}{\eta} \left[1 + \frac{R_e}{R_i} (1 - \eta) \right] \times$$

$$\times \left[\cos(\Delta\varphi + \varphi_c) - \frac{U}{U_0} \cos \varphi_c \right]. \tag{18}$$

For the problem in question Eq. (14) gives $\varphi_c = 31° 35'$; Eq. (17) gives $\Delta\varphi = -1° 55'$; Eq. (18) gives $I_c/I_{c0} = 1.44$. Since $(\varphi_{c0} - \varphi_c) < \Delta\varphi < 2(\varphi_{c0} - \varphi_c)$ (Fig. 6b), the capture factor is determined by Eq. (9) and is equal to $\varkappa = 0.57$.

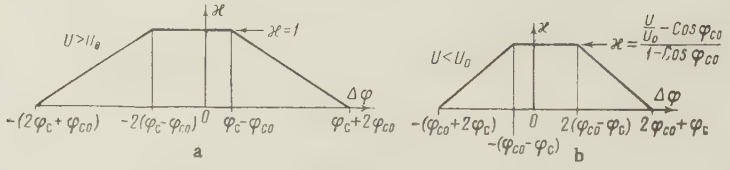

Fig. 6. The dependence of the capture factor for the accelerator resonator when operating in tandem with a similar resonator, on the phase difference between them.

Let us define the ratio between the current at the resonator input in the new state to the current in the initial state as

$$k = \frac{I_{in}}{I_{in\,0}} = \frac{I_{in}}{I_{out\,0}}. \tag{19}$$

Then $\varkappa$ in the new state (from Eqs. (3) and (19) is equal to:

$$\varkappa = \frac{I_{out}}{I_{in}} = \frac{I_{out}}{kI_{put\,0}} = \frac{\frac{I_c}{2\nu}}{k\frac{I_{c0}}{2\nu}} = \frac{1}{k}\frac{I_c}{I_{c0}}.$$

From the above expression

$$k = \frac{1}{\varkappa}\frac{I_c}{I_{c0}} = 2{,}5.$$

Given this increase in current at the resonator input, the voltage in it is reduced by 10% and the capture factor is reduced from 1 to 0.57.

The experimental part of this research was carried out jointly by Yu. K. Solodkov, N.P. Popov, Ye. A. Sidorov and V.B. Stepanov. A.D. Grishina took part in the initial stages of the work. Useful advice was given by V.A. Teplyakov and G.M. Anisimov. The authors express their gratitude to all those listed above.

REFERENCES

1. Semenov, N.N., Zel'manov, I.L. Kompaneyetz, A.S., Stepanov, B.M., Shembel', B.K. Some problems in designing heavy-current linear accelerators. Reports of the conference on high energy accelerators, Geneva, 1956.
2. Lawrence, E.O.,Science, 1955, 122, 3180, 1127.
3. Shembel', B.K., Teplyakov, V.A., A.P. Fedotov, Prokunin, L.M., Grishina, A.D. Design problems of linear accelerators for heavy particles. Reports of the conference on charged particle accelerators, Moscow, 1954.
4. Konpaneyets, A.S., Variation in resonator frequency due to synchronous beam load. Report of IKhF AN SSR, 1952.
5. Fedotov, A.P., Shembel', B.K., Measurement Techniques, 1955, 6, 43.
6. Teplyakov, V.A., Shembel' B.K., Radio Engineering and Electronics, 1956, 1, 4, 443.
7. Klystrons, translated from English and edited by Ye. D. Naumenko, Soviet Radio, 1952.
8. Mel'nikov, V.K. and Yu. S. Sayazov. Theory of capture of particles under synchronous conditions of acceleration taking into account non-conservation in the equations of motion. Unified Nuclear Research Institute, Dubna, 1958.
9. Teplyakov, V.A., Analysis of operation of complex bunchers, Report of IKhF An SSR, 1959.

Received by editors 3 May 1960

GAS DISCHARGE DETECTOR OF MICROWAVE OSCILLATIONS

G.D. Lobov

This article makes a theoretical analysis of one of the possible hypothesis regarding the operation of the gas discharge detector. On the basis of analysis an estimate is given for the rise time of the pulse, and the transmission factor of the gas-discharge detector is determined. The theoretical results have been verified experimentally.

INTRODUCTION

A great deal of work has been done on the effect of a microwave electromagnetic field on a gas discharge, and, in particular, on detection using a gas discharge tube. The following facts can be considered to have been established analytically up to the present time.

1. When a microwave field is superimposed on a gas discharge, apart from a variation in the dc component of the discharge current [1 - 5], there is also a variation of the rate of recombination of electrons with ions [6, 7] and in the number of collisions between electrons and gas particles [8, 9].

2. When different regions of the gas discharge are irradiated with pulse modulated microwave energy, the voltage pulse obtained across the load resistance differs in magnitude, polarity and shape [4,5]. The maximum signal is obtained when irradiating the discharge region lying between the end of the negative glow and the beginning of the positive column [4,5].

3. The voltage pulse varies with a variation in the pressure and nature of the gas, the size of the discharge gap, the applied power and the discharge current [1, 3, 4 and 5].

Published data, however, do not give any idea of the parameters of the gas discharge detector, since the detection mechanism is only considered qualitatively, and the results are contradictory and do not always agree with experimental data.

This article gives a theoretical analysis of one of the possible hypotheses for the operation of a gas discharge detector. The basis of the analysis is the fact that when a microwave field is superimposed on a gas discharge, the electron energy varies. The variation in electron energy may lead to variation in certain parameters of the gas discharge, which in the final analysis has an effect on the dc component of the discharge current through the tube. It may be assumed that the variation in energy has a greater effect at places where the total electron energy is minimum. This region of the discharge is the Faraday dark space.

1. EQUATION FOR THE ELECTRON ENERGY BALANCE IN GASEOUS DISCHARGE

The energy increment obtained by an electron when a microwave field is superimposed can be found by means of the equation for the balance in electron energy.

As shown in Ref. 10, the mean energy balance for an electron, ignoring the propagation of heat, can be described by the equation

$$\frac{dQ}{dt} = Q_{acq}^{(1)} - Q_{los}^{(1)} \qquad (1)$$

in which $Q_{acq}^{(1)}$ and $Q_{los}^{(1)}$ are the energy acquired and lost per second.

In the case of a decaying plasma we usually only calculate the energy received by electrons from the field, which is equal to [10, 11]

$$Q_{acq}^{(1)} \approx \frac{e^2 |E_{\sim}|^2 \nu}{2m(\omega^2 + \nu^2)}.$$

If there is a constant electric field, we have to take into account the energy acquired by the electron from the constant field:

$$Q_{acq}^{(1)} = \frac{e^2 E_{=}^2}{m\nu}.$$

The energy lost by an electron during elastic and non-elastic collisions is

$$Q_{los}^{(1)} = \delta\nu_y (Q - Q_M).$$

Here

$$\delta = \delta_y \left(1 + \frac{\delta_{Hy}\nu_{Hy}}{\delta_y \nu_y}\right).$$

$Q - Q_m$ is the difference in the energy of the electron and molecules; δ_y and δ_{Hy} are the coefficients of transfer of electron energy to a gas particle during elastic and non-elastic collisions.

Substituting Q_{acq} and Q_{los} into Eq. (1) and replacing Q in terms of 3/2 kT, we obtain

$$\frac{dT}{dt} = \frac{2e^2E_=^2}{3km\nu} + \frac{e^2|E_\sim|^2\nu}{3km(\omega^2+\nu^2)} - \delta\nu_y(T - T_м).$$

This expression may be transformed if it is assumed that before the arrival of the microwave pulse $T = T_Н$, and $\nu = \nu_Н$; but when the microwave pulse is effective in steady-state operation, $T = T_к$ and $\nu = \nu_к$. The substitution of these conditions into the previous expression gives us three equalities that will be useful from here on:

$$\frac{2e^2E_=^2}{3km\nu_н} = \delta_н\nu_{yн}(T_н - T_м),$$

$$\delta_к\nu_к\nu_{yк}(T_к - T_м) - \delta_н\nu_н\nu_{yн}(T_н - T_м) = \frac{e^2|E_\sim|^2\nu_н^2}{3km(\omega^2+\nu_н^2)}, \tag{2}$$

$$\frac{dT}{dt} = \frac{\delta_н\nu_н\nu_{yн}(T_н - T_м)}{\nu} +$$

$$+ \frac{\delta_к\nu_к\nu_{yк}(T_к - T_м) - \delta_н\nu_н\nu_{yн}(T_н - T_м)}{\nu_к^2}\frac{\omega^2+\nu_н^2}{\omega^2+\nu^2}\nu - \delta\nu(T - T_м). \tag{3}$$

2. TEMPERATURE INCREMENT AND TEMPERATURE RISE TIME IN A GAS DISCHARGE WHEN A MICROWAVE FIELD IS SUPERIMPOSED

Equations (2) and (3) can be used to determine the increment and temperature rise time when a microwave field is superimposed.

For the sake of simplicity we will make the vollowing assumptions in our solution.

1. The entire microwave power is applied to the Faraday dark space, where the transfer of energy from electrons to gas particles is mainly effected by elastic collisions, i.e., $\nu = \nu_y$ and $\delta = \delta_y = 2m/M$ (M is the mass of a molecule).

2. The temperature of the molecules is considerably less than that of the electrons;

$$T_м \ll T_Н,\ T_к.$$

3. The applied power is small, so that $T_K - T_H = \Delta T \ll T_H,\ T_K$.

4. When calculating the temperature rise time we will ignore the variation ν in the expression $1/(\omega^2 + \nu^2)$.

Taking these assumptions into account, we have

$$\frac{dT}{dt} = \frac{\delta\nu_н^2T}{\nu} + \frac{\delta(\nu_к^2T_к - \nu_н^2T_н)}{\nu_к^2}\nu - \delta\nu T. \tag{4}$$

If it is taken that the principal collisions are collisions between electrons and molecules, Eq. (4) can be rewritten in the form

$$\frac{\nu^2d\nu}{dt} = \frac{\delta}{2}\left[\nu_н^4 + \frac{\nu_к^4 - \nu_н^4}{\nu_к^2}\nu^2 - \nu^4\right].$$

The solution of this equation at the boundary condition $\nu = \nu_H|_{t=0}$ is the function

$$\ln\frac{(\nu - \nu_к)(\nu_н + \nu_к)}{(\nu + \nu_к)(\nu_н - \nu_к)} + 2\frac{\nu_к^2}{\nu_н^2}\left(\operatorname{arc\,tg}\frac{\nu\nu_к}{\nu_н^2} - \operatorname{arc\,tg}\frac{\nu_к}{\nu_н}\right) = -\delta\left(\nu_к + \frac{\nu_н^4}{\nu_к^3}\right)t.$$

Keeping the former assumptions, this function can be simplified if we take $\nu_K \simeq \nu_H$. In this case we have

$$\nu \simeq \nu_к + (\nu_н - \nu_к)e^{-2\delta\nu_Ht} = \nu_н + \Delta\nu\left(1 - e^{-\frac{t}{\tau}}\right)$$

or

$$T^{\frac{1}{2}} \simeq T_{\text{н}}^{\frac{1}{2}} e^{-2\delta\nu_{\text{н}}t} + T_{\text{к}}^{\frac{1}{2}}(1 - e^{-2\delta\nu_{\text{н}}t}) = T_{\text{н}}^{\frac{1}{2}} + \frac{\Delta T}{T_{\text{н}}^{\frac{1}{2}}}(1 - e^{-\frac{t}{\tau}}).$$

The rise time of the temperature pulse from 0.1 to 0.9 ΔT is equal to

$$\tau_{\text{f}} = \frac{1{,}1}{\delta\nu_{\text{н}}} = \frac{1{,}1\tau_0}{pT_{\text{н}}^{\frac{1}{2}}}, \tag{5}$$

in which $\tau_0 = 1/\delta\nu_0$; ν_0 = the frequency of the elastic collisions between electrons and gas molecules at the pressure p = 1 mm of mercury and electron temperature T = 1°K.

Table 1 gives the values of δ, ν_0 and τ_0 for certain gases.

Table 1

Gas	He	Ne	Ar
$\delta = \frac{2m}{M}$	$2{,}8\cdot10^{-4}$	$5{,}5\cdot10^{-5}$	$2{,}8\cdot10^{-5}$
ν_0, sec^{-1}	$8{,}2\cdot10^{-6}$	$1{,}21\cdot10^{-7}$	$1{,}78\cdot10^{-7}$
τ_0, μsec	440	1500	2000

To find the temperature increment we use Eq. (2). Assuming the same simplifications as when determining the rise time, we have for a small sign

$$\Delta T = \frac{e^2 |E_\sim|^2}{6km\delta(\omega^2 + \nu^2)}.$$

The electric field intensity E can be expressed in terms of power flow through the waveguide P, in accordance with Ref. 12, by the relationship

$$|E_\sim|^2 = \frac{4P \operatorname{Re} W}{S},$$

where S and W are the cross section and characteristic impedance of the wave guide. In a waveguide with an H_{10} wave, filled with a dielectric,

$$W_{H_{10}} = \frac{377}{\sqrt{\varepsilon - \left(\frac{\omega_{\text{к}}}{\omega}\right)^2}}.$$

If we consider as a first approximation that the gas discharge occupies the entire volume of the waveguide, and that the dielectric constant of the ionized gas is expressed in accordance with Ref. 11 by

$$\varepsilon = 1 - \frac{\omega_0^2}{\omega^2 + \nu^2} - i\frac{\omega_0^2\nu}{\omega(\omega^2 + \nu^2)},$$

in which $\omega_0^2 = 3.2 \cdot 10^9$ n, then when substituting E, W and ϵ into the expression for ΔT, we have

$$\Delta T = \frac{250e^2P}{Skm\delta(\omega^2 + \nu^2)} \operatorname{Re}\left[1 - \frac{\omega_0^2}{\omega^2 + \nu^2} - \frac{\omega_{\text{к}}^2}{\omega^2} - i\frac{\omega_0^2\nu}{\omega(\omega^2 + \nu^2)}\right]^{-\frac{1}{2}} \tag{6}$$

Let us consider two cases.

1. $\omega^2 + \nu^2 \gg \omega_0^2$. When substituting all the constants we obtain

$$\Delta T = \frac{1{,}4\cdot10^{16}P}{\delta\left(1 + \frac{\nu_0^2p^2T_{\text{н}}}{\omega^2}\right)}\frac{W_0}{S\omega^2} = \frac{\varkappa P}{1 + \frac{\nu_0^2p^2T_{\text{н}}}{\omega^2}}, \tag{7}$$

in which $W_0 = 377/\sqrt{1-(\omega_к/\omega)^2}$ (ohm); S is the cross-section of the waveguide (cm^2); P is the power (mw); p is the pressure (mm Hg); ΔT and T are temperature (°K). The value $\varkappa$ describing the increase in temperature when one mw of microwave power is applied is given in Table 2.

2. $\omega^2 \gg \nu^2$. In this case

$$\Delta T = \varkappa P \sqrt{1-\left(\frac{\omega_к}{\omega}\right)^2}\,\mathrm{Re}\left[1-\frac{\omega_к^2+\omega_0^2}{\omega^2}-i\frac{\omega_0^2}{\omega^2}\frac{\nu}{\omega}\right]^{-\frac{1}{2}} \tag{8}$$

Table 2

Gas	He	Ne	Ar
$\varkappa$, degree/mw	1,6	8	16

Analysis of Eq. (8) shows that when the frequency and signal power are constant, ΔT increases with n to a certain limit. If there is further increase in the concentration, ΔT drops; roughly speaking, there will be a decrease when the expression $1 - (\omega_K^2 + \omega_0^2)\omega^{-2}$ becomes less than zero. Hence the maximum concentration and the maximum temperature increase can be found from the condition $1 - (\omega_K^2 + \omega_0^2)\omega^{-2} = 0$, from which

$$n_{con} = 3\cdot 10^{10}\,\omega^2\left[\left(1-\frac{\omega_к}{\omega}\right)^2\right];$$

$$\Delta T_{max} = \frac{\varkappa}{\sqrt{2}} P \sqrt{\frac{\omega}{\nu}}. \tag{9}$$

3. GAS-DISCHARGE DETECTOR TRANSMISSION FACTOR

Equations (6), (7) and (8) can be used to find the dependence of the variation in the discharge current on the applied microwave power, since certain parameters affecting the discharge current vary with temperature. Indeed, the density of the electron current (the ionic part of the current in the Faraday dark space will be ignored) in the discharge is determined by the relationship [13]

$$J = eD\frac{dn}{dl} + enKE,$$

in which D and K are, respectively, the difusion factor and the electron mobility.

Since D, K and n are exponential functions of electron temperature T^k, the increment in the discharge current in steady-state operation when the temperature varies by ΔT is given by

$$\Delta I \quad CI_0\frac{\Delta T}{T_н},$$

in which I_0 is the dc component of the discharge current through the detector; C is a constant depending on that parameter whose role is considered fundamental in the variation of the discharge current.

When considering different extreme cases, i.e., when considering the current to be either purely diffusional or solely a conduction current, and also when taking into account the change in electron concentrations, as a function of the change in the recombination coefficient, we can determine a number of extreme values for the constant C, which varies from 3/2 to -1.

It is quite possible that all the processes play a part in some way or other in varying the discharge current, and that the role of a process may be predominant in different parts of the discharge. This may explain the variation in the amplitude, polarity and shape of the pulse when illuminating different parts of the gaseous discharge.

On the basis of the experimentally extablished fact that in the region of maximum detection the discharge current increases when a microwave field is applied, and also taking into account the large part played by diffusion and recombination in the Faraday dark space, we can assume C = 1/2.

If a discharge tube is included in the circuit containing an emf in series with a load resistance r_H, a change in the temperature of the electrons in the discharge tube will lead to a change in the load voltage:

$$\Delta U = -\frac{1}{2} I_0 \frac{r_H}{1+\frac{r_H}{r_p}} \frac{\Delta T}{T_H} \simeq -\frac{I_0 r_H \varkappa P}{2\left(1+\frac{r_H}{r_p}\right)\left(1+\frac{\nu^2}{\omega^2}\right) T_H},$$

where r_p is the internal resistance of the discharge gap.

For small load resistances and high frequencies this expression can be simplified:

$$\Delta U \simeq -\frac{I_0 r_H \varkappa P}{2T_H}. \tag{10}$$

Hence the gas detector transmission factor is

$$\beta = \left|\frac{\Delta U}{P}\right| = I_0 r_H \beta_0. \tag{11}$$

Here β_0 is the transmission factor at I_0 = 1 ma and r_H = 1 kilohm.

The temperature of the electrons in the Faraday dark space lies somewhere between the molecule temperature T_m = 300°K and the electron temperature in the positive column of the gas discharge T_{pos}.

Table 3 shows the extreme values of the transmission factor calculated according to Eq. (11). For $\beta_{0\min}$ it was assumed that $T = T_{0pos}$ and T is taken at high gas pressures.

When determining β_{0max} T was taken as 300°K. To obtain ΔT we used Eq. (2), in which $T_H = T_M$ = 300°K.

Table 3

Gas	He	Ne	Ar
β_0 min mv/mw	0,03	0,2	0,8
β_0 max mv/mw	5	25,6	54

4. EXPERIMENTAL VERIFICATION

The conclusions were checked experimentally using gas discharge tubes both soldered to and temporarily joined to a vacuum system. As soldered tubes we used neon signal lamps of different types.

The experiment was made at three wavelengths: λ_1, λ_2, = $4\lambda_1$ and $\lambda_3 = 12\lambda_1$. The block diagram of the circuit used for the experiment is described in Refs. 1 and 2. Basically, we tested certain relationships resulting from the analysis of Eqs. (5) - (10), and we studied the effect of microwaves on different parts of the glow discharge. Various parts of the discharge were excited by a cavity resonator fed from a klystron generator (λ = 10 cm). The graph in Fig. 1b shows that the maximum signal was obtained when the Faraday dark space was irradiated.

According to Eq. (10) the values of the detected signal at $\Delta T \ll T_H$ and T_K are proportional to the applied power. Figure 2 confirms this conclusion. Zdornova [3] came to the same conclusion when she studied the behavior of a gas detector with microwaves.

Table 4

λ	λ_1	λ_2
n_{exp} / n_{theor}	1,6	0,9

Examination of the dependence of the amplitude of the detected voltage on the discharge current (Fig. 3) shows that the transmission factor only increases monotonically with an increase in the current up to a certain value. Comparison of Fig. 3 with Fig. 4 makes it possible to compare the maximum concentration obtained theoretically and experimentally.

Table 4 gives the results of this comparison. The calculation of the maximum concentration was based on Eq. (9).

It is clear from Table 4 and Eq. (10) that the maximum concentrations and current increase with the signal frequency. Consequently, the transmission factor may be increased together with the signal frequency by increasing the discharge current. This is confirmed in Fig. 5 which shows the mean of the functional relationship between the transmission factor and the discharge current for two wavelengths λ_1 and $4\lambda_1$.

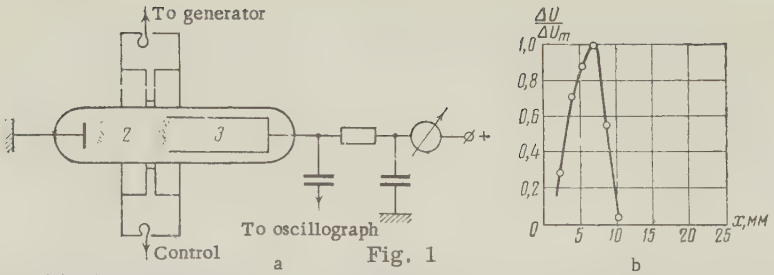

Fig. 1

Fig. 1. a) block diagram for a study of the effect of microwave radiation on different regions of the discharge (1: negative glow; 2) Faraday dark space; 3) positive discharge column;); b) change in detected load resistance voltage as a function of the illuminated discharge region.

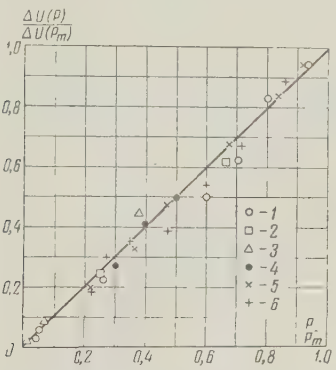

Fig. 2

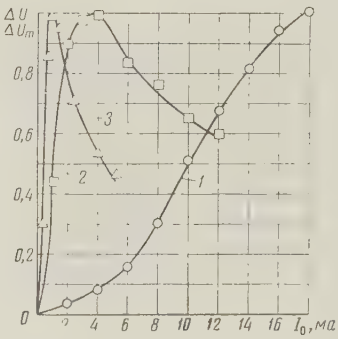

Fig. 3

Fig. 2. Dependence of detected load voltage on power input:
1 — λ_1, I_0 = 4 ma, P_M = 1.4 mw, MN-6; 2 — λ_1, I_0 = 10 ma, P_M = 1.4 mw, MN-6;
3 — λ_1, I_0 = 16 ma, P_M = 0.8 mw, MN-6; 4 — λ_2, I_0 = 2 ma, P_M = 10 mw, FN-2;
5 — λ_2, I_0 = 2.4 ma, P_M = 16 mw, MN-15; 6 — λ_2, I_0 = 3.4 ma, P_M = 10 mw, MN-15.

Fig. 3. Dependence of the amplitude of the detected voltage on the dc component of discharge current for the same tube MN-6: 1 — λ_1; 2 — $\lambda_2 = 4\lambda_1$; 3 — $\lambda_3 = 12\lambda_1$

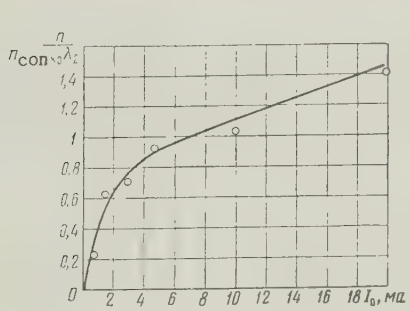

Fig. 4

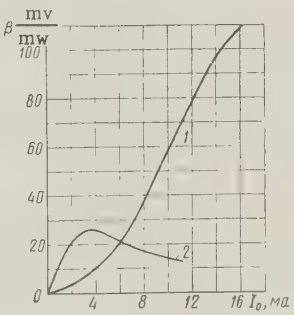

Fig. 5

Fig. 4. Dependence of the mean concentration of electrons in a discharge tube on the dc component of discharge current.

Figure 5. Averaged transmission factor for a gas-discharge detector with MN-6 n neon tube: 1 — $\lambda_2 = 4\lambda_1$; 2 — λ_1

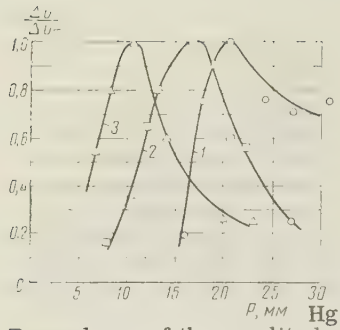

Fig. 6. Dependence of the amplitude of the detected voltage on gas pressure for Ne: 1 — λ_1; 2 — $\lambda_2 = 4\lambda_1$; 3 — $\lambda_3 = 12\lambda_1$

According to Eq. (7), as the gas pressure increases, the transmission factor of the gas discharge detector should drop. A decrease in the detected voltage is observed later as the signal frequency becomes higher. It is clear from Fig. 6 that this is qualitatively confirmed for Ne. The behavior of Ar and He is similar. A reduction in the transmission factor at low pressures may be explained by the fact that we ignored the non-elastic collisions, the number of which is inversely proportional to the pressure. Since $\delta_{HY} = 1/p^k$, the detected voltage should drop appreciably at fairly small pressures.

Figures 7 a, b and c show the dependence of the rise time on the gas pressure. The solid lines mark the theoretical values of the relationships plotted.

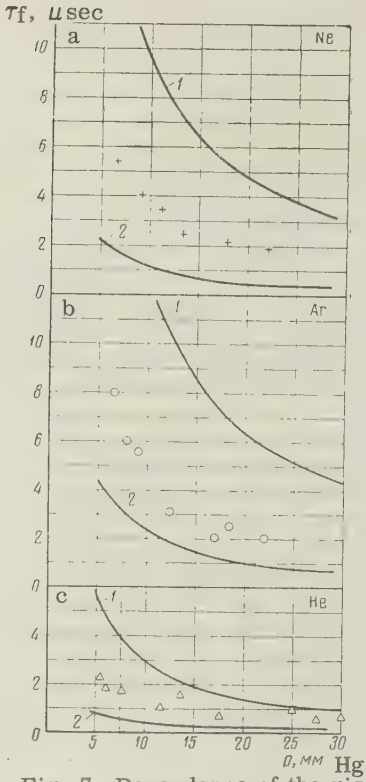

Fig. 7. Dependence of the rise time of the pulse on gas pressure for Ne (a), Ar (b) and He (c). Theoretical curves plotted from Eq. (5): 1) for T = 300°K; 2) for $T = T_{pos}$ (T_{pos} taken from Ref. 14).

CONCLUSIONS

1. The gas discharge detector follows a square law at small input power values.
2. The transmission factor of a gas-discharge detector is proportional to the power distribution of the signal being detected and inversely proportional to the square of the signal frequency. When standard waveguides are used as the spaces in which the gas discharge detectors are mounted, the transmission factor does not depend on the signal frequency, since the power density increases with the frequency. The transmission factor increases with the discharge current up to a certain optimum current, which can be determined by the ratio between the electron concentration and the signal frequency. This value increases as the signal frequency gets higher.
3. The afterglow of a gas discharge detector depends on the nature and pressure of the gas. As the gas pressure increases, the afterglow decreases.

The author takes the opportunity to express his appreciation to E. V. Dmitriyeva for her assistance.

REFERENCES

1. Barrouz, G. and Brenvel, A. Gas-discharge tube as microwave detector. Problems of Radar Technology, 1953, 1, 159.
2. Lobov, G. D., Mikhaylovskiy, L. K., Microwave and millimeter wave gas detector,

NDVSh (Radio Engineering and Electronics), 1958, 1, 1, 232.
3. Zdornova, Ye. A., Some results of experimental investigation of a gas-discharge microwave detector, Izv. Vuzov MVO SSR (Radio Physics), 1959, 2, 2, 262.
4. Burton, J. Udelson, Effect of microwave signals incident upon different regions of a hydrogen glow discharge, J. Appl. Phys., 1957, 28, 3, 380.
5. M.A. Lampert, A.D. White, Microwave technique for studying discharges, Electr. Commun., 1953, 30, 2, 124.
6. L. Goldstein, J. Anderson, Quenching of afterglow in gaseous discharge plasmas by low power microwaves, Phys. Rev., 1953, 90, 3, 486.
7. J.M. Anderson, Quenching of the negative glow by microwaves in cold-cathode gaseous discharges, Phys. Rev., 1957, 108, 3, 898.
8. L. Goldstein, J. Anderson, Interaction of microwaves propagated through a gaseous discharge plasma, Phys. Rev., 1953, 90, 1, 151.
9. L. Goldstein, J. Anderson, Momentum transfer crossection, Phys. Rev., 1956, 102, 2, 388.
10. Rayzer, M.D. and Spigel', I.S., Investigation of plasma using microwaves, Progress of Physical Sciences, 1953, 164, 4, 34.
11. Al'pert, Ya. L., Ginzburg, V.L. Feynburg, Ye. L., Propagation of radio waves, GTTI 1953.
12. Measurements at super-high frequencies, Soviet Radio, 1952.
13. Granovskiy, V.L., Electric current in gas, I, GTTI, 1952.
14. Engel', A., Shtenbek, M., The Physics and the technology of electric discharge in gases. 1, 2, NKTP SSSR, 1935.

Moscow Power Engineering Institute
Department of Theoretical
Fundamentals of Radio

Received by the editors 9 April 196

SOME THEORETICAL PROBLEMS IN THE OPERATION OF A MICROWAVE PHASEMETER

S.B. Rubin

The paper discusses theoretical aspects of the operational accuracy of the individual sections of a serrodyne microwave phasemeter: the influence of frequency instability of the klystron oscillator, nonideality of the characteristics of the serrodyne method of frequency translation, standing waves in waveguides, and nonideality of amplitude limiters and phase detectors, upon the phenomenon of parasitic phase excursions in the high-frequency and low-frequency sections of the phasemeter.

INTRODUCTION

The use of the various methods of microwave phase measurement depends on requirements for accuracy, rates of processes, automaticity of measurements, etc. Phasemetric systems with frequency conversion are convenient for measurement and automatic recording of rapidly varying phase shifts. In such systems the measurement of microwave phase shifts reduces to the measurement of the phase shift of the signal at a lower frequency, which simplifies the use of automatic measuring devices. It is possible to eliminate much of the error in phase measurement due to a change in single amplitude without thereby increasing lag of the system.

Frequency conversion in the phase measurement system is achieved by many methods.

The method of frequency translation by means of a traveling-wave or ferrite inserts into a waveguide [1, 2, 3] possesses a number of advantages.

We shall examine below some theoretical accuracy problems of a phasemeter employing the so-called serrodyne method of frequency translation — translation of frequency by velocity modulation of the electron stream in a traveling-wave tube by means of a sawtooth voltage*. The phasemeter is intended for the recording of one-time processes with rapidly varying phase shifts at microwave frequencies**.

A simplified block diagram of the phasemeter is shown in Fig. 1. The phasemeter consists of a closed high-frequency waveguide circuit and an intermediate-frequency circuit. The waveguide circuit includes: 1, klystron oscillator; 2, traveling-wave tube; 3, crystal mixer; 4, decoupling ferrite isolators, matching elements, etc; 5, a so-called "special waveguide gap." The i-f circuit consists of: 6, quartz-stabilized oscillator; 7, sawtooth voltage generator, modulating the traveling-wave tube and synchronized with the quartz oscillator; 8, phase inverter; 9, i-f amplifier with r-f filter and 10 — two phase detectors: with direct indication of phase and with m-times amplification of measured phase shift; 11, amplitude limiters; 12, m-th harmonic filters. The recording and indicating elements are not shown on the block diagram.

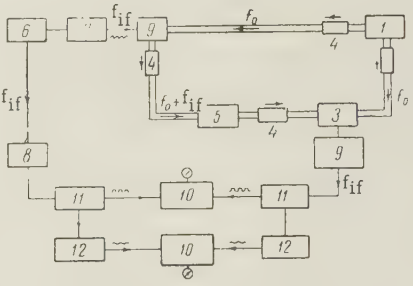

Figure 1. Block diagram of phasemeter.

Phase shift and partial change in amplitude of the microwave signal occur in one of the arms of the high-frequency section due to a change in electrodynamic properties of the medium filling the special waveguide gap (hereafter referred to as the Q-gap).

A signal of frequency f_0 is applied to the TWT input from the klystron oscillator. As the result of sawtooth modulation of the tube with the intermediate frequency f_{if} a signal with translated frequency $f = f_0 + f_{if}$ (or $f = f_0 - f_{if}$) travels from the output of this tube into the Q-gap and on to the mixer. Also applied to the mixer is a reference signal directly from the klystron oscillator.

The intermediate frequency f_{if} is so chosen that it is considerably higher than the highest expected frequency components of the phase shift.

The beat-frequency output signal is filtered so that only the f_{if} frequency component is extracted. The resulting signal is generally proportional to the amplitude of the input signal; the phase shift of the microwave signal obtained in the Q-gap is, in principle, entirely translated to the phase of the output signal. Final measurement of the phase shift is performed at intermediate frequency f_{if} by comparing the output signal with the reference signal from the quartz-stabilized oscillator. The phase inverter in the reference-signal circuit permits establishment of the initial phase shift.

In comparison with the superheterodyne method of frequency conversion, the system discussed does not require accurate stabilization of the frequency difference of the two microwave signals, since the system is a phase-coherent system. The use of a traveling-wave tube for frequency translation insures excellent isolation between the input and output signals at the translated frequency.

---

*A detailed description of the process of frequency translation by means of a TWT is given in Ref. 1.

**A model of such a phasemeter has been developed by A.M. Piltakyan, I.A. Khmel'nitskiy, A.M. Kuznetsov and S.B. Rubin.

The phasemeter described is designed for recording a transient non-repetitive change in phase excursion of the microwave signal passing through the investigated Q-gap. Hence, the various internal or external factors causing a phase excursion which is constant or varies slowly need not be taken into account. They only lead to a change in the reference level at which the dynamic process of change in phase shift begins. Thus, in considering the causes of parasitic phase excursions it is first necessary to determine whether or not these excursions are sufficiently rapid in variation.

The causes of error in phase measurement with the phasemeter, limiting its sensitivity, are many. The chief of these are discussed below.

1. PARASITIC PHASE EXCURSIONS IN THE HIGH-FREQUENCY SECTION

Influence of Standing Waves in Waveguide Sections. Despite the presence of ferrite isolators and matching elements, complete elimination of the reflection of signals in the waveguide elements is not possible. With alignment of the system the standing-wave ratios are relatively small, which permits neglecting multiple reflections of waves in the first approximation. Hence, we discuss below only the case wherein, in addition to the direct wave, only one reflected wave reaches the detector of the mixer.

Let the detector be located at section x of a waveguide. Then the direct signal of frequency $f_0 + f_{if}$ reaching the mixer from the TWT output and passing through the Q-gap is described by the expression

$$U_1 = A(t)\cos\left[(\omega+\Omega)t - \frac{2\pi}{\lambda}x + \Psi(t)\right], \tag{1}$$

where $\Psi(t)$, the phase shift acquired in the Q-gap, is the principal quantity to be measured; A(t) is the amplitude of the principal signal; $\omega = 2\pi f_0$; $\Omega = 2\pi f_{if}$; λ is the waveguide wavelength corresponding to frequency ω. The value of A(t) depends on the electrodynamic properties of the medium in the Q-gap and is determined by attenuation of the signal in this medium. Hence it, also, varies over certain limits with time. The change in amplitude of the principal signal proves to be an unavoidable additional phenomenon complitcating phase measurement.

Also reaching the detector of the mixer is the reference signal of frequency f_0

$$U_2 = D\cos\left(\omega t - \frac{2\pi}{\lambda}x + \psi\right), \tag{2}$$

of constant amplitude and phase, and the corresponding reflected signals.

The detector of the mixer usually operates in the standing-wave mode. In this case $x = l - \frac{\lambda}{4}$, where l is the distance of the shorting plunger from the coordinate origin. The complex reflection coefficient R of the waveguide discontinuity which is small in comparison with the wavelength and which represents the admittance Y an odd number of quarter wavelengths from the shorting plunger is approximately equal to [4]

$$R \simeq 1 - Z_0 Y, \tag{3}$$

where Z_0 is the characteristic impedance of the waveguide. In the present case the detector represents such a discontinuity. Under these conditions the sum signals of frequencies $f_0 + f_{if}$ and f_0 will have amplitudes

$$A_1(t) = A(t)\sqrt{1+2\rho\cos\gamma+\rho^2},\quad D_1 = D\sqrt{1+2\rho'\cos\gamma'+\rho'^2} \tag{4}$$

and the additional phase shifts

$$s = \frac{\pi}{2} - \frac{2\pi l}{\lambda} + \operatorname{arc\,tg}\frac{\rho\sin\gamma}{1+\rho\cos\gamma},\quad s' = \frac{\pi}{2} - \frac{2\pi l'}{\lambda} + \operatorname{arc\,tg}\frac{\rho'\sin\gamma'}{1+\rho'\cos\gamma'}, \tag{5}$$

where ρ and ρ' are the moduli of the reflection coefficients and $|\gamma|$ and $|\gamma'| < \pi$. The presence of the second terms in (5) may lead to phase distortion. If the quantity Y in Eq. (3) remains constant (or changes little) with a change in amplitude and phase of the incoming signal over the entire dynamic range, then the parasitic phase shift introduced is constant. Thus, this

shift is not detrimental in the investigation of the dynamic process.

Influence of Crystal Mixer Characteristics. For a determination of the possible distortions arising in the mixer at various levels of the principal and reference signals let us use the fundamental formulas of the conventional theory of crystal mixers. The equivalent circuit of the mixer is shown in Fig. 2. The i-f load impedance Z_{if} is quite small for high-frequency signals. The principal signal u_c and the reference signal u_r may be dealt with in the from of Eqs. (1) and (2), including, for brevity, the constant phase difference of Ψ (t).

As was mentioned above, the rate of change of the functions A(t) and Ψ (t) is much slower than the change in the principal harmonic component of the i-f voltage u_{if}.

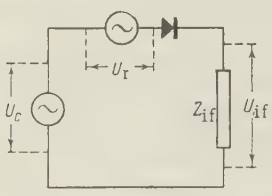

Fig. 2. Equivalent circuit of mixer.

With excellent accuracy the static characteristic of the detector at voltages less than 1 v may be considered exponential:

$$i_d = j_0 (e^{au_d} - 1), \tag{6}$$

where j_d is the detector current, j_0, a is the detection parameter and $u_d = u_c + u_r - u_{if}$ is the voltage drop at the detector. Considering the small magnitude of u_{if} and using the formulas for series expansion of e^x in Bessel functions, let us extract the i-f current component $(j_d)_{if}$. The alternating i-f component is then represented in the form

$$u_{if}^{\sim} = \frac{2j_0 Z_{if} I_1(aA) I_1(aD)}{1 + aj_0 I_0(aD) I_0(aA) Z_n} \cos(\Omega t + \Psi). \tag{7}$$

If the signal amplitude A(t) is sufficiently small and the amplitude D of the reference signal is large (that is, conversion is achieved at a high level), then Eq. (7) reduces to the form

$$u_{if}^{\sim} \simeq \frac{aj_0' Z_{if} I_1(aD)}{1 + aj_0 Z_{if} I_0(aD)} A \cos(\Omega t + \Psi). \tag{8}$$

Equations (7) and (8) show that in both cases the phase shift Ψ (t) is entirely transferred to the i-f signal. The amplitude distortion which occurs in the first case (i.e., if the level of the principal signal is also sufficiently high) may not be sufficiently high for the measurement of the phase shift if I_1 (aA(t)) does not vanish.

Thus, in the phasemeter mixer an increase in the power of the principal singal is permissible in comparison with the usual case of conversion at high level. At large losses of the principal signal in the Q-gap this factor is of considerable importance.

Equation (7) or Eq. (8) may be used for the case where the sum signal $u_c + u_r$ is presented in the form of Eqs. (4) and (5). Considering, for the sake of simplicity, that the amplitude A(t) is sufficiently small, from Eq. (8) we obtain

$$u_{if}^{\sim} \simeq \frac{aj_0 Z_{if} I_1(aD_1)}{1 + aj_0 Z_{if} I_0(aD_1)} A_1(t) \cos[\Omega t + \Psi(t) - \psi + s - s']. \tag{9}$$

Thus, the phase error due to the reflected wave in the mixer is expressed in the form

$$F = s - s' + \psi, \tag{10}$$

ψ is an insignificant constant phase shift; the difference s-s' may depend only slightly on time and distorts the measurements during transients.

Nonideality of TWT Characteristics and of Sawtooth-Voltage Generator. It was assumed above that an ideal translation of frequency is achieved by means of a traveling-wave tube. In practice it develops that the output signal contains not a single spectral line corresponding to the translated frequency $f_0 + f_{if}$ (or $f_0 - f_{if}$) but a band of frequencies separated from the frequency of the output signal by harmonics of the frequency of the sawtooth voltage f_s. With proper adjustment of the tube and amplitude of the sawtooth voltage the amplitudes of these harmonics are considerably lower than the amplitude of the main output signal. These

harmonics are caused by [1, 2]: (1) amplitude modulation of the r-f signal, since in sawtooth modulation of the voltage at the helix of the tube its gain varies slightly; (2) a nonlinear relation between the input-signal phase shift and the sawtooth voltage (modulating the electron-beam velocity) causing this shift; (3) sawtooth defects: finite flyback time, nonlinearity, variable slope, incorrect choice of slope.

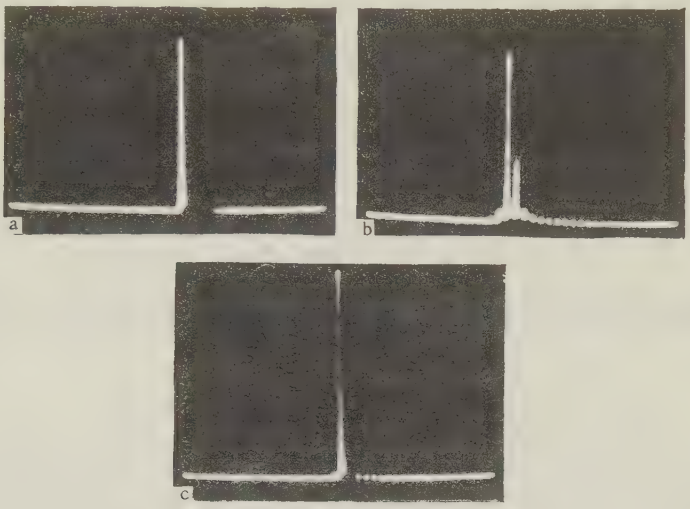

Fig. 3. Signal spectrum after serrodyne conversion.

Frequency conversion by means of a traveling-wave tube may be observed, for example, by the use of a spectrum analyzer. Figure 3 gives photographs of the spectrum of the output signal of a tube for the 3-cm band: a, spectral line corresponding to the initial frequency $f_0 = 10^4$ Mc (without sawtooth modulation); b, spectrum of the output signal with sawtooth-voltage modulation of frequency $f_{if} = 250$ kc (here we see the lines for the signals of the principal frequency f_0, the translated frequency $f_0 + f_{if}$ and the harmonics); c, spectrum of the output signal after adjustment of the tube and the correct selection of the sawtooth-voltage amplitude (we see essentially only one spectral line $f_0 + f_{if}$; the amplitudes of the signal f_0 and the residual harmonics are largely suppressed).

The the reasons given above it is not possible to completely eliminate additional harmonics. In the mixing of the output signal with the reference signal there is obtained at the mixer output a signal of complex spectral composition, containing harmonics which are multiples of frequency f_{if}. Due to the resonance properties of the i-f amplifier (tuned to f_{if}) most of the harmonics do not contribute to the parasitic phase excursion. The harmonic resulting from the presence of the incompletely suppressed image-frequency signal $f_0 - f_{if}$ at the tube output is detrimental.

Assume that the signal at the output consists of only three frequencies: $\omega + \Omega$ (the principal frequency and frequencies not wholly suppressed), $\omega - \Omega$ (the image frequency) and ω (the initial frequency). The corresponding ratio of amplitudes is 1: $\alpha : \beta$, where α and β are small in comparison with unity. Since all three frequencies are extremely close, the properties of the medium in the Q-gap are identical for all three signal components. Hence, the phase excursion and change of amplitudes with time in the passage of the signal through the Q-gap will also be identical for the components.

The intermediate-frequency signal at the mixer output may be expressed in the form

$$u_{if} = \frac{Z_{if} j_0 [I_0(aD) - 1 + \beta a I_1(aD) A(t) \cos \Psi(t)]}{1 + a j_0 Z_{if} I_0(aD)} - \\ + \frac{a j_0 Z_{if} I_1(aD)}{1 + a j_0 Z_{if} I_0(aD)} A(t) \sqrt{1 + \alpha^2} \cos [\Omega t + F(t)], \tag{11}$$

where

$$F(t) = \operatorname{arc\,tg}\left[\frac{1-\alpha}{1+\alpha}\operatorname{tg}\Psi(t)\right].$$

It follows from Eq. (11) that the frequency component of the initial signal affects only the "dc component of current." The component at the image frequency leads to phase-shift distortion. Since α is small, with $|\Psi(t)| < \pi/2$ we may write

$$F(t) \simeq \Psi(t) + \alpha \sin 2\Psi(t). \tag{12}$$

The second term in Eq. (12) evidently represents the phase distortion in the high-frequency section due to the presence of the uncompensated image-frequency signal.

The influence of parasitic sawtooth modulation of gain with frequency f_{if} may be examined directly. In this case the signal at the mixer input may be expressed in the form

$$u_c = \left(1 - \frac{b}{\pi}\sum_{n=1}^{\infty}\frac{\sin n\Omega t}{n}\right) A(t)\cos[(\omega+\Omega)t + \Psi(t)], \tag{13}$$

where b is the percentage modulation. As the result of conversion the i-f signal at the mixer output is

$$\widetilde{u_{if}} = \frac{aj_0 I_1(aD)Z_{if}}{1 + aj_0 Z_{if} I_0(aD)} A(t)\left\{\cos[\Omega t + \Psi(t)] - \frac{b}{2\pi}\sin[\Omega t - \Psi(t)\right\}; \tag{14}$$

and, as was to be expected, it differs from Eq. (11) only in the constant phase shift. Thus, knowing the index of parasitic modulation of gain of a traveling-wave tube it is possible to determine the magnitude of phase distortion caused by this modulation.

Influence of Klystron Instability. Due to the face that the system is coherent in principle, in the ideal case frequency instability of the klystron should not lead to distortion of the investigated effective phase shift obtained in one of the channels. Actually, however, due to a dependence of the parameters of the elements of the section on frequency and due to nonidentical electrical lengths of the two channels, klystron instability affects the accuracy of phase-shift measurements.

(a) Influence of Delay in One of the Channels. Let us represent the signal of a klystron with frequency instability in the form

$$u = B\cos[\omega_0 + \Delta\omega(t)]t, \tag{15}$$

where $\angle\omega(t)$ is a function satisfying the condition $\max|\Delta\omega(t)| \ll \omega_0$ and indicating the frequency drift of the klystron.

This signal is divided into two signals arriving at the mixer through different channels with a delay of one of these signals relative to the other. The signal passing through the TWT and Q-gap arrives with translated frequency and an additional (effective) phase shift $\Psi(t)$. For the case of conversion at high level on the condition that the value of delay τ is small, phase distortion is represented as a function of time

$$F(t) = \tau\frac{d\Delta\omega}{dt}t. \tag{16}$$

(b) Influence of Nonideality of the Frequency Characteristics of the Reference-Signal Channel and the Principal-Signal Channel. For the sake of simplicity let us assume that there is only one element (for example, in the reference-signal channel) with a nonideal frequency characteristic. The signals at the input and output of this element are related as follows

$$u_{out} = H(u_{in}) = H\left(\frac{\omega(t)}{\omega_0}\right)D\cos\left[\omega(t)t + \varphi\left(\frac{\omega(t)}{\omega_0}\right)\right], \tag{17}$$

where the quantity $H\left(\frac{\omega(t)}{\omega_0}\right) \simeq 1 + \frac{\Delta\omega}{\omega_0}\frac{dH}{d\omega}$ indicates the change in amplitude and $\varphi\left(\frac{\omega(t)}{\omega_0}\right) \simeq \frac{\Delta\omega}{\omega_0}\frac{d\varphi}{d\omega}$ the change in phase of the signal. In addition, $H(1) = 1$ and $\varphi(1) = 0$, that is, at the nonimal

frequency no distortion is introduced.

With these assumptions the i-f signal at the mixer output is represented in the form

$$u_{if} = \frac{aj_0 Z_{if} I_1[aD(1+\alpha)]}{1 + aj_0 Z_{if} I_0[aD(1+\alpha)]} A \cos\left[\Omega t + \Psi(t) + \frac{\Delta\omega}{\omega_0}\frac{d\varphi}{d\omega}\right], \quad (18$$

where $\alpha(t)$ denots a small absolute value of $\frac{\Delta\omega(t)}{\omega o}\frac{dH}{d\omega}$. In the given case phase distortion in the high-frequency section is expressed by the term

$$F(t) = \frac{1}{\omega_0}\frac{d\varphi}{d\omega}\Delta\omega(t), \quad (19$$

where $\Delta\omega(t)$ is some (possibly random) function of time.

2. PARASITIC PHASE EXCURSIONS IN THE INTERMEDIATE-FREQUENCY SECTION

It was shown in the preceding paragraphs that under certain conditions the signal reaching the intermediate-frequency section from the mixer and i-f amplifier has the form

$$u = QA(t)\cos[\Omega t + \Psi(t)], \quad (20$$

where Q = const and Ψ (t) is the measured phase shift.

Dependence of the signal amplitude on time complicates direct measurement of phase at the intermediate frequency. Within the intermediate-frequency section this dependence may b eliminated by two methods: by automatic gain control or by signal amplitude limiting. With automatic gain control there may occur time-dependent parasitic phase shifts, which always arise in the presence of feedback in combinations of linear and nonlinear elements [5]. Hence the second method is more suitable. Distortions introduced in using the method of signal amplitude limiting are discussed in greater detail below.

1. In the ideal case bilateral limiting of the signal must be achieved by means of an element with the volt-ampere characteristic show in Fig. 4. In actual cases the limiter characteristic is a compound curve or, in the simplified case, a combination of broken lines as shown, for example, in Fig. 5. In calculating the analythical form of the functions j = f(u) represented in Figs. 4 and 5 (as well as for other more complex cases) the following formula is convenient:

$$j(u) = -\frac{H_0}{2} + \frac{1}{2\pi i}\int_{\sigma-i\infty}^{\sigma+i\infty} \xi(p)\, e^{pu} dp, \quad (21$$

where $\xi(p)$ is the Laplace transform of these functions displaced upward along the ordinate axi by $H_0/2$. For the first case (Fig. 4)

$$\xi(p) = \xi_1(p) = \frac{II_0}{p}; \quad (22$$

for the second case (Fig. 5)

$$\xi(p) = \xi_2(p) = H_0 \operatorname{tg}\theta\left[\frac{1}{p^2} - \frac{e^{-pb}}{p^2}\right]. \quad (23$$

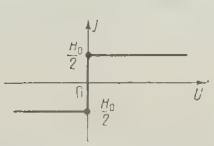

Fig. 4. Characteristic of ideal limiter.

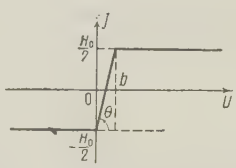

Fig. 5. Limiter characteristic.

The signal is a function of time u = u(t). In order to determine the spectral composition of current as a function of time j(t) by means of Eq. (21) in many cases it is sufficient to determine the spectrum of function epu(t).

Let us use Eq. (21) for a signal of the form (20). Let

$$u(t) = E(t)\sin[\Omega t + \Psi(t)] + u_0. \tag{24}$$

Let us also assume that amplitude modulation does not reach 100%, i.e., $E(t) \geqslant E_0 > 0$. We may write

$$\exp\{p[u_0 + E\sin(\Omega t + \Psi)]\} =$$

$$= e^{pu_0}\left\{I_0(pE) + 2\sum_{k=1}^{\infty}(-1)^{k-1}I_{2k-1}(pE)\sin[(2k-1)(\Omega t + \Psi)] + \right.$$

$$\left. + 2\sum_{k=1}^{\infty}(-1)^k I_{2k}(pE)\cos 2k(\Omega t + \Psi)\right\}. \tag{25}$$

Substituting this uniformly converging series into Eq. (21) and integrating term by term, we obtain the expansion of the current j(t) in a series of the Taylor type (in this case the series cannot be termed a Taylor series since its coefficients are slowly varying functions of time). The corresponding coefficients are easily calculated if we use the known integral representation of the functions $I_m(q)$:

$$I_m(q) = \frac{1}{\pi}\int_0^{\pi} e^{q\cos\psi}\cos m\psi d\psi. \tag{26}$$

In the case of the nonideal characteristic (Fig. 5) the precise expressions for the coefficients are quite lengthy. For the sake of simplicity let us assume (as does in fact occur) that the current rise occurs quite rapidly (i.e., tg θ is large and $b = H_0 \operatorname{ctg}\theta$ is small). In addition, let us proceed directly to an examination of symmetrical limiting wherein $u_0 = b/2$. Then we obtain an approximate form in which the errors in the coefficients of the series are at least one order less than b/E.

$$j(t) = \frac{2H_0}{\pi}\sum_{k=0}^{\infty}\frac{\cos\left[(2k+1)\frac{b}{E(t)}\right]}{2k+1}\sin[(2k+1)(\Omega t + \Psi(t))]. \tag{27}$$

Thus, the current j(t) depends on the change in amplitude of the input signal. In the ideal case b = 0.

$$j(t) = \frac{2H_0}{\pi}\sum_{k=0}^{\infty}\frac{\sin[(2k+1)(\Omega t + \Psi(t))]}{2k+1}, \tag{28}$$

j(t) is independent of changes in the amplitude of E(t).

2. Final detection of phase shift in the phasemeter occurs by comparison of the principal signal with the reference signal from the quartz-controlled oscillator. After passage through the limiter, in accordance with Eq. (27) we have

$$u_c = u_0\sum_{k=0}^{\infty}\frac{\cos\left[(2k+1)\frac{b}{E(t)}\right]}{2k+1}\sin[(2k+1)(\Omega t + \Psi(t))]. \tag{29}$$

After passage through the limiter in the reference-signal channel the sinusoidal signal of the quartz-controlled oscillator also acquires the form of Eq. (29):

$$u_{ref} = u_0\sum_{k=0}^{\infty}\frac{\cos\left[(2k+1)\frac{b'}{E_{ref}}\right]}{2k+1}\sin(2k+1)\Omega t, \tag{30}$$

where b' is a limiter parameter similar to the parameter b, E_{ref} is the amplitude of the reference signal. In contrast with Eq. (29), E_{ref} is independent of time.

Comparison of the principal signal and the reference signal is performed in two parallel channels by means of coarse and fine phase detectors on the condition (stated above) that the change in amplitude E(t) and phase $\Psi(t)$ occurs many times more slowly than the change in the function sin Ωt.

(a) "Coarse Channel." The sum voltage $u = \alpha u_c(t) + \beta u_{ref}(t)$ is applied to a diode detector which, for reasons of simplicity, we shall assume is a square-law detector. The coefficients α and β characterize the summing element.

The detector characteristic is $j_d = s_1 u_d^2 + s_2 u_d + s_3$, where j_d is the detector current, $u_d = \alpha u_c + \beta u_{ref} - v$ is the detector voltage and v is the low-frequency voltage at the load resistance r of the detector. The low-frequency component of current is obtained in the form

$$(j_d)_= = s_3 - vs_2 + r^2 s_1 + U_0^2 s_1 \left\{ \frac{\alpha^2}{2} \sum_{k=0}^{\infty} \frac{\cos^2 (2k+1) \frac{b}{E}}{(2k+1)^2} + \right.$$

$$+ \frac{\beta^2}{2} \sum_{k=0}^{\infty} \frac{\cos^2 (2k+1) \frac{b'}{E_{ref}}}{(2k+1)^2} + \alpha\beta \sum_{k=0}^{\infty} \frac{\cos \left[(2k+1) \frac{b}{E} \right] \cos \left[(2k+1) \frac{b'}{E_{ref}} \right]}{(2k+1)^2}$$

$$\left. \times \cos (2k+1) \Psi \right\}. \tag{31}$$

The sums are calculated in final form and, as the result, we have

$$(j_d)_= = s_3 - vs_2 + v^2 s_1 + U_0^2 s_1 \left\{ \frac{\pi^2}{16} (\alpha+\beta)^2 - \frac{\pi}{8} \left[\alpha^2 \frac{b}{E} + \beta^2 \frac{b'}{E_{ref}} \right] - \right.$$

$$- \frac{\pi\alpha\beta}{16} \left[\left| \frac{b}{E} + \frac{b'}{E_{ref}} - \Psi \right| + \left| \frac{b}{E} + \frac{b'}{E_{ref}} + \Psi \right| + \left| \frac{b}{E} - \frac{b'}{E_{ref}} - \Psi \right| - \right.$$

$$\left. \left. + \left| \frac{b}{E} - \frac{b'}{E_{ref}} + \Psi \right| \right] \right\}. \tag{32}$$

Equation (32) is valid in the case where the values within the absolute signs are less than π. Designating the expression within braces in Eq. (32) as $F(\Psi)$ and considering the usual relationship of $v = r(j_d)_=$, we find

$$v = \frac{1 + rs_2 \pm \sqrt{(1+rs_2)^2 - 4rs_1 [s_3 + U_0^2 s_1 F(\Psi)]}}{2rs_1}. \tag{33}$$

Thus, the indicator displaying the output voltage of the coarse channel of the phasemeter must in this case be calibrated in accordance with Eq. (33).

Let us discuss the expression of $F(\Psi)$ in greater detail. In the ideal case $b = b' = 0$, $\alpha = \beta$

$$F(\Psi) = \frac{\alpha^2 \pi}{4} [\pi - |\Psi(t)|] \tag{34}$$

That is, the phase may vary continuously from zero to π. If the summing element is a symmetrical (that is, if $\alpha \neq \beta$), then the constant phase shift is insignificant. In the general case b and b' are other than zero but sufficiently small. With $\alpha = \beta$ we have

$$F(\Psi) = \frac{\pi\alpha^2}{4} \left[\pi - |\Psi(t)| + \frac{1}{2} \left(\frac{b}{E(t)} + \frac{b'}{E_{ref}} \right) \right]. \tag{35}$$

The time-dependent additional component takes into account phase distortion owing to limiter imperfection.

With phase shifts

$$|\Psi(t)| \leqslant \frac{b}{E(t)} + \frac{b'}{E_{ref}} \tag{36}$$

$F(\Psi)$ may vary in steps. This indicates that within the limits of Eq. (36) there exist zones of insensitivity.

(b) "Fine Channel." In this channel, from Eqs. (29) and (30) there is eliminated any

m-th harmonic of frequency Ω and then there is performed a measurement of the relative phase shift, which thus proves to be increased by m times (m = 2 k + 1, k = 1, 2, 3, . . .). The input signals of the phase detector are

$$w_c = U_0 \cos \frac{mb}{E(t)} \sin m[\Omega t + \Psi(t)], \tag{37}$$

$$w_{ref} = U_0 \cos \frac{mb'}{E_{ref}} \sin m\Omega t. \tag{38}$$

As is seen from Eq. (37), the principal signal is obtained as an amplitude-modulated signal although the percentage modulation due to the smallness of parameter b is not great.

Phase-shift detection by means of a balanced peak detector adjusted for linear operation leads to the following result: the indicator of the balanced peak detector must react to a quantity v proportional to the amplitude difference of the sum $w_c + w_{ref}$ and difference $w_c - w_{ref}$ signals. In view of the small value of mb/E and mb'/E_{ref}, this quantity may be reduced to the form

$$v \simeq 2U_0 \sqrt{1 - m^2 \left[\left(\frac{b}{E(t)} \right)^2 + \left(\frac{b'}{E_{on}} \right)^2 \right]} \left\{ \cos \frac{m}{2} \Psi(t) - \sin \frac{m}{2} \Psi(t) \right\}. \tag{39}$$

The coefficient preceding the brace depends on the change in amplitude E(t) of the input signals and leads to distortion of the results of the measurement. In order to eliminate this distortion it is convenient to limit the amplitude of the input signals of Eqs. (37) and (38) before detection.

CONCLUSIONS

We have listed a number of factors which have proved to be of probable influence on the accuracy of phasemeter operation. Theoretical examination of the effect of these factors has been based on the following principle: the measurement distortion introduced by each of these factors is considerable in the event that the error is a function of time varying at a rate comparable with the rate of change in the measured phase shift (i.e., if it leads to distortion of measurements of the transient process). This principle follows directly from the prupose of the device.

On the basis of theoretical examination several practical conclusions have been obtained concerning requirements for the various units of the installation. The chief conclusions (in addition to the obvious conclusions concerning the necessity for optimum matching of all elements of the high-frequency section, decrease in the gain modulation of the traveling-wave, high stability of the klystron oscillator, high quality of amplitude limiters, etc) are as follows.

1. In designing the crystal mixer it is necessary to insure constancy of detector admittance over the entire range.
2. The basic circuit permits conversion of a high frequency to an intermediate frequency at an increased level of the principal signal. At large losses of the principal signal, with a change in properties of the medium in the Q-gap, this circumstance is of great importance.
3. Among the detrimental harmonics entering the i-f section greatest harm is caused by the harmonic resulting from the presence of the image-frequency signal. This places special requirements on the i-f amplifier.
4. In order to eliminate the influence of changes in amplitude of the input signals an additional amplitude limiter must be installed in the fine phase-detection channel.
5. If it is not possible to eliminate the detrimental factors by practical methods, we may evaluate their effect from the formulas given in the appropriate sections of the paper.

REFERENCES

1. R.C. Cumming, The serrodyne frequency translator, Proc. IRE, 1957, 45, 2, 175.
2. G.W.C. Mathers, Homodyne generator and detection system, IRE Wescon Convention

Record, Part I, Microwaves, Antennas and Propagation, 1957.
3. E.M. Rutz, I.E. Dye, Frequency translation by phase modulation, IRE Wescon Convention Record, Part I, Microwaves, Antennas and Propagation, 1957.
4. Microwave measurements, translated from English under editorial supervision of V.B. Shteynshleyger, Izd. Sovetskoye radio, 1952.
5. A.M. Bonch-Bruyevich, V.I. Shirokiy, ZhTF, 1955, 25, 10, 1925.

Submitted to the editors 1 March 1960

OPTIMAL ELECTRON BEAM FOCUSING IN A PERIODIC TRAVELING-WAVE TUBE FOCUSING DEVICE

A. L. Igritskiy

A new analytical method is presented for determining the parameters of a traveling-wave tube(TWT) periodic focusing device for optimal electron beam focusing. It is shown that the proposed method ensures considerably less rippling of the beam in the periodic device than the Chang method used at the present time. The new method makes it possible to obtain the correct beam configuration which is also a function of the conditions at the input to the periodic device. It is shown that the best focusing conditions are obtained when the electrons enter the periodic field at maximum induction.

INTRODUCTION

One of the most important problems in designing a periodic travelling wave tube (TWT) focusing device is to ensure a small degree of ripple in the electron beam. It is only in the case of small electron oscillations around an equilibrium radius that the greatest percentage of cathode current can be passed to the collector and minimum noise factor in the tube ensured.

Analysis shows that the ripple of the electron beam in a periodic device is determined by the following three focusing parameters: the maximum induction of the periodic magnetic field B_{z0}, the period of the magnetic field L, and the axial component of induction at the tube cathode B_{zk}. The conditions under which the electrons enter the periodic field also have an effect on the ripple.

The analytical method of ensuring a small degree of ripple of the beam is set forth in Ref. 1. As shown below, however, this method does not provide conditions for optimum focusing. On the basis of an analysis of the electron trajectory equation in the periodic device, given in Ref. 2, this article determines the conditions for optimum focusing, ensuring correct

shape and small amplitudes of the beam ripple. Theoretical formulas are derived which make it possible to determine the maximum focusing conditions for any tube parameters.

1. SIMPLIFIED EQUATION FOR ELECTRON TRAJECTORY IN PERIODIC DEVICE

The electron trajectory equation for the periodic focusing device obtained in Ref. 2 may be used to determine the principal parameters of this device: B_{z0}, L and B_{zk}, at which optimum focusing of the electron beam is ensured. But to obtain simple and convenient relationships, this equation has to be simplified to the maximum extent. The calculation of the electron trajectory, made in Ref. 2, and a number of other computations show that the main contribution to the amplitude of the electron oscillations in the periodic device is made by the principal oscillation harmonics in the solution of a uniform Mathieu equation determined by the stability zone n. The amplitude factor of this harmonic is equal to c_n. The amplitude coefficients of the higher and lower [c_{n+2} etc.] harmonics c_{n+2}, c_{n-2} are one or two orders smaller than the coefficient c_n. Hence, we can ignore the terms containing the coefficients c_{n+2} and c_{n-2}, with a comparatively small loss in accuracy, in the formula for beam ripple given in Ref. 2. As a result of a series of simple transformations, we then obtain the following equation for the ripple δ of the electron beam:

$$\delta(t) = \frac{b}{a}\cos[\sqrt{a}(t-t_0)] - \frac{q}{(\sqrt{a}-2)\sqrt{a}}\cos[\sqrt{a}(t-t_0)+2t_0] - \frac{q}{(\sqrt{a}+2)\sqrt{a}}\cos[\sqrt{a}(t-t_0)-2t_0] - \frac{b}{a}+\frac{2q}{a-4}\cos 2t. \quad (1)$$

In Eq. (1) the values δ and t are related to the radial and axial coordinates of the electron r and z by the following

$$t = \frac{2\pi}{L}z, \quad (2)$$

$$r = r_0(1+\delta). \quad (3)$$

Here, r_0 = const and represents the radius, close to which there are slight oscillations of the electron.

The constant coefficients, a, b and q in Eq. (1) are expressed in terms of the TWT parameters and the periodic magnetic field. From Ref. 2 we have

$$a = \frac{1}{2}\left(\frac{L}{\lambda_p}\right)^2\left[\frac{B_{z0}^2}{2B_b^2}+\alpha^2+3\alpha^4\frac{B_{zK}^2}{B_b^2}\right], \quad (4)$$

$$2q = \left(\frac{L}{\lambda_p}\right)^2\frac{B_{z0}^2}{4B_b^2}, \quad (5)$$

$$b = \frac{1}{2}\left(\frac{L}{\lambda_p}\right)^2\left[\frac{B_{z0}^2}{2B_b^2}-\alpha^2-\alpha^4\frac{B_{zK}^2}{B_b^2}\right], \quad (6)$$

$$\lambda_p = \frac{4\pi\sqrt{\Phi}}{\sqrt{\eta}B_b}, \quad (7)$$

$$B_b^2 = \frac{\sqrt{2}I}{\pi\varepsilon_0\eta^{3/2}\Phi^{1/2}r_K^2}, \quad (8)$$

$$\alpha = \frac{r_K}{r_0}. \quad (9)$$

In these equations Φ is the potential of the second anode in the electron gun, η is the ratio of the charge to the mass for an electron; I is the current in the tube beam, ϵ_0 is the dielectric constant of vacuum, and r_k is the radial coordinate of the peripheral electron at the cathode, whose trajectory determines the configuration of the electron beam.

When deriving Eq. (1) it is assumed that the magnetic field varies sinusoidally:

$$B_z = B_{z0} \sin\left(\frac{2\pi}{L} z\right) \tag{10}$$

and that the extreme electron enters the periodic magnetic field at the point $z = z_0$, with a radial coordinate $r = r_0$, moving parallel to the axis z. In accordance with Eqs. (2) and (3), the initial conditions were taken for

$$t = t_0 = \frac{2\pi}{L} z_0, \quad \delta_0 = \delta_0' = 0.$$

Next, let us consider the calculation of the parameters of the periodic focusing device for two particular values $t_0 = 0$ and $t_0 = \pi/2$. The first value of t_0 corresponds to a case in which the electron enters the periodic magnetic field at a point where the induction is zero, and the second case is for a point where the induction is maximum.

2. CALCULATION OF PARAMETERS OF A PERIODIC FOCUSING DEVICE FOR THE CASE IN WHICH THE ELECTRONS ENTER THE FIELD AT MAXIMUM INDUCTION

Setting $t_0 = \pi/2$ in Eq. (1) we obtain an equation for the ripple of the electron beam in the form

$$\delta(t) = \left[\frac{b}{a} + \frac{2q}{a-4}\right] \cos\left[\sqrt{a}\left(t - \frac{\pi}{2}\right)\right] - \frac{b}{a} + \frac{2q}{a-4} \cos 2t. \tag{11}$$

It is desirable to have the ripple of the beam as small as possible. Let us consider methods by which this may be done.

a) Chang's method [1]. By selecting a relationship between the induction at the cathode B_{zk} and maximum induction of the periodic field B_{z0}, we try to make the coefficient $b = 0$, and then reduce q to the maximum extent by selecting the lowest possible magnetic field period L. As is clear from Eqs. (4) and (5), as L decreases, a and 2q decrease as well. For fairly small periods L $a \ll r$, so they can be ignored. As a result, at $b = 0$, Eq. (11) can be written in the form

$$\delta = -\frac{2q}{4}\left\{\cos 2t + \cos\left[\sqrt{a}\left(t - \frac{\pi}{2}\right)\right]\right\}. \tag{12}$$

We can see from Eq. (12) that as $q \to 0$, $\delta \to 0$, i.e., the ripple of the beam can be made as small as we please with a corresponding reduction in the period L. From Eqs. (11), (2) and (3) the configuration of the beam at $b = 0$ can be described by the equation

$$r = r_0 + r_0 \frac{2q}{a-4}\left\{\cos\left[\sqrt{a}\left(\frac{2\pi}{L} z - \frac{\pi}{2}\right)\right] + \cos\left(\frac{4\pi}{L} z\right)\right\}, \tag{13}$$

in which $z \geqslant L/4$. As an example let us determine the configuration of the beam $r = f(z)$ for a TWT working in a periodic magnetic field with induction $B_{z0} = 3.4 \cdot 10^{-2}$ webers/m^2, and period L = 1.4 cm; $B_{zk} = 2.22 \cdot 10^{-2}$ webers/m^2. For this tube the parameters as determined by Eqs. (7) and (8) are $\lambda_p = 7.75 \cdot 10^{-2}$, and $B_b^2 = 0.89 \cdot 10^{-4}$, and the coefficient α will be taken as equal to unity. As a result of calculation by Eqs. (4) - (6) we have $a = 0.396$, $q = 0.0533$ and $b = 0$. Figure 1a shows the configuration of the electron beam $r = f(z)$ in the case of Chang's method of focusing for these values of the coefficients when derived by Eq. (13). We see that the beam has a highly regular boundary. The oscillation of the extreme electron occurs about the input radius r_0 and the maximum amplitude of the oscillation is

$$A_m = \pm r_0 \frac{4q}{a-4}. \tag{14}$$

The radius of the electron beam in the periodic device may be greater than at the input by a factor $r_0 \frac{4q}{a-4}$. The maximum relative variation in the radius due to oscillations of the

electrons is $\frac{8q}{a-4}100\%$. Using Eq. (14) and taking Eqs. (4) and (5) into account, we show in Fig. 2 the dependence of the amplitude of the ripple on the magnetic field period in the case of focusing by the Chang method.

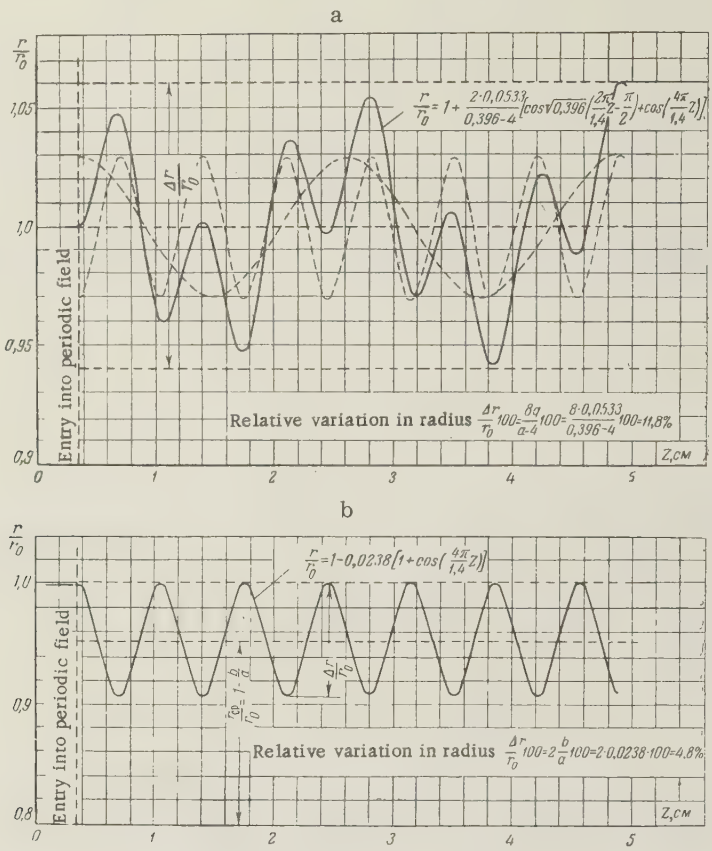

Fig. 1. Configuration of electron beam $r/r_0 = f(z)$ in periodic magnetic field ($t_0 = \pi/2$): a) focusing by Chang's method; b) by the new method.

b) New method of ensuring small ripple of the electron beam. This method is better and consists of the following. The parameters of the periodic focusing device B_{z0}, L and the induction at the tube cathode B_{zk} will be selected in such a way that the first term in Eq. (11) vanishes. This will clearly happen when

$$\frac{2q}{a-4} = -\frac{b}{a}. \tag{15}$$

The ripple of the electron beam in this case is equal to

$$\delta(t) = -\frac{b}{a}(1+\cos 2t) = \frac{2q}{a-4}(1+\cos 2t). \tag{16}$$

Using Eq. (16), it can be shown, in the same way as was done for Chang's method, that as the magnetic field period decreases, the ripple of the beam tends to zero.

After substitution of values from Eqs. (4) - (6), Eq. (15) will relate to three parameters B_{z0}, L and B_{zk}. On this basis we can arbitrarily choose two of them, and determine the

third from Eq. (15). We will deal in detail with a case in which the amplitude of the periodic magnetic field is given and constant: B_{z0} = const, while the induction at the cathode B_{zk} may vary. Let us see how in this case the amplitude of the beam ripple b/a and the magnetic period L vary with B_{zk}. In order to save space we will introduce the symbols

$$k = \frac{B_b^2}{B_{z0}^2}; \quad \gamma = \frac{B_{zk}^2}{B_{z0}^2}; \quad \frac{B_{zk}^2}{B_b^2} = \frac{\gamma}{k}. \tag{17}$$

Taking into account Eqs. (17), (4) and (6), the expression b/a can be written in the form

$$\frac{b}{a} = \frac{1 - 2k\alpha^2 - 2\alpha^4\gamma}{1 + 2k\alpha^2 + 6\alpha^4\gamma}. \tag{18}$$

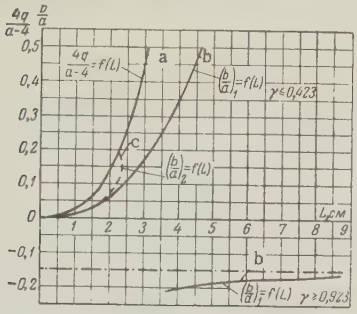

Fig. 2. Amplitude of beam ripple as a function of magnetic field period: a) focusing by Chang's method ($4q/(a-4) = f(L)$); b) by the new method ($t_0 = \pi/2$) ($(b/a)_1 = f(L)$); c) by the new method ($t_0 = 0$) ($(b/a)_2 = f(L)$).

For the given tube at B_{z0} = const, the coefficient k = const. Fig. 3 shows the relationship $b/a = f(\gamma)$ from Eq. (18). The parameters of the tube and the field were given before.

Now let us see how the period L varies

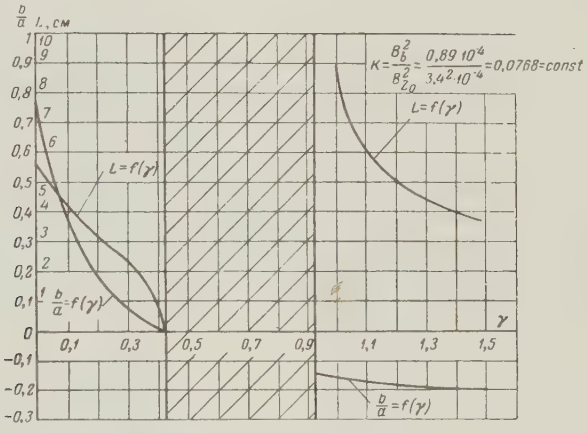

Fig. 3. Amplitude of beam ripple $b/a = f(\gamma)$ and magnetic field period $L = f(\gamma)$ as a function of the degree of screening of cathode γ when focusing by new method ($t_0 = \pi/2$).

with γ. To do this we will substitute values from Eqs. (4) - (6) into Eq. (15). Solving the equation obtained with respect to L, taking into account the symbols in Eq. (17), we have

$$L = \lambda_p \sqrt{\frac{8k(1 - 2k\alpha^2 - 2\alpha^4\gamma)}{(1 + 2k\alpha^2 + 6\alpha^4\gamma)(1 - k\alpha^2 - \alpha^4\gamma)}}. \tag{19}$$

Figure 3 shows the relationship $L = f(\gamma)$ from Eq. (19). The hatched area is where the magnetic field period is imaginary and where, consequently, it is not possible to focus by the new method.

Using Fig. 3, we have plotted a graph on Fig. 2 showing the amplitude of the beam ripple as a function of the magnetic field period $(b/a)_1 = f(L)$ when focusing by the new method. Figure 2 shows that at this period, the amplitude is approximately half, when using the new method, of what it is by the Chang method.

An equation describing the configuration of the beam can be obtained from Eqs. (2), (3) and (16), as follows

$$r = r_0 - r_0 \frac{b}{a}\left[1 + \cos\left(\frac{4\pi}{L} z\right)\right], \tag{20}$$

where $z \geqslant \frac{L}{4}$. It is not difficult to see from Eq. (20) that for values of γ on the left of the hatched area in Fig. 3 the radius of the beam during oscillation cannot exceed its value at the input to the periodic device. The configuration calculated by Eq. (18) - (20) for a TWT with the above-mentioned parameters at maximum induction of the periodic field $B_{z0} = 3.4 \cdot 10^{-2}$ webers/m^2 and cathode induction $B_{zk} = 2.1 \cdot 10^{-2}$ webers/m^2 is given in Fig. 1b. We see that the oscillations of the extreme electron are around the mean radius $r_{mea} = r_0(1 - \frac{b}{a})$ and the maximum amplitude is $r_0 \frac{b}{a}$. The radius of the electron beam in the periodic device cannot be greater than that at the input to the device, and this gives the new method of reducing ripple a further advantage over Chang's method. The maximum relative variation in beam radius during oscillations which has an effect on the tube's noise factor is $2\frac{b}{a}$, using the new method. This variation is approximately half as much as in the Chang method.

A periodic device with the parameters calculated above was built for experimental purposes. The periodic field was created with permanent ring magnets. The exact value of induction at the cathode was found by an electromagnet placed in the region of the TWT electron gun. Tests showed that for this device there was a 98% current transfer to the collector of the tube.

We studied focusing by the new method in the region of small γ. At large γ, i.e., for the focusing region on the right of the hatched area in Fig. 3, b/a is negative and, consequently, during oscillation the beam radius cannot be less than r_0. The chief advantage of the new method of selecting focusing parameters at large γ is the possibility of using magnetic fields with a large period, but, in view of the high amplitudes of oscillation, the focusing area with large γ is hardly suitable for low-noise TWT's.

As has already been pointed out, Eq. (15) relates the three parameters, B_{z0}, L and B_{zk}. We have considered in detail a case in which B_{z0} and B_{zk} have been given. The period of the magnetic field L and the amplitude of the beam ripple were calculated from Eq. (19) and (18). But in practice it often happens that the parameters of the periodic field — L and B_{z0} — are given. In this case the induction at the cathode may be found from

$$B_{zk} = \sqrt{\gamma} B_{z0},$$

in which

$$\gamma_{1,2} = \frac{-\left[c_2 - 6c_3 - 16k\left(\frac{\lambda_p}{L}\right)^2\right] \pm}{12\alpha^4}$$
$$\frac{\pm\sqrt{\left[c_2 - 6c_3 - 16k\left(\frac{\lambda_p}{L}\right)^2\right]^2 - 24\left[8k\left(\frac{\lambda_p}{L}\right)^2 c_1 - c_2 c_3\right]}}{12\alpha^4}; \tag{21}$$
$$c_1 = 1 - 2k\alpha^2; \quad c_2 = 1 + 2k\alpha^2; \quad c_3 = 1 - k\alpha^2.$$

Equation (21) is obtained from Eq. (19).

If the cathode induction B_{zk} and the period L are given, the maximum induction required for focusing can be determined from Eq. (16). Substituting the values obtained from Eqs. (4), (5) and (6) into it, and solving the equation obtained, we have

$$B_{z0} = B_b \sqrt{2x},$$

in which

$$x_{1,2} = \frac{-\left(\beta d_2 - \frac{1}{2}\beta d_1 - 4\right) \pm \sqrt{\left(\beta d_2 - \frac{1}{2}\beta d_1 - 4\right)^2 - 4\beta\left(4d_1 - \frac{1}{2}\beta d_1 d_2\right)}}{2\beta};$$
$$\beta = \left(\frac{L}{\lambda_p}\right)^2; \qquad d_1 = \alpha^2 + \alpha^4 \frac{B_{zk}^2}{B_b^2}; \quad d_2 = \alpha^2 + 3\alpha^4 \frac{B_{zk}^2}{B_b^2}.$$

Considering that there are three parameters B_{z0}, B_{zk} and L requiring calculation, and only one equation relating them, we can introduce any additional condition, for example, the condition of constancy of the beam ripple amplitude

$$\frac{b}{a} = \frac{1 - 2k\alpha^2 - 2\alpha^4\gamma}{1 + 2k\alpha^2 + 6\alpha^4\gamma} = A = \text{const}. \tag{22}$$

In this case only one of the parameters may be given arbitrarily, and the two others must be found from Eqs. (15) and (22).

3. CALCULATION OF PARAMETERS OF A PERIODIC MAGNETIC FIELD FOR THE CASE IN WHICH ELECTRONS ENTER THE FIELD WITH ZERO INDUCTION

If an electron enters the periodic magnetic field at the beginning of the period at zero induction, we can assume $t_0 = 0$, in Eq. (1), taking Eq. (10) into account. As a result we have

$$\delta(t) = \left(\frac{b}{a} - \frac{2q}{a-4}\right)\cos(\sqrt{a}\,t) - \frac{b}{a} + \frac{2q}{a-4}\cos 2t. \tag{23}$$

Using the method proposed in the foregoing section, we will select the parameters of the focusing device in such a way that the first term of Eq. (23) vanishes. This will obviously occur when

$$\frac{b}{a} - \frac{2q}{a-4} = 0. \tag{24}$$

In this case the ripple of electron beam will be equal to

$$\delta(t) = -\frac{b}{a}(1 - \cos 2t). \tag{25}$$

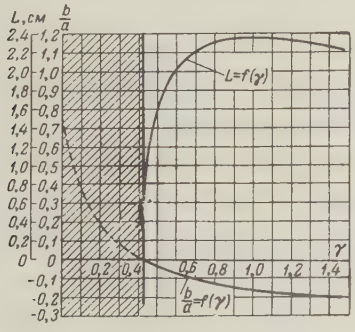

Fig. 4. Amplitude of beam ripple $b/a = f(\gamma)$ and magnetic field period $L = f(\gamma)$ as a function of the degree of screening of cathode γ when focusing by new method ($t_0 = 0$)

As in the foregoing section, let us consider in detail the calculation of parameters of the focusing device when B_{z0} is the only constant. Here it will be assumed that the induction at the cathode may vary continuously, and we will determine the variation in the magnetic field period and beam ripple amplitude accordingly. In the given case the amplitude can be determined as before by Eq. (18) and the graph for the above-mentioned tube is plotted in Fig. 4. It was assumed that $B_{z0} = 3.4 \cdot 10^{-2}$ webers/m^2. The formula for the magnetic field period is obtained from Eq. (24) after substitution of values from Eqs. (4) - (6) and Eq. (17):

$$L = \lambda_p \sqrt{-\frac{8k(1 - 2k\alpha^2 - 2\alpha^4\gamma)}{(1 + 2k\alpha^2 + 6\alpha^4\gamma)(k\alpha^2 + \alpha^4\gamma)}}. \tag{26}$$

Fig. 4 is a plot of the relationship $L = f(\gamma)$ from Eq. (26). The hatching shows the region in which the magnetic field period is imaginary, and, consequently, the new method cannot be used for focusing. The dotted line in Fig. 2 derived from Fig. 4 represents the variation in the amplitude of oscillation due to the magnetic field period $(b/a)_2 = f(L)$. By comparing the curves we can see that in this case as well, for small L the increase in amplitude with the increase in period is slower than in Chang's method. From Eqs. (2), (3) and (25), the configuration of the beam in the given case will be determined by the equation

$$r = r_0 - r_0 \frac{b}{a}\left(1 - \cos\frac{4\pi}{L} z\right), \qquad (27)$$

in which $z \geqslant 0$.

Figure 5 shows the configuration of the electron beam calculated from Eqs. (18), (26) and (27) for a TWT with the above-given parameters at maximum induction of the magnetic

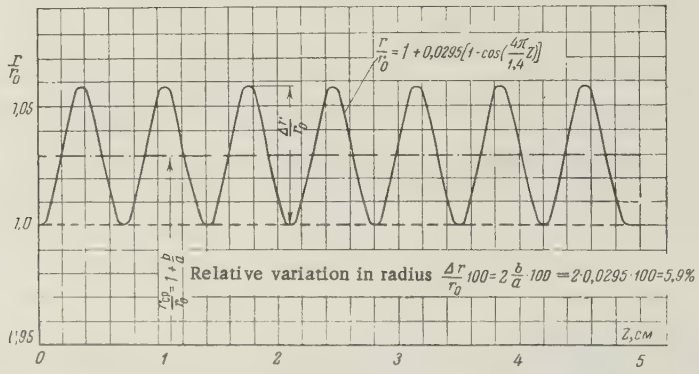

Fig. 5. Configuration of electron beam $r/r_0 = f(z)$ in a periodic magnetic field when focusing by the new method ($t_0 = 0$)

field $B_{z0} = 3.4 \cdot 10^{-2}$ webers/m^2 and cathode induction $B_{zk} = 2.36 \cdot 10^{-2}$ webers/m^2. We see that the oscillations of the extreme electron occur near the mean radius ($r_{mea} = r_0 (1 + \frac{b}{a})$ and the maximum amplitude is equal to $r_0 \frac{b}{a}$. The radius of the electron beam in the periodic device cannot be smaller than at the input to the device. This shows that in the given case the focusing is worse than when electrons enter the field at maximum induction, since it is more probable that the electrons reach the helix. Furthermore, we can see from Fig. 2 that the oscillation amplitude in the given case increases more rapidly with an increase in L. The maximum relative variation in beam radius during oscillations is $2\frac{b}{a}$. This variation at small values of the magnetic field period is approximately half of what it is in Chang's method.

CONCLUSION

The new method for calculating the parameters of the periodic TWT focusing device for optimum focusing of an electron beam differs from Chang's analytical method used at the present time. Chang's method uses the condition $b = 0$, but in the new method the condition $\frac{b}{a} + \frac{2q}{a-4} = 0$ is used in selecting parameters for the device. As a result the new method has a number of advantages. They are as follows:

1. It ensures considerably less ripple in the electron beam in the focusing device, which is particularly important in making low-noise TWT's.

2. It makes it possible to obtain a given correct configuration of the electron beam. Here, (1) if the electron beam enters the periodic field at maximum induction, the radius of the beam during oscillation of the electrons in the periodic device cannot be greater than that at the input to the device (see Fig. 1b). This fact makes it easier to adjust the focusing device by increasing the gap between the beam and the TWT helix; and (2) when the electron beam enters the periodic field at zero induction, the radius of the beam, conversely cannot be less than the radius r_0 (see Fig. 5).

3. To ensure conditions for the best focusing when using the new method of determining the parameters of the device, the aim should be to make the electrons enter the periodic field at maximum induction.

REFERENCES

1. K.K.N. Chang, Beam focusing by periodic and complementary fields Proc. I.R.E., 1955, 43, 1, 62.
2. A.L. Igritskiy, Calculation of electron trajectories in a periodic TW tube focusing device. Radio Engineering and Electronics, 1960, 5, 2, 255.

Received by the editors 5 August 1959

SOME RESULTS OF AN INVESTIGATION OF TRANSMISSION SECONDARY ELECTRON EMISSION OF MgO EMITTERS

N.L. Yasnopol'skiy, N.A. Karelina, V.S. Malysheva

This paper describes a transmission secondary electron emitter. The transmission secondary emission of aluminum films 100—1000 Å thick with MgO emitters deposited on them is discussed. It is shown that a decrease in Al thickness from 3000 to 350 Å permits lowering the operating voltage from 11-18 to 3-4 kv with secondary-emission ratios of 5-8. It is noted that in such emitters the transmission secondary electron emission under certain conditions may change to self-maintained emission.

INTRODUCTION

Investigation of transmission secondary electron emission for the purpose of creating efficient emitters has become a subject of constant attention. For the creation of transmission emitters substances possessing high surface reflection secondary electron emission are used.

E. Sternglass [1] has described emitters consisting of a layer of KCl (an efficient emitter with thickness of ~ 600 Å, with a conducting sublayer of Au 15—20 Å thick, and a supporting layer of SiO 100 Å applied to a fine-structured mesh. Such emitters possess a secondary-electron ration of $\sigma_{max} \simeq 8.4$ with a primary-electron energy of $V_p = 3.2$ kev. However, in transmission operation (as in surface reflection operation) KCl emitters show a yield decreasing with time under the influence of electron bombardment. This decrease in σ is caused by the formation of centers of deterioration.

A.I. Pyatnitskiy [2] prepared antimony-cessium transmission emitters (antimony layer 400 Å) on a glass film of 7500 Å. These emitters yielded σ xx 2.7 with $V_p = 20$ kev taking into account the primary current incident at the glass base layer and $\sigma_{max} = 4.7$ with $V_p = 16$ kev taking into account the current passing through the glass base layer.

Ye. A. Krasovskiy [3] has reported on an antimony-cesium emitter on a metal base layer yielding $\sigma_{max} = 7$.

It is contended that MgO is an extremely favorable substance for the creation of a secondary-electron emitter. In surface reflection operation MgO emitters show maximum secondary-emission ratios $\sigma = 16 - 24$. They possess maximum stability in comparison with other emitters, sustaining a primary current density of 5 ma/cm^2 at Vp = 300 ev for 800 hours [5].

V.G. Butkevich and M.M. Butslov [4] have created transmission emitters which consist of MgO on conducting film of Al with thickness ~ 3000 Å. With MgO thickness of 0.19 mg/cm^2 these yielded $\sigma_{max} = 3.2$ with $V_p = 13$ kev and with thickness of 0.73 mg/cm^2 yielded $\sigma_{max} = 8$ with $V_p = 18$ kev. It may be assumed that the high primary-electron energies required for the operation of these emitters are caused by the large energy losses of the primary electrons and the loss of primary electrons themselves in passage through the relatively thick metal base layer.

For our work we constructed effective emitters of MgO with an aluminum base layer

on a fine mesh. This permitted decreasing the base layer thickness by one order of magnitude and obtaining high values of σ by transmission at considerably lower primary-electron energies.

1. EXPERIMENTAL PROCEDURE

Investigation of the emitters was performed on a demountable vacuum system under a bell with rubber gasketing and evacuation by an oil diffusion pump. The trap was cooled by liquid nitrogen. Measurements were made at a vacuum on the order of 10^{-6} mm Hg.

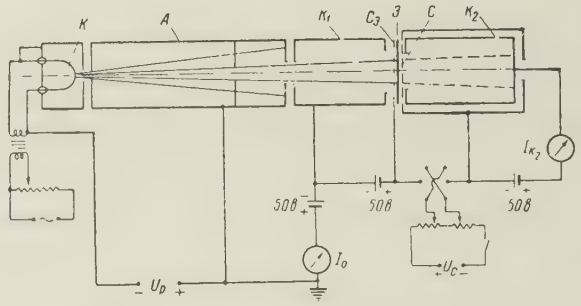

Fig. 1. Basic diagram of measurement setup. K, cathode; A, anode; K_1, collector of reflected primaries and surface reflection secondary electrons; E, emitter of secondary electrons; C_e, grid, the emitter base; C, grid trapping scattered secondary electrons; K_2, collector of primary and transmission secondary electrons passing through the emitter.

The basic diagram of the measurement device and measurement circuit is shown in Fig. 1. The electron gun is simple in construction and consists of a tungsten cathode K and anode A. The anode apertures limit the beam and determine its diameter, which permits simple determination of the average current density in the beam. The energy of primary electrons V_p is determined by the accelerating voltage U_p applied between cathode and anode. In this arrangement the average current density in the beam increases with the accelerating voltage. In our measurements it did not exceed 10^{-6} amp/cm^2. The field trapping the secondary electrons determines the potential difference between the emitter base C_e and the grid C. The grid C with 95% open area fastened to a cylinder shielding transmission secondary electrons K_2 is made in the form of a Faraday cage. Its inner surface is coated with aquadag in order to lower the reflection coefficient and secondary emission from the collector surface. Between grid C and collector K_2 there is applied a potential difference of 50 v which returns the secondary electrons excited from the collector. The distance of the grid from the emitter is 3 mm, the beam diameter at the target surface is 6 mm. The secondary-emission ratio α is calculated, taking into account the penetrability coefficient of grid C_e, from

$$\sigma = \frac{I_{K_2}}{I_0 \alpha} = \frac{I_{K_2}}{I_p},$$

where I_{k2} is the current in the secondary electron collector, I_0 is the beam current, and I_p is the primary-electron current at the free surface of the film.

Thus, we and the above-mentioned authors have determined the total secondary-emission ratio, for the current I_{k2} includes both the true secondaries and the primaries passing through the film.

2. TRANSMISSION SECONDARY ELECTRON EMISSION OF THIN Al FILMS

An aluminum layer was made by depositing in vacuum on a fine copper or tungsten mesh with a pre-applied organic film. Removal of the organic film was achieved by baking

under the vacuum at a temperature of 250° C and a pressure of the order of several mm of Hg. The thickness of the Al layer was determined approximately from the weight of the evaporated material, assuming spherically uniform evaporation. The density of Al in the film was assumed to be equal to the density of the solid metal.

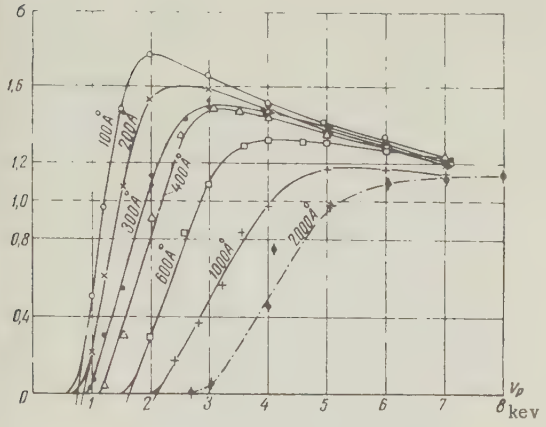

Fig. 2. Curves for $\sigma = f(V_p)$ for Al films of various thickness. Dotted curves indicate data of Ref. 4.

The transmission secondary emission of layers of Al was investigated in the thickness range from 100 to 1000 Å in Fig. 2 the secondary-emission ratio is shown as a function of V_p. As was to be expected, in the thinner films transmission secondary emission appears at lower values of V_p, rises more rapidly and at maximum attains larger values than in the case of thicker films. After reaching the maximum the value of σ gradually decreases, approaching a limit at unity, which corresponds to passage of the electrons through the film without loss. For the sake of comparison Fig. 2 shows the curve for δ = 2000 Å taken from Ref. 4. It fits well into the family of curves obtained by us.

The primary-electron energy V_{p0} corresponding to the beginning of penetration is approximately defined by the point of intersection of the straight-line segment of the curve $\sigma = f(V_p)$ with the horizontal axis. Figure 3 shows V_{p0} as a function of δ, where δ is the layer thickness.

In the investigated range of thicknesses the energy of beginning of penetration V_{p0} lies within the range from 0.7 to 2.2 kev. The point for δ = 2000 Å fits well on the curves obtained by us.

3. TRANSMISSION SECONDARY EMISSION WITH MgO LAYER

Efficient MgO emitters were made on Al films with thickness of 350-400 Å. The MgO layer was applied by the combustion of Mg in air and deposition of the MgO "smoke" on the specimen. In addition, as is known, a porous layer of MgO is formed. Its thickness is calculated from the increase in specimen weight after application of the layer.

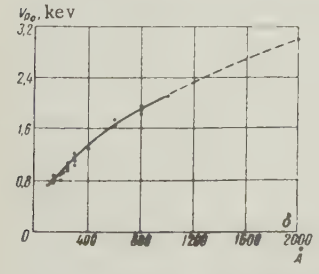

Fig. 3. Energy at the beginning of penetration of the film as a function of Al thickness. Point at 2000 Å taken from data of Ref. 4.

Investigation of such emitters showed that preheating in vacuum at 450° C leads to an increase in σ. Figure 4 shows σ as a function of V_p for an Al film with an applied layer of MgO before and after preheating. The value of σ of the preheated emitter reaches approximately 7 at V_p = 3 kev and $\sigma_{max} \simeq 9$ at V_p = 5 kev. Let it be noted that such emitters at the current densities used show a considerable decrease in σ with time under the influence of electron bombardment.

We also investigated emitters compressed after application of an MgO layer by treatment in the vapors of a volatile liquid. Such emitters possess lower σ but are more stable under load. Figure 5 shows σ as a function of V_p for an Al base layer and MgO coatings of different thickness. The various thicknesses of coating were achieved by successive applications of MgO to the same specimen. After each application the emitter was compressed and heated. The curves show that

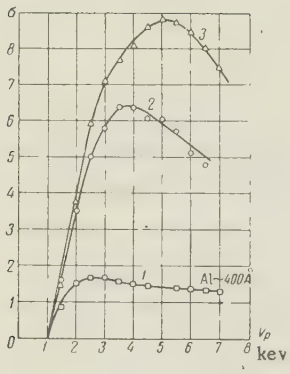

Figure 4. σ as a function of V_p for an Al layer of 400 Å (1) and an MgO coating of 0.05 mg/cm^2 before preheating (2) and after (3).

an increase in the MgO layer up to 0.19 mg/cm^2 has practically no effect on the starting energy of penetration, which is approximately 1 kev. An increase in MgO thickness leads to an increase in σ and shift of the maximum of the $\sigma = f(V_p)$ curve toward higher primary-electron energies.

The dependence of σ on layer thickness, obtained by a study of a number of specimens in the range from 0.016 to 0.19 mg/cm^2, is shown in Fig. 6. Values of thickness are plotted on the axis both in milligrams per square centimeter and in microns. Recalculation was performed on the assumption that the layer density was 3.2 g/cm3, which corresponds to a dense layer of MgO. It is possible that the films obtained by us, although compressed, had greater thickness. The curves show that in the investigated range of thicknesses σ increases monotonically with thickness. For the maximum investigated thickness the resulting values are: $\sigma \sim 5$ at $V_p = 3$ kev and $\sigma_{max} \simeq 7$. It is of interest to note that the secondary-electron yield for the given thickness of MgO exceeds by at least one order or magnitude the secondary-electron yield for solid layers of MgO (δ = 800 Å), indicated by N.R. Whetten and A.B. Leponsky [5]. This phenomenon is evidently associated with the porosity of the film.

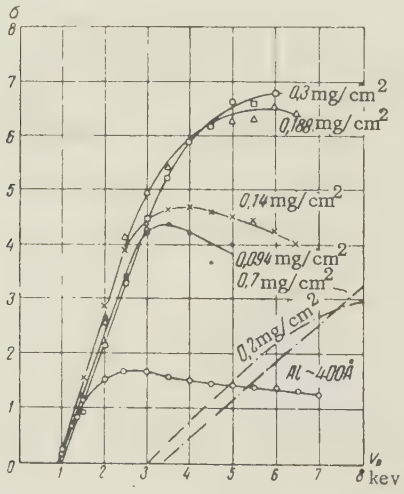

Figure 5

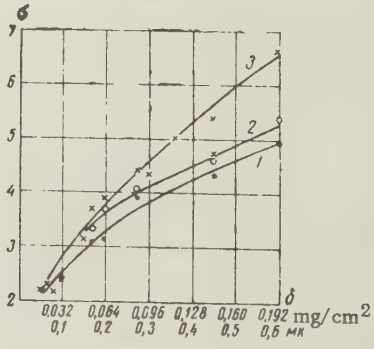

Figure 6

Figure 5. σ as a function of V_p for an Al film and applied emitter with compressed and preheated MgO layers of different thickness. Dotted curves are plotted from data given in Ref. 4.

Figure 6. Dependence of σ for transmission secondary emission on MgO layer thickness for compressed and preheated emitters with $V_p = 3$ kev (1); with $V_p = 3.5$ kev (2); with V_p corresponding to maximum values of σ (3).

Figure 7 shows σ as a function of V_p for the specimen which gave maximum values of σ. For an evaluation of the results obtained by us, as in Fig. 5, the dotted curves are plots of the results obtained by V.G. Butkevich and M.M. Butslov [4] with similar emitters differing by one order of magnitude in the thickness of the aluminum sublayer. Comparison shows that a decrease in the thickness of the base layer permits a decrease in the energy V_{p0} required for penetration of the emitter from 3-3.5 to 1-1.5 kev and permits high values of σ for transmission secondary emission on the order of 5-8 with V_p = 3-4 instead of 11-18 kev.

4. SELF-MAINTAINING TRANSMISSION EMISSION

The above results were obtained with a potential difference U_c of 50 v for secondary-electron capture. It was seen that for compressed specimens saturation of the curves for $\sigma = f(U_c)$ sets in at $U_c = 30$ v and that further increase in U_c up to 450 v has practically no effect on the secondary current. With uncompressed specimens at $U_c > 30$ v there is observed a small monotonic increase in secondary current with an increase in the capture potential difference.

In some uncompressed samples there are observed at $U_c = 120$-170 v a spontaneous increase in secondary-emission current and self-maintained emission upon removal of the beam current. Dependence of the transmission emission current on the capture potential difference for films with thickness of 0.12 mg/cm^2 at $V_p = 6$ kev is shown in Fig. 8. The

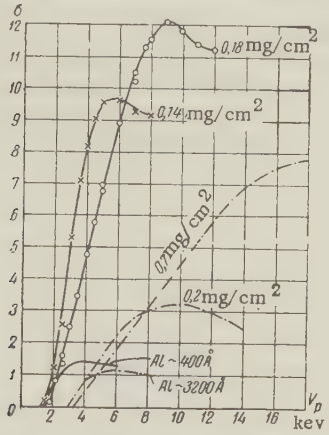

Figure 7

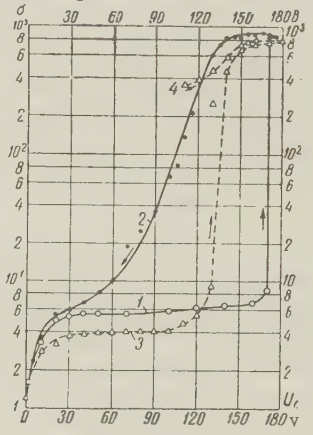

Figure 8

Figure 7. σ as a function of Vp for the emitter specimen with maximum yield. Dotted curves plotted from data in Ref. 4.

Figure 8. Dependence of the ratio of the transmission emission current to primary beam current on the capture potential difference U_c. 1, with an increase in U_c; 2, with a decrease in U_c; 3, with repeated increase in U_c; 4, with decrease in U_c upon removal of beam current.

corresponding values of σ are plotted on a logarithmic scale. With an increase in the capture potential difference, when U_c reaches 170 v, there occurs a spontaneous increase of current (curve 1) up to a value approximately 900 times greater than the primary current, (I_p). The value of current is limited by the voltage drop at a resistor (2 megohms) in the collector circuit. With a decrease in voltage from 170 to 140 v (curve 2) the current is practically unchanged, but then it begins to decrease. However, in the reverse direction the curve proceeds considerably higher than the initial curve before spontaneous increase occurs and returns to normal values of σ at $U_c = 30$ v. Repeated increase in the capture potential difference (curve 3) again leads to a spontaneous increase of current to a value on the order of 800 I_p. Upon removing the current of the primary beam the emission current continues to flow. A decrease in the capture potential difference (curve 4) after removing the beam current leads to a decrease in the self-maintained emission current and to its cessation at a particular value of U_c. It is interesting to note that in the absence of a stabilizing resistor in the circuit, removal of the beam current not only does not cause a disappearance of the emission current but, to the contrary, leads to a considerable increase in current (by 1.5-2 times).

At the beginning of the investigation of a given specimen the self-maintaining emission is relatively stable and easily excited. However, during investigation partial or complete interruptions of self-maintained emission are observed with subsequent recovery showing considerable time lag. In the course of time the process of recovery falters and finally

ceases altogether. This is apparently associated with the deterioration of the secondary-emission properties of the MgO layer with time.

It is suggested that the cause of the spontaneous increase of current and transition to self-maintained emission, as stated in Ref. 6, is the development of an independent discharge in the solid dielectric. In addition, impact ionization leads to an increase in current either due to avalanche formation [7] or redistribution of the field within the layer, with the result that there arises a large current due to tunnel emission from the sublayer[8].

CONCLUSIONS

1. An efficient transmission secondary-electron emitter has been obtained consisting of an MgO layer with a thin conductive layer of Al on a fine grid.
2. It has been shown that decreasing the conductive layer of such an emitter from 3000 to 350 Å permits decreasing the energy losses of primary electrons and losses of the primary electrons themselves in the conductive layer and, as a result, permits reducing the emitter operating voltages from 11-18 to 3-4 kv with a secondary-emission ratio $\sigma = 5-8$.
3. It is observed that in such emitters with an uncompressed MgO layer under certain conditions a transition of transmission secondary emission to self-maintained emission occurs.

REFERENCES

1. E.J. Sternglass, M.M. Wachtel, IRE Trans. Nucl. Sci., 1956, 3, 4, 29.
2. A.I. Pyatnitskiy, Izv. AN SSSR, Ser. fiz., 1958, 22, 4, 464.
3. Ye. A. Krasovskiy, Izv. AN SSSR, Ser. Fiz., 1958, 22, 4,472.
4. V.G. Butkevich, M.M. Butslov, Radio Engineering and Electronics, 1958, 3, 3, 355.
5. N. Rey Whetten, A.B. Laponsky, J. Appl. Phys., 1959, 30, 3, 432.
6. D.V. Zernov, Izv. AN SSSR, Division of Technical Sciences, 1950, 6, 866.
7. H. Jacobs, J. Freely, F.A. Brand, Phys. Rev., 1952, 88, 3, 492.
8. M.I. Yelison, D.V. Zernov, Radio Engineering and Electronics, 1957, 2, 1, 75.

Submitted to the editors 15 June 1960

THEORY OF OPERATION OF THE ELECTROSTATIC FLUXMETER IN PLASMA

Ya. M. Shvarts

This article considers methods of increasing the signal-to-noise ratio at the electrostatic fluxmeter output when the fluxmeter is used for measurements in plasma. It is shown that when a synchronous detector is included in the circuit and dc voltage feedback is applied, this ratio is considerably increased. The article gives theoretical ratios. An evaluation is made of the maximum signal-to-noise ratio at the fluxmeter output.

INTRODUCTION

Until recently instruments for measuring an electrostatic field were only used in a medium with low electric conductivity. Hence, the result of conduction currents was not considered when formulating the theory of these instruments. Nevertheless, the conduction

currents modulated by the screen plate in an electrostatic fluxmeter, and flowing through the electrostatic generator load, cause a voltage drop which constitutes noise. In Ref. 1 there is a description of methods of suppressing noise at the output of an instrument for measuring the electrostatic field intensity when used to measure the field on the surface of bodies in a particularly ionizing medium such a ionospheric plasma. But this article deals with the problems superficially, in particular, the methods of enhancing the signal-to-noise ratio at the instrument output.

The fundamental principle of the electrostatic fluxmeter and the factors leading to the occurrence of a noise voltage are discussed in Refs. 1 and 2. We will therefore not deal with this, but go on to discuss the basis of the problem.

1. THE EQUATION OF AN ELECTROSTATIC GENERATOR AND ITS SIMPLIFICATION

Fig. 1 a shows the equivalent circuit for an electrostatic generator, taking the noise current into account. Applying Kirchhoff's law, we can obtain an equation relating the voltage u at the load z with the current i flowing through it. The load on electrostatic generators is usually a resistance R and a variable condenser C, connected in parallel. In this case the equation takes the form

$$\frac{du}{dt} + \left(\frac{dC}{dt} R + 1\right)\frac{u}{RC} = \frac{i}{C}. \tag{1}$$

Analysis of the equation in its general form is extremely cumbersome and complicated, since, apart from the variation in the condenser, we have to take into account the possibility of the resistance R being shunted by the medium*.

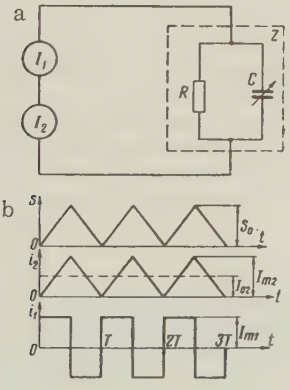

Fig. 1. a) equivalent circuit for electrostatic generator; I_1 and I_2 are signal and noise current generators; b) variation in area of measuring plate and generator currents with time.

Hence, it is essential to consider which simplifications can be introduced into the theoretical circuit.

First of all, we can always select a load resistance considerably less than the shunt resistance. To do this we have to make sure that the drop in load voltage due to the noise and signal currents is considerably less than the potential of the body surface at the point where the measuring plate of the fluxmeter is positioned. The potential of the surface of the body is determined with respect to the potential of the medium in the vicinity of the body.

Secondly, in a number of designs now in existence the following inequalities are satisfied

$$\frac{dC}{dt} R \ll 1, \tag{2}$$

$$\frac{C_\sim}{C_0} \ll 1 \tag{3}$$

provided $C = C_0 + C_\sim$, where C_0 is the mean capacitance, and $C_\sim$ is the variable part of the capacitance.

Physically speaking, satisfying condition (2) means ignoring the variation in the time constant of the load during the operational cycle of the fluxmeter, and satisfying condition (3)

---

* The shunting effect when using the instrument for ionospheric plasma shows up in the fact that the variation in the potential of the measuring plate due to a load voltage drop, caused by the signal and wire currents, leads to an additional noise current and to variation in the field intensity on the surface of the measuring plate. To make allowance for this, a certain additional load-shunting resistance R' should be introduced and its value would depend on u.

means taking the capacitance as constant.

The analysis is simplified if we assume that the variation in the potential of the measuring plate in the fluxmeter due to the load voltage drop when one of the currents flows through it does not affect the value of the other current. Calculation of the effect of noise currents on the operation of the electrostatic generator can then be made separately. In actual fact, this is done when the electrostatic generator load is correctly chosen, i.e., when the voltage drop due to noise and signal currents is considerably less than the potential of the body surface at the site of the measuring plate. This is quite feasible, since the potentials of artificial satellites and rockets are measured in volts [3] and we only need the resistance $R < 10^4$ ohm for the voltage drop at z due to the noise currents to be at least two orders smaller than the surface potential [1]. The load voltage drop due to operating currents does not normally exceed thousandths of a volt.

Let us designate the useful current of the electrostatic generator due to the presence of the electrostatic field E on the surface of the measuring plate as i_1, and the corresponding load voltage as u_1. The noise current flowing through the load z will be designated i_2 and the noise voltage u_2.

On the basis of the above we can reduce Eq. (1) to the following two equations:

$$\frac{du_1}{dt} + \frac{u_1}{RC} = \frac{i_1}{C}, \quad \frac{du_2}{dt} + \frac{u_2}{RC} = \frac{i_2}{C}.$$

The total load voltage is equal to

$$u_1 + u_2 = u.$$

2. RELATIONS BETWEEN ELECTROSTATIC GENERATOR CURRENTS AND VOLTAGES

Let us assume that the area of the measuring plate S exposed to the field varies linearly, as often happens in practice. Then, during the period the measuring plate is unscreened $S = at$, and during the period the plate is screened $S = S_0 - at$.

The variation in the plate area with time is shown in Fig. 1 b. It is obvious that if the electrostatic field at the surface of the plate is equal to ϵ, while the screening frequency is f, the operating current i_1 is determined by the formula

$$i_1 = \frac{\varepsilon E}{4\pi} \frac{dS}{dt} = \pm \frac{\varepsilon E S_0 f}{2\pi}.$$

Since the noise current is created by a current flowing onto the open part of the measuring plate, and since it can be considered as a first approximation that the part of the measuring plate exposed to the field is equal to the part into which the noise current flows (for particle streams vertically incident on the measuring plate, this is ideally the case), its value can be measured from the following equality:

$$i_2 = j_2 S,$$

where j_2 is the density of the noise current.

A graph showing the variation in the signal and noise currents with time is given in Fig. 1 b. It is clear that the noise current has been shifted 90° with respect to the signal current.

The total voltage u across the load z should be the result of the action of rectangular signal current pulses and triangular noise current pulses on the circuit z. Expressing the signal and noise currents in the form of a Fourier series and designating the dc component of the noise current I_{02}, and the maximum amplitudes of the signal and noise currents as I_{m1} and I_{m2}, respectively, we obtain the following expressions for voltages at the load z:

$$u_1 = \sum_{n=1}^{\infty} u_{1n} \sin(n\omega t + \varphi_n),$$

$$u_2 = U_{02} - \sum_{n=1}^{\infty} u_{2n} \cos(n\omega t + \varphi_n),$$

in which

$$u_{1n} = \frac{4I_{m1}R}{\pi n \sqrt{n^2 R^2 \omega^2 C^2 + 1}};$$

$$u_{2n} = \frac{8I_{m2}R}{\pi^2 n^2 \sqrt{n^2 R^2 \omega^2 C^2 + 1}};$$

$$U_{02} = I_{02}R; \quad \varphi_n = \operatorname{arc\,tg} nR\omega C;$$

$$\omega = 2\pi f; \quad n = 1, 3, 5, 7, \ldots .$$

The following conclusions can be drawn.

1. The phase shift between the corresponding harmonics of voltages u_1 and u_2 remains equal to the phase shift between currents i_1 and i_2.

2. The shape of the voltages u_1 and u_2 varies, compared with that of i_1 and i_2.

3. The relative amplitude of the first harmonics in the voltages u_1 and u_2 increases, compared with that of the corresponding harmonics of the currents i_1 and i_2, since the load impedance is an inverse function of the frequency.

In order to select an effective way of combating noise we have to make a rough estimate of the ratio of the signal voltage to the noise voltage at the electrostatic generator output, i.e., at the measuring circuit output. This ratio can be calculated approximately by the ratio of the amplitudes of the harmonics of the signal and noise voltages

$$m \simeq \pi \frac{I_{m1}}{I_{m2}} = \frac{Ef}{2j_2}.$$

Making use of the results given in Refs. 1 and 2, and substituting E = 1 v/cm, f = 1500 cps and $j_2 = 10^{-7}$ amp/cm^2, we find that when using the instrument for measurements in the ionospheric plasma, m may drop to approximately 1/100. This means that for the above values of E, f, and j_2, the input noise voltage exceeds the mean theoretical input signal voltage by a factor of 100. It stands to reason that when measuring the signal voltage with a given degree of accuracy, the noise has to be suppressed by much more than a factor of 100.

3. USE OF A SYNCHRONOUS DETECTOR

The analysis of the solution of the quation for the operation of the electrostatic generator, taking noise into account, leads to the conclusion that the corresponding harmonics of the noise and signal voltages at the generator output are shifted by 90°. Consequently, the incorporation of a phase-sensitive element into the measuring circuit makes it possible to greatly attenuate one of the signals.

Such an element is the synchronous detector, usually used in the measuring circuits of electrostatic fluxmeters, [4]. Indeed, when manufacturing the instrument on the basis of the block diagram shown in Fig. 2a, and when tuning the synchronous detector to the first harmonic of the signal voltage, the relationship between the input and output signal and noise voltages (for an ideal detector) is determined by the following equations:

$$U_1 = \sum_{n=1}^{\infty} \frac{u_{1n} k(nf_1) \cos \Delta\psi_n}{n},$$

$$U_2 = \sum_{n=1}^{\infty} \frac{u_{2n} k(nf_1) \sin \Delta\psi_n}{n}.$$

U_1 and U_2 are the dc signal and noise voltages at the synchronous detector output; f_1 is the frequency of the first harmonic; $k(nf_1)$ is the amplification factor of the measuring circuit at the frequency of the corresponding harmonic; $\Delta\psi_n$ is the detuning of the synchronous detector for the corresponding harmonic, i.e., the phase shift between the switching voltage of the

corresponding signal voltage harmonic*:

$$\Delta\psi_n = n\Delta\psi_0 + \Delta\psi(nf_1) + \varphi_n - \varphi_1 n,$$

where $\Delta\psi_0$ is the tuning error of the synchronous detector and the corresponding signal voltage; $\Delta\psi$ (nf_1) is the phase shift due to the dependence of the amplifier phase characteristic on frequency, at the tuning frequency of the synchronous detector $\Delta\psi = 0$; $\varphi_n - \varphi_1 n$ is the phase shift due to the action of the electrostatic generator load.

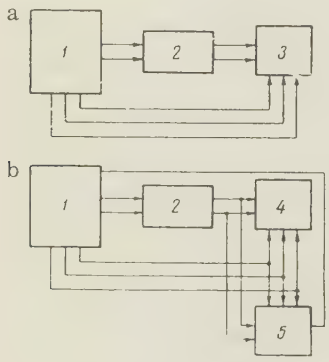

Fig. 2. Block diagram of intrument: a) with synchronous detector; b) with negative feedback; 1) electrostatic generator; switching voltage generator; 2) amplifier; 3) synchronous detector; 4) principal synchronous detector; 5) additional synchronous detector

The ratio between the dc signal and noise voltage at the synchronous detector output is equal to

$$M = \pi \frac{I_{m1}}{I_{m2}} \frac{\sum_{n=1}^{\infty} \frac{k(nf_1)\cos\Delta\psi_n}{n^2\sqrt{n^2R^2\omega^2C^2+1}}}{\sum_{n=1}^{\infty} \frac{k(nf_1)\sin\Delta\psi_n}{n^3\sqrt{n^2R^2\omega^2C^2+1}}}.$$

In measuring circuit with sensibly chosen parameters, in which $k(f_1) > k(nf_1)$ and $\sin\Delta\psi_n/n^3$ decreases as n increases, it is enough to restrict oneself to the ratios of the dc voltages which result from the first harmonics of the signal and noise voltages for the purpose of the calculation. In this case

$$M = \pi \frac{I_{m1}}{I_{m2}} \operatorname{ctg} \Delta\psi_1.$$

This means that it is possible to suppress the noise voltage at the instrument output to a high degree.

Nevertheless, it is harly possible to make $\Delta\psi_1 < 1'$. The greatest shortcoming of this method of suppressing noise is the fact that the suppression is effected at the instrument output, i.e., an enormous noise voltage has to pass through the whole amplification channel without overloading it, which is very difficult to achieve in practice. Thus, methods of combatting noise should reduce the effective noise voltage at the instrument output.

4. USE OF NEGATIVE FEEDBACK

One of these methods is to use negative feedback for the dc noise voltage [4]. To do this we have to use in parallel with the principal synchronous detector another synchronous detector tuned to the voltage shifted by 90° with respect to the signal voltage (Fig. 2b). The rectified voltage from this detector is used for the negative voltage feedback.

In its general form, the additional synchronous detector can be made by placing an additional measuring plate of the same form as the generator plate under it and connecting the two plates electrically. The negative feedback voltage is fed to the special electrode in the form of a graduated plate [5]. Between this electrode and the auxiliary plate is an extra screen plate fitted onto the same axis as the principal screen plate. The two plates are mounted in such a way that the ac voltage at the output of the negative feedback electrostatic generator is 180° out of phase with the ac noise voltage. This is done, for example, by shifting the vanes of the extra screen plate 90 electrical degrees with respect to the principal plate, with an

---

* The phase shift between the nearest zero crossings of the switching voltage and the corresponding harmonic of the signal voltage is measured in degrees of the harmonic.

approximate positioning of the measuring plates.

A few theoretical ratios are given below. Without negative feedback

$$U = \sum_{n=1}^{\infty} \frac{u_{1n} k\,(nf_1) \cos \Delta\psi_n}{n} - \sum_{n=1}^{\infty} \frac{u_{2n} k\,(nf_1) \sin \Delta\psi_n}{n},$$

where U is the output voltage of the principal synchronous detector.

The output voltage of the additional synchronous detector U' is in this case determined by the expression

$$U' = \sum_{n=1}^{\infty} \frac{u_{1n}\, k\,(nf_1) \sin \Delta\psi'_n}{n} - \sum_{n=1}^{\infty} \frac{u_{2n}\, k\,(nf_1) \cos \Delta\psi'_n}{n},$$

in which $\Delta\psi'_n$ is the detuning of the additional synchronous detector.

The addition of negative feedback reduces the noise voltage at this synchronous detector input by a factor of $1 + k(nf_1)\,\beta_n$ (β_n is the feedback factor). For $k(nf_1)\,\beta_n \gg 1$, taking into account the effect of feedback,

$$U = \sum_{n=1}^{\infty} \frac{u_{1n}\, k\,(nf_1) \cos \Delta\psi_n}{n} - \sum_{n=1}^{\infty} \frac{u_{2n} \cos \Delta\psi'_n \sin \Delta\psi_n}{n\beta_n} + \\ + \sum_{n=1}^{\infty} \frac{u_{1n} \sin \Delta\psi_n \sin \Delta\psi'_n}{n\beta_n}.$$

Clearly,

$$\sum_{n=1}^{\infty} \frac{u_{1n} \sin \Delta\psi_n \sin \Delta\psi'_n}{n\beta_n} \ll \sum_{n=1}^{\infty} \frac{u_{1n}\, k\,(nf_1) \cos \Delta\psi_n}{n}.$$

Hence, limiting ourselves, as in the foregoing section, to the calculation of the signal-to-noise ratio of the dc values at the synchronous detector output due to the first harmonics of the signal and noise voltages, and taking into account that $\cos \Delta\psi' \simeq 1$, we find the following coefficient M':

$$M' = \pi \frac{I_{m1} k\,(f_1)\, \beta_1 \operatorname{ctg} \Delta\psi_1}{I_{m2}}.$$

It follows from this expression that for the negative noise voltage feedback the signal-to-noise ratio at tge output of the instrument increases by a factor of $k(f_1)\,\beta_1$.

Let us recall another way of suppressing noise — the use of special grid electrodes in the electrostatic generator. This method is described fairly fully in Ref. 1. It makes it possible to reduce the ac component of the noise current in the electrostatic generator load by a factor of b,

$$b = b_1 b_2,$$

where b_1 is the attenuation factor of the ac noise currents due to the reduction in the modulation effect of the screen plate, and b_2 is the coefficient describing the recudtion in the absolute flow of particles striking the measuring grid electrode.

CONCLUSION

When using all three methods of suppressing noise, the signal noise ratio at the synchronous detector output is determined by the expression

$$M' = \pi \frac{I_{m1} k\,(f_1)\, \beta_1 \operatorname{ctg} \Delta\psi_1 b_1 b_2}{I_{m2}}. \qquad (4)$$

It follows from Eq. (4) that by applying special t4chniques we can measure small electrostatic fields against a background of a large noise current. An approximate evaluation of the product $k(f_1)\beta \operatorname{cotan} \Delta\psi_1 b$ gives a value which is at least of the order of $10^5 - 10^6$, i.e., for example, against a background of the greatest possible noise current with a density 10^{-6} amp/cm^2 [1] we can measure fields on the surface of the sounding body which create a current of 10^{-11} and per unit of surface of the measuring plate in the electrostatic generator. For a generator with am exposure frequency f = 1500 cps this is equivalent to a field $E \simeq 3 \cdot 10^{-2}$ v/cm.

In conclusion I would like to express appreciation to I. M. Imyanitov for his constant interest in this work.

REFERENCES

1. Imyanitov, I. M., Shvarts, Ya. M. Methods of combatting noise currents at the electrostatic fluxmeter input when the fluxmeter operates in a conducting medium. Artificial earth satellites, 1959, 3, 77.
2. Imyanitov, I. M. Variation in electrostatic fields in upper layers of the earth's atmosphere, Progress of Physical Sciences, 1957, LXIII, 1b, 267.
3. Krasovskiy, V.I., Soviet investigation of the ionosphere with the aid of rockets and artificial earth satellites. Artificial earth satellites, 1959, 2, 32; Istomin, V.G., Investigation of ionic composition of earth's atmosphere with rockets and artificial earth satellites. Artificial earth satellites, 1959, 2, 36.
4. Ya. M. Shvarts. Author's patent, No. 123247, class 21e, 5_{01}, 1959.
5. Imyanitov, I. M., Instruments and methods for studying electricity in the atmosphere, GITTL, 1957.

Received by the editors 4 April 1960

EXPERIMENTAL INVESTIGATION OF TUNNEL CURRENT IN THIN GERMANIUM p-n JUNCTIONS

N.A. Belova and A.N. Kovalev

An experimental investigation was made of the effect of the degree of alloying of germanium on tunnel-type diode characteristics. An attempt is made to evaluate the results quantitatively in accordance with Ref. 2.

The effect of dislocations in the intrinsic germanium and the effect of temperature on the tunnel current in thin p — n functions are investigated.

As follows from a qualitative description [1] and the following theoretical work, the volt-ampere characteristic of a tunnel diode should be strongly affected by the concentration of mobile charge carriers both in the n and p regions. We were interested in experimentally ascertaining the dependence of the tunnel current on such determining parameters as the degree of alloying of the n and p regions.

1. MAXIMUM TUNNEL CURRENT

In view of the lack of a complete expression for a tunnel current across the p — n junction in the form of a continuous function of the applied voltage, the current may be

described by such extreme points as the maximum and minimum of the volt-ampere characteristic. Ref. 2, in which the question of the effect of alloying conditions on tunnel diode characteristics is considered theoretically, an expression is obtained within the limits of the model for potential differences corresponding to the maximum tunnel current.

$$eV_{\max} = \frac{1}{6}\{2(E_V - \mu) - (\mu - E_c) + \\ + \sqrt{[2(E_V - \mu) + \mu - E_c]^2 + 4(E_V - \mu)(\mu - E_c)}\}, \quad (1)$$

where μ is the chemical potential; E_c and E_V are the top and bottom boundaries of the forbidden zone (see Fig. 1); e is the electron charge.

Equation (1) is obtained on the assumption that the p region is alloyed more strongly than the n region.

In order to make a quantitative evaluation we have to know the position of the Fermi level on both sides of the p — junction for different concentrations of p and n. By knowing the concentration n, we can determine the position of the Fermi level in the n region, i.e., $\mu - E_c$, from the following relationship:

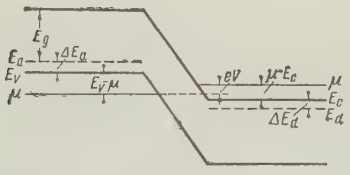

Fig. 1. Approximate position of zones.

$$n = 2\left(\frac{2\pi kTm^*}{h^2}\right)^{3/2} \delta \frac{2}{\sqrt{\pi}} \int_0^\infty \frac{\sqrt{x}\,dx}{e^{x-\eta}+1}, \quad (2)$$

where m* is the effective mass of the electron, k is Boltzman's constant, T is the absolute temperature, h is Planck's constant, δ is the number of minima in the conduction zone, and $\eta = (\mu - E_c)/kT$. The integral is tabulated, and the value of η determined from tables in Ref. 4.

In this article the concentration of the mobile carriers n in the experimental specimens of germanium was determined by the measurement of the Hall constant R from the formula $n = 1/eR$. The Hall constant was measured in a magnetic field of intensity 5500 oersteds.

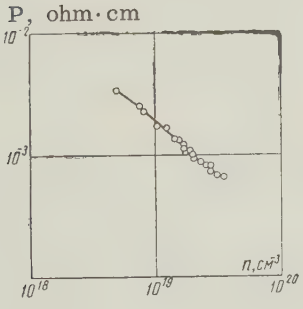

Fig. 2

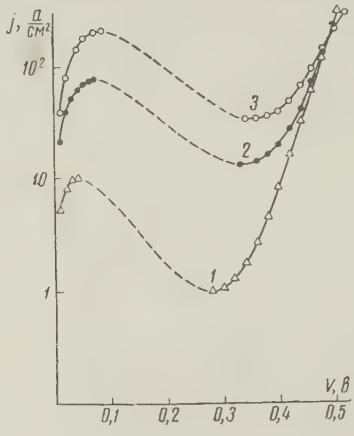

Fig. 3

Fig. 2. Specific resistance as a function of electron concentration in n type germanium.

Fig. 3. Volt-ampere characteristics of tunnel diodes with different degrees of alloying of the p region: 1) for diode whose p region is formed by inclusion of In + 0.5% Ga; 2) In + 1% Ga; 3) In + 1.5% Ga.

Figure 2 gives the concentrations obtained in this way as a function of the specific

resistance for n type germanium alloyed with arsenic or phosphorous.

Table 1 gives the calculated Fermi level in the conduction zone for two different n concentrations.

Table 1

ρ, ohm·cm	n, $см^{-3}$	$\mu - E_c$
0,00065	$3,5 \cdot 10^{19}$	$1,4\,kT$
0,0009	$2,2 \cdot 10^{19}$	$0,5\,kT$

Table 2

ρ ohm·cm	$\mu - E_c$	V_{max}, mv	$E_V - \mu$
0,0009	$0,5\,kT$	40	$2,2\,kT$
0,0009	$0,5\,kT$	68	$3,8\,kT$
0,0009	$0,5\,kT$	82	$4,6\,kT$

The position of the Fermi level in the valence zone for experimental diodes can be determined by Eq. (1), since it is not possible to measure the concentration in the p region obtained during melting by an independent method.

We investigated experimentally the effect of the carrier concentration in the p region on the position of the tunnel current maximum. To do this we manufactured diodes from germanium with a mixture of arsenic (specific resistance 0.0009 ohm·cm). The different concentrations in the p region were obtained by using different after-charges of gallium in indium (from 0.5 to 1.5%), and for all the experimental diodes the concentration in the p region was intentionally greater than in the n region on account of the high solubility of gallium in germanium ($5.10^{20}\,cm^{-3}$). This makes it possible to use Eq. (1)

Figure 3 shows the volt-ampere characteristics for three typical diodes. As the concentration in the p region increases, the position of the maximum tunnel current shifts towards the higher voltage region.

Table 2 shows the values, calculated from Eq. (1), for the Fermi level in the p region as a function of the position of the tunnel current maximum. (The values of V_{max} are taken from the experiment, and those of $\mu - E_c$ from Table 1).

As follows from Eq. (1), the position of the maximum depends to a very slight extent on the degree of alloying in the n region.

To check this experimentally we manufactured diodes from n type germanium with different concentrations on the basic carriers. The hole region was obtained by melting drops of indium containing 0.5% gallium and 0.5% zinc into the germanium. The additives were introduced in a crystallographic direction (III), which made it possible to obtain a flat melting front. Slow cooling was used to make the distribution of the additives in the recrystallized layer near the p — n junction more uniform.

The volt-ampere characteristics of the diodes made in this way are shown in Fig. 4, from which it is clear that the position of the maximum is for practical purposes not a function of the concentration of the n region.

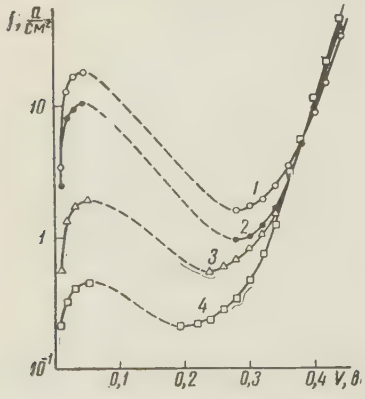

Fig. 4. Volt-amperes characteristics of tunnel diodes with different degrees of alloying of n region: 1) intrinsic germanium, ρ = 0.00065 ohm·cm; 2) intrinsic germanium ρ = 0.0009 ohm·cm; 3) intrinsic germanium ρ = 0.0011 ohm·cm; 4) intrinsic germanium ρ = 0.0016 ohm·cm.

Thus, for diodes with a more strongly alloyed p region the maximum is determined by the degree of degeneracy in the p region.

The experimental curves in Figs. 3 and 4, which agree well with Eq. (1), also reveal a strong dependence of the tunnel current on the concentration in the n and p regions. As is known, [3], one of the basic characteristics of a thin p — n junction determining the tunnel current is the probability of tunnel leakage of electrons through the potential barrier. This probability is proportional to the following expression:

$$P \sim \exp\left(-\frac{\pi^2 m^{*1/2} E_g^{3/2}}{\sqrt{2}\, heE}\right), \qquad (3)$$

in which E is the electric field intensity in the p — n junction and E_g is the width of the

forbidden zone in the germanium.

Since the exponent contains the field intensity E, this probability is naturally very sensitive to the position of the Fermi level on both sides of the junction, i.e., to the degree of alloying of the n and p regions. Consequently, to check the soundness of the results obtained for the position of the Fermi level in the diodes, we can evaluate the variation in the probability of tunnel leakage P as a function of the degree of alloying and compare the result with the variation in the density of the tunnel current obtained by experiment.

To calculate the field intensity at the junction we have to know its thickness, and this was determined from the formula

$$W = \sqrt{\frac{\varepsilon U}{2\pi e n}},$$

in which ϵ is the dielectric constant of germanium; U is the potential difference between the n and the p side, determined from the relationship (see Fig. 1)

$$eU = E_g + (E_V - \mu) + (\mu - E_c) - eV;$$

where V is the applied voltage.

The calculation shows that in diode 3 (Fig. 3) the probability of tunnel leakage is 13 times as great as in diode 1. From experimental data the ratio of the currents at the maximum for these diodes is $\sim$ 20. The same calculation for diodes 1 and 3 (Fig. 4) gives a probability ratio of $\sim$ 30. According to the experimental data, the current at the maximum for diode 1 is greater than for diode 3 by a factor of 10.

2. TEMPERATURE DEPENDENCE OF TUNNEL CURRENT

It was shown experimentally in Ref. 5 that the temperature dependence of the tunnel current may be both positive and negative, and the author associated the nature of the temperature dependence with the alloying additive (arsenic, antimony).

Measurement of the dependence of the tunnel current on temperature was made for diodes with different concentrations in the n and p regions. The intrinsic germanium was alloyed with arsenic or antimony. Experiments showed that when the degree of alloying of the p region is high (p $\gg$ n), we observe a reduction in the tunnel current when the temperature is lowered, regardless of the nature of the additive in the n type germanium. At a lower concentration of carriers in the p region (p $\geqslant$ n) the tunnel current increases as the temperature decreases. Furthermore, it is possible to obtain different temperature dependence of the tunnel current for the same concentration of arsenic in the intrinsic germanium, by varying the degree of alloying of the p region.

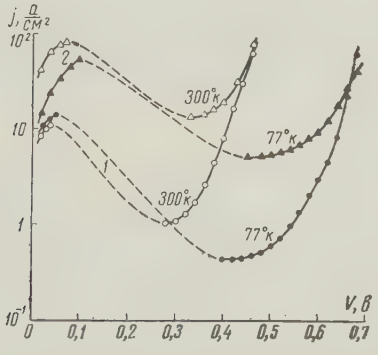

Fig. 5. Temperature dependence of tunnel diode; intrinsic germanium $\rho = 0.0009$ ohm · cm.

Figure 5 shows the volt-ampere characteristics for two diodes with an identical concentration in the n region, but with different degrees of alloying in the p region. Curves 2 stand for the diode with greater degeneracy in the p region than the one presented by curves 1. The characteristics are taken at room temperature (293°K) and at the temperature of liquid nitrogen (77°K). There is a positive temperature dependence for curve 2 and a negative one for curve 1. Thus, the nature of the temperature dependence of the tunnel current is determined first and foremost by the degree of decay in the n and p regions of the tunnel diode.

3. MINIMUM VOLT-AMPERE CHARACTERISTIC

It is known from Ref. 2, that in germanium, even at an impurity concentration of 10^{18} cm^{-3}, the local levels of the elements of the third and fifth group shift and form impurity zones which at concentrations of the order of $10^{19} - 10^{20}$ cm^{-3} may overlap with the nearby "normal" semiconductor bands. Clearly, for the concentrations which we used we have to take into account the presence of impurity zones and above all, their effect on the position of the volt-ampere characteristic minimum. Reference 2 gives the following expression for the potential difference applied to the p — n junction at which there is complete disappearance of the tunnel current:

$$eV_{\min} = \Delta E_a + \Delta E_d + (\mu - E_c) + (E_v - \mu), \tag{4}$$

in which ΔE_a is the width of the acceptor impurity zone; ΔE_d is the width of the donor impurity zone.

Thus, the position of the minimum is a direct function of the width of the impurity zones, and consequently, it can provide information on the energy spectrum of the semiconductor.

The above cited experimental data tally qualitatively with Eq. (4). For example, it is clear from Figs. 3 and 4 that the position of the volt-ampere characteristic minimum shifts towards higher voltages as the concentration increases in n and p regions. Furthermore, using Eq. (4) we can evaluate the width of the impurity zones, for example, for the diode whose characteristic, 2, is given in Fig. 4. The voltage at which we observe a minimum in the characteristic can be taken as the potential difference at which there is complete disappearance of the tunnel current, since at the minimum for this diode it amounts to 10% of the current at the maximum. It turns out that $\Delta E_a + \Delta E_d \simeq 0.2$ ev.

Reference 2 expresses the view that the tunnel current may possibly be affected by the various extended defects in the semi-conductor lattice, in particular, dislocations, the presence of which may lead to the appearance of allowed bands in the forbidden zone. On the other hand, the imperfections of the crystal lattice in germanium cause non-uniformity of the recrystallization layer when the diodes are melted, which may also lead to the non-uniformity of p — n junction and different types of leakage. In view of this we carried out experiments aimed at ascertaining the effect of dislocations in intrinsic germanium on the volt-ampere characteristics of tunnel diodes. To do this we manufactured diodes from germanium with different dislocation densities (from 20 to 1000 cm^{-2}). The experiments showed that there is smoother and, apparently, more uniformly distributed melting in the crystals without dislocations. We should point out that the largest current differential ($I_{max} - I_{min}$) is obtained from just those diodes made from germanium with a low dislocation density. At the same time we did not find any marked dependence on the tunnel current on dislocation density. This was most probably due to the small size of the tunnel current flowing along the dislocation zone, the carrier density in which is small compared with the carrier density in the zone of germanium proper.

CONCLUSION

It was experimentally shown that the degree of alloying of the n and p regions of a narrow p — n junction substantially affects the tunnel current and, especially the magnitude and position of the maximum and minimum volt-ampere characteristic. For diodes with a more strongly alloyed p region, the position of the maximum is determined basically by the degree of degeneracy in the p region. The position of the minimum volt-ampere characteristic shifts towards the higher voltages when the degree of alloying of the n and p regions increases; this may be due to the presence of impurity zones in the heavily alloyed semiconductor.

It also follows from the experiment that the nature of the temperature dependence of the tunnel current is determined by the degree of degeneracy in the n and p regions.

No appreciable dependence of the tunnel current on the dislocation density was found.

In conclusion we consider it our duty to express our gratitude to N. Ye. Skvortsova for the suggested topic of study and for her permanent interest in our work. We sincerely thank V. L. Bonch-Bruyevich for valuable advice during discussions of our work; we also thank S. G. Kalashnikov for his fruitful comments.

REFERENCES

1. L. Esaki, Phys. Rev., 1958, 190, 603.
2. V. L. Bonch-Bruyevich, Radio Engineering and Electronics, 1960, 5, 12, 2033.
3. J. A. Lesk, N. Holonyak, IRE Wescon Convention Record, 1959, 3, 8.
4. J. McDougall, E.C. Stoner, Philos. Trans. Roy. Soc. London A, 1939, 237, 67.
5. V. Furukawa, Phys. Soc. Japan, 1960, 15, 6.

Institute of Radio Engineering and
Electronics of the AN USSR

Received by the editors 10 September 1960

FLUCTUATIONS IN A REFLEX KLYSTRON OSCILLATOR DUE TO ELECTRON VELOCITY SPREADING SHOT AND HEAT EFFECTS

Ye. N. Bazarov and M. Ye. Zhabotinskiy

Using the method of symbolic equations and correlation theory we consider fluctuations in a reflex klystron oscillator due to velocity spreading in the electron stream and the shot and heat effects. We obtained expressions for the mean square fluctuations in amplitude and phase, and for the oscillation spectrum. We show that under certain conditions the electron velocity spreading in the stream may have a substantial effect on the fluctuations.

References 1 and 2 consider fluctuations in the amplitude and phase of the oscillation of an oscillator consisting of a reflex klystron, due solely to the shot and heat effects. Using the symbolic equation method and correlation theory as in Ref. 3, it is not difficult to take into account as well the effect of the velocity spreading of electrons in the stream on fluctuations in the amplitude and phase of the oscillator. To do this, we ignore the actual structure of the electron stream and assume it to have one velocity [4] and represent the electron velocity at the klystron resonator gap input in the form

$$v_1(t) = v_0(1 + p_0(t)),$$

where v_0 is the dc component of the electron velocity; P_0 (t) is the fluctuation in velocity, and t is time.

The convection current at the klystron resonator gap input is written in the form

$$i_1(t) = I_0(1 + f_0(t)).$$

Here I_0 is the mean cathode current and $f_0(t)$ is the current fluctuation.

Since the system under investigation is a narrow-band one, it can be taken that the fluctuation spectra of the velocity and the current are uniform within the system pass band. This makes it possible to replace the actual correlation functions of p_0 and f_0 by δ-functions, i.e., to write

$$\overline{p_0(t)\,p_0(t')} = A_0\delta(t - t'),$$

$$\overline{f_0(t)\,f_0(t')} = B_0\delta(t - t').$$

In the general case, p_0 and f_0 are correlated:

$$\overline{p_0(t) f_0(t')} = C_0 \delta(t - t').$$

The coefficients A_0, B_0, and C_0 are determined by the operating conditions of the cathode and the design of the electron gun in the klystron, and can be found for each case from the fluctuation spectra obtained in Ref. 4.

The klystron resonator can be replaced, as is well known, by a lumped equivalent circuit with an inductance L, capacitance C and resistance r. In this case it is easy to write the equation for the voltage at the resonator gap. The equation is different from the corresponding equation in Ref. 2 in that we now take into account the electron velocity spreading in its coefficients. Since the system under consideration is closely approximated by a linear conservative system, we can obtain expressions for: 1) the mean square amplitude fluctuation of the voltage at the resonator gap:

$$\bar{\rho}^2 = \frac{L_{11} + 2L_{21} \exp(-p_1\theta_0)}{8p_1}, \tag{1}$$

2) the spectral density of the amplitude fluctuations:

$$g(\Omega) = \frac{L_{11} + 2L_{21} \cos\frac{\theta_0}{\omega}\Omega}{4\pi p_1^2} \frac{1}{1 + \left(\frac{\Omega}{\omega p_1}\right)^2}, \tag{2}$$

and 3) the mean square phase fluctuations where $\omega p_1 t \gg 1$:

$$\bar{\chi}^2 = \left\{ \frac{q_1^2}{4p_1^2}(L_{11} + 2L_{21}) + \frac{1}{4R_0^2}(L_{12} + 2L_{22}) - \right.$$
$$\left. - \frac{q_1^2}{4p_1R_0}[P_{11} + P_{12} + 2(P_{21} + P_{22})] \right\} \omega t. \tag{3}$$

using the same method as in Ref. 2.

The first term in Eq. (3) is due to amplitude fluctuations, the second is due to the direct effect of random surges, and the third is due to the correlation of the fluctuations in the amplitude and the surges.

The values L and P in Eqs. (1) - (3) are determined by both the fluctuation properties of the electron stream and the operating characteristics of the klystron. They take the form

$$\left.\begin{matrix} L_{11} \\ L_{12} \end{matrix}\right\} = 2\left\{ 2rk_0T\omega_0 + \frac{I_0^2}{\omega_0 C^2}[2B_0 + A_0\theta_0^2 \pm \right.$$
$$\left. \pm (2\theta_0 C_0 \sin 2\theta_0 + (\theta_0^2 A_0 - B_0)\cos 2\theta_0) J_2(2z_0)] \right\},$$
$$\left.\begin{matrix} L_{21} \\ L_{22} \end{matrix}\right\} = 2\frac{I_0^2}{\omega_0 C^2}[J_0(z_0) \mp J_2(z_0)](\theta_0 C_0 \sin\theta_0 - B_0\cos\theta_0),$$
$$\left.\begin{matrix} P_{11} \\ P_{12} \end{matrix}\right\} = 2\frac{I_0^2}{\omega_0 C^2}[2\theta_0 C_0 \cos 2\theta_0 + (B_0 - \theta_0^2 A_0)\sin 2\theta_0] J_2(2z_0), \tag{4}$$
$$\left.\begin{matrix} P_{21} \\ P_{22} \end{matrix}\right\} = -2\frac{I_0^2}{\omega_0 C^2}(B_0 \sin\theta_0 + C_0\theta_0\cos\theta_0) J_2(z_0).$$

Here k_0 is Boltzman's constant, T is the absolute temperature; $\omega_0^2 = 1/LC$; $z_0 = \frac{\eta_0\theta_0}{v_0^2} R_0$; $\eta_0 = e/m$ — is the ratio of the electron charge to its mass; θ_0 is the mean transit angle of the electrons in the reflex space; R_0 is the stationary amplitude of the ac voltage at the resonator gap; ω is the frequency generated by the klystron; $J_k(z_0)$ is a Bessel function of the first kind and k-th order, $\Lambda_1(z_0) = \frac{2}{z_0} J_1(z_0)$.

The values p_1 and q_1 are determined by the expressions

$$p_1 = \frac{I_0\eta_0\theta_0}{2\omega_0 C v_0^2} z_0 \frac{d\Lambda_1(z_0)}{dz_0} \sin\theta_0,$$

$$q_1 = \frac{I_0\eta_0\theta_0}{2\omega_0 C v_0^2} \frac{d\Lambda_1(z_0)}{dz_0} \cos\theta_0, \tag{5}$$

in which the stationary values of z_0 and the frequency ω are determined by the equations

$$1 + \frac{I_0\eta_0\theta_0}{r\omega_0^2 C^2 v_0^2} \Lambda_1(z_0) \sin\theta_0 = 0,$$

$$\omega \simeq \omega_0 - \frac{I_0\eta_0\theta_0}{C v_0^2} \Lambda_1(z_0) \cos\theta_0. \tag{6}$$

In Eq. (4) the terms containing A_0, B_0, and C_0 are determined by the fluctuations in the velocity, the convection current and the correlation of the fluctuation in velocity and convection current, respectively. We should point out that if the fluctuation in electron velocity and the thermal fluctuations are ignored ($A_0 = C_0 = 0$), and assuming optimum electron transit angle in the reflex space $\left(\theta_0 = \theta_0^{opt} = \left(\frac{3}{4} + n\right)2\pi,\ n = 1, 2, 3, \ldots\right)$, Eqs. (1) - (3), according to Eq. (4), indeed coincide with the similar expressions in Ref. 1 to within the accuracy of the coefficient 1/2 for $J_2(2z_0)$. For $\theta_0 \neq \theta_0^{opt}$ and $A_0 = C_0 = 0$, Eqs. (1) and (3) correspond, to within an accuracy of the order of $(p_1\theta_0)^2$, with similar expressions in Ref. 2. The fluxtuations in velocity of the electrons ($A_0 \neq 0$) and the correlation of the fluctuations in velocity and convection current ($C_0 \neq 0$) give rise to terms in Eqs. (1) - (3) which can be compared with the terms due to the fluctuations of the convection current. Indeed, if, for example, the transit angle of the cathode - resonator gap is ~ 9, then, according to Ref. 4, we have for the coefficients A_0, B_0, and C_0

$$A_0 \simeq \frac{e}{I_0} 10^{-4},$$

$$B_0 \simeq \frac{e}{I_0} 10^{-2},$$

$$C_0 \simeq \frac{e}{I_0} 10^{-5},$$

and since A_0 is always multiplied by θ_0^2, the terms containing A_0 may be of the same order as those containing B_0. Conversely, the terms due to the correlation of the fluctuations in velocity and convection current can almost always be ignored. We then obtain from Eqs. (3) and (4) for the mean square fluctuations in phase at the optimum transit angle θ_0:

$$\overline{\chi^2} = \frac{eI_0}{R_0^2 C^2}\left[1 + \frac{\theta_0^2}{2} 10^{-2} + \frac{\theta_0^2 \cdot 10^{-2} - 1}{2} J_2(2Z_0)\right] 10^{-2} t.$$

For the sake of clarity we have omitted here the term describing the effect of thermal fluctuations, which is of the same small order of magnitude as the terms for the correlation of the fluctuations in velocity and convection currents.

When the klystron operates in the second mode $\theta_0 \simeq 17$, and when operating in the fourth mode $\theta_0 \simeq 30$. It follows from this that fluctuations in velocity may substantially influence fluctuations in the output phase, and the higher the number of the operating mode, the greater the effect.

REFERENCES

1. Bernshteyn, I. L. Reports of the AS USSR, 1956, 106, 453.
2. Bazarov, Ye. N., Zhabotinskiy, M. Ye, Radio Engineering and Electronics, 1959, 4, 10, 1685.
3. Rytov, S. M., ZhETF, 1955, 29, 304.

4. Gvozdover, S.D., Theory of microwave instruments, GITTL, 1956, p. 248.

Submitted to the editors 15 June 1960

BRIEF COMMUNICATIONS

TWT GAIN WITH FINITE VALUES OF THE GAIN PARAMETER C

M.B. Tseymlin, Ye. M. Il'ina

Analysis of the interaction of a stream of electrons with the traveling electromagnetic wave in a traveling-wave tube leads to a fourth-power equation with complex coefficients for the propagation constants (e.g., see Refs. 1, 2). It is usually assumed that the gain per unit length of wave is small, that is, that the gain parameter C introduced by Pierce [1] is considerably less than unity. On this assumption a third-power equation is derived for the propagation constants.

However, in medium- and high-power tubes the parameter C may reach values of 0.1 - 0.2. In this case, in determining the propagation constants it is necessary to consider finite values of C (i.e., to solve the fourth-power equation [3]). Numerical solution of this equation presents considerable difficulty.

The power method of calculation described in Ref. 4 permits a relatively simple determination of TWT gain with finite values of the gain parameter C. This method consists of finding the amplitude distribution of the r-f field along the tube from the real-power balance equation. It is assumed that the field within the line may be represented by a single wave with constant phase velocity.

In Ref. 4 the following asymptotic equation was derived for TWT gain:

$$G = BCN + A = 8{,}68\mu z + 20 \lg \frac{mk}{\mu^2 (\mu^2 + \nu^2)} \text{ db}, \tag{1}$$

where

$$\mu = \beta_e C \sqrt{\sqrt{2b\gamma^2 + 4b^2 q} - (q + b^2)};$$

$$\nu = \beta_e C \sqrt{\sqrt{2b\gamma^2 + 4b^2 q} + (q + b^2)}; \tag{2}$$

$$\gamma = \frac{\beta}{\beta_e} = 1 + bC; \tag{3}$$

$$m = \beta_e \beta^2 C^3; \quad k = \beta_e C b; \tag{4}$$

$q = \beta_q^2 / \beta_e^2 C^2$ is the space-charge parameter; $b = (u_0 - v_\Phi) / C v_\Phi$ is the asynchronism parameter for the disturbed wave; β_e is the phase constant of the electron stream; β is the phase constant for a wave in a system with a beam*.

* In Ref. 4 β is taken to represent the phase constant of the wave in a system without a beam. For $C \ll 1$ this would not lead to error, for in this case it could be assumed that $\gamma = 1 + bC \simeq 1$.

For finite values of the gain parameter C it cannot be assumed that $\gamma = 1$, but it is necessary to use Eq. (3).

Equations (1) - (3) permit a calculation of TWT gain (with finite values of the parameter C) as a function of the phase velocity of the disturbed wave. However, practical interest attaches to the dependence of the gain on the phase velocity of the undisturbed wave, for it is this wave which is associated with the geometric parameters of the line. The relationship between the phase velocities of the disturbed and undistrubed waves may be obtained from the reactive-power balance equation.

Reactive power in the line may be determined from

$$P_{lr} = \frac{(\beta - \beta_0) E_1^2(z)}{2\mu\beta^2 K_c} - \frac{(\beta - \beta_0) E_1^2(0)}{2\mu\beta^2 K_c}, \tag{5}$$

where β_0 is the phase constant of the undisturbed wave and K_c is the coupling impedance.

This relationship is easily derived from the expression for the total power flux over a segment dz in the presence of a beam of electrons [5[:

$$dP_l = \frac{EE^*}{K_c\beta^2}(\Gamma - \Gamma_0)\, dz, \tag{5'}$$

where E is the r-f field intensity along the line, $\Gamma = \mu - j\beta$ is the propagation constant of the disturbed wave, $\Gamma_0 = j\beta_0$ is the propagation constant of the undisturbed wave in the absence of losses.

Assuming that the r-f field intensity within the line varies exponentially (as $e^{\mu z}$), integrating Eq. (5') over the limits from zero to z and eliminating the imaginary part, we arrive at Eq. (5) for the reactive power flux within the line.

On the other hand, the reactive power of interaction may be represented in the form

$$P_{rr} = -\frac{1}{2}\,\mathrm{Im}\int_0^z E(z)\, i^*(z)\, dz, \tag{6}$$

where E(z) and i(z) are the r-f components of field intensity and current as defined by the following equations from Ref. 4

$$E(z) = E_1(z)\, e^{-j\beta_e(1+bC)z}; \tag{7}$$

$$i(z) = j\,\frac{I_0\beta_e}{2U_0}\int_0^z E(x)\,\frac{\sin\beta_q(z-x)}{\beta_q}\, e^{-j\beta_e(z-x)}\, dx; \tag{8}$$

$E_1(z)$ is the amplitude of field intensity, I_0 and U_0 are the dc components of the beam current and voltage, respectively.

Substituting Eqs. (7) and (8) into Eq. (6) and using the condition of reactive-power balance $P_{rr} = P_{lr}$, we obtain

$$\frac{\beta - \beta_0}{2\mu\beta^2 K_c}\,[E_1^2(z) - E_1^2(0)] = -\frac{I_0\beta_e}{4U_0\beta_q}\int_0^z E_1(x)\, dx \int_0^x E_1(t)\cos k(x-t)\sin\beta_q(x-t)\, dt. \tag{9}$$

Using the expression for the field amplitude $E_1(z)$ under conditions of asymptotic gain [4],

$$\frac{E_1(z)}{E_1(0)} = \frac{mk}{\mu^2(\mu^2 + \nu^2)}\, e^{\mu z},$$

after appropriate transposition we find

$$\beta - \beta_0 = \frac{\mu^2 + \beta_q^2 - k^2}{2k}. \tag{10}$$

The value of $\beta - \beta_0$ may be expressed in terms of the asynchronism parameters b and b_x

for the disturbed and undisturbed waves, respectively, from

$$b - b_x = \frac{\beta - \beta_0}{\beta_e C} \tag{11}$$

From Eqs. (10), (11), (2) and (3) let us find the desired relationship between b and b_x:

$$b_x = 2b - \frac{1}{2b}\sqrt{2b(1+bC)^2 + 4b^2 q}. \tag{12}$$

For $C \ll 1$ Eq. (12) takes the form

$$b_x = 2b - \sqrt{\frac{1}{2b} + q}. \tag{13}$$

In the case of considerable space charge ($q > 1$), we may obtain from Eq. (13)

$$b_x \simeq 2b - \sqrt{q}. \tag{14}$$

It was shown in Ref. 4 that for $q > 1$ $b_{opt} = \sqrt{q}$. It follows from Eq. (14) that in this case $b_x \simeq b = \sqrt{q}$. Consequently, with considerable space charge under maximum-gain conditions the phase velocity of the wave is practically unaffected by the electron stream. This statement is also borne out by the results of more rigorous analysis [6].

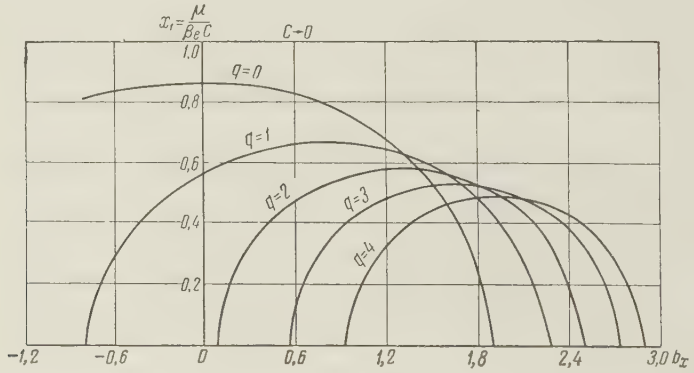

Figure 1. Dependence of the increasing wave parameter $x_1 = \mu/\beta_e C$ on the asynchronism parameter b_x for $C \to 0$.

Equations (2), (3) and (12) permit a calculation of the dependence of the increasing wave parameter $x_1 = \mu/\beta_c C$ on the asynchronism parameter b_x for the undisturbed wave and the space-charge parameter q for various values of C. This dependence is shown in Figs. 1-3. Figure 4 shows the dependence of the maximum value of $x_1 = \mu/\beta_e C$ on q for various values of C. From these plots it is seen that the curve for the dependence of x_1 on q becomes less steep as C increases. With finite values of C maximum gain occurs when $x_1/1 + b_x C$ (proportional to the gain per unit length) is maximum. Figure 5 shows the dependence of the maximum value of $x_1/1 + b_x C$ on q for various values of C.

Upon determining the optimum value of b corresponding to the maximum value of $x_1/1 + b_x C$ we may calculate the initial-loss parameter A for finite values of C from

$$A = 20 \lg \frac{mk}{\mu^2(\mu^2 + \nu^2)}. \tag{15}$$

The dependence of A on q for various values of C is shown in Fig. 6.

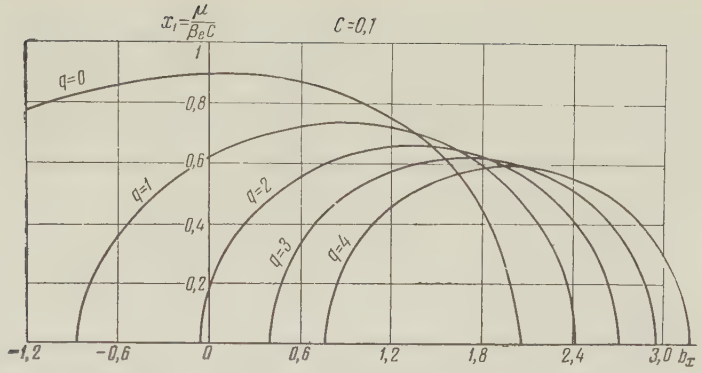

Figure 2. Dependence of the increasing wave parameter $x_1 = \mu/\beta_e C$ on the asynchronism parameter b_x for C = 0.1.

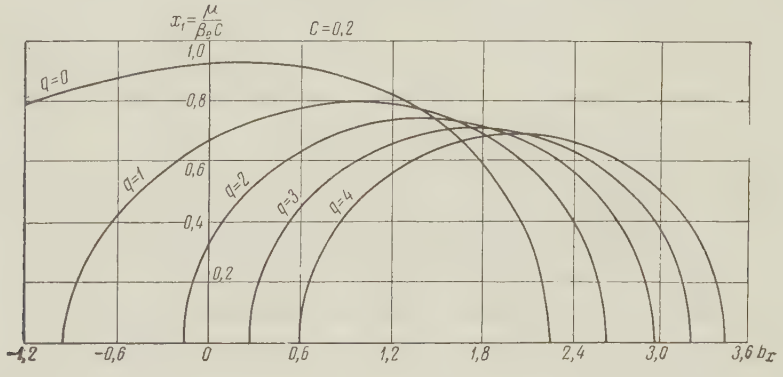

Figure 3. Dependence of the increasing wave parameter $x_1 = \mu/\beta_e C$ on the asynchronism parameter b_x for C = 0.2.

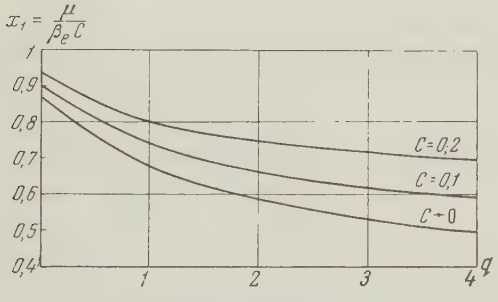

Figure 4. Dependence of the maximum value of the increasing wave parameter x_1 on q for various values of the gain parameter C.

The approximate calculation of the attenuation within the line (performed in Ref. 4 may be generalized in the case of finite values of C.

Figures 7 and 8 show the dependence of the increasing wave parameter $x_1 = \mu/\beta_e C$ on the attenuation parameter d for various values of C and q.

It was shown in Ref. 1 that the dependence of the increasing wave parameter x_1 on the attenuation parameter d for $C \ll 1$ may be approximately described by

$$x_1 = x_{10} - \frac{d}{3},$$

where x_{10} is the value of x_1 at d = 0. It may be shown that a similar dependence occurs at finite values of C. In Figs. 7 and 8 the broken lines represent $x_1 = x_{10} - d/3$ for values of C = 0.1 and 0.2. The correspondence of the solid and broken curves is quite adequate. The results obtained in the present paper coincide with those of Ref. 3 for zero space charge.

For space charge other than zero, in comparing the results it is necessary to use the

relationship [3]

$$4QC = \frac{q}{(1 + C\sqrt{q})^2}. \qquad (16)$$

A comparison performed taking Eq. (16) into account shows that the values of the parameter x_1 calculated in Ref. 3 exceed the values of $x_1 = \mu/\beta_e C$ calculated from Eq. (2). This is

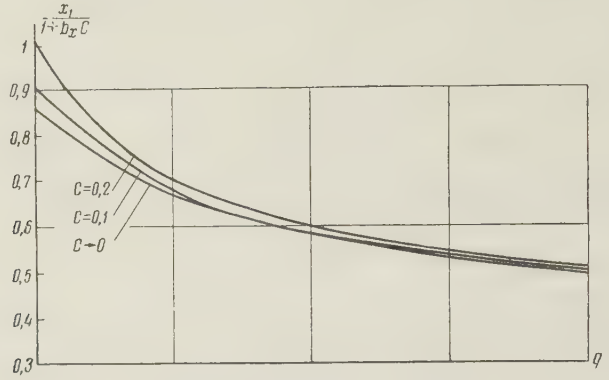

Figure 5. Dependence of the maximum value of $x_1/1 + b_x C$ on q for various values of C.

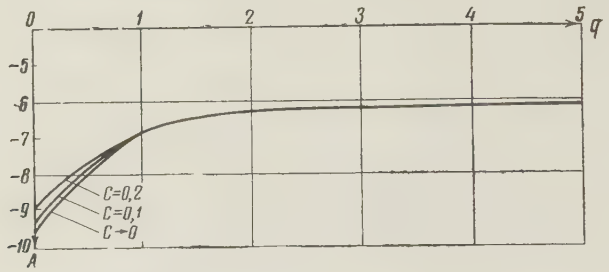

Figure 6. Dependence on the initial-loss parameter A in optimum operation on space charge q for various values of C.

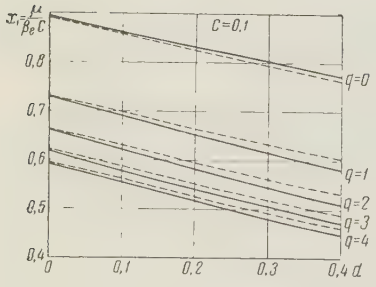

Fig. 7

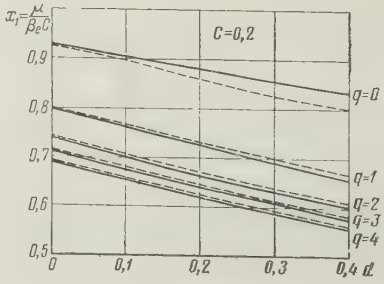

Fig. 8

Figure 7. Dependence of the increasing wave parameter $x_1 = \mu/\beta_e C$ on the attenuation parameter d for C = 0.1.

Figure 8. Dependence of the increasing wave parameter $x_1 = \mu/\beta_e C$ on the attenuation parameter d for C = 0.2.

apparently explained by the fact that the authors of Ref. 3 used for the finite values of C the characteristic equation presented in Ref. 1 where the space charge was not sufficiently accurately calculated. As preliminary calculations have shown, the values of $x_1 = \mu/\beta_e C$ obtained in the present paper are in complete agreement with the values of the increasing wave parameter calculated from the characteristic equation (VII. 18) in Ref. 2.

REFERENCES

1. J. Pierce. Traveling-wave tubes, Published by Sovetskoye radio, 1952.
2. A.H. Beck, Space-charge waves and slow electromagnetic waves, Pergamon Press, London, 1958, p. 223.
3. C. Birdsall, G. Brewer, IRE Trans., 1954, ED-1, 3, 1.
4. M.B. Tseytlin, Ye. M. Il'ina, Radio Engineering and Electronics, 1960, 5, 4, 700.
5. V.N. Shevchik, Fundamentals of microwave electronics, Published by Sovetskoye radio, 1959, p. 148.
6. L.N. Loshakov, ZhTF, 1953, 23, 10, 1833.

Submitted to the editors 19 April 1960

AMMONIA-BEAM MASER OPERATING WITHOUT LIQUID NITROGEN

V.V. Grigor'yants, M. Ye. Zhabotinskiy

In collaboration with G.A. Vasneva we previously proved the possibility of creating an ammonia-beam maser [1] operating without freezing of the ammonia molecules [2]. It was shown that such a maser requires beam sources with directivity of 5 - 10° or, in the absence of such sources, division of the operating volume of the maser into two chambers: an operating chamber and a source chamber, with separate evacuation of each. The chambers are separated by a diaphragm, the position and orifice of which are so chosen that they insure the required directivity of the beam into the operating chamber (see Fig. 1). The required pump capacity is determined for each chamber from

$$S = 2{,}8 \cdot 10^{-20} \frac{N}{P}, \qquad (1)$$

where S is the pump capacity in liters per second, P is the operating pressure in the chamber in mm Hg, and N is the number of molecules per second entering the chamber.

As is known, maser output is of the order of 10^{-9} w. In order to obtain this power, taking saturation into account, approximately 10^{15} active molecules in the energy state being used must enter the cavity resonator per second. For the line (3,3) these molecules constitute approximately 2 percent of the total number of molecules in the beam. Hence for full use of the beam approximately 1×10^{17} molecules must enter the maser per second. For evacuation of this number of molecules at a vacuum of 2×10^{-5} mm Hg is sufficient. This is provided by a pump with capacity of approximately 100 l/sec. The use of directional sources permits substantial reduction in this capacity.

In the case of the two-chamber model nondirectional sources of the fine-grating type

may be used. The total intensity of the beam entering the source chamber rises to approximately 3 x 10^{18} molecules per second. Since in the source chamber the beam must travel a path of less than 1 cm, in order to insure the required mean free path a vacuum of the order of 10^{-3} mm Hg is sufficient. This is provided by a pump with capacity of approximately 100 l/sec. The use of directional sources permits substantial reduction in this capacity.

An experimental check of the efficiency of a maser without liquid nitrogen was performed on a standard laboratory maser with the following data (unchanged throughout the experiments discussed below): cavity length, 100 mm; length of quadrupole condenser, 100 mm; diameter of input pupil, 6 mm; U_{kv} = 32 kv. The source was an array of long tubes*: tube diameter, 0.25mm; tube length, 5 mm; number of tubes, 185. Total diameter of the array was 4 mm. Distance between the cavity resonator and quadrupoles was 7 mm; distance between the grating and the quadrupoles was 14.5 mm. The operating chamber was evacuated by a standard diffusion pump N-5 with oil seal and a capacity of approximately 250 l/sec. In the experiments with a dual-chamber maser the source chamber was evacuated by a TsBL-100 pump through a vacuum line with length 0.5 m and diameter 60 mm, which lowered the effective rate of evacuation. Oscillation was observed by means of a microwave receiver with a crystal-stabilized local oscillator, an intermediate frequency f_0 = 56 Mc, and a band width Δf = 0.4 Mc. Measurements during maser operating without liquid nitrogen were compared with similar measurements for the same maser with liquid nitrogen. Results of the experiments are given in the table.

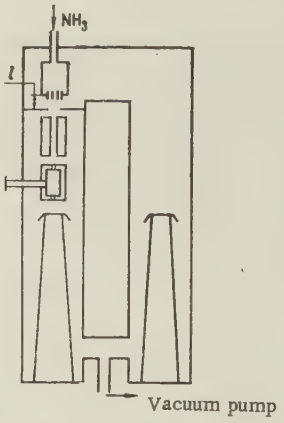

Figure 1. Dual-chamber maser.

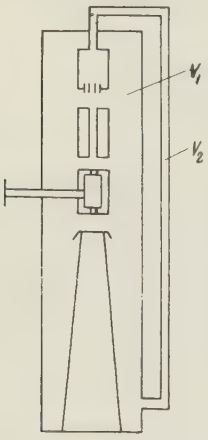

Figure 2. Maser with ammonia circulation.

It is seen from the table that the dual-chamber maser without liquid nitrogen has a signal-to-noise ratio half as good as that of a maser with liquid nitrogen, even though the former is, of course, not of optimum construction.

It is necessary to point out that in starting the maser without liquid nitrogen with a single pump the pressure at the source was 6.5 x 10^{-2} mm Hg, which corresponds to a mean free path of approximately 0.6 mm, whereas the tube length was 5 mm. This indicates that, due to the low beam intensity, the directivity of the array was not fully exploited. Hence, it is necessary to increase the number of tubes of the array while preserving the ratio of length to radius.

Successful starting of a maser without liquid nitrogen permits achievement of a practical maser with ammonia circulation [2] (see Fig. 2). The possibility of such circulation is insured by the fact that the outlet pressure of ordinary high-vacuum pumps is of the same magnitude as the operating pressure of the gas at the source (i.e., 10^{-2} — 1.0 mm Hg). If at the initial moment there is introduced into the system (degassed and evacuated to a high vacuum) pure ammonia up to a pressure of 1 x 10^{-3} mm Hg and we have $V_1/V_2 \simeq 10^2$ (see Figure 2), then upon switching in a pump with a capacity chosen from Eq. (1) practically all of the gas will pass into V_2, that is, to the source, where the pressure will be V_1/V_2 times greater than the initial pressure (i.e., approximately 10^{-1} mm Hg). Both the maser and the vacuum pump will be made for the same operating conditions. Prolonged operation of such a design requires oil with high heat

---

* The procedure for making these arrays was developed by G.A. Semenov.

Maser type	Source pressure mm Hg	Pressure in operating chamber mm Hg	Pressure in source chamber mm Hg	Minimum pressure in source mm Hg	Signal / Noise
Single-chamber, without liquid nitrogen	$6.5 \cdot 10^{-2}$	$2.7 \cdot 10^{-5}$	—	$2.2 \cdot 10^{-2}$	~ 10
Dual-chamber, ι = 3 mm	$1.2 \cdot 10^{-1}$	$2.2 \cdot 10^{-5}$	$1.6 \cdot 10^{-4}$	$1.5 \cdot 10^{-2}$	~ 16
Dual-chamber, ι = 6 mm	$1.3 \cdot 10^{-1}$	$2.0 \cdot 10^{-5}$	$1.8 \cdot 10^{-4}$	$2.0 \cdot 10^{-2}$	~ 20
Maser with Liquid nitrogen	$2.5 \cdot 10^{-1}$	$6.3 \cdot 10^{-6}$	—	$1.7 \cdot 10^{-2}$	~ 40
Maser with Liquid nitrogen	$6.5 \cdot 10^{-2}$	$2.1 \cdot 10^{-6}$	—	—	~ 25

resistance and a getter which does not absorb ammonia. The maser with circulation may also be made in the dual-chamber variant.

The authors express their thanks to I. N. Orayevskiy and G.N. Barykin for their assistance in the experiments.

REFERENCES

1. N.G. Basov, Experimental Equipment and Techniques, 1957, 1, 71.
2. G.A. Vasneva, V.V. Grigor'yants, M.Ye. Zhabotinskiy, Reports at the Second All-Union Conference of MVO SSSR on radio electronics, Radio Engineering and Electronics, 1958, 3, 3, 442.

Submitted to the editors 12 July 1960

LETTERS TO THE EDITOR

EXCITATION MECHANISM OF ELECTRON PLASMA OSCILLATIONS

In a number of papers [2, 3] devoted to the investigation of plasma oscillations it was assumed that in the experiments of Merill, Webb and associates [1] the oscillations are excited by means of a mechanism close to the klystron mechanism [5, 7]. It was subsequently shown in Ref. 4 that the phenomena observed under such conditions may be explained on the basis of a combination of the principle of phase focusing and coherent interaction with the plasma of the electron bundles being formed.

The successful development of the theory of spatial interaction of the electron stream with the plasma [5-11] (henceforth we shall refer to this interaction as the TWT mechanism) and experimental verification of this theory [12-16] led to re-examination of the explanations of earlier experiments, particularly the experiments in Refs. 17 and 1. Criticism of the initial explanation of the experiments of Looney and Brown, made on the basis of serious theoretical and experimental observations [19, 18] was evidently correct, although the new

ideas of various authors differ. Analysis of the experiments of Merill and Webb was primitive and the opinions expressed are not conclusive. There is an opinion [11, 20] that these experiments [1] are explained by the TWT mechanism. In support of this it is stated in Ref. 20 only that the rate of increase in amplitude of the plasma wave (calculated on the basis of the theory in Ref. 10, which is in poor agreement with experiment) may be quite high. Another opinion [16, 18] consists of the fact that the excitation of oscillations in the experiments [1] is associated with the oscillations of electrons within the potential well and is not accompanied by a demonstration. In the papers mentioned [16, 11, 18, 20] there is no detailed analysis of the correspondence between the experimental observations of Ref. 1 and the assumptions stated concerning the nature of these observations.

In connection with such variety of opinion concerning the essentials of such fundamental experiments as those of Merill and Webb it is our intention to show that there is at this time no basis for questioning the klystron mechanism of excitation and to call attention to the fact that in any attempt to explain these experiments it is necessary to explain an entire series of facts.

In the case of the TWT mechanism the regions of modulation and transmission of energy from the electron stream to the plasma must coincide, and in the case of the klystron mechanism they must be spatially separate and concentrated in sharply delimited zones. As the basis for determining the possibility of a klystron plasma oscillator it is first necessary to demonstrate the existence at the plasma boundary of an alternating microwave field with sufficient amplitude, which is verified by direct experiments [21]. The beam of electrons passing through such a plasma boundary is modulated and is converted into a train of bundles with maximum density at the site of the phase focus. At this site there occurs more intense interaction of the beam with the plasma (coherent interaction of the bundle charges with the plasma) and, in addition, it is possible that there is feedback from the modulation zone due, for example, to a wave propagated from the region of the phase focus. In the presence of stable feedback (in practice it is achieved by careful choice of the combination of current and energy of the electron beam) in the phase focus region there is noticed not only anomalous scattering but also "monochromatic" oscillations. In the absence of the required feedback, phase focusing will exist for isolated, short intervals of time. The anomalous scattering is preserved, but as the result of oscillations in the form of more or less short wave trains the usual indicating devices reveal no definite frequency but a wide spectrum of frequencies (noise). This klystron mechanism, in combination with coherent interaction [4], permits explaining the following facts.

1. The formation of sharply delimited scatter zones and an oscillatory zone, their relative positions, their displacement toward the cathode with a decrease in electron velocity or with an increase in plasma concentration (a decrease in phase focal length upon an increase in frequency).

2. The order of magnitude of energy interaction (loss of energy, energy of anomalous fast electrons), the increase in energy losses with an increase in current or a decrease in electron energy, the nondependence of losses on the concentration of external plasma.

3. The existence of critical interaction. The energy losses increase with the electron beam current, but at a certain value of current the losses cease to increase (see curves 7 and 8, Figure 2, Ref. 4). It may be shown that this is associated with spreading of the electron bundles under the influence of the natural space charge. At a certain beam current the minimum bundle dimensions begin to exceed the plasma wavelength.

4. The occurrence, along with anomalous scattering, of noise or oscillations with fixed frequency (see above).

An indication of the difference in the mechanisms of interaction — for example, in cases of Refs. 4 and 16 — is also found in the fact that with electron beam power of the same order the oscillatory power in Ref. 4 proved to be greater by many orders of magnitude. It should be pointed out that coherent interaction of electron bundles and plasma was proposed as a means of introducing energy into the plasma [22, 23]. Also detracting from the role of the TWT mechanism is the fact that the extent of the oscillatory zone in the experiments discussed is less than the plasma wavelength.

Thus, the abovementioned trend toward a unified explanation of the various experiments does not always yield positive results. No one now doubts the existence of the TWT mechanism, but this does not exclude the fact that in some cases the excitation of oscillations is due also to a mechanism having much in common with the klystron mechanism. Moreover, in discussing the creation of self-excited plasma oscillators it is necessary to

consider, not two, but three possibilities, for there is also the analog of a positive-grid oscillator examined in detail in Ref. 18.

REFERENCES

1. I. Merill, W. Webb, Phys. Rev., 1939, 55, 1191.
2. G. Wehner, J. Appl. Phys., 1951, 22, 761.
3. T.R. Neill, K.G. Emeleus, Proc. Roy. Irish Acad. A., 1951, 53, 197.
4. M.D. Gabovich, L.L. Pasechnik, ZhETF, 1959, 36, 1025.
5. D. Bohm, D. Gross, Phys. Rev., 1949, 75, 1851, 1864; 1950, 79, 992.
6. A.I. Akhiyezer, Ya. B. Faynberg, ZhETF, 1951, 21, 1262.
7. A.A. Vlasov, Multiple particle theory, GITTL, 1950.
8. L.D. Landau ZhETF, 1946, 16, 574.
9. M.A. Lampert, J. Appl. Phys., 1956, 27, 5.
10. M.Sumi, J. Phys. Soc. Japan, 1959, 14, 653.
11. Yu. L. Klimontovich, ZhETF, 1959, 36, 1405.
12. G.D. Boyd, L.M. Field, W. Gould, Phys. Rev., 1958, 109, 1393.
13. M.D. Gabovich, L.L. Pasechnik, Reports at the Second All-Union Conference on Gaseous Electronics, 1958; Radio Engineering and Electronics, 1959, 4, 11, 1850.
14. Ye.V. Bogdanov, V.Ya. Kislov, Z.S. Chernov, Radio Engineering and Electronics, 1960, 5, 2, 229.
15. A.A. Zaytsev, ZhETF, 1959, 36, 1332.
16. R.A. Demirkhanov, A.K. Gevorkov, A.F. Popov, ZhTF, 1960, 30, 315.
17. D.H. Looney, S.C. Brown, Phys. Rev., 1954, 93, 965.
18. R.A. Demirkhanov, A.K. Gevorkov, A.F. Popov, G.I. Zverev, ZhTF, 1960, 30, 306.
19. M. Sumi, J. Phys. Soc. Japan, 1954, 14, 1093.
20. M. Sumi, J. Phys. Soc. Japan, 1954, 9, 88
21. D. Gabor, E. Ash, D. Dracott, Nature, 1955, 176, 916.
22. K.D. Sinelnikov et al., Proc. of the Geneva conference, 1958, No. 2211.
23. A.I. Akhiyezer et al., Proc. of the Geneva conference, 1958, No. 2300.

Institute of Physics
AN SSSR

M.D. Gabovich

Submitted to the editors 21 April 1960

ACADEMICIAN ABRAM FEDOROVICH IOFFE

Academician Abram Fedorovich Ioffe, a prominent Soviet scientist who enriched science and engineering with many discoveries and investigations, passed away on 14 October 1960.

A.F. Ioffe was born in Romna (formerly Poltavskaya guberniya) on 29 October 1880. Upon the completion of his studies at Petersburg Technological Institute in 1902, not being satisfied with the level of science in tsarist Russia, he entered Munich University and graduated from that institution in 1905 with the degree of doctor of philosophy. Returning to Petersburg in 1906, he began his work as a scientist, pedagogue and organizer, which he pursued indefatigably until the very last day of his life.

Even A.F. Ioffe's early investigations of the atomic nature of electricity and the elementary photoelectric effect were of fundamental importance and are included among the classical experiments of modern physics.

Of no less importance were the widely known works of A.F. Ioffe and his students in the investigation of the mechanical and electrical properties of crystals. These researches were the first conclusive explanation for the marked difference between the molecular and bulk strengths of crystals, while investigations of electrical conductivity and breakdown of crystals contributed to the explanation of the intricate phenomena of the movement of

electrical charges and polarization in dielectric crystals.

A.F. Ioffe's investigations of semiconductors, begun as early as 1930, cannot be overestimated in importance. He and his close associates engaged in detailed studies of electrical, magnetic and thermal phenomena in semiconductors, which permitted a general description of the complex phenomena of extrinsic and intrinsic conductivity of semiconductors as well as the mechanism of electron and hole conductivity. As early as 1937 A.F. Ioffe and A.V. Ioffe expressed their opinion concerning the nature of the rectification of electrical current at the junction between two semiconductors with different conductivity; this opinion was later brilliantly developed in the works of Soviet and foreign scientists and lies at the foundation of all the extremely important modern applications of semiconductors. A.F. Ioffe's investigations in thermoelectricity, leading to the creation of laboratory models of semiconductor thermoelectric generators and refrigerators with practical efficiency, have been a particular contribution to investigations abroad and are serving as the basis for the development of a new branch of power engineering.

The works of A.F. Ioffe have gained wide acclaim. He was chosen as a member of the academies and scientific societies of many countries.

A.F. Ioffe's activities in the organization of scientific investigations in the Soviet Union were truly unmatched. On his initiative or with his help physical-technical institutes were organized in Leningrad, Khar'kov, Sverdlovsk, Dnepropetrovsk, and Tomsk. The Institute of Chemical Physics and the Electrico Physics Institute in Leningrad, as well as the Leningrad Agricultural Engineering Institute, are unique among such institutes. A.F. Ioffe taught numerous brilliant scientists, many of whom in turn enriched mankind with important discoveries which are the pride of Soviet science.

In his intense activity A.F. Ioffe constantly proved himself to be not only a prominent scientist but also a patriot of the entire Soviet fatherland. Immediately after the Great October Socialist Revolution he was one of the first great scientists actively participating in the development of Soviet science and engineering, devoting all his energy to this honorable task. A.F. Ioffe always combined his interest in the principal problems of physics with an interest in engineering and was always concerned that the achievements of physics be used for the development of the technical might of the Soviet Union.

The Soviet government placed high value on A.F. Ioffe's work and achievements, awarding him many prizes and bestowing on him in 1955 the rank of Hero of Socialist Labor.

Editorial Staff

RADIO ENGINEERING AND ELECTRONIC PHYSICS

The English Edition of Radio Engineering and Electronic Physics is mailed to subscribers within 18 weeks after the publication of the original Russian issue.

Russian electronic journals published by the
American Institute of Electrical Engineers
Translated by Royer and Roger, Inc.

	Subscription rates			
	Individuals		Libraries	
	$	£	$	£
Radio Engineering and Electronic Physics	28.50	10	57.00	20
Radio Engineering	14.25	5	28.50	20
Telecommunications	14.25	5	28.50	20

Royer and Roger translates and produces
the following Russian scientific journals:

Biophysics
Entomological Review
Geochemistry
Geodesy and Cartography
Izvestiya, Academy of Sciences of the USSR, Geologic Series
Pavlov Journal of Higher Nervous Activity
Problems of Oncology
Radio Engineering
Radio Engineering and Electronic Physics
Refractories
Sechenov Physiological Journal of the USSR
Soil Science
Telecommunications

Comments and inquiries regarding *Radio Engineering and Electronic Physics* and other translation journals should be sent to:

International Division
Royer and Roger, Inc.

1000 Vermont Avenue, N.W.
Washington 5, D.C.

41 East 28th Street
New York 16, New York

RADIO ENGINEERING AND ELECTRONIC PHYSICS

РАДИОТЕХНИКА И ЭЛЕКТРОНИКА

NUMBER 1 1961

CONTENTS